A specialized exit route: Specific recognition and cell cycle-dependent transport of exomer-dependent cargoes in *Saccharomyces cerevisiae*

Inauguraldissertation

zur

Erlangung der Würde eines Doktors der Philosophie

vorgelegt der

Philosophisch-Naturwissenschaftlichen Fakultät

der Universität Basel

von

Uli Rockenbauch

aus Stuttgart, Deutschland

UNI
BASEL

Basel, 2012

Genehmigt von der Philosophisch-Naturwissenschaftlichen Fakultät

auf Antrag von

Prof. Dr. Anne Spang

Prof. Dr. Margaret Robinson

Basel, den 21. Februar 2012

Prof. Dr. Martin Spiess

Dekan der Philosophisch-
Naturwissenschaftlichen Fakultät

creative commons

Namensnennung-Keine kommerzielle Nutzung-Keine Bearbeitung 2.5 Schweiz

---

Sie dürfen:

das Werk vervielfältigen, verbreiten und öffentlich zugänglich machen

Zu den folgenden Bedingungen:

Namensnennung. Sie müssen den Namen des Autors/Rechteinhabers in der von ihm festgelegten Weise nennen (wodurch aber nicht der Eindruck entstehen darf, Sie oder die Nutzung des Werkes durch Sie würden entlohnt).

Keine kommerzielle Nutzung. Dieses Werk darf nicht für kommerzielle Zwecke verwendet werden.

Keine Bearbeitung. Dieses Werk darf nicht bearbeitet oder in anderer Weise verändert werden.

- Im Falle einer Verbreitung müssen Sie anderen die Lizenzbedingungen, unter welche dieses Werk fällt, mitteilen. Am Einfachsten ist es, einen Link auf diese Seite einzubinden.
- Jede der vorgenannten Bedingungen kann aufgehoben werden, sofern Sie die Einwilligung des Rechteinhabers dazu erhalten.
- Diese Lizenz lässt die Urheberpersönlichkeitsrechte unberührt.

Die gesetzlichen Schranken des Urheberrechts bleiben hiervon unberührt.

Die Commons Deed ist eine Zusammenfassung des Lizenzvertrags in allgemeinverständlicher Sprache: http://creativecommons.org/licenses/by-nc-nd/2.5/ch/legalcode.de

Haftungsausschluss:
Die Commons Deed ist kein Lizenzvertrag. Sie ist lediglich ein Referenztext, der den zugrundeliegenden Lizenzvertrag übersichtlich und in allgemeinverständlicher Sprache wiedergibt. Die Deed selbst entfaltet keine juristische Wirkung und erscheint im eigentlichen Lizenzvertrag nicht. Creative Commons ist keine Rechtsanwaltsgesellschaft und leistet keine Rechtsberatung. Die Weitergabe und Verlinkung des Commons Deeds führt zu keinem Mandatsverhältnis.

Quelle: http://creativecommons.org/licenses/by-nc-nd/2.5/ch/ Datum: 3.4.2009

BIOZENTRUM
Universität Basel
The Center for
Molecular Life Sciences

For clarification purposes, the figure numbering of Chapter 6 has been adapted to suit this document.

This work has been funded by the Werner Siemens Foundation (Zug, Switzerland) and by the Human Frontier Science Programme (HFSP).

"Ufundza ute uyakufa."

(You learn until you die.)

Swazi proverb

1. Table of Contents

2. Summary

In yeast, the exomer complex – consisting of Chs5p and the ChAPs family – mediates the exit of a subset of cargoes from the trans-Golgi network via secretory vesicles. The best-characterized protein of this pathway is Chs3p, which localizes to the bud neck in a cell cycle-dependent manner. This work aimed to create a better understanding of the role of exomer in cargo export to the plasma membrane.

In a candidate-based screen, we found that most of the factors required for correct delivery of Chs3p to the plasma membrane also affected exomer-independent cargoes such as Hxt2p or Pma1p. However, a *SRO7* deletion specifically impaired exocytosis of Chs3p-containing vesicles. Moreover, in *Δsro7* as well as *Δypt31,* bud neck localization of Chs3p was particularly affected in large- or small-budded cells, respectively. These findings suggest that traffic to, as well as endocytosis from the plasma membrane, is regulated differently according to the cell cycle stage.

In an attempt to gain a better understanding of how exomer components associate with each other and recognize cargoes, we found that the ChAPs contain five essential tetratricopeptide repeats (TPRs). These repeats are interchangeable between the ChAPs and form a conserved structural backbone. TPR1-4 forms a binding site for Chs5p, while TPR5 may have a more structural role in exomer complex assembly. Surprisingly, using domain-switch chimeras, we found that the cargo specificity of the ChAPs is not determined by a single domain, but rather by large stretches distributed throughout their sequence. Unlike COPI, COPII or clathrin/AP coats, exomer therefore appears to employ an extensive, three-dimensional surface for cargo recognition.

These findings opened up the possibility that exomer-dependent cargoes may be sorted into different secretory vesicles than exomer-independent cargoes. We therefore sought to establish a protocol for differential vesicle immunoprecipitation, which would also allow us to characterize the cargo content of individual vesicle populations. Unfortunately, contaminating endosomes in the vesicle preparation rendered our experiments inconclusive. In parallel, we tested mass spectrometry on purified plasma membranes as an alternative strategy to identifying novel exomer-dependent cargoes. However, this approach turned out to be not ideally suited, as judged by the amount of time and resources required for optimization. We might therefore have to turn to new technologies – or define more suitable methods – in order to be able to characterize vesicle sub-populations.

Introduction

3. Introduction

A hallmark of eukaryotic cells is their compartmentalization into different organelles. These provide reaction spaces that are separate from the cytoplasm and include the nucleus, the endoplasmic reticulum (ER), the Golgi apparatus, endosomes, lysosomes, mitochondria and peroxisomes. Each of these organelles is limited by one or two lipid bilayers and harbors a characteristic repertoire of proteins, lipids, ions and other chemical compounds, which marks its identity and allows it to fulfill its functions. At the same time, this complexity requires mechanisms to ensure the correct sub-cellular localization of the different classes of molecules.

The processes governing the traffic of proteins within the cell has received great attention in recent decades. Budding yeast expresses about 5,000 proteins at a given time, about two thirds of which are synthesized by free ribosomes in the cytoplasm. Most of them remain cytoplasmic, while some undergo post-translational import into e.g. the nucleus, peroxisomes and mitochondria. Import into organelles is enabled by targeting sequences and allows a set of proteins to cross the lipid membrane (or double membrane), while others are prevented from entering the organelle. On the other hand, about one third of proteins are synthesized by ribosomes on the surface of the rough endoplasmic reticulum. This process is controlled by an ER signal sequence, which in turn is recognized by a signal recognition particle (SRP) that directs the nascent ribosome to the ER surface. Proteins are then co-translationally inserted into the ER by the Sec61 translocon complex and either enter the lumen of the ER, or they remain in the ER membrane. In yeast and bacteria, proteins can also be inserted into the ER post-translationally (Rapoport, 2007).

3.1. The secretory pathway

The ER is the entry point of the secretory pathway, from where material is transported to the Golgi apparatus, the endosomal system, the lysosome/vacuole and the plasma membrane (PM). The flow of proteins between these organelles is mediated by means of vesicular intermediates. These are formed by bending of the lipid bilayer, inclusion of cargo into the forming vesicle, formation of a bud, and scission. Various vesicle coats have been described to date (Fig. 3.1), whose function it is to mediate both membrane deformation and cargo recruitment. In order to prevent homogenization of organelles, concentration of cargoes into nascent vesicles has to be specific, so that some proteins are transported to the next organelle while others are retained. Furthermore, it has been demonstrated that lipid sorting also occurs at the stage of vesicle formation (Klemm *et al.*, 2009). Eventually, a vesicle fuses with its target membrane, thus releasing transmembrane proteins into the

membrane and soluble proteins into the lumen. If the acceptor membrane is the plasma membrane, soluble protein become released into the extracellular space.

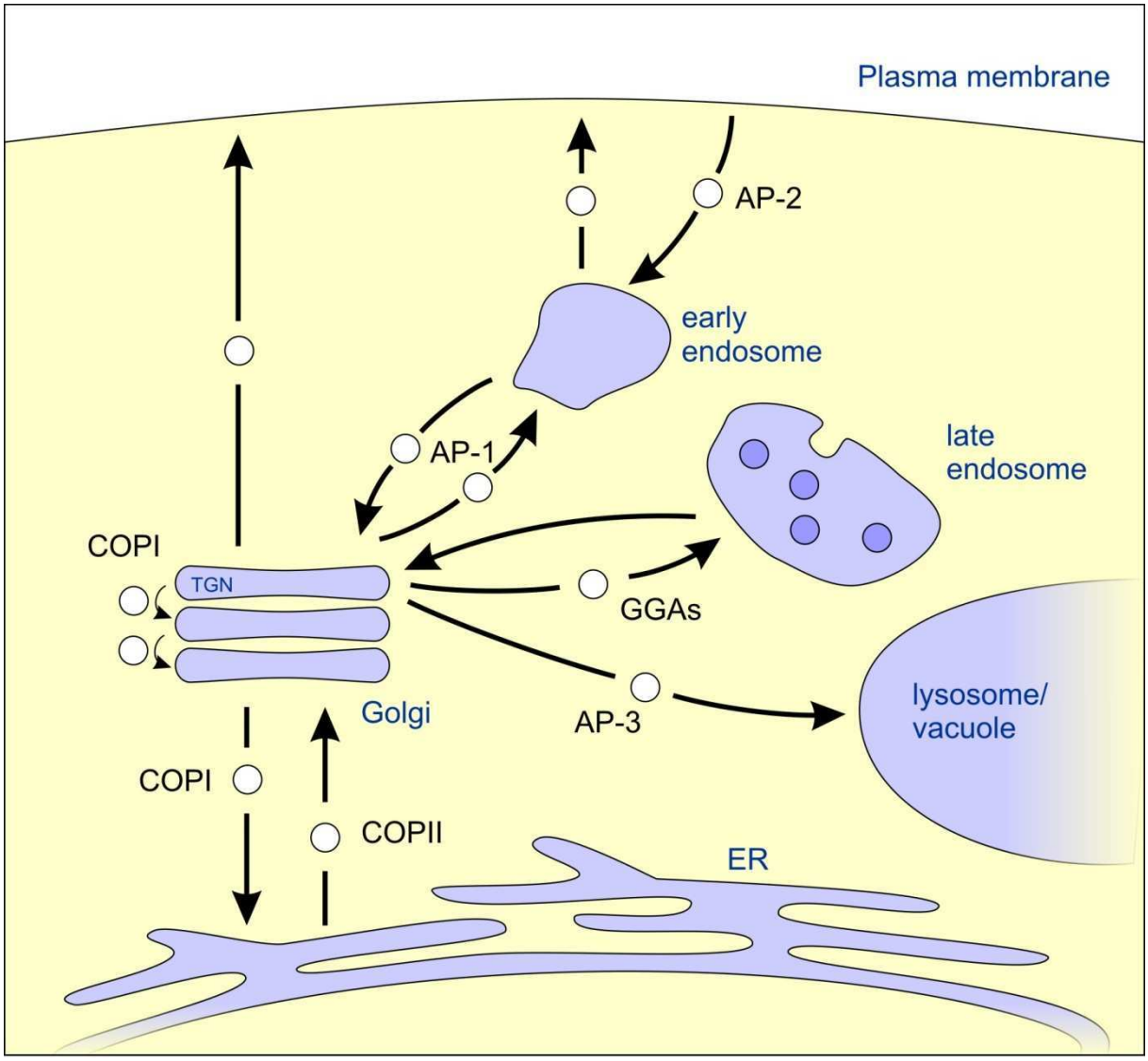

Fig. 3.1 Vesicular transport steps of the secretory pathway. The flow of proteins (and lipids) between the endoplasmic reticulum (ER), Golgi apparatus, endosomes, vacuole and plasma membrane is mediated by transport vesicles, whose coats are indicated: COPII is involved in anterograde traffic from the ER to the Golgi, while COPI vesicles act in retrograde cargo transport within the Golgi and from the Golgi to the ER. Clathrin-coated vesicles with different adaptor proteins (APs) act in post-Golgi sorting: AP-1 mediates traffic between the trans-Golgi network (TGN) and early endosomes, GGAs transport cargo to late endosomes, and AP-3 vesicles travel from the Golgi to the vacuole. Cargo retrieval from endosomes is also mediated by the retromer complex, which is not a "classical" coat and does not form spherical vesicles. The coats for the two classes of secretory vesicles from the TGN and endosomes are unknown.

3.2. The Golgi apparatus

The flow of proteins through the secretory pathway allows them to become chemically modified, e.g. by disulfide bridge formation in the ER, or by glycosylation. The latter takes place in the ER (N-linked glycosylation), or in both the ER and Golgi (O-linked glycosylation), where different glycosyltransferases act in specific stacks of the Golgi apparatus. Glycosylation not only serves as a quality control mechanism in protein folding, but can also act as a surface delivery determinant (Scheiffele *et al.*, 1995; Proszynski *et al.*, 2004). Various models have been proposed how transport through the Golgi apparatus might work. The most widely accepted idea is that Golgi cisternae undergo maturation: In this scenario, cargo would enter at the *cis*-side and progress through the Golgi stack as the cisterna matures (Pelham, 2001; Nakano and Luini, 2010). For maturation to occur, the environment within the cisternae must gradually change over time, so that resident enzymes are thought to undergo retrograde transport via COPI vesicles. Strong evidence for this comes from studies in yeast, where maturation of Golgi cisternae from *cis* to *trans* has been followed by live imaging (Losev *et al.*, 2006; Matsuura-Tokita *et al.*, 2006). Consistent with this, some studies found peri-Golgi vesicles to contain Golgi-resident enzymes, while anterograde cargo appeared to be excluded (Love *et al.*, 1998; Martinez-Menarguez *et al.*, 2001). However, other works have challenged this view, as they showed COPI vesicles to be depleted of resident enzymes, or to contain both retrograde and anterograde cargo (Orci *et al.*, 1997; Kweon *et al.*, 2004). Moreover, diffusion-based models for intra-Golgi transport exist, as it was observed that a three-dimensionally reconstructed Golgi apparatus showed cisternal connections under high cargo load (Marsh *et al.*, 2004; Trucco *et al.*, 2004). Therefore, intra-Golgi transport is still a matter of debate and may even comprise several different mechanisms acting in parallel or under different physiological conditions.

In mammalian cells, the *trans*-side of the Golgi stack appears as a network of tubular extensions. That this so-called trans-Golgi network (TGN) is distinct from the Golgi cisternae became clear when the effect of the drug Brefeldin A (BFA) was studied: While the Golgi cisternae fused with the ER upon BFA treatment, the TGN instead fused with the endosomal system (Lippincott-Schwartz *et al.*, 1991; Wood *et al.*, 1991). Indeed, the TGN is the exit site for post-Golgi carriers which deliver cargo to endosomes, lysosomes – whose analogue in yeast is the vacuole –, or the plasma membrane. At least in mammalian cells, these carriers are heterogeneous and range from spherical vesicles to long tubules (Hirschberg *et al.*, 1998; Bard and Malhotra, 2006; De Matteis and Luini, 2008). This may reflect the role of the TGN as a branching point in the secretory pathway, from where cargoes are sorted to multiple destinations in different carriers. However, much remains to be learned about the formation of these carriers.

3.3. Endocytosis and degradation in the lysosome/vacuole

Endocytosis, allows the internalization of molecules from the cell surface and occurs continuously in all eukaryotic cells. Multiple endocytic pathways have been described that can be distinguished by their molecular requirements, the internalized cargoes and the endocytic vesicles formed (Mayor and Pagano, 2007; Kumari *et al.*, 2010). After endocytosis, cargoes are found in organelles termed endosomes, which serve as sorting stations for proteins that need to be recycled or that are destined for degradation in the vacuole. Based on their kinetics of protein and lipid uptake from the cell surface, "early" and "late" endosomes can be distinguished. Late endosomes mature from early endosomes (Rink *et al.*, 2005; Huotari and Helenius, 2011) but are morphologically different, as intra-luminal vesicles can typically be seen inside them by electron microscopy (Fig. 3.1). Hence, late endosomes are also referred to as multi-vesicular bodies (MVBs). Formation of the intra-luminal vesicles is carried out by the ESCRT complexes and occurs similarly to cytoplasmic transport vesicles, but in this case the membrane is bent away from the cytoplasm (Hanson *et al.*, 2009). Concurrently, proteins are either sorted into these vesicles for subsequent degradation, or they are excluded and recycled. When MVBs fuse with the lysosome/vacuole, the intra-luminal vesicles are released into the vacuolar lumen where they are degraded by peptidases and lipases. Interestingly, the proteins that control MVB formation have also been implicated in viral budding at the plasma membrane, a process which also requires budding away from the cytoplasm (Garrus *et al.*, 2001).

3.4. The late secretory pathway

Given the multiple routes that cargoes can take within the cell, it is no surprise that the secretory and endocytic pathway intersect: From the TGN, proteins cannot only travel directly to the plasma membrane, but also via endosomes. This creates alternative surface delivery routes, e.g. in polarized epithelial cells that display two distinct PM domains, an apical and a basolateral side. While the exocytic and endocytic pathways in these cells are quite complex, it is commonly accepted that the TGN and endosomes act as sorting stations for apical and basolateral cargoes, ensuring that each PM domain maintains its specific protein and lipid composition (Fölsch, 2008). Traffic to these domains is thought to occur in distinct membrane carriers.

Somewhat similar to this, two types of secretory vesicles have been distinguished in yeast, based on their biophysical properties, genetic requirements, and cargo (Harsay and Bretscher, 1995; Gurunathan *et al.*, 2002; Harsay and Schekman, 2002). In an key experiment, secretory vesicles were separated by density gradient centrifugation and shown to fractionate in two peaks (Harsay and Bretscher, 1995). The two vesicle vesicle types were indistinguishable by morphology but contained

different cargoes: Low-density secretory vesicles (LDSVs) transport the majority of exocytic cargoes that travel directly from the TGN to the PM, e.g. the plasma membrane ATPase Pma1p, the endoglucanase Bgl2p, the GPI-anchored protein Gas1p and chitin synthase III (Chs3p). In turn, high-density secretory vesicles (HDSVs) originate from endosomes and contain the periplasmic enzymes invertase, acid phosphatase and exoglucanase. Therefore, the HDSV pathway appears to specifically transport soluble secretory enzymes. However, it is not known whether the two pathways – in particular LDSVs – contain additional sub-populations.

Temperature-sensitive mutants of proteins involved in late steps of secretion, such as *sec6-4*, accumulate both types of secretory vesicles, demonstrating that some mechanisms of vesicle targeting and fusion are shared among HDSVs and LDSVs. Additionally, there are mutations which individually affect only one branch of exocytosis: The *cdc42-6* and *exo70-38* alleles accumulate LDSVs upon shift to the restrictive temperature, but secretion of invertase via HDSVs is unaffected (Adamo *et al.*, 2001; He *et al.*, 2007). On the other hand, mutations in yeast actin (Act1p) as well as in the actin cytoskeleton-organizing protein Sla2p affect only the secretion of invertase (Mulholland *et al.*, 1997; Gall *et al.*, 2002). These studies suggested that the factors governing secretory vesicle delivery to the PM are partially distinct for the direct route from the TGN to the PM, and for the route via endosomes. This may allow the cell to differentially regulate the secretory flow of two cargo classes, perhaps based on the cell cycle stage or in response to environmental conditions. It should be noted that the *cdc42-6* and *exo70-38* mutants accumulated vesicles preferentially in the small-budded stage, indicating that secretion may be regulated in a cell cycle-dependent manner. However, no detailed analysis has yet been presented.

Finally, many cargoes in the late yeast secretory pathway are able to travel via multiple routes. For instance, deletions of *VPS1*, *VPS4*, *PEP12* or clathrin abolish the formation of HDSVs (Gurunathan *et al.*, 2002; Harsay and Schekman, 2002). In these strains, the periplasmic enzymes which are normally secreted via HDSVs reach the cell surface via LDSVs. This indicates that these cargoes can interact with multiple sorting machineries in the same TGN compartment, enabling them to enter more than one type of vesicle. The "decision" into which vesicle they become incorporated may depend on the kinetics with which they are recognized by different cargo receptors.

Another example of cargo re-routing is Vps10p, a sorting receptor for vacuolar hydrolases. Vps10p normally cycles directly between the TGN and endosomes via clathrin-coated vesicles (Deloche *et al.*, 2001). However, upon clathrin deletion, the distribution of Vps10p is not significantly changed because it arrives at endosomes via export to the plasma membrane and subsequent endocytosis (Deloche and Schekman, 2002). In summary, while the early secretory pathway is organized in a

relatively linear fashion, the post-Golgi trafficking pathways are more complex and allow multiple possible routes.

3.5. Polarized exocytosis in yeast

Exocytosis in yeast is tightly coupled to cell polarity and to cell cycle progression: Early in the cell cycle, the primary site of secretory vesicle delivery is the daughter cell (i.e. the bud), where new proteins are deposited and membrane expansion occurs. During this phase, the bud tip is marked by key polarity proteins such Cdc42p (Madden and Snyder, 1998) (Fig. 3.2). The site of exocytosis then broadens in G2/M phase, so that isotropic growth occurs in the bud. Finally, during cytokinesis, secretory vesicles are delivered to the bud neck between mother and daughter cell (Brennwald and Rossi, 2007; Park and Bi, 2007).

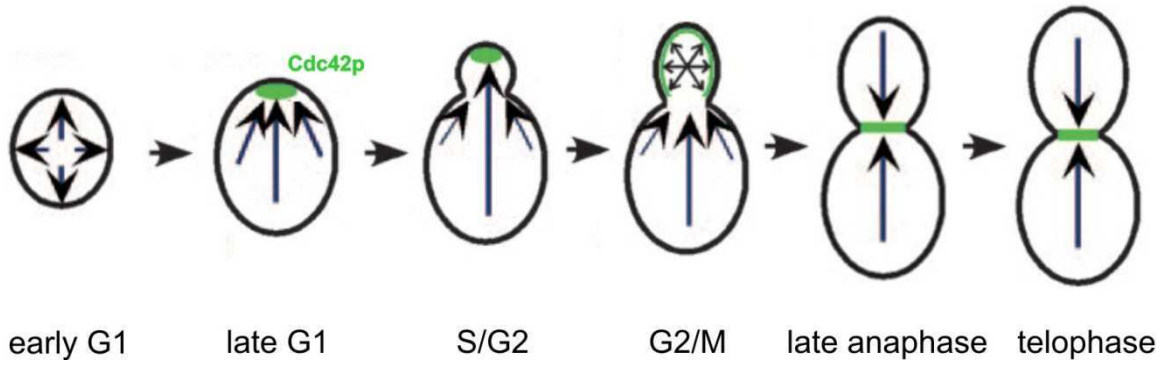

Fig. 3.2 Polarized growth and sites of vesicle delivery in *S. cerevisiae*. During the cell cycle, sites of exocytosis (indicated by arrows) correlate with the localization of polarity factors like the Rho GTPase Cdc42p. Vesicles are delivered to the incipient bud site in G1 phase and to the bud tip in S/G2. Isotropic growth occurs in G2/M, after which vesicles are delivered to the site of septum formation until the cell cycle is completed. Adapted from Park and Bi (2007).

The key players in bud neck organization are members of the septin family, soluble GTP binding proteins which are conserved from yeast to humans. Several minutes before an growing bud can be discerned by microscopy, a ring of septins is deposited at the incipient bud site. This ring is transformed into an hourglass shape during S and G2/M phase, and splits into two rings during cytokinesis (Gladfelter *et al.*, 2001). Importantly, the bud neck is not only the site of septum formation, but also contributes to the spatial organization of the cell cortex: While serving as an anchoring scaffold for a number of proteins (DeMarini *et al.*, 1997; Oh and Bi, 2011), septins have also been shown to act as diffusion barriers for transmembrane proteins and cell polarity factors (Barral *et al.*, 2000; Takizawa *et al.*, 2000; Dobbelaere and Barral, 2004). Although these functions are

reminiscent of tight junctions in epithelial cells, septins lack transmembrane domains and therefore assemble beneath the plasma membrane. How exactly septins perform the above described functions is therefore still incompletely understood. Importantly, at least in epithelial cells and neurons, septins interact with the exocyst complex and SNARE proteins, indicating they may also participate in secretory vesicle delivery (Hsu *et al.*, 1998; Beites *et al.*, 2005; Spiliotis *et al.*, 2008; Ito *et al.*, 2009). However, this role has not yet been demonstrated in yeast.

3.6. Molecular mechanisms of vesicle generation

Several landmark studies in the early 1980s opened the way to identifying numerous genes and proteins involved in vesicle budding and fusion (Novick *et al.*, 1980; Balch *et al.*, 1984). Since then, the mechanisms of vesicular transport have been studied in great detail. In particular, three types of vesicle coats have been characterized at a molecular level: COPII (involved in anterograde transport from the ER to the Golgi apparatus), COPI (retrograde transport from the Golgi to the ER as well as intra-Golgi transport), and several types of clathrin-coated vesicles which operate between the trans-Golgi network, the endosomal/lysosomal system, and the plasma membrane (Kirchhausen, 2000; Bonifacino and Glick, 2004) (Fig. 3.1). While these coats are structurally and mechanistically distinct, they share the following principles:

1. Coat recruitment is mediated by a small GTPase of the Arf/Sar1 family, which is anchored to the donor membrane by an alpha-helix in the GTP-bound (activated) state.
2. Coat proteins are recruited from the cytosol to the donor membrane where their polymerization is initiated (Fig. 3.3). They serve a dual function, firstly to induce membrane curvature, and secondly to recruit transmembrane cargoes into the nascent vesicle.
3. Vesicle formation is completed by "pinching off", i.e. by scission of the neck that connects the vesicle and the donor membrane.
4. At some point, the coat is shed to allow fusion with the acceptor membrane. It is, however, still debated when uncoating occurs during a vesicle's life cycle. Recent evidence suggests that COPI and COPII vesicles are still at least partially coated upon arrival at their respective target membranes (Cai *et al.*, 2007; Zink *et al.*, 2009; Lord *et al.*, 2011).
5. Medium-range contact between the vesicle and the acceptor membrane occurs through tethering factors. This process is mediated by members of the Rab GTPase family (Zerial and McBride, 2001).
6. Fusion requires the formation of SNARE complexes from cognate pairs of v-SNAREs (in the vesicle) and t-SNAREs (on the target membrane).

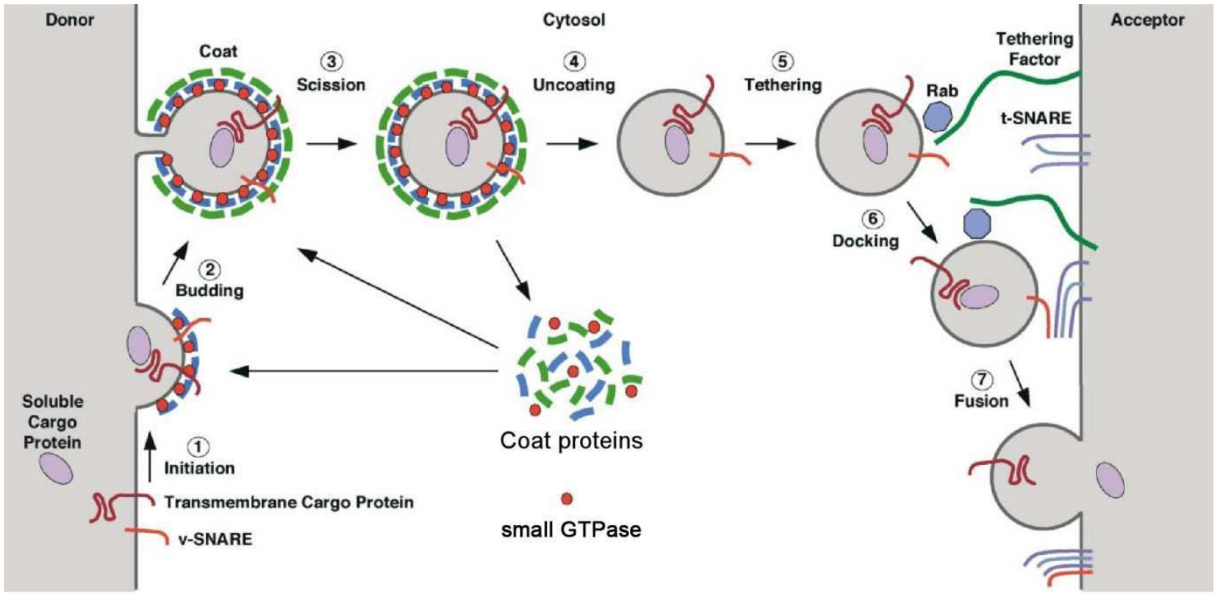

Fig. 3.3 General mechanisms of vesicle budding and fusion (adapted from Bonifacino and Glick, 2004) (1) Initiation of budding requires the activation of a small GTPase, which recruits coat proteins from the cytosol to the donor membrane. The coat deforms the membrane and binds transmembrane cargoes. Some transmembrane proteins act as receptors for soluble cargoes, which cannot be recognized by the coat itself. At this stage, v-SNAREs are also incorporated into the vesicle. (2) Budding proceeds as the coat polymerizes. Some coats are deposited in two layers. (3) Scission of the neck releases the vesicle from the donor membrane. (4) The vesicle coat is shed, thus allowing recycling of the coat proteins. (5) Organelle-specific tethering factors make contact with the vesicle; this process is mediated by Rab proteins. (6) Docking occurs when t-SNAREs of the target membrane and the v-SNARE engage in a *trans*-SNARE complex. (7) The adjacent lipid bilayers mix, and the vesicle fuses with the acceptor organelle.

In the following sections, different vesicle coats and the major players that participate in the life cycle of a vesicle are discussed in more detail.

3.7. Small GTPases of the Arf/Sar1 family

A conserved branch of the Ras superfamily of GTPases is formed by the ADP ribosylation factor (Arf) proteins and Sar1, which is closely related to Arfs and has a similar function in vesicle transport. Mammals have up to six Arf proteins (ARF1-6), which are divided into three groups, class I (ARF1-3), class II (ARF4 and ARF5), and class III (ARF6) (Kahn *et al.*, 2006). Humans appear to have lost the ARF2 gene and therefore express five Arfs, whereas yeast has three: Yeast Arf1p and Arf2p represent the class I Arfs, while yeast Arf3p is probably the homologue of mammalian ARF6. Arf1p and Arf2p are 96% identical (Stearns *et al.*, 1990; Kahn *et al.*, 2006) and are functionally interchangeable, so that only a *Δarf1/2* double deletion is lethal.

Arf1p has a well-studied role in vesicle traffic but also participates in several other cellular processes: For instance, Arf1p has been shown to act in phospholipid metabolism via activation of phospholipase D and phospholipid kinases (Brown *et al.*, 1993; Jones *et al.*, 2000), and to regulate actin cytoskeleton assembly on Golgi membranes (Fucini *et al.*, 2000). Furthermore, the repertoire of ARF functions is still expanding, as more recent studies have implicated Arf1p in mRNA transport and turnover (Trautwein *et al.*, 2004; Kilchert *et al.*, 2010; Kilchert and Spang, 2011). Lastly, the exomer complex, which is the focus of the work presented here, was identified as a novel Arf1p effector and controls the exit of specialized cargo proteins from the TGN (see section 3.14).

Arf1p and other small GTPases use guanine nucleotides as co-factors and undergo cycles of activation and inactivation, depending on whether GTP or GDP is bound (Chavrier and Goud, 1999). This nucleotide-dependent "on/off" switch correlates with the binding of the protein to a cellular membrane in the activated state (Fig. 3.4). Upon activation, which is mediated by exchange of GDP to GTP by a guanine nucleotide exchange factor (GEF), Arf1p undergoes a conformational change: A myristoylated N-terminal amphipathic helix, buried in a hydrophobic pocket in Arf1p-GDP, flips out in Arf1p-GTP and is inserted into the lipid bilayer. This altered fold also affects two other surfaces on the protein – termed switch 1 and switch 2 – which present a surface for various effector proteins (Amor *et al.*, 1994; Pasqualato *et al.*, 2002). Finally, inactivation is caused by GTP hydrolysis by the GTPase itself. As the intrinsic rate of hydrolysis is slow, GTPase activating proteins (GAPs) are required to efficiently complete the activation/deactivation cycle (Spang *et al.*, 2010).

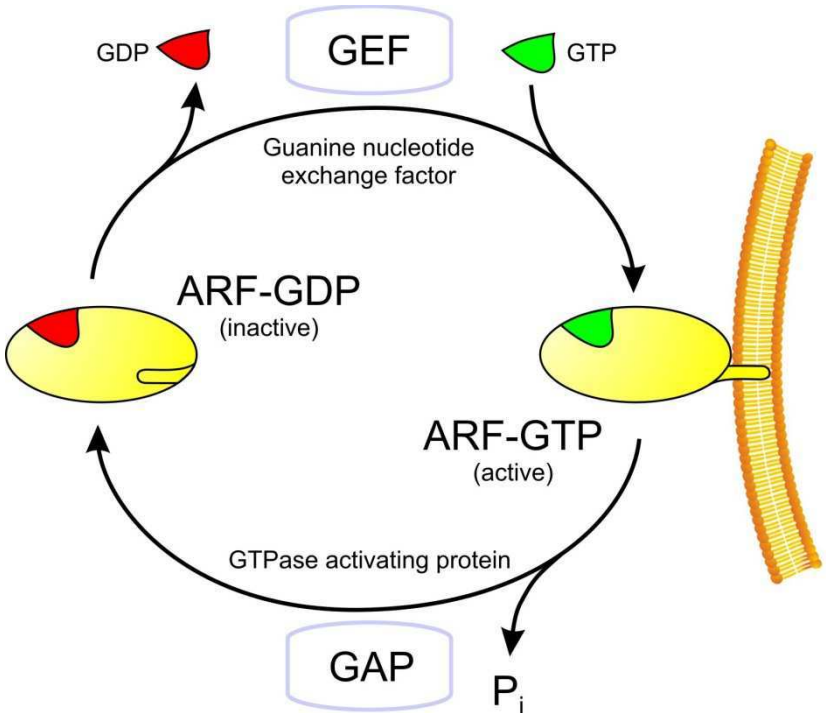

Fig. 3.4 The GTPase cycle of ARF proteins. Active (GTP-bound) ARF is tethered to the lipid bilayer by its amphipathic helix. This helix is buried in the protein in the GDP-bound (inactive) state. Transition from ARF-GDP to ARF-GTP is mediated by guanine nucleotide exchange factors (GEFs), which catalyze the exchange from GDP to GTP. GTPase-activating proteins (GAPs) stimulate the GTPase activity of ARF, causing hydrolysis of GTP to GDP and phosphate.

Vesicle coats are the most well-studied effectors of Arf/Sar1 GTPases, and the cycle of coat protein recruitment, vesicle budding and uncoating closely correlates with the GTPase cycle. The following section therefore describes the different vesicle types whose formation is controlled by Arf1p and Sar1p.

3.8. COPII

The minimal machinery for the formation of COPII vesicles, which typically have a diameter of 50 - 90 nm, consists of the small GTPase Sar1p and the coat proteins Sec23p, Sec24p, Sec13p and Sec31p (Barlowe *et al.*, 1994; Dancourt and Barlowe, 2010). Budding can be reconstituted *in vitro* using the purified proteins components and chemically defined liposomes together with GMP-PNP, a non-hydrolyzable GTP analogue (Matsuoka *et al.*, 1998). *In vivo*, the guanine nucleotide exchange factor (GEF) Sec12p is required for activation of Sar1p, which results in Sar1p recruitment to the ER membrane and subsequent recruitment of the coat (Barlowe et al., 1993; Barlowe and Schekman, 1993) (Fig. 3.5). COPII has a membrane-proximal layer consisting of Sec23p and Sec24p, and a membrane-distal layer made up of Sec13p and Sec31p. The two layers are sequentially recruited and serve different functions: All known cargo binding sites have been mapped to the Sec23p/Sec24p heterodimer (Miller *et al.*, 2003; Mossessova *et al.*, 2003; Mancias and Goldberg, 2007), which recognize multiple motifs, including di-phenylalanine, di-tyrosine, di-leucine, di-isoleucine, di-acidic or valine-based sequences (Nishimura and Balch, 1997; Nufer *et al.*, 2002; Wendeler *et al.*, 2007; Wendeler *et al.*, 2007). The Sec13p/Sec31p subcomplex is thought to have a more structural role in defining the vesicle shape (Fath *et al.*, 2007). Recent data suggest that several cage lattices of different geometry might be formed by the COPII components, thus providing the flexibility to accommodate for cargoes of varying sizes (Stagg *et al.*, 2006; reviewed in Zanetti *et al.*, 2011).

Sar1p is inactivated by Sec23p, which has an intrinsic GAP activity (Yoshihisa *et al.*, 1993). Interestingly, this GAP activity is stimulated by the Sec13p/Sec31p subunits, suggesting that proceeding polymerization of the coat might trigger its own disassembly (Antonny *et al.*, 2001). However, the presence of cargo appears to delay this process and may thus prevent premature uncoating of nascent vesicles (Forster *et al.*, 2006).

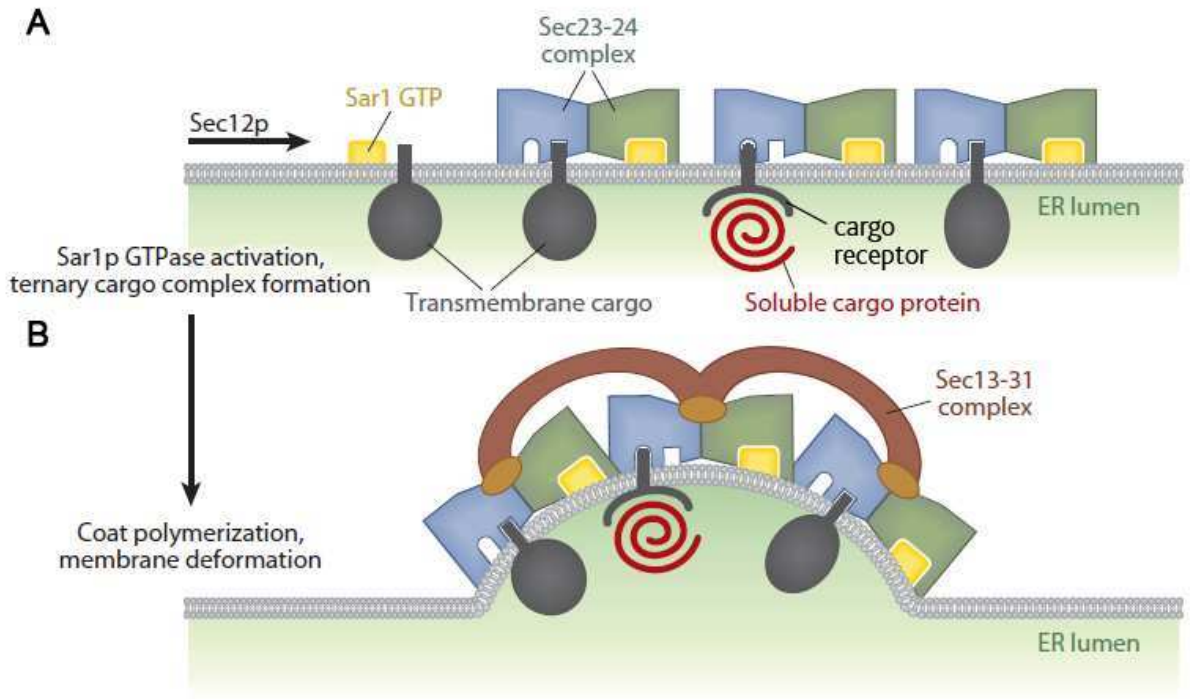

Fig. 3.5 Early steps of COPII vesicle formation (adapted from Dancourt and Barlowe, 2010). (A) Budding is initiated by the activation of the small GTPase Sar1p through the GEF Sec12p. Sar1p-GTP recruits the Sec23p/Sec24p subcomplex, which harbors several binding sites for cargoes in the ER membrane that carry specific ER export signals. Soluble luminal proteins are recruited by cargo receptors, which themselves bind to Sec23p/Sec24p. (B) The membrane-distal layer of the COPII coat consists of Sec13p and Sec31p, which assemble onto Sec23p/Sec24p. The donor membrane is deformed as the coat polymerizes, eventually giving rise to a bud which undergoes scission from the ER membrane.

3.9. COPI

COPI vesicles mediate retrograde transport, both within the Golgi apparatus and between the Golgi and the ER. Retrieval of cargoes to the ER is essential to maintain the localization of ER-resident proteins that have escaped to the Golgi, and for recycling of SNAREs after COPII vesicle fusion. The coat of COPI vesicles consists of the small GTPase Arf1p and coatomer, a heptameric complex consisting of the subunits α, β, β', γ, δ, ε and ζ (Beck *et al.*, 2009). Like the COPII coat, coatomer is recruited to the Golgi membrane by Arf1p, and the cage lattice of COPI resembles that of COPII and clathrin coats (Lee and Goldberg, 2010). However, its subunits are not deposited in subsequent layers but bind as one complex (Fig. 3.6), which polymerizes and produces vesicles of 40 – 70 nm diameter. This process has also been reconstituted *in vitro* (Spang *et al.*, 1998).

In COPI vesicle formation, Arf1p is activated by the GEFs Gea1p and Gea2p, which have overlapping functions in yeast but are not redundant (Spang *et al.*, 2001). In turn, two yeast Arf GAPs are involved retrograde transport from the Golgi to the ER: Gcs1p, the homologue of mammalian ARFGAP1, and Glo3p, corresponding to mammalian ARFGAP2/3. Glo3p and Gcs1p stimulate the GTPase activtity of

Arf1p, thus causing disassembly of the coat, similar to the action of the GAP Sec23p in the COPII coat. Interestingly, mammalian ARFGAP1 and yeast Gcs1p have an ALPS (ARFGAP1 lipid-packing sensor) domain which allows them to associate preferentially with highly curved lipid bilayers (Bigay *et al.*, 2005). Moreover, increasing curvature up-regulates the activity of ARFGAP1 (Bigay *et al.*, 2003), which may provide an explanation how Arf1p-GTP hydrolysis is coupled to progressing vesicle formation. However, other GAPs like Glo3p lack an ALPS motif, so that this mechanism cannot be applicable to Arf GAPs in general.

Two main types of signals are known to be recognized by the COPI coat: C-terminal di-lysine motifs (KKXX) are bound by the WD40 domains of the large α/β' subunits (Eugster *et al.*, 2004). In addition, arginine-based motifs are recognized by β- and δ-COP (Michelsen *et al.*, 2007). Both of these signals mediate efficient cargo retrieval to the ER.

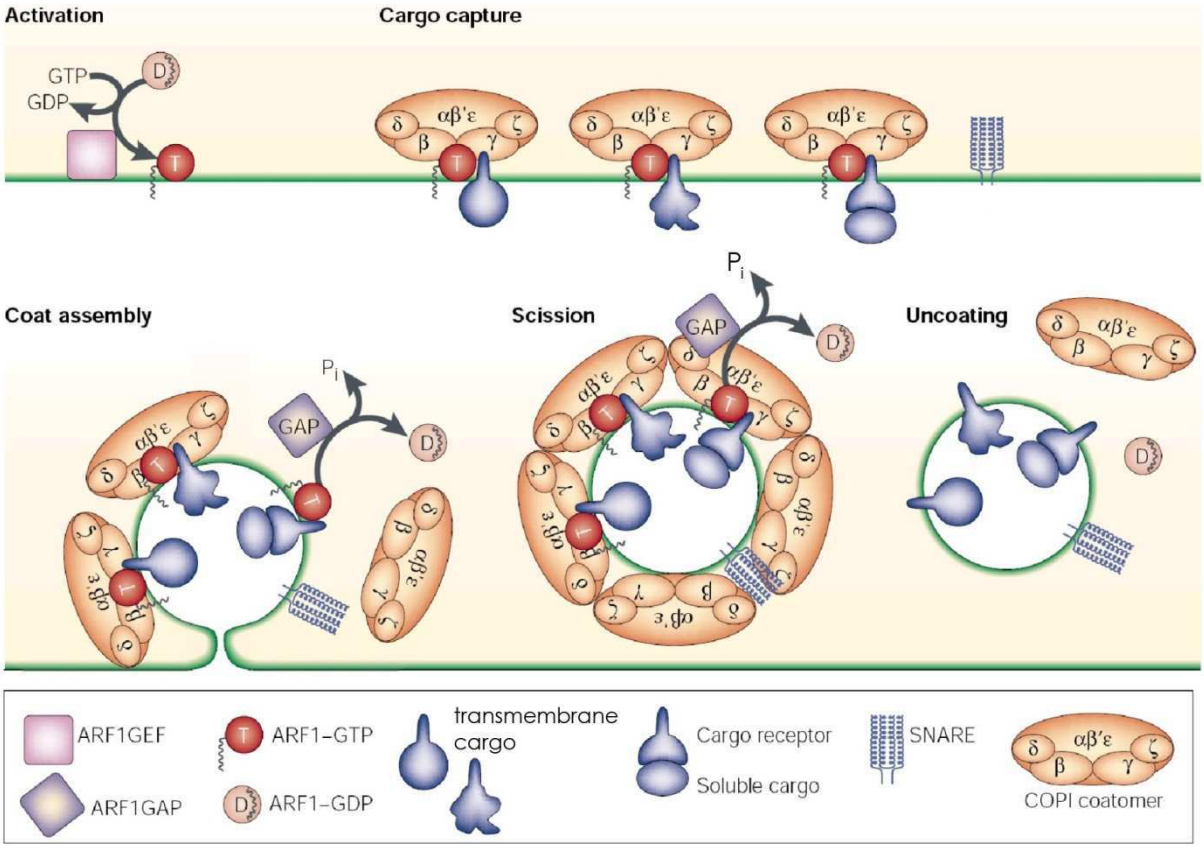

Fig. 3.6 Formation of COPI vesicles. Coat formation requires the activation of Arf1p and capture of coatomer, cargo and SNAREs. Cargoes lacking a transmembrane domain are bound by cargo receptors. As for COPII, coat polymerization drives vesicle formation. Arf1p-GTP is inactivated by a GAP, leading to disassembly of the coat (adapted from Kirchhausen, 2000).

3.10. Clathrin/AP coats

Clathrin-coated vesicles (CCVs) are more heterogeneous than COPI or COPII, as they act in multiple pathways and employ several adaptor protein (AP) complexes. These include the heterotetramers AP-1, AP-2, AP3 and AP4, as well as the monomeric GGA (Golgi-localized, gamma-ear-containing, Arf-binding) proteins (Nakatsu and Ohno, 2003; Robinson, 2004). AP-1-4 are each composed of four subunits, a small one (σ), a medium one (μ) and two large subunits (γ/β1, α/β2, δ/β3 and ε/β4). The variable large subunits (γ, α, δ, ε) mediate binding to the target membrane, while at least β1-3 have a "clathrin box" motif that mediates clathrin binding. Cargo binding sites for YXXΦ and di-leucine-based motifs have been identified in the γσ heterodimer and in the μ subunit (Owen and Evans, 1998; Janvier *et al.*, 2003; Jackson *et al.*, 2010). While the GGA proteins are very different from APs, they show significant similarity to the "ear domain" of the γ subunit (Collins *et al.*, 2003).

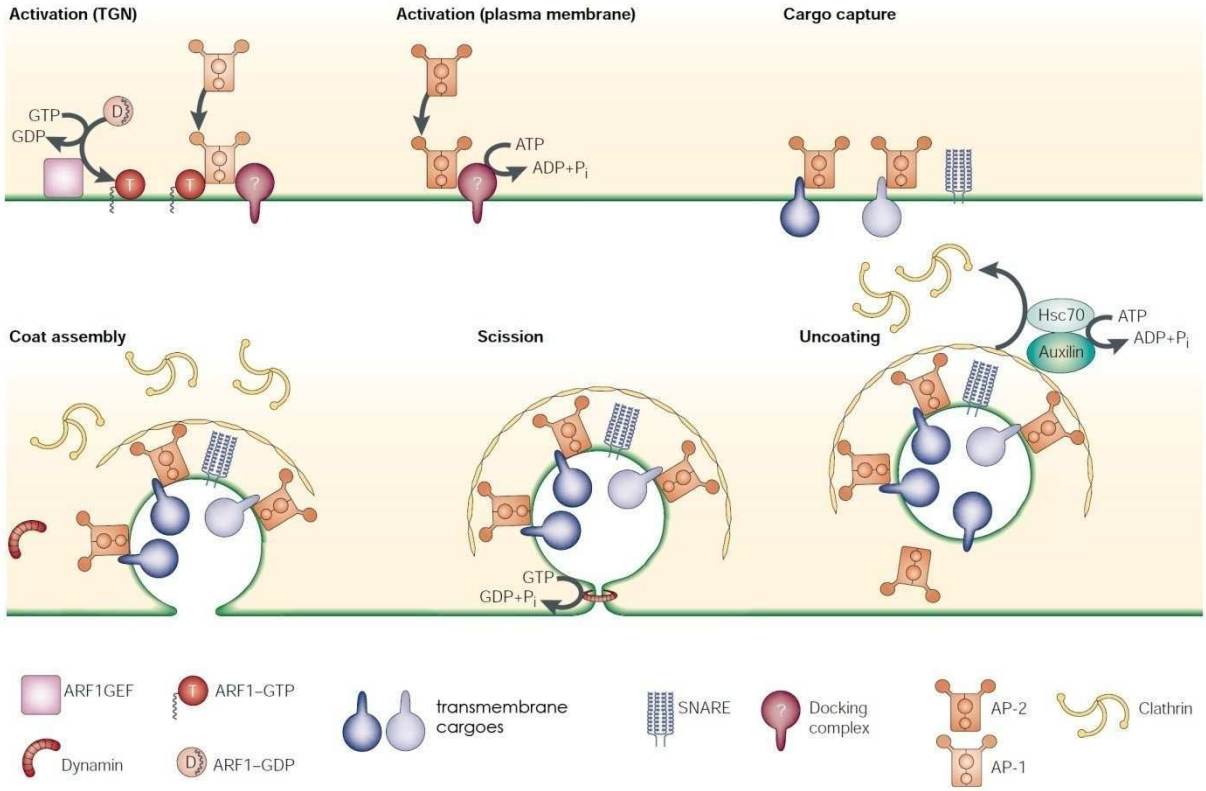

Fig. 3.7 Formation of clathrin-coated vesicles (CCVs) (adapted from Kirchhausen, 2000). Most clathrin coats depend on activated Arf1p; additionally, a cytosolic docking factor is thought to facilitate the initial association of AP-1 with the membrane. Recruitment of AP-2 is independent of Arf1p. Upon polymerization of the coat, scission of the vesicle neck is mediated by the GTPase dynamin (although in yeast the role of dynamin is less clear). Another distinguishing feature of CCVs is that uncoating is actively promoted by HSC70 and Auxilin.

Like COPI, AP-1, AP3, AP4 and GGA coats are all recruited to the membrane by activated Arf1p (Fig. 3.7). Moreover, *in vitro* experiments suggest that a cytosolic docking factor facilitates AP-1 recruitment to the membrane (Meyer *et al.*, 2005). Clathrin itself, which forms the outer layer of the coat, assembles into a characteristic triskelion structure that has the ability to polymerize into a spherical lattice (Fotin *et al.*, 2004; Traub, 2005). As clathrin itself has no membrane-binding activity, it assembles onto an inner layer of APs, which bridge the interaction of clathrin with transmembrane cargo proteins. However, this only applies to AP-1 and AP-2 coats: AP3 and AP4 do not appear to be present in isolated CCVs and may therefore function independently of clathrin (Dell'Angelica *et al.*, 1997; Hirst *et al.*, 1999).

CCVs operate in several transport pathways: AP-2 is required for clathrin-dependent endocytosis, AP3 mediates traffic from the TGN to the lysosome/vacuole, and AP-1 participates in the transport of proteins between the TGN and early endosomes, although there is conflicting data concerning the directionality of the transport (Meyer *et al.*, 2000; Valdivia *et al.*, 2002; Foote and Nothwehr, 2006; Canuel *et al.*, 2008). GGAs have a function in TGN-to-endosome transport, probably independently of AP-1 (Hirst *et al.*, 2009). Little is known about AP-4, which is only found in some organisms, including mammals and plants but not yeast, and which may have a role in cargo exit from the TGN (Dell'Angelica *et al.*, 1999; Boehm *et al.*, 2001; Simmen *et al.*, 2002). The diverse transport routes in which CCVs operate require the targeting of APs to specific membranes. However, this specificity cannot be achieved through Arf1p which is relatively promiscuous and engages in multiple CCV pathways. Some specificity may therefore come from phosphoinositides, which are markers of membrane identity and to which AP-1 and AP-2 have been shown to bind. Particularly AP-2, which functions independently of Arf1p, seems to rely at least partially on the PM-localized lipid phosphatidylinositol-(4,5)-bisphosphate for correct membrane recruitment (Gaidarov and Keen, 1999; Rohde *et al.*, 2002).

A recent study reported the identification of a fifth clathrin adaptor, AP-5 (Hirst *et al.*, 2011). AP-5 does not bind clathrin and is insensitive to Brefeldin A, suggesting that it functions independently of Arf1p, like AP-2. AP-5 appears to localize to late endosomes and is required for the correct trafficking of the mannose-6-phosphate receptor. Like some of the other APs, AP-5 has been lost from some organisms, including fungi.

3.11. Retromer

Clathrin/AP-1-coated vesicles are not the only pathway involved in recycling cargoes from endosomes to the TGN: A second key player is the so-called retromer complex, which is conserved from yeast to mammals (Bonifacino and Rojas, 2006). Retromer consists of five core subunits, Vps5p, Vps17p, Vps26p, Vps29p and Vps35p. Vps26p, Vps29p and Vps35p are thought to form a subcomplex for cargo interaction, while Vps5p and Vps17p are mostly responsible for membrane deformation and carrier generation (McGough and Cullen, 2011). The latter two proteins belong to the family of sorting nexins (SNX) and contain a BAR (Bin/amphiphysin/Rvs) domain that allows them to bind to curved membranes with high affinity (Carlton *et al.*, 2004). Additionally, some sorting nexins have a PX (Phox homology) domain, which recognizes phosphoinositides on endosomal membranes (Pylypenko *et al.*, 2007). A considerable number of additional sorting nexins have been identified in mammals and yeast, which may allow retromer to act on multiple membranes (e.g. both early and late endosomes). While the cargo binding and membrane deformation activity of retromer is reminiscent of a protein coat, it has not been observed as an electron-dense structure around spherical vesicles, but rather seems to coat membrane tubules (Arighi *et al.*, 2004; Carlton *et al.*, 2004). The way in which retromer generates transport carriers therefore appears to be distinct from COPI/II and clathrin-coated vesicles.

3.12. Active vesicle transport and tethering

The movement of vesicles to their respective target membranes can be facilitated by active transport. The yeast actin cytoskeleton is a good example for this, as it has a vital function in the transport of secretory vesicles. Early in the cell cycle, actin filament nucleation by formins occurs mostly at the growing bud tip, so that so-called actin cables emanate from the daughter cell and extend into the mother. Vesicles are transported along these cables by the type V myosin Myo2p, at a speed of ~3 µm/s (Schott *et al.*, 2002). The moving Myo2p binds to the vesicle-associated Rab proteins Sec4p and Ypt31p/32p (Santiago-Tirado *et al.*, 2011), ensuring that secretory vesicles efficiently reach the bud tip, where they rapidly fuse with the PM. During later stages of the cell cycle, when key polarity factors such as Cdc42p and the formin Bni1p change their localisation (Fig. 3.2), actin cables are also re-oriented, so that vesicle delivery occurs isotropically during G2/M, and at the bud neck during late anaphase and cytokinesis (reviewed in Park and Bi, 2007).

Vesicle tethering, which mediates the initial contact between vesicles and the target membrane, is a crucial step that precedes fusion. Various tethering complexes have been identified on all organelles of the secretory pathway, such as the Dsl complex (ER), the TRAPPI/II, COG and GARP complexes

(Golgi), the exocyst (PM), as well as the CORVET and HOPS complexes (endosome and vacuole, respectively) (Cai *et al.*, 2007). Except for the TRAPP complexes, all tethers are effectors of Rab GTPases, of which there are 11 in yeast. Mammals, in contrast, have more than 60 Rab GTPases, likely reflecting a larger complexity of their intracellular trafficking network.

The exocyst complex, consisting of Sec3p, Sec5p, Sec6p Sec8p, Sec10p, Sec15p, Exo70p and Exo84p, is essential for tethering at the PM, and conditional mutants in exocyst components cause an accumulation of secretory vesicles. Sec3p and Exo70p can directly interact with PM phospholipids, while the other components are thought to arrive at the PM by association with the vesicle (He and Guo, 2009). The function of the exocyst is controlled by the Rab GTPase Sec4p, its GEF, Sec2p, and two GAPs, Msb3p and Msb4p (Park and Bi, 2007).

3.13. SNAREs

The fusion of a vesicle with the correct target membrane is ensured by SNARE (soluble NSF attachment protein receptor) proteins. They provide the energy required for overcoming the repulsive forces of the two adjacent membranes and allow fusion to occur (reviewed in Malsam *et al.*, 2008). At the same time, SNAREs provide the cell with a molecular code to match a transport vesicle with its correct target organelle. SNAREs are type II transmembrane proteins with a cytoplasmic domain that contains a helical SNARE motif and an N-terminus which is variable between individual family members. Some SNAREs like SNAP-25 lack a transmembrane domain but instead have an acyl moiety which anchors them to the membrane (Vogel and Roche, 1999). Two classes of so-called v- and t-SNAREs exist (v and t for "vesicle" and "target membrane"). For a particular fusion event, three t-SNAREs must pair with a cognate v-SNARE on an opposing membrane, leading to formation of a four-helix bundle (Sutton *et al.*, 1998). The "zippering up" of the SNARE complex brings the membranes into close proximity and drives membrane fusion (Weber *et al.*, 1998), although it is still debated whether the energy provided by this is sufficient for fusion *in vivo*. *In vitro* studies of 300 different SNARE combinations identified only 9 which were fusogenic, indicating that SNAREs are key players in providing specificity to vesicle delivery within the cell (McNew *et al.*, 2000; Parlati *et al.*, 2002).

Since every single vesicle must contain a v-SNARE, this leads to the question: How is the loading of SNAREs co-ordinated with vesicle formation? To date, several different mechanisms have been identified: As one example, the ER-Golgi v-SNAREs Bet1p and Bos1p bind directly to the Sar1p GTPase (Springer and Schekman, 1998). Together with the Sec23p/Sec24p dimer, this ternary "priming complex" then nucleates COPII vesicle budding (Springer *et al.*, 1999). As a second example,

the yeast ARFGAPs Glo3p and Gcs1p are able to induce a conformational change in a number of SNARE proteins, including the ER-Golgi v-SNAREs Bet1p, Bos1p and Sec22p. This altered conformation allows them to bind to Arf1p (Rein *et al.*, 2002; Robinson *et al.*, 2006; Schindler and Spang, 2007). The coatomer complex is then thought to assemble onto the Arf1p-SNARE-complex, thus ensuring that the SNAREs are included into COPI vesicles. A third mechanism found for some clathrin-coated vesicles depends on epsinR, a cargo-specific clathrin adaptor, which specifically binds and recruits the SNARE Vti1b into CCVs. The binding site on epsinR does not overlap with that for other cargoes, which probably ensures that SNARE loading cannot be outcompeted by high cargo load (Miller *et al.*, 2007).

In summary, the loading of SNARE proteins is not based on one, but on diverse strategies, depending on the vesicle type. However, a common theme appears to be that recognition of v-SNAREs is carried out by separate mechanisms from other classes of cargoes, so that no competition can occur.

3.14. The exomer complex

In recent years, the so-called exomer complex has emerged to be essential for the sorting of a subset of cargoes into secretory vesicles at the yeast TGN. The exomer components are almost exclusively found in the fungal kingdom, suggesting that fungi may have a separate route for exporting specialized cargoes to the plasma membrane. However, the principles how cargoes are recognized and sorted by the exomer complex could serve as a valuable model system for analogous processes in higher organisms.

3.14.1. Genetic and functional characteristics

Historically, the first components of the pathway were identified in the context of chitin synthesis: Deposition of chitin, a major constituent of the yeast cell wall, required the genes *CHS1-6* (Bulawa *et al.*, 1986; Silverman *et al.*, 1988; Cabib *et al.*, 1989; Bulawa, 1992; Santos *et al.*, 1997; Trilla *et al.*, 1997). Chs1p, Chs2p and Chs3p were subsequently shown to be the catalytically active chitin synthases, while Chs4p, Chs5p and Chs6p were involved in regulating the activity and transport of Chs3p, to date the best-studied cargo of this pathway. In G1/S phase and during mitosis (i.e. in small- and large-budded cells), Chs3p localizes to the bud neck where it synthesizes a chitin ring that makes up ~90% of the total cell wall chitin (Bulawa, 1993; Chuang and Schekman, 1996; Ziman *et al.*, 1996). In G2, Chs3p is present in internal membranes (sometimes called "chitosomes"), representing both endosomes and the TGN (Valdivia *et al.*, 2002). Activation and anchoring of Chs3p at the bud neck requires Chs4p (Reyes *et al.*, 2007), while recycling of Chs3p from the PM is mediated via endocytosis

and retrieval from early endosomes to the TGN by an AP-1-dependent pathway (Valdivia *et al.*, 2002).

In turn, Chs5p and Chs6p are essential for Chs3p export from the Golgi apparatus, as *Δchs5* or *Δchs6* mutants accumulate Chs3p in the TGN, where it prevented from entering secretory vesicles (Santos and Snyder, 1997; Ziman *et al.*, 1998; Valdivia *et al.*, 2002). Chs6p has three paralogues in *S. cerevisiae*: Bud7p (a protein involved in bud site selection), Bch1p and Bch2p ("BCH" for Bud7p-Chs6p-homologue). A functional connection between them could be drawn when Bch1p and Chs5p were identified as novel biochemical interactors of Arf1p by a differential affinity chromatography approach (Trautwein *et al.*, 2004; Trautwein *et al.*, 2006). Since all four paralogues were found to bind both Arf1p and Chs5p, they were termed "ChAPs" for "Chs5p-Arf1p-binding proteins". The ChAPs also co-precipitate with each other, but only in the presence of Chs5p, which is therefore thought to mediate the interaction between the ChAPs (Sanchatjate and Schekman, 2006; Trautwein *et al.*, 2006). Together, the set of Chs5p and the ChAPs were later termed "exomer complex" (Wang *et al.*, 2006).

Deletions of Chs5p and the ChAPs are viable, but single ChAP deletions show distinct phenotypes: As described above, *Δchs6* strains are chitin synthesis-deficient. Diploid *Δbud7* cells show a random budding pattern (while wild-type diploid yeast cells bud from alternating poles) (Zahner *et al.*, 1996), and cells carrying a *BCH1* deletion are sensitive to ammonium (Trautwein *et al.*, 2006). No specific phenotype has yet been described for cells lacking *BCH2*. It is therefore thought that not only Chs3p, but also other specialized cargoes such as budding landmarks or ion transporters depend on the exomer complex for exiting the TGN, so that in ChAP deletions these cargoes are retained and specific cellular phenotypes are observed. Moreover, some ChAPs appear to be partially redundant, as the trafficking defect for Chs3p is not only observed in *Δchs6* cells, but also in a *Δbch1Δbud7* double deletion (Trautwein *et al.*, 2006).

Only two exomer-dependent cargoes have been described in the literature: Chs3p and Fus1p, a protein involved in cell fusion during mating (Santos and Snyder, 2003; Barfield *et al.*, 2009). A third candidate, Crh2p, may also depend on Chs5p for correct localization, but it is currently not clear whether the observed mis-localization in *Δchs5* is really a surface delivery defect, or re-routing to the vacuole by indirect effects (Rodriguez-Pena *et al.*, 2002). The cargoes responsible for the *Δbud7* and *Δbch1* phenotypes have not yet been identified. Importantly, all ChAP-related phenotypes are collectively found in a *Δchs5* strain (Trautwein *et al.*, 2006). This demonstrates that Chs5p is functionally upstream of the ChAPs, and that the cargoes affected by ChAP deletions are also TGN-retained in *Δchs5* cells. Since only a specific subset of cargoes depends on this pathway, it suggests

that exomer may be either a vesicle coat or a sorting complex at the TGN and might constitute a third route to the cell surface, in addition to the known high- and low-density secretory vesicles.

3.14.2. Biochemical characteristics and membrane association

Chs5p is a 761 aa protein with a calculated molecular weight of 74 kDa. The domain structure of Chs5p consists of a fibronectin 3 (FN3) domain and a BRCT domain at the N-terminus; a region corresponding to these two domains interacted with Chs6p in a yeast two-hybrid assay (Wang *et al.*, 2006). On the other hand, the C-terminal half, partly composed of heptad repeats with the consensus sequence $(NKPFEDS)_n$, is predicted to be intrinsically disordered (unpublished data). This domain has been shown to bind anionic lipids but is, surprisingly, dispensable for function *in vivo*, while only the FN3 and BRCT domains are essential (Wang *et al.*, 2006; Martin-Garcia *et al.*, 2010). Less is known about the domain structure of the ChAPs: The four *S. cerevisiae* paralogues are between 82 and 88 kDa in size and show an overall sequence identity of ~25%. While it is known that the C-terminal 13 amino acids of the ChAPs are required for association with Chs5p (Trautwein *et al.*, 2006), their domain structure has not yet been analyzed in detail.

Chs5p and the ChAPs require Arf1p and its GEF Sec7p *in vivo* for recruitment from the cytoplasm to the TGN (Wang *et al.*, 2006). The ChAPs also depend on Chs5p for TGN recruitment, although their degree of membrane localization at steady state appears variable, with Bch1p being the most cytoplasmic and Bch2p the most Golgi-associated ChAP (Trautwein *et al.*, 2006). *In vitro*, activated Arf1p can also recruit the exomer components to liposomes, where they are able to form defined, spiked structures covering the liposome surface (Trautwein *et al.*, 2006; Wang *et al.*, 2006). However, under the conditions tested, neither budding of vesicles nor formation of coated buds was observed. This could mean either that exomer is not a coat complex, i.e. it may sort cargo into vesicles without carrying out the budding process itself. Alternatively, Chs5p and the ChAPs could be part of a coat and form, for instance, only the inner, cargo-binding layer.

Exomer has been isolated from yeast cell extracts, and a molecular ratio of 5:4:1:1:1 (Chs5p:Bch1p:Bud7p:Chs6p:Bch2p) was determined (Sanchatjate and Schekman, 2006). However, reconstitution of exomer from recombinant proteins resulted in a complex with a different stoichiometry (Wang *et al.*, 2006). In addition, immunoprecipitation experiments showed that the ratio of the ChAPs varied, depending on the paralogue against which the antibody was directed (Trautwein *et al.*, 2006). It therefore seems likely that the ChAPs can assemble with Chs5p into complexes of varying stoichiometries. Moreover, Chs5p appears to be able to oligomerize *in vitro* (Sanchatjate and Schekman, 2006) and may therefore provide a structural scaffold for association with different ChAP family members, perhaps depending the cargo to be transported.

3.14.3. Cargo recognition

Because specific phenotypes are associated with individual ChAP deletions, and since the efficient export of Chs3p and Fus1p specifically requires one or several ChAPs, there is little doubt that the ChAPs have a central role in cargo recognition. Although a direct interaction has not yet been demonstrated, the ChAPs can be crosslinked to Chs3p (Sanchatjate and Schekman, 2006; Trautwein *et al.*, 2006). Furthermore, an IXTPK motif has been discovered in the cytoplasmic tail of Fus1p. This motif is necessary for exomer binding and export of Fus1p to the cell surface (Barfield *et al.*, 2009). However, the IXTPK sequence only functions in a restricted context and is not found in Chs3p, which raises the question whether exomer-dependent cargoes share any common sorting motif. Furthermore, while the ChAPs are similar to each other in their primary structure, they apparently recognize different cargoes. How exactly this is achieved, and what conveys cargo specificity to the ChAPs, has not been investigated.

4. Aim of this study

Recent work has identified the TGN-associated exomer complex as an essential mediator of Golgi export for a subset of cargoes. These cargoes are thought to be recognized by the ChAPs protein family. However, only few proteins are currently known to travel via this pathway: an example is Chs3p, which shows a cell cycle-dependent bud neck localization. Additionally, at least early in the cell cycle, Chs3p localization at the bud neck does not match with the localization of the exocyst, which marks the bud tip as the general site of exocytosis. This raised several questions: Is the machinery required for plasma membrane delivery of exomer-dependent cargoes generally different from that of exomer-independent cargoes? Or are they similar, and the requirement for exomer is the only distinguishing factor? Are the determinants for plasma membrane delivery of Chs3p different early and late in the cell cycle?

Moreover, little is known about how specific cargo recognition is achieved by the ChAPs. Finally, we do not know whether exomer-dependent and –independent cargoes travel in the same type of secretory vesicle or in separate carriers.

The goals of this study were therefore:

1. To perform a screen for determinants of Chs3p transport to the plasma membrane, compared to exomer-independent cargoes. At the same time, to investigate whether factors exist that specifically affect Chs3p surface localization in G1/S phase or during M phase.
2. To investigate the domain structure of the ChAPs, assign specific functions to motifs or domains, and identify the region(s) conveying cargo specificity to the ChAPs.
3. To establish a protocol that would allow the differential precipitation of secretory vesicles containing Chs3p or exomer-independent cargoes. By the same approach, we aimed to characterize these vesicles and identify additional cargoes which are exported via the exomer pathway.

Chapter 5

Cell cycle-dependent traffic to the plasma membrane

5. Transport to the plasma membrane is regulated differently early and late in the cell cycle in *Saccharomyces cerevisiae*

The following manuscript was submitted to the *Journal of Cell Science* and was accepted on November 13, 2010. The authors' contributions are outlined below.

Bettina Zanolari performed the screen on the localization of Chs3p and Hxt2p, and constructed most of the mutants including *sec6-4* and *sec3-2*. She also took the time-lapse images of Chs3p and Sec8p over the cell cycle.

Uli Rockenbauch assessed the localization of Itr1p, and the localization of Chs3p in additional exocyst mutants (*sec5-24*, *sec10-2*, *exo84-117*). He provided critical comments on the manuscript.

Mark Trautwein supervised Bettina Zanolari's work and contributed to the FRAP experiments. He also performed the *GAL1-SEC6* shutoff experiments and quantified the effect of *ypt31/ypt32* mutants on Chs3p bud neck localization.

Lorena Clay performed the FRAP experiments.

Yes Barral provided critical comments on the manuscript.

Anne Spang supervised the experiments, assessed the localization of Pma1p, Cwp2p and CPY, and wrote the manuscript.

Transport to the plasma membrane is regulated differently early and late in the cell cycle in *Saccharomyces cerevisiae*

Bettina Zanolari[1,*], Uli Rockenbauch[1,*], Mark Trautwein[1], Lorena Clay[2], Yves Barral[2] and Anne Spang[1,‡]

[1]Biozentrum, University Basel, CH-4056 Basel, Switzerland
[2]ETH Zürich Hönggerberg, CH-8049 Zürich, Switzerland

*These authors contributed equally to this work
‡Author for correspondence (anne.spang@unibas.ch)

Accepted 13 November 2010
Journal of Cell Science 124, 1055-1066

doi:10.1242/jcs.072371

Summary

Traffic from the *trans*-Golgi network to the plasma membrane is thought to occur through at least two different independent pathways. The chitin synthase Chs3p requires the exomer complex and Arf1p to reach the bud neck of yeast cells in a cell-cycle-dependent manner, whereas the hexose transporter Hxt2p localizes over the entire plasma membrane independently of the exomer complex. Here, we conducted a visual screen for communalities and differences between the exomer-dependent and exomer-independent transport to the plasma membrane in *Saccharomyces cerevisiae*. We found that most of the components that are required for the fusion of transport vesicles with the plasma membrane, are involved in localization of both Chs3p and Hxt2p. However, the lethal giant larva homologue Sro7p is required primarily for the targeting of Chs3p, and not Hxt2p or other cargoes such as Itr1p, Cwp2p and Pma1p. Interestingly, this transport defect was more pronounced in large-budded cells just before cytokinesis than in small-budded cells. In addition, we found that the yeast Rab11 homologue Ypt31p determines the residence time of Chs3p in the bud neck of small-budded, but not large-budded, cells. We propose that transport to and from the bud neck is regulated differently in small- and large-budded cells, and differs early and late in the cell cycle.

Key words: Small GTPases, Intracellular traffic, Cell cycle, Yeast, Exocytosis, Endocytosis

Introduction

Various transport pathways operate to localize cargo to the plasma membrane. At least two different transport pathways have been identified in yeast by the buoyant density of the transport carriers and the cargo they contain (Gurunathan et al., 2002; Harsay and Bretscher, 1995; Harsay and Schekman, 2002). The high-density fraction transports exoglucanase and invertase, whereas the low-density pool brings the plasma membrane ATPase Pma1p, the glucose transporter Hxt2p, Fus1p and the chitin synthase III Chs3p, and probably a large variety of other cargo to the plasma membrane (Bagnat and Simons, 2002; Barfield et al., 2009; Harsay and Schekman, 2002; Kruckeberg et al., 1999). The lighter pool of transport containers can probably be further split into subclasses. Chs3p and Fus1p have distinct transport requirements from Pma1p or Hxt2p, because they need the action of the exomer complex for exit from the *trans*-Golgi network (TGN) (Sanchatjate and Schekman, 2006; Trautwein et al., 2006; Wang et al., 2006). The exomer complex consists of the peripheral Golgi protein Chs5p and the ChAP proteins (Wang et al., 2006). The ChAPs are four homologous proteins that can interact with both the small GTPase Arf1p and Chs5p (Trautwein et al., 2006). They form complexes of varying stoichiometries and might act as receptors for cargoes to be transported by the exomer-dependent pathway (Sanchatjate and Schekman, 2006; Trautwein et al., 2006). Whether exomer is a sorting complex at the TGN, similarly to the ESCRTIII complex at the endosome (Saksena et al., 2009) or a novel coat, remains to be established. The exomer complex fulfils two of the hallmarks of a vesicle coat because it interacts directly with both a small GTPase of the Arf/Sar family and cargo proteins (Trautwein et al., 2006). However, unlike the COPI and COPII coats (Matsuoka et al., 1998; Spang et al., 1998), the exomer complex, with Arf1p, fails to change the membrane curvature of liposomes or to bud off vesicles (Wang et al., 2006).

Chs3p displays an interesting localization pattern as it changes over the cell-cycle. Early in the cell-cycle in G1 and S phase, Chs3p is located at the incipient bud site and at the bud neck of small-budded cells. In G2, when the bud is medium sized, Chs3p is present in internal structures referred to as chitosomes (Chuang and Schekman, 1996; Ziman et al., 1996), which are endosomes. In mitosis, when also the actin cytoskeleton re-polarizes from the bud tip to the bud neck, Chs3p is exported to the bud neck again. By contrast, the fusion of secretory transport vesicles is thought to occur at the incipient bud site and then in G1 and S phase of the cell cycle, at the bud tip. During G2, vesicles fuse all over the bud surface and subsequently, during cytokinesis, relocalization of the vesicle fusion site to the bud neck occurs. This raises the question whether fusion of Chs3p-containing transport vesicles is governed by the same regulatory factors as that of general transport vesicles. It is assumed that the exocyst is required for fusion of transport vesicles with the plasma membrane because mutants in the exocyst component *SEC6* accumulate vesicles (TerBush et al., 1996), some of which contain Chs3p (Valdivia et al., 2002). However, no detailed analysis is available.

Here, we investigate how the transport of Chs3p to the bud neck region of the plasma membrane is controlled in *Saccharomyces cerevisiae*. We show that delivery of Chs3p to the bud neck region

Journal of Cell Science

continues, even when the vesicle fusion machinery is only apparent in the bud tip. To gain a better understanding of the regulation of Chs3p localization at the plasma membrane, we performed a visual screen comparing the transport of Chs3p and Hxt2p to the plasma membrane using fluorescently labeled variants. We found that the general fusion machinery at the plasma membrane is essential for the efficient delivery of both cargoes to the plasma membrane, independent of whether the cargo is localized to the bud neck region or the entire plasma membrane. However, some transport mutants affected the localization of Chs3p and Hxt2p, and other exomer-independent cargo differentially. Moreover, we found that the residence time of Chs3p at the bud neck is determined in different ways in small- and large-budded cells. Our data therefore indicate that general transport factors can selectively influence the temporal and spatial localization of different cargoes.

Results

Transport dynamics of Chs3p and the exocyst complex over the yeast cell cycle

To gain further insight into the temporal and spatial aspects of Chs3p transport, we observed localization of Chs3p–GFP over the cell cycle. As reported previously (Valdivia et al., 2002), Chs3p–GFP is present in the bud-neck in small-budded cells immediately after bud emergence (G1–S phase), it disappears from the bud neck in medium-budded cells (G2 phase), to reappear only in the bud neck of large-budded cells (M-phase), where it persists until the end of cytokinesis (Fig. 1A). Transport vesicles generally fuse at the bud tip of small-budded cells, all over the bud surface in medium-sized cells and then vesicle fusion is restricted to the bud neck region at cytokinesis. The site of vesicle fusion is marked by the presence of the exocyst complex, which serves as tethering complex for vesicles with the plasma membrane (Guo et al., 1999). We used Sec8p, a member of the exocyst complex (TerBush and Novick, 1995), fused to GFP to visualize the localization of the exocyst complex over the cell cycle (Fig. 1A). Sec8p–GFP was functional because a chromosomal fusion to the essential *SEC8* was generated at the endogenous locus, and the resulting strain grew indistinguishably from an untagged control. Interestingly, Chs3p–GFP remained restricted to the bud neck when the fusion machinery was localized to the bud tip. This observation could be explained by two different possibilities. First, Chs3p–GFP transport is restricted to the short time-window of initiation of bud emergence. Second, Chs3p–GFP transport to the bud neck persists after bud emergence. In the latter case, Chs3p could be delivered either directly to the bud neck or to the bud tip and then a 'diffusion-and-trapping' mechanism would anchor Chs3p at the bud neck. To determine whether Chs3p could be delivered to the bud neck after the initial bud growth had been initiated, we performed a FRAP analysis. We bleached the Chs3p–GFP signal in small-budded cells and determined the reappearance of the Chs3p–GFP signal in the bud neck 10 minutes after the initial bleaching (Fig. 1B). In 80% (n=16) of the small-budded cells, we observed reappearance of the Chs3p signal in the bud neck after photobleaching, indicating that Chs3p pools at the plasma membrane can be replenished after initiation of the budding process.

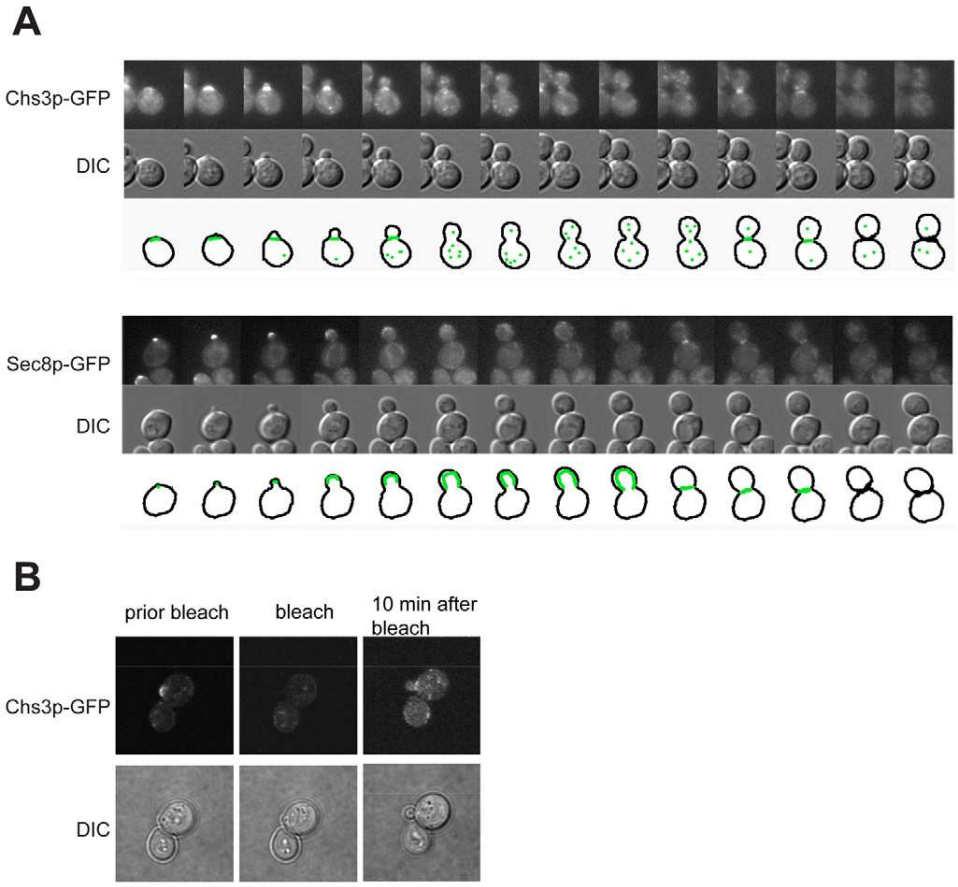

Fig. 1. Cell-cycle-dependent transport of Chs3p–GFP. (**A**) Time-lapse images of wild-type yeast cells bearing either Chs3p–GFP or Sec8p–GFP. The images in the DIC and GFP channels were acquired every 10 minutes. The schematic drawings underneath the time-lapse images illustrate the localization of the GFP-tagged proteins. (**B**) Chs3p–GFP reaches the bud neck even after bud emergence in small-budded cells. Cells expressing Chs3p–GFP, which had just initiated bud formation were used for FRAP experiments. A *Z*-stack was acquired before and 10 minutes after bleaching the incipient bud site. For the analysis, cells were taken into account in which the bud grew during the 10 minute period after the bleaching. Representative single plane images are shown.

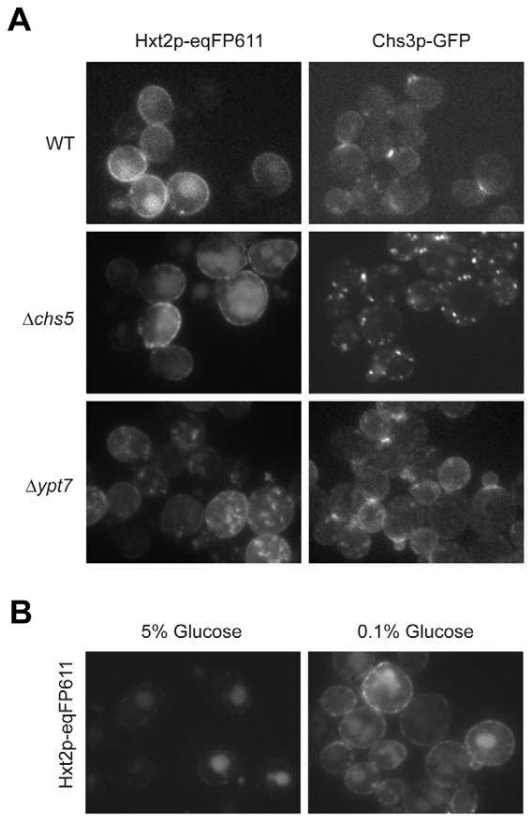

Fig. 2. Trafficking of Hxt2p–eqFP611 and Chs3p–GFP. (**A**) Hxt2p–eqFP611 and Chs3p–GFP have different requirements for plasma membrane localization. Chs3p–GFP and Hxt2p–eqFP611 were expressed from their endogenous loci in different strains. Chs3p–GFP was specifically retained in *Δchs5* cells, whereas prominent mislocalization of Hxt2p–eqFP611 was observed in *Δypt7* cells. (**B**) Hxt2p–eqFP611 is exported to the plasma membrane upon shift from high-glucose to low-glucose medium. Cells were grown to log phase in medium containing 5% glucose at 30°C, harvested and resuspended in medium with 0.1% glucose and incubated again. The images were acquired 1.5 hours after downshift.

Chs3p and Hxt2p travel independently to the plasma membrane

To gain a better understanding of the plasma membrane localization of Chs3p, we used a strain in which Chs3p was appended with 2×GFP and the plasma-membrane-localized hexose transporter Hxt2p with the red fluorescent protein eqFP611 (Wiedenmann et al., 2002) (Fig. 2A). We decided to use Hxt2p because it can be used for steady state as well as pulse–chase analysis (Kruckeberg et al., 1999). In medium containing high levels of glucose (5%) Hxt2p did not localize to the plasma membrane, but was instead routed to the vacuole (Fig. 2B). Upon shift to low-glucose medium (0.1% glucose), Hxt2p was transported to the plasma membrane. Therefore, Hxt2p provides a suitable cargo model for steady state and pulse analysis. Hxt2p localization is independent of exomer because in a *Δchs5* mutant, in which Chs3p–GFP is retained in the Golgi, Hxt2p–eqFP611 still reached the plasma membrane under normal and low-glucose conditions (Fig. 2A, Table 1 and data not shown). Conversely, in a *Δypt7* strain, in which Chs3p–GFP traffic is only mildly affected, Hxt2p–eqFP611 staining at the plasma membrane was clearly reduced, and the protein was instead enriched in the vacuole (which is fragmented in the absence of Ypt7p) (Fig. 2A). The mislocalization of Hxt2p in *Δypt7* was specific and no significant changes in plasma membrane localization were observed for the plasma membrane ATPase Pma1p, the GPI-anchored cell-wall protein Cwp2p or the inositol transporter Itr1p (supplementary material Fig. S1) (Table 1). By contrast, as expected, the vacuolar carboxypeptidase Y (CPY) showed abnormal localization in *Δypt7* cells (supplementary material Fig. S1) (Table 1). These data demonstrate, that Chs3p and Hxt2p have different requirements to ensure their proper delivery to the plasma membrane.

The exocyst is required for localization of Chs3p–GFP to the bud neck

First, we wanted to investigate whether both Hxt2p transport and Chs3p traffic requires the same exocyst tethering complex. All exocyst components are essential and therefore deletions are not available. The use of temperature-sensitive strains for the investigation of Chs3p traffic is limited because Chs3p is involved in acute heat-shock response (Fig. 3A) (Valdivia and Schekman, 2003). Upon shift of wild-type cells to 37°C, Chs3p was rapidly endocytosed and appeared at the plasma membrane in a delocalized manner. After 2.5 hours at 37°C, cells had adapted to the new environment and Chs3p relocated to the bud neck. Therefore, upon shift of temperature-sensitive mutant cells to the restrictive temperature (37°C), we would only be able to observe the effect of mutants on heat-shock-induced trafficking of Chs3p, and not its normal delivery to the bud neck. However, some temperature-sensitive mutants show an effect at the permissive temperature (23°C). Thus, we determined the localization of Chs3p–GFP and Hxt2p–eqFP611 in exocyst mutants at 23°C. Whereas *sec6-4* cells showed wild-type localization of both markers, Chs3p–GFP was at least partially delocalized over the plasma membrane in *sec3-2* cells. Under these conditions, Hxt2p–eqFP611 was still properly localized (Fig. 3A) (Table 1). To corroborate the transport defect, we screened more temperature-sensitive transport mutants for a transport defect at the permissive (23°C) or semi-permissive temperature (30°C) using Pma1p–GFP, Itr1p–GFP and GFP–Cwp2p as markers. While *sec5-24* showed no transport defect at the indicated temperatures, *sec10-2* showed aberrant localizations of the markers at 30°C and *exo84-117* at 23°C (Fig. 3B) (Table 1). As expected, localization of Chs3p–GFP at the bud neck was impaired under the same conditions in which the other markers had failed to localize properly (Fig. 3B,C) (Table 1). More importantly, *sec5-24* cells failed to correctly localize Chs3p–GFP to the bud neck at 30°C, indicating that Chs3p localization is strongly dependent on a functional exocyst complex. Moreover, the data suggest, that Chs3p trafficking might be more sensitive to non-functional exocyst than other cargo transported to the bud tip.

Another way to test for exocyst requirement in Chs3p transport is to selectively downregulate one of its components. To this end, we constructed a strain in which *SEC6* is under *GAL1* promoter control and Chs3p is tagged with GFP, and performed a *GAL1* shut-off experiment. Growth of this strain in glucose represses the *GAL1* promoter and leads to a depletion of Sec6p. After 13 hours of growth in glucose-containing medium, when about 70% of the cells were still alive (data not shown), Chs3p–GFP was found in a diffuse pattern in the cells, indicating that Chs3p was trapped in vesicles that failed to fuse with the plasma membrane (Fig. 3D). This result is consistent with the absence of exocyst function and hence the accumulation of vesicles in the cell. This accumulation

Table 1. Summary of localization phenotypes in various mutants

Genotype	Function	Correct localization					
		Chs3p	Hxt2p	Cwp2	Pma1p	Itr1p	CPY
WT		++	++	++	++	++	++
Δchs5	Chs3p trafficking to bud neck	– –	++	++	++	++	++
Δypt6	Intra Golgi trafficking	+	+	ND	ND	ND	ND
Δypt7	LE>Lysosome	+	–	++	++	++	–
Δypt10	Endosomal transport	+	++	ND	ND	ND	ND
Δypt11	Organelle inheritance	+	++	ND	ND	ND	ND
Δypt51	EE>LE, TGN>LE	++	+	ND	ND	ND	ND
Δypt51/Δypt52/Δypt53	EE>LE, TGN>LE	– –	–	–	–	–	+
Δmsb3	GAP of Sec4p	++	++	ND	ND	ND	ND
Δmsb4	GAP of Sec4p	+	++	ND	ND	ND	ND
Δmsb3/Δmsb4	GAP of Sec4p	– –	– –	ND	ND	ND	ND
Δsro7	Regulation of exocytosis	–	++	+	++	–[a] ++[b]	++
Δsro77	Regulation of exocytosis	+	++	++	++	++	++
Δsro7/Δsro77	Regulation of exocytosis	– –	– –	–	–	+	+
Δbni4	Anchoring of Chs3p at bud neck	–	ND	ND	ND	ND	ND
Δchs4	Activation of Chs3p at bud neck	–	ND	ND	ND	ND	ND
Δbni4/Δchs4	Function of Chs3p at bud neck	– –	ND	ND	ND	ND	ND
Δypt31	TGN>PM	–	++	+	++	+	++
Δypt32	TGN>PM	+	++	++	++	++	++
Δsur2	Sphingolipid synthesis	++	++	ND	ND	ND	ND
Δelo3	Sphingolipid synthesis	+	+	ND	ND	ND	ND
Δypt31/ypt32A141D[c]	TGN>PM	++	+	ND	++	+	ND
Δypt31/ypt32A141D[d]	TGN>PM	– –	–	–	–	+	ND
sec6-4[c]	Exocyst	++	++	ND	ND	ND	ND
sec3-2[c]	Exocyst	+	++	ND	ND	ND	ND
sec5-24[d]	Exocyst	–	ND	+	+	+	ND
sec10-2[c]	Exocyst	–	ND	+	++	+	ND
sec10-2[d]	Exocyst	– –	ND	– –	–	– –	ND
exo-84-117[c]	Exocyst	–	ND	–	+	+	ND
exo-84-117[d]	Exocyst	– –	ND	– –	–	–	ND
sec4-8[c]	Golgi>PM	–	++	ND	ND	ND	ND
sec2-41[c]	GEF for Sec4p	–	++	ND	ND	ND	ND
ypt1-3[c]	ER>Golgi	++	++	ND	ND	ND	ND

++, Localization indistinguishable from wild type; + slight changes in localization or mislocalization in ≤10% of cells; –, obvious changes in localization or mislocalization in a large number of cells; – –, strong mislocalization defect in almost all (or all) cells. [a]Early chase times; [b]late chase times and steady state; [c]temperature-sensitive mutants, tested at 23°C; [d]temperature-sensitive mutants, tested at 30°C (semi-permissive temperature).

of vesicles has been demonstrated in vitro by gradient fractionation of a *sec6-4* strain after shift for 1 hour to the non-permissive temperature (Valdivia et al., 2002). Chs3p–GFP co-migrated with the plasma membrane marker Pma1p in the vesicle fraction upon depletion of Sec6p by incubating a strain containing *SEC6* under the control of the *GAL1* promoter in medium containing glucose (Fig. 4). In a wild-type strain, this peak was not observed because no transport vesicles accumulate. Moreover, growing the cells in galactose, which keeps the promoter active did not interfere with plasma membrane transport (Fig. 4).

To extend our finding on the exocyst requirement for localization of Chs3p at the bud neck, we used mutant exocyst-associated proteins. The lethal giant larva homologue Sro7p and its close homologue Sro77p appear to bridge the interaction between the t-SNARE in the plasma membrane, Sec9p and the exocyst. Deletions of *SRO7* and *SRO77* are viable, and the growth of the double deletion is strongly impaired. In a *Δsro7* strain, Chs3p–GFP was enriched in internal structures, whereas Hxt2p–eqFP611 was properly localized (Fig. 5A, Table 1). This phenotype seemed to be more pronounced in large-budded than in small-budded cells (Fig. 5B). The effect on transport of Chs3p–GFP in *Δsro7* cells was specific, because Hxt2p–eqFP611 was also exported to the plasma membrane after shift from high-glucose to low-glucose medium (Fig. 5C). In the double deletion *Δsro7 Δsro77*, both markers were aberrantly localized under normal growth conditions, which is consistent with the notion that Sro7p and Sro77p have overlapping functions. Interestingly, under the high-to-low glucose regime, Hxt2p–eqFP611 was efficiently exported to the plasma membrane even in a *Δsro7 Δsro77* strain (Fig. 5C), indicating that under these conditions Hxt2p was routed into a Sro7/Sro77p-independent pathway. This prompted us to test another cargo, Itr1p, whose transport to the plasma membrane is dependent on inositol availability. Little Itr1p–GFP is found at the plasma membrane when cells are grown in rich medium. However, growth in minimal medium causes the inositol transporter to be efficiently expressed at the plasma membrane (Miyashita et al., 2003) (Fig. 5D). At steady state conditions, the localization of Itr1p was not compromised by the loss of either *SRO7* or *SRO77* (Fig. 5E), yet in *Δsro7 Δsro77* cells Itr1p–GFP was partially mislocalized, to a much lower extent than that observed for Hxt2p–eqFP611 (Table 1). By contrast, when we shifted *Δsro7* cells from rich medium to minimal medium and determined Itr1p–GFP localization after 20 minutes, Itr1p did not efficiently reach the plasma membrane in 10–20% of the cells (Fig. 5F). Interestingly, 1.5 hours after the shift, this partial mislocalization defect was rescued, indicating that vesicle fusion with the plasma membrane is slowed down in *Δsro7* cells, but is not detectable for cargo that is continuously present in large amounts at the plasma membrane, or which is cycling very slowly. Most important, however, is the observation that while mislocalized Itr1p–GFP appeared as a haze mostly distributed over the entire cell irrespective of the cell cycle stage, Chs3p–GFP was

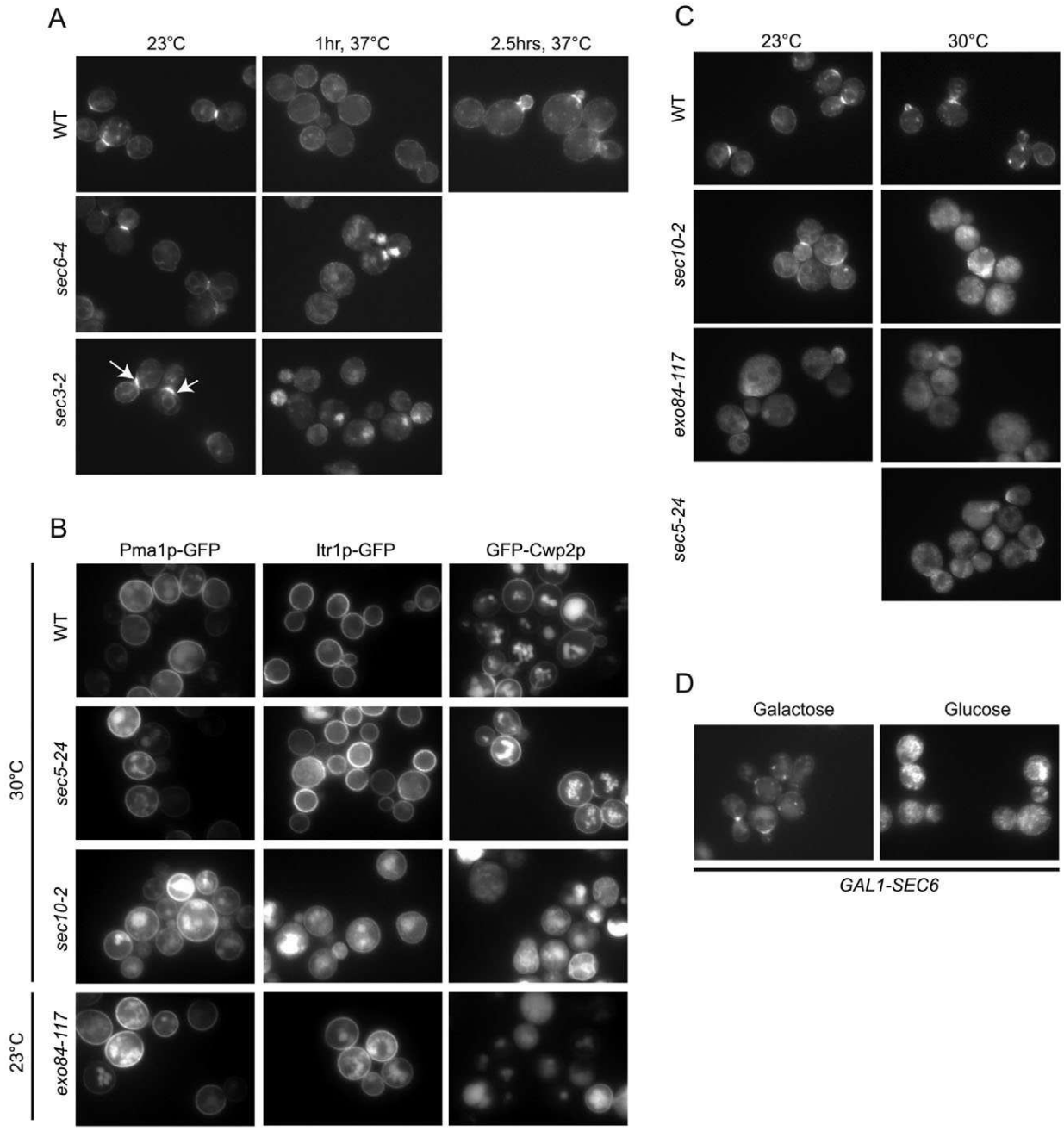

Fig. 3. The exocyst is required for proper plasma membrane localization of Chs3p–GFP and Hxt2p–eqFP611. (**A**) Mutants in the exocyst complex inhibit plasma membrane localization of Chs3p–GFP in response to heat shock. Logarithmically growing cells at 23°C were shifted to 37°C for indicated times and Chs3p–GFP localization was determined by live-cell imaging. The arrows indicate the broader Chs3p–GFP bud-neck localization in *sec3-2* cells at 23°C. (**B**) Plasma membrane localization of Itr1p–GFP and GFP–Cwp2 is impaired at the permissive or semi-permissive temperature in a subset of temperature-sensitive exocyst mutants. Logarithmically growing cells at 23°C were shifted to 30°C for 6 hours, where indicated before analysis. (**C**) Chs3p trafficking is impaired in a subset of exocyst mutants grown at the permissive or semi-permissive temperature. Logarithmically growing cells at 23°C were shifted to 30°C for 6 hours, where indicated before analysis. (**D**) *GAL1* shut-off of *SEC6* leads to intracellular accumulation of Chs3p–GFP. Endogenous *SEC6* was put under the control of the galactose-induced *GAL1* promoter in a strain expressing Chs3p–GFP. Cells grown on galactose were shifted into glucose-containing medium, which causes repression of the *GAL1* promoter. Images were taken 13.5 hours after the shift from galactose into glucose-containing medium.

clustered in the bud neck region early and more pronounced late in the cell cycle. Hence, it is unlikely that both cargoes travel in the same vesicle. Taken together, our data demonstrate that the exocyst is required for the correct localization of Chs3p–GFP at the bud neck. Moreover, they also indicate that similarly to inclusion of Hxt2p and Chs3p in vesicles at the Golgi, fusion at the plasma membrane could also be regulated differently, depending on the cell-cycle stage.

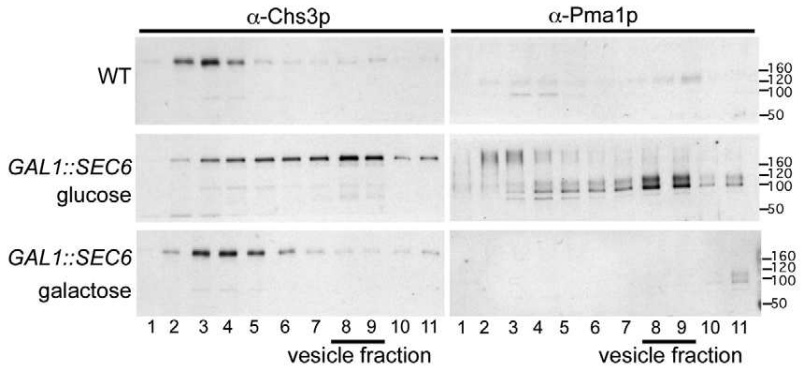

Fig. 4. Chs3p accumulates in the vesicle fraction after *SEC6 GAL1* shut-off. Strains containing *SEC6* under the *GAL1* promoter were incubated for 13 hours in glucose-containing medium, or were cultured in galactose. The supernatant of a 13,000 ***g*** spin was loaded on a sucrose gradient. The gradient fractions were separated by SDS-PAGE, and immunoblots were developed with anti-Chs3p and anti-Pma1p antibodies. The TGN fraction stays close to the top, whereas the vesicle fraction migrates towards the bottom. After *GAL1* shut-off, Chs3p co-migrates with the vesicle fraction containing the plasma membrane ATPase Pma1p, which is not detected without vesicle accumulation.

Sec4p is required for the correct localization of Chs3p

Other key regulators of intracellular traffic are small GTPases of the Rab family, most of which appear to act in post-Golgi traffic in yeast. We wanted to test whether one of the Rab proteins would specifically act on Chs3p–GFP traffic. Only 2 of the 11 Rab proteins in yeast are essential, and conditional mutants are available. Ypt1p is the homologue of Rab1 and is involved in anterograde and retrograde transport in the ER shuttle (Kamena et al., 2008), whereas Sec4p is the Rab required for fusion of transport vesicles with the plasma membrane (Guo et al., 1999). The temperature-sensitive mutant *ypt1-3* did not affect transport of either Chs3p or Hxt2p to the plasma membrane at 23°C (Fig. 6A). By contrast, Chs3p was mislocalized at 37°C, whereas Hxt2p still reached the plasma membrane efficiently. The effect of the *ypt1-3* mutation on Chs3p traffic could be indirect because in this mutant, Golgi morphology and composition is strongly affected (Kamena et al., 2008), to which Chs3p could be more sensitive than Hxt2p.

By contrast, both proteins were affected in *sec4-8* mutant cells at 23°C (Fig. 6) and strong intracellular staining was observed at 37°C. A similar phenotype was observed when we analyzed a mutant in the GEF for Sec4p, Sec2p, indicating that the observed phenotype is specific (Fig. 6B, Table 1). Interestingly, after the shift from high-glucose to low-glucose medium, most Hxt2p was correctly targeted to the plasma membrane at the permissive temperature (Fig. 6C). To corroborate the findings of a role of Sec4p in Chs3p transport, we also analyzed mutants in the non-essential GAPs for Sec4p, Msb3p and Msb4p. Deletion of either *MSB3* or *MSB4* had little to no impact on Hxt2p–eqFP611 and Chs3–pGFP, whereas they were severely mislocalized in *Δmsb3 Δmsb4* (Fig. 6D, Table 1). We conclude that Sec4p and its regulators have a central role in localization of both Chs3p and Hxt2p.

Ypt31p and Ypt32p are required for proper Chs3p–GFP traffic

The function of Ypt1p and Sec4p is central for the transport of all cargo proteins that have to reach the plasma membrane. Therefore, an effect on both cargoes tested here is not unexpected. However, it is conceivable that one of the non-essential Rab proteins could have a more important role in one of the transport pathways than in the others. Therefore, we screened deletion strains of Rab GTPases for localization defects of either Hxt2p or Chs3p. Most of the individual deletions of the Rab GTPases did not impede the localization of Chs3p or Hxt2p (Fig. 7, Table 1). In a *Δypt11* strain, the Chs3p–GFP signal seemed occasionally a bit broader, but Chs3p still reached the bud neck efficiently. Hxt2p transport was affected more than Chs3p plasma membrane localization in a *Δypt7* strain. Ypt7p is the orthologue of Rab7 and is required for all membrane-fusion steps with the yeast lysosome, the vacuole (Fig. 2, Table 1). Although the single deletion of *YPT51* had only mild effects on Chs3p–GFP and Hxt2–eqFP611, loss of all Rab5 activity (*Δypt51 Δypt52 Δypt53*) severely altered the localization of Hxt2p and Chs3p, because neither Chs3p nor Hxt2p could be efficiently endocytosed anymore, and therefore internal structures were almost completely absent (Fig. 7, Table 1). A similar phenotype was observed in a *Δend3* mutant, which is defective in an early phase of endocytosis (supplementary material Fig. S2). As a consequence of failed endocytosis, Chs3p–GFP accumulated at the plasma membrane in medium-sized buds (data not shown). More importantly, when we analyzed *Δypt31* and *Δypt32* mutants, localization of Chs3p–GFP, but not Hxt2p–eqFP611, was impaired (Fig. 7, Table 1). In both mutants, more Chs3p-positive internal structures were visible, which seemed to accumulate sometimes at the bud neck. Moreover, in the temperature-sensitive double mutant, *Δypt31 ypt32A141D*, this phenotype was evident at the permissive temperature (23°C) (Fig. 6, Table 1).

The residence time of Chs3p–GFP is shortened in the small bud neck of *Δypt31* cells

We investigated the phenotype of *Δypt31* and *Δypt32* more closely and determined the level of Chs3p–GFP staining in small-, medium- and large-budded cells. Interestingly, although the levels of Chs3p–GFP in the bud neck of large-budded cells was not altered in *Δypt31* or *Δypt32*, significantly fewer small-budded cells showed correct Chs3p–GFP localization in *Δypt31* cells (Fig. 8A). Because of the large variability of the Chs3p localization in the *Δypt32* strain, we focused our analysis on *Δypt31*. The observed phenotype could be explained by either the lack of transport of Chs3p–GFP to the bud neck in a fraction of cells or a decrease in residence time of Chs3p–GFP in the bud neck of small-budded cells. To distinguish between these possibilities, we performed a time-lapse analysis, for which we took pictures of individual cells every 10 minutes and counted the number of frames in which we could observe a Chs3p–GFP signal in the bud neck of small cells (Fig. 8B,C). These data indicate that the average residence time of Chs3p–GFP is about 1.5 frames (which corresponds to about 15 minutes) shorter in *Δypt31* than in wild-type cells. The initial transport to the bud neck did not seem to be affected in the *Δypt31* mutant, suggesting that either less Chs3p–GFP is transported to the bud neck, or Chs3p–GFP is endocytosed faster from the bud. To distinguish between these possibilities, we measured the intensity of Chs3p–GFP in the bud neck of small-budded wild-type and *Δypt31* cells. However, we did not find any significant differences in the signal intensity in the bud neck (data not shown), favoring the more rapid endocytosis of Chs3p–GFP in the absence

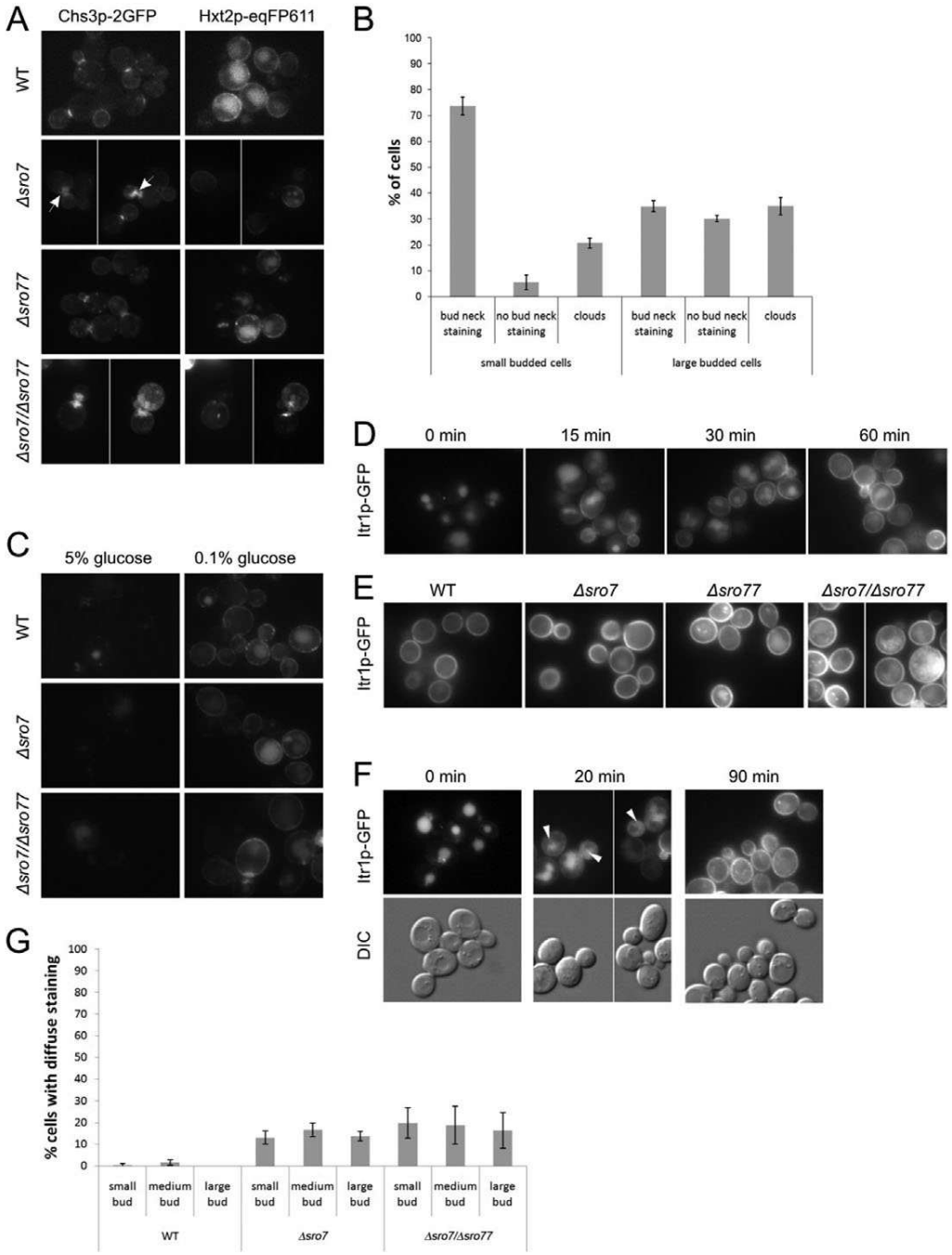

Fig. 5. Sro7p is required for proper bud neck localization of Chs3p especially in large-budded cells. (**A**) *Δsro7* affects trafficking of Chs3p–GFP, but not Hxt2p–eqFP611, to the plasma membrane. Various strains expressing Chs3p–GFP and Hxt2p–eqFP611 were grown to log phase in YPAD at 30°C and subjected to live-cell imaging. The arrows indicate apparent vesicles clouds containing Chs3p–GFP in the bud neck of the *Δsro7* mutant. (**B**) Quantification of the mislocalization of Chs3p–GFP in *Δsro7* cells compared with the wild type. Cells were scored for bud-neck localization of Chs3p–GFP. 'clouds' represents the class of mislocalized Chs3p close to the bud neck. (**C**) Hxt2p–eqFP611 still appears at the plasma membrane in *Δsro7* and in *Δsro7 Δsro77* cells after glucose induction. A high-to-low glucose shift experiment was performed as described in Fig. 2B. (**D**) Itr1p–GFP is transported to the plasma membrane in response to low inositol levels. Cells expressing Itr1p–GFP were grown in YPAD and then shifted into minimal medium, which caused plasma membrane expression of Itr1p–GFP. Pictures were taken 0, 15, 30 and 60 minutes after shift into minimal medium. (**E**) Itr1p–GFP localization at the plasma membrane is only mildly affected in *Δsro7Δsro77* cells under steady state conditions. The localization of Itr1p–GFP was analyzed in WT, *Δsro7*, *Δsro77* and *Δsro7Δsro77* cells grown in minimal medium. (**F**) Itr1p–GFP transport to the plasma membrane is delayed upon induction in *Δsro7* cells. *Δsro7* cells expressing Itr1p–GFP were shifted from rich to minimal medium and the plasma membrane appearance of Itr1p–GFP was followed over time. Initially a haze of Itr1p–GFP signal populated the cytoplasm in some cells. Note that the bright staining represents vacuole-localized Itr1p–GFP. After 90 minutes, Itr1p–GFP was localized at the plasma membrane and was indistinguishable from that in the wild type. The arrowheads point to the haze. (**G**) Quantification of the *Δsro7* and *Δsro7Δsro77* cells that had a delay in Itr1p–GFP transport to the plasma membrane.

of Ypt31p. Because we did not see a difference for the residence time in large-budded cells in the *Δypt31* strain, our data provide evidence that the localization of Chs3p at the bud neck in small-budded cells is regulated in a different manner than in large-budded cells. Furthermore, they suggest that transport to and from a particular location in the cell might require different factors depending on the stage of the cell cycle.

Discussion

We investigated the requirements for plasma membrane localization of Chs3p by conducting a visual screen with mutants of regulators of vesicle fusion at the plasma membrane and Rab GTPases. We found that the requirements for the fusion of transport vesicles containing Chs3p or Hxt2p are mainly the same. However, bud neck localization of Chs3p was specifically affected in *Δsro7*, when compared with Hxt2p, or other exomer-independent cargo such as Itr1p, Pma1p and Cwp2p. Although export of Itr1p to the plasma membrane was delayed in *Δsro7* cells under pulse–chase conditions, no defect was observed under steady-state levels. No role for Sro7p in the formation of transport carriers has been established. It seems to be required rather in later stages of the life cycle of a vesicle, such as the fusion stage. These differences

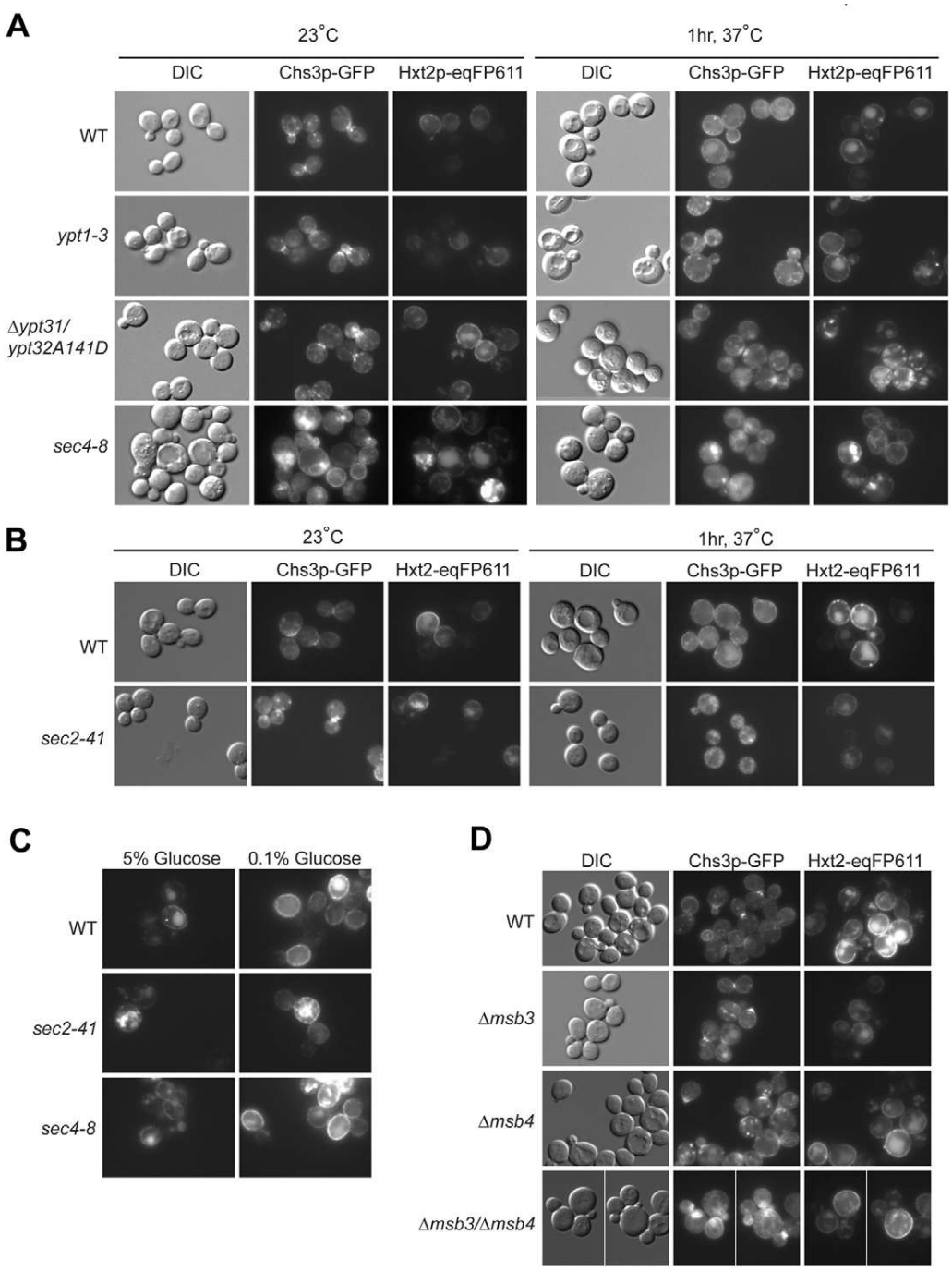

Fig. 6. Several Rab GTPases and the Sec4p GEF influence traffic of cargo to the plasma membrane. (**A**) Strains of the temperature-sensitive mutations of the essential Rab proteins *YPT1* and *SEC4* and the essential pair *YPT31–YPT32* were grown to log phase at 23°C and then shifted to 37°C for 1 hour. Cells were mounted and imaged immediately thereafter. In contrast to *sec4-8*, *ypt1-3* is not required for Chs3p–GFP and Hxt2p–eqFP611 at 23°C. (**B**) *sec2-41* mutant cells are defective in Hxt2p and Chs3p traffic. Wild-type and *sec2-41* strains were grown to log phase at 23°C and then shifted for 1 hour to 37°C. Images were taken immediately after sample preparation. (**C**) *sec4-8* and *sec2-41* are not impaired in Hxt2 transport after glucose shift at 23°C. Cells were grown in 5% glucose, harvested and resuspended in medium containing 0.1% glucose, causing transport of Hxt2p to the plasma membrane. (**D**) The Sec4p-GAPs Msb3p and Msb4p are required for trafficking of Chs3p and Hxt2p–eqFP611 to the bud neck.

suggest either that Chs3p and Hxt2p travel in separate transport containers or that because Chs3p transport is dependent on the cell-cycle state, transport to the plasma membrane is regulated differently according to the cell-cycle phase. These two possibilities are not mutually exclusive and could both operate to control plasma membrane localization of a variety of proteins. Alternatively, a transcytosis type of transport could be envisaged for Chs3p localization. In this scenario, Chs3p would be transported to the bud tip in the same vesicle as Hxt2p and other exomer-independent cargo. Because the bud tip is also the major place for endocytosis, Chs3p could be internalized immediately into special transport containers and routed to the bud neck. There is little evidence for this latter model so far, but it could help explain how the chitin ring can form asymmetrically on the mother-cell side of the neck (DeMarini et al., 1997).

Although we identified mutants that more strongly affected transport to the plasma membrane of Chs3p than of Hxt2p and vice versa, our study does not allow us to definitively conclude the presence of two separate transport containers for Chs3p and Hxt2p. It is likely that the inclusion of Chs3p into nascent vesicles at the TGN is favored at particular times in the cell cycle and that at these times (G1–S phase, cytokinesis) also fusion at the plasma membrane is differently regulated compared with the rest of the cell cycle. Transport of vesicles to the plasma membrane seems to occur by distinct pathways because *cdc42-6* mutants only accumulated vesicles at the restrictive temperature in small-budded but not large-budded cells (Adamo et al., 2001). In contrast to our results, no differential trafficking of cargoes to the plasma membrane was detected. The differential localization patterns for distinct cargoes are probably achieved not only by the fusion of vesicles with the plasma membrane, but also by how quickly the cargo is endocytosed again (Valdez-Taubas and Pelham, 2005).

Interestingly, we found that the residence time of Chs3p at the plasma membrane seems to be regulated differently over the cell cycle, because loss of the Rab11 homologue Ypt31p reduced specifically the time of Chs3p plasma membrane localization in small-budded but not in large-budded cells. We did not detect a reduction in the fluorescence intensity of Chs3p–GFP at the bud neck of *Δypt31* cells, suggesting that the export from the TGN and the arrival at the plasma membrane of Chs3p–GFP are not impaired. Since Sec4p is essential for the fusion of Chs3p-containing transport vesicles, it is unlikely that Ypt31p has a role in the final steps of Chs3p deposition at the plasma membrane. Finally, endocytosis of Chs3p involves the three Rab5 homologues Ypt51p, Ypt52p and Ypt53p, indicating that Ypt31p might not be the determining factor in early steps of Chs3p internalization. However, we cannot definitely exclude a role of Ypt31p in endocytosis, because Singer-Krüger and colleagues (Singer-Krüger et al., 1994) demonstrated no defect in early stages of α-factor receptor endocytosis in *Δypt51Δypt52Δypt53*. Nevertheless, when we tested different cargoes in our triple deletion strain, all cargoes were trapped at the plasma membrane similarly to the phenotype observed in a *Δend3* strain (supplementary material Fig. S2), in which early stages of endocytosis are blocked (Raths et al., 1993). No data are available to our knowledge elucidating the cause of the internalization of Chs3p in G2 phase or after cytokinesis. However, our data suggest that Ypt31p might be a factor contributing to the timely endocytosis of Chs3p, specifically in small-budded cells, for example, early in the cell cycle. Interestingly, Ypt31p is required for the establishment of the bipolar budding pattern in diploid cells (Ni and Snyder, 2001), a function, which is shared by Chs5p and Bud7p. Moreover,

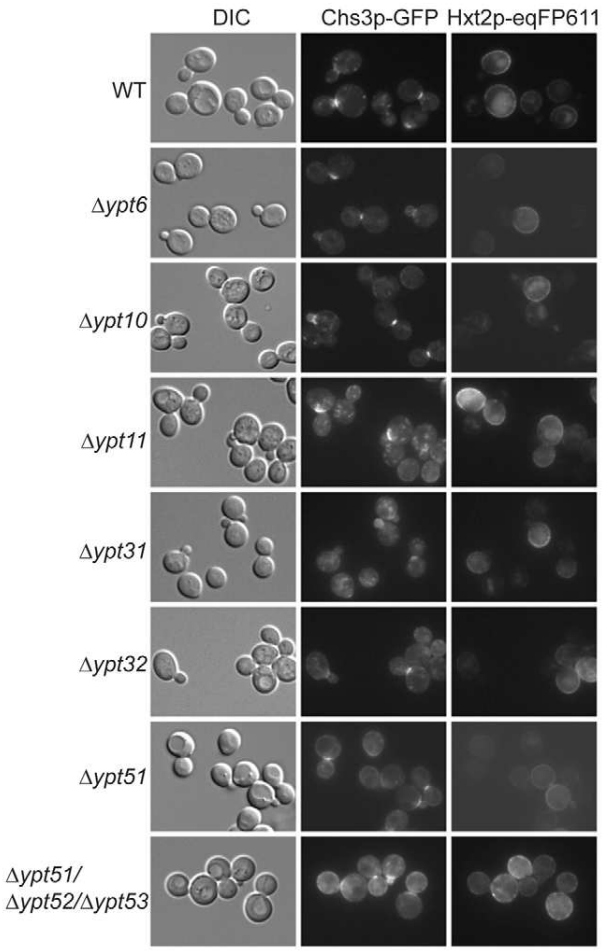

Fig. 7. Analysis of the effect of the deletion of the non-essential Rab proteins on Chs3p and Hxt2p transport. Various Rab genes were deleted in a strain in which Chs3p–GFP and Hxt2p–eqFP611 were expressed. The effect of loss of the Rab proteins on plasma membrane traffic of the markers was assessed after growth of the cells to log phase at 30°C.

Ypt31p localizes to the incipient bud site and to small-budded cells (Jedd et al., 1997), indicating that it might be involved in Chs3p trafficking early in the cell cycle, and that this function could be independent of the function of Ypt31p at the Golgi.

Interestingly, deletion of the lethal giant larva homologue Sro7p specifically interfered with transport of Chs3p to the plasma membrane. Sro77p, which is 54% identical to Sro7p did not have a significant role in transport of either Chs3p or Hxt2p to the plasma membrane. However, simultaneous loss of *SRO7* and *SRO77* resulted in accumulation of both cargoes in internal structures. Although transport to the plasma membrane seems to be heavily impaired, and the double mutant has severe growth defects, *Δsro7 Δsro77* cells still survive. Thus, a Sro7/Sro77p-independent pathway to the plasma membrane must exist. The existence of such a pathway is illustrated by our finding that Hxt2p reaches the plasma membrane efficiently after shift from high to low glucose, which induces Hxt2p expression at the plasma membrane.

The only other implication of Sro7p in the fusion of the specific carriers comes from its initial identification: Sro7p is required for

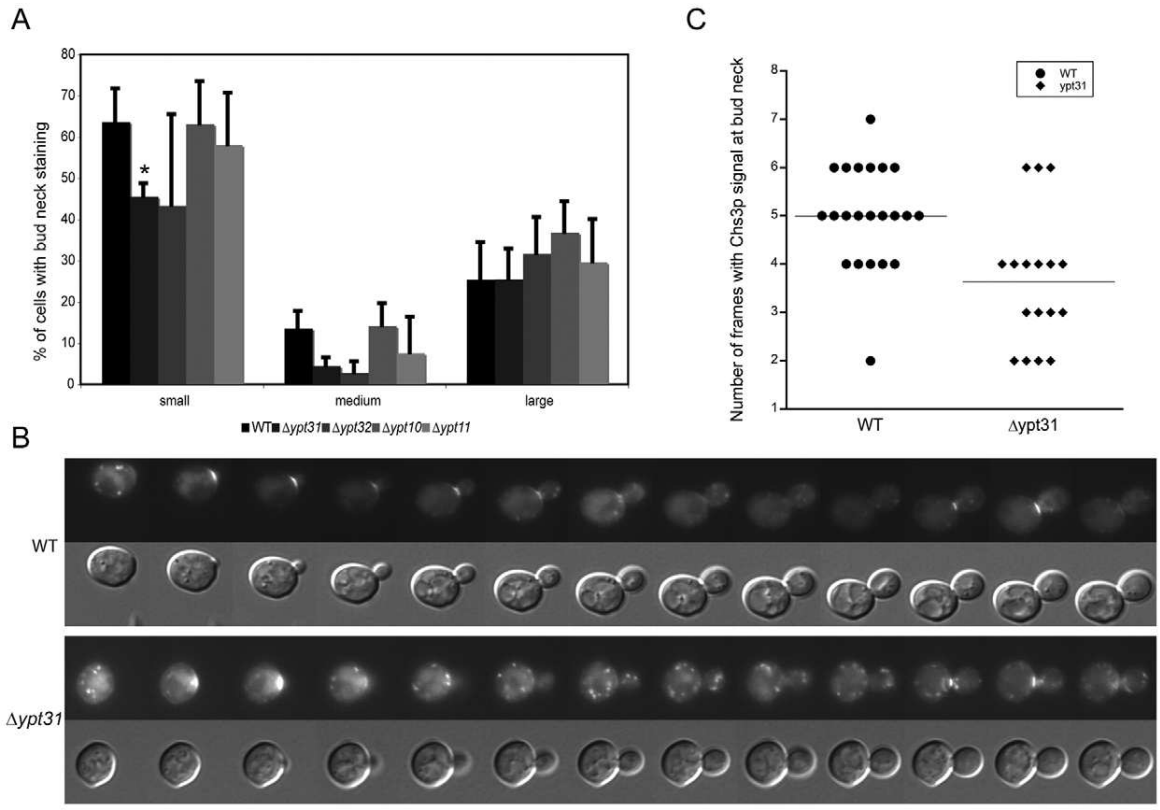

Fig. 8. The residence time of Chs3p–GFP is reduced in the bud neck of small-budded but not large-budded *Δypt31* cells. (**A**) Several *Δrab* strains were grown to log phase and the bud neck localization of Chs3p–GFP was determined in small-, medium- and large-budded cells. Deletion of *YPT31* caused a significant ($P<0.01$; Student's *t*-test) reduction of Chs3p–GFP bud-neck localization specifically in small-budded cells. (**B**) The drop in bud-neck localization in *Δypt31* is due to a shortened residence time of Chs3p at the bud neck. Time-lapse recording of a wild-type cell and a *Δypt31* cell. Although the initial transport of Chs3p–GFP was unaffected, the Chs3p–GFP signal disappears faster from the bud-neck region in *Δypt31* cells. The pictures were taken in 10 minute time intervals. (**C**) Quantification of the effect in B from 22 wild-type and 17 *Δypt31* individual recordings. The difference is statistically significant at $P<0.01$ (Mann-Whitney-U-Test, two-tailed).

the plasma membrane localization of the sodium transporter Ena1p under high-salt stress (Larsson et al., 1998; Wadskog et al., 2006). Our findings, however, show a differential requirement under normal growth conditions. The effect of mislocalization of Chs3p–GFP was more pronounced in large-budded than in small-budded cells. This result reinforces the notion that bud neck localization of Chs3p is governed, at least in part, by different factors during the cell cycle. In addition, it also points to a possible role of exomer-dependent transport in polarity maintenance. The metazoan homologue of Sro7p LGL has been shown to be required for epithelial polarity, and loss of function resulted in epithelial–mesenchymal transition, a key event in metastatic formation of tumors (Reischauer et al., 2009).

Another metazoan homologue, tomosyn, appears to negatively regulate vesicle exocytosis in several systems by regulating the formation of the SNARE complex. By contrast, deletion of *SRO7* led to an accumulation of vesicles containing Chs3p, but not Hxt2p, indicating that formation of SNARE complexes might be impaired in *Δsro7* cells. Our findings are in agreement with a recent report showing that Sro7p promotes SNARE complex assembly (Williams and Novick, 2009). It remains unclear why the vesicle fusion defect in *Δsro7* cells was much more pronounced late in the cell cycle compared with early stages of bud emergence. One possible explanation is that the bud neck is differently organized in small-budded versus large-budded cells (McMurray and Thorner, 2009). During mitosis, the septin collar is split into two rings, one in the mother cell and one in the daughter cell. Chs3p-containing vesicles will have to fuse in between these two rings to synthesize chitin for cytokinesis, whereas most cargo could fuse to either side, and the precise targeting might be not so important. Thus, one of the functions of Sro7p could be to ensure the correct fusion of Chs3p-containing vesicles. This precise targeting might be less important in G1, when the old septin ring from the previous cytokinesis is removed and only one new septin ring is assembled at the emerging bud, which is then transformed in an ordered array, referred to as the septin collar.

Our data suggest that more pathways exist than those previously established for low- and high-density vesicles. The population of low-density vesicles probably consists of several subclasses, one of which is involved in Chs3p transport to the bud neck. A recent report demonstrated the segregation of sphingolipids and sterol during secretory transport vesicle formation (Klemm et al., 2009). However, deletion of two key components in sphingolipid biosynthesis, *ELO3* and *SUR2*, did not differentially affect trafficking of Hxt2p and Chs3p, indicating that sphingolipids would not act as a sorting determinant in our paradigm (Table 1). We cannot exclude the possibility that Hxt2p and Chs3p travel in the same type of vesicles, and sorting at the TGN is the crucial step.

This type of regulation is not unprecedented because different types of COPII vesicles exist, which only can be distinguished by the cargo they transport. For example GPI-anchored proteins are sorted away from other cargo at the ER, but still exit using the COPII machinery (Muniz et al., 2001; Muniz et al., 2000). Moreover, COPI vesicles bud at different levels of the Golgi and hence must also contain different cargo proteins. The finding that only a subset of cargo is misrouted in cells with compromised Golgi function (Kamena et al., 2008) is also consistent with this notion.

Taken together, our results suggest that cargo is sorted in different low-density transport containers at the TGN, and that the fate of a subset of these containers might be regulated differently depending on the cell-cycle state.

Materials and Methods

Yeast methods and antibodies

Standard genetic techniques and media were used throughout (Sherman, 1991). Chromosomal tagging and deletions were performed as described (Gueldener et al., 2002; Janke et al., 2004; Knop et al., 1999). For the chromosomal 3×GFP fusions, we used the template plasmid pYM-3×GFP–TRP1. To construct the template plasmid, 3×GFP along with TRP1 was amplified from plasmid pBS-3×GFP–TRP1 (a gift from John A. Cooper, Washington University, St Louis, MO) and cloned into a pYM7 backbone digested with *Bam*HI–*Sac*I. The Chs3p-2×GFP strain used throughout this study was recovered by a spontaneous loss of one copy of GFP during the homologous recombination. Since we used YPH500/YPH499 as background for all experiments, we introduced mutations either by allelic replacement or through crosses. *sec6-4* and *sec4-8* were cloned into pRS406 (Sikorski and Hieter, 1989) using *Xma*I–*Sac*II. The plasmids were digested with *Bcl*I and transformed into yeast. Positive colonies were subjected to selection on 5-FOA, and temperature-sensitive mutants were used for further analysis. *sec5-24* and *sec10-2* were amplified from strains generously provided by Wei Guo (University of Pennsylvania, PA) and cloned into pRS304 using *Bam*HI and *Not*I. The plasmids were cut with *Nco*I and *Bsr*GI and transformed into yeast. Positive clones were selected on 5-FAA, and temperature-sensitive mutants were used for further analysis. The *exo84-117* mutant strain was constructed by transforming pRS315-*exo84-117* (pGS99; a gift from Wei Guo) into YPH499 and the chromosomal *EXO84* was deleted as described above. The strains used in this study are listed in supplementary material Table S1. The plasmids expressing CPY–GFP, Pma1–GFP and GFP–Cwp2 were generous gifts from Olivier Deloche (University of Geneva, Switzerland), Aaron Neiman (Stony Brook, NY) and Howard Riezman (University of Geneva, Switzerland), respectively. Antibodies against Chs3p and Pma1p have been described earlier (Serrano et al., 1986; Trautwein et al., 2006).

Wide-field microscopy of yeast strains

Strains were grown in YPAD to early to mid-log phase at 23°C or 30°C and shifted to 37°C for various times where indicated. Strains containing a plasmid were grown O/N in HC-URA at 23°C or 30°C, diluted in YPAD and grown for another 4–6 hours at either 23°C or 30°C. Itr1p–GFP strains were grown overnight and diluted in HC complete medium to allow for Itr1p sorting to the plasma membrane. For pulse–chase experiments, strains were grown overnight and diluted in YPAD, grown for 4–6 hours, then harvested and resuspended in HC medium. Cells were harvested by low-speed centrifugation, resuspended in a small volume of HC-complete medium, and an aliquot was spread on a microscope slide. The cells were inspected immediately on an Axioplan 2 microscope equipped with a Axio Cam MRm camera (Carl Zeiss, Aalen Oberkochen, Germany) and a Plan Apochromat 63×/1.40 objective. Axiovision 3.1 software was used to control hardware and to acquire and to process images.

For quantitative analysis, random fields of cells were selected in the DIC channel and pictures were taken in the DIC, GFP and eqFP611 channels. On the DIC image, the cells were classified into small-, medium- and large-budded cells, and then the localization of Chs3p–GFP in the bud neck was scored accordingly using images of the GFP channel.

For time-lapse analysis, cells were mounted onto agarose pads. Images were acquired every 10 minutes at 30°C. Cells were kept in focus by controlling the focal plane either manually or by using the autofocus option in the Axiovision software. The temperature of the slide was controlled using a thermo-controlled stage.

FRAP experiments

Cells were grown on YPD plates, resuspended in liquid non-fluorescent medium and immobilized on non-fluorescent medium (Waddle et al., 1996) containing 1.6% agarose. Imaging was performed on a Zeiss 510 confocal microscope using a Plan-Apochromat 100× objective at room temperature. Fluorescent molecules in the bleaching regions were photobleached. Bleaching regions were irradiated with 250 iterations of 50% laser intensity at 30% output of an argon laser (488 nm) and scans were collected with typically 1% laser intensity under the same condition. Scans were performed before, immediately after and 10 minutes after the bleach.

Gradient separation of secretory vesicles

Strains were precultured in YPD or YP 1% raffinose 1% galactose (YP-GAL). The preculture was then used to inoculate larger cultures in YPD or YP-GAL. For GAL shut-off, strains were grown for 13 hours at 30°C in YPD to reach an OD_{600} of about 0.5. The equivalent of 10 OD_{600} was harvested, resuspended in 200 µl of 10% sucrose (w/w), 20 mM triethanolamine pH 7.2, 1 mM EDTA, 1 mM PMSF, and subjected to glass bead lysis. The lysate was centrifuged at 13,000 ***g*** and 4°C for 6 minutes, and 30 µl of the supernatant was loaded on a 35–60% sucrose step gradient. The gradient was developed by centrifugation for 1 hour at 4°C and 75,000 r.p.m. in a TLA100 rotor (Beckman-Coulter, Krefeld, Germany). Twenty µl fractions were collected from the top and analyzed by immunoblot.

We thank A. Reyes, C. Roncero, J. A. Cooper, O. Deloche, W. Guo, A. Nieman, H. Riezman and R. Schekman for strains and plasmids. Present and past members of the Spang lab are acknowledged for thoughtful discussions and comments. This work was supported by Swiss National Science Foundation, the University of Basel and the ETH Zürich.

Supplementary material available online at
http://jcs.biologists.org/cgi/content/full/124/7/1055/DC1

References

Adamo, J. E., Moskow, J. J., Gladfelter, A. S., Viterbo, D., Lew, D. J. and Brennwald, P. J. (2001). Yeast Cdc42 functions at a late step in exocytosis, specifically during polarized growth of the emerging bud. *J. Cell Biol.* **155**, 581-592.

Bagnat, M. and Simons, K. (2002). Cell surface polarization during yeast mating. *Proc. Natl. Acad. Sci. USA* **99**, 14183-14188.

Barfield, R. M., Fromme, J. C. and Schekman, R. (2009). The exomer coat complex transports Fus1p to the plasma membrane via a novel plasma membrane sorting signal in yeast. *Mol. Biol. Cell* **20**, 4985-4996.

Chuang, J. S. and Schekman, R. W. (1996). Differential trafficking and timed localization of two chitin synthase proteins, Chs2p and Chs3p. *J. Cell Biol.* **135**, 597-610.

DeMarini, D. J., Adams, A. E., Fares, H., De Virgilio, C., Valle, G., Chuang, J. S. and Pringle, J. R. (1997). A septin-based hierarchy of proteins required for localized deposition of chitin in the Saccharomyces cerevisiae cell wall. *J. Cell Biol.* **139**, 75-93.

Gueldener, U., Heinisch, J., Koehler, G. J., Voss, D. and Hegemann, J. H. (2002). A second set of loxP marker cassettes for Cre-mediated multiple gene knockouts in budding yeast. *Nucleic Acids Res.* **30**, e23.

Guo, W., Roth, D., Walch-Solimena, C. and Novick, P. (1999). The exocyst is an effector for Sec4p, targeting secretory vesicles to sites of exocytosis. *EMBO J.* **18**, 1071-1080.

Gurunathan, S., David, D. and Gerst, J. E. (2002). Dynamin and clathrin are required for the biogenesis of a distinct class of secretory vesicles in yeast. *EMBO J.* **21**, 602-614.

Harsay, E. and Bretscher, A. (1995). Parallel secretory pathways to the cell surface in yeast. *J. Cell Biol.* **131**, 297-310.

Harsay, E. and Schekman, R. (2002). A subset of yeast vacuolar protein sorting mutants is blocked in one branch of the exocytic pathway. *J. Cell Biol.* **156**, 271-285.

Janke, C., Magiera, M. M., Rathfelder, N., Taxis, C., Reber, S., Maekawa, H., Moreno-Borchart, A., Doenges, G., Schwob, E., Schiebel, E. et al. (2004). A versatile toolbox for PCR-based tagging of yeast genes: new fluorescent proteins, more markers and promoter substitution cassettes. *Yeast* **21**, 947-962.

Jedd, G., Mulholland, J. and Segev, N. (1997). Two new Ypt GTPases are required for exit from the yeast trans-Golgi compartment. *J. Cell Biol.* **137**, 563-580.

Kamena, F., Diefenbacher, M., Kilchert, C., Schwarz, H. and Spang, A. (2008). Ypt1p is essential for retrograde Golgi-ER transport and for Golgi maintenance in S. cerevisiae. *J. Cell Sci.* **121**, 1293-1302.

Klemm, R. W., Ejsing, C. S., Surma, M. A., Kaiser, H. J., Gerl, M. J., Sampaio, J. L., de Robillard, Q., Ferguson, C., Proszynski, T. J., Shevchenko, A. et al. (2009). Segregation of sphingolipids and sterols during formation of secretory vesicles at the trans-Golgi network. *J. Cell Biol.* **185**, 601-612.

Knop, M., Siegers, K., Pereira, G., Zachariae, W., Winsor, B., Nasmyth, K. and Schiebel, E. (1999). Epitope tagging of yeast genes using a PCR-based strategy: more tags and improved practical routines. *Yeast* **15**, 963-972.

Kruckeberg, A. L., Ye, L., Berden, J. A. and van Dam, K. (1999). Functional expression, quantification and cellular localization of the Hxt2 hexose transporter of Saccharomyces cerevisiae tagged with the green fluorescent protein. *Biochem. J.* **339**, 299-307.

Larsson, K., Bohl, F., Sjostrom, I., Akhtar, N., Strand, D., Mechler, B. M., Grabowski, R. and Adler, L. (1998). The Saccharomyces cerevisiae SOP1 and SOP2 genes, which act in cation homeostasis, can be functionally substituted by the Drosophila lethal(2)giant larvae tumor suppressor gene. *J. Biol. Chem.* **273**, 33610-33618.

Matsuoka, K., Orci, L., Amherdt, M., Bednarek, S. Y., Hamamoto, S., Schekman, R. and Yeung, T. (1998). COPII-coated vesicle formation reconstituted with purified coat proteins and chemically defined liposomes. *Cell* **93**, 263-275.

McMurray, M. A. and Thorner, J. (2009). Septins: molecular partitioning and the generation of cellular asymmetry. *Cell Div.* **4**, 18.

Miyashita, M., Shugyo, M. and Nikawa, J. (2003). Mutational analysis and localization of the inositol transporters of Saccharomyces cerevisiae. *J. Biosci. Bioeng.* **96**, 291-297.

Muniz, M., Nuoffer, C., Hauri, H. P. and Riezman, H. (2000). The Emp24 complex recruits a specific cargo molecule into endoplasmic reticulum-derived vesicles. *J. Cell Biol.* **148**, 925-930.

Muniz, M., Morsomme, P. and Riezman, H. (2001). Protein sorting upon exit from the endoplasmic reticulum. *Cell* **104**, 313-320.

Ni, L. and Snyder, M. (2001). A genomic study of the bipolar bud site selection pattern in Saccharomyces cerevisiae. *Mol. Biol. Cell* **12**, 2147-2170.

Raths, S., Rohrer, J., Crausaz, F. and Riezman, H. (1993). end3 and end4: two mutants defective in receptor-mediated and fluid-phase endocytosis in Saccharomyces cerevisiae. *J. Cell Biol.* **120**, 55-65.

Reischauer, S., Levesque, M. P., Nusslein-Volhard, C. and Sonawane, M. (2009). Lgl2 executes its function as a tumor suppressor by regulating ErbB signaling in the zebrafish epidermis. *PLoS Genet.* **5**, e1000720.

Saksena, S., Wahlman, J., Teis, D., Johnson, A. E. and Emr, S. D. (2009). Functional reconstitution of ESCRT-III assembly and disassembly. *Cell* **136**, 97-109.

Sanchatjate, S. and Schekman, R. (2006). Chs5/6 complex: a multiprotein complex that interacts with and conveys chitin synthase III from the trans-Golgi network to the cell surface. *Mol. Biol. Cell* **17**, 4157-4166.

Serrano, R., Kielland-Brandt, M. C. and Fink, G. R. (1986). Yeast plasma membrane ATPase is essential for growth and has homology with (Na+ + K+), K+- and Ca2+-ATPases. *Nature* **319**, 689-693.

Sherman, F. (1991). Getting started with yeast. *Methods Enzymol.* **194**, 3-21.

Sikorski, R. S. and Hieter, P. (1989). A system of shuttle vectors and yeast host strains designed for efficient manipulation of DNA in Saccharomyces cerevisiae. *Genetics* **122**, 19-27.

Singer-Kruger, B., Stenmark, H., Dusterhoft, A., Philippsen, P., Yoo, J. S., Gallwitz, D. and Zerial, M. (1994). Role of three rab5-like GTPases, Ypt51p, Ypt52p, and Ypt53p, in the endocytic and vacuolar protein sorting pathways of yeast. *J. Cell Biol.* **125**, 283-298.

Spang, A., Matsuoka, K., Hamamoto, S., Schekman, R. and Orci, L. (1998). Coatomer, Arf1p, and nucleotide are required to bud coat protein complex I-coated vesicles from large synthetic liposomes. *Proc. Natl. Acad. Sci. USA* **95**, 11199-11204.

TerBush, D. R. and Novick, P. (1995). Sec6, Sec8, and Sec15 are components of a multisubunit complex which localizes to small bud tips in Saccharomyces cerevisiae. *J. Cell Biol.* **130**, 299-312.

TerBush, D. R., Maurice, T., Roth, D. and Novick, P. (1996). The exocyst is a multiprotein complex required for exocytosis in Saccharomyces cerevisiae. *EMBO J.* **15**, 6483-6494.

Trautwein, M., Schindler, C., Gauss, R., Dengjel, J., Hartmann, E. and Spang, A. (2006). Arf1p, Chs5p and the ChAPs are required for export of specialized cargo from the Golgi. *EMBO J.* **25**, 943-954.

Valdez-Taubas, J. and Pelham, H. (2005). Swf1-dependent palmitoylation of the SNARE Tlg1 prevents its ubiquitination and degradation. *EMBO J.* **24**, 2524-2532.

Valdivia, R. H. and Schekman, R. (2003). The yeasts Rho1p and Pkc1p regulate the transport of chitin synthase III (Chs3p) from internal stores to the plasma membrane. *Proc. Natl. Acad. Sci. USA* **100**, 10287-10292.

Valdivia, R. H., Baggott, D., Chuang, J. S. and Schekman, R. W. (2002). The yeast clathrin adaptor protein complex 1 is required for the efficient retention of a subset of late Golgi membrane proteins. *Dev. Cell* **2**, 283-294.

Waddle, J. A., Karpova, T. S., Waterston, R. H. and Cooper, J. A. (1996). Movement of cortical actin patches in yeast. *J. Cell Biol.* **132**, 861-870.

Wadskog, I., Forsmark, A., Rossi, G., Konopka, C., Oyen, M., Goksor, M., Ronne, H., Brennwald, P. and Adler, L. (2006). The yeast tumor suppressor homologue Sro7p is required for targeting of the sodium pumping ATPase to the cell surface. *Mol. Biol. Cell* **17**, 4988-5003.

Wang, C. W., Hamamoto, S., Orci, L. and Schekman, R. (2006). Exomer: a coat complex for transport of select membrane proteins from the trans-Golgi network to the plasma membrane in yeast. *J. Cell Biol.* **174**, 973-983.

Wiedenmann, J., Schenk, A., Rocker, C., Girod, A., Spindler, K. D. and Nienhaus, G. U. (2002). A far-red fluorescent protein with fast maturation and reduced oligomerization tendency from *Entacmaea quadricolor* (Anthozoa, Actinaria). *Proc. Natl. Acad. Sci. USA* **99**, 11646-11651.

Williams, D. C. and Novick, P. J. (2009). Analysis of SEC9 suppression reveals a relationship of SNARE function to cell physiology. *PLoS One* **4**, e5449.

Ziman, M., Chuang, J. S. and Schekman, R. W. (1996). Chs1p and Chs3p, two proteins involved in chitin synthesis, populate a compartment of the Saccharomyces cerevisiae endocytic pathway. *Mol. Biol. Cell* **7**, 1909-1919.

5.1. Supplementary figures

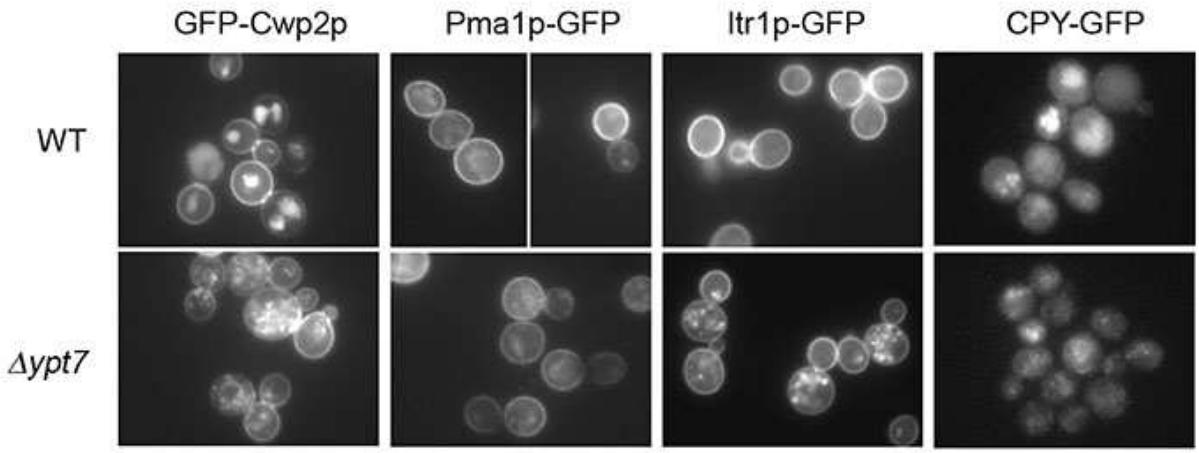

Fig. S1. Plasma membrane appearance of Cwp2, Pma1p and Itr1p is not impaired in *Δypt7* cells. The localization of GFP–Cwp2p, Pma1p–GFP. Itr1p–GFP and CPY–GFP was analyzed in logarithmically growing cells. In *Δypt7* cells, the transport of the vacuolar protein CPY was strongly affected, whereas the plasma membrane appearance of the other cargoes remained unchanged.

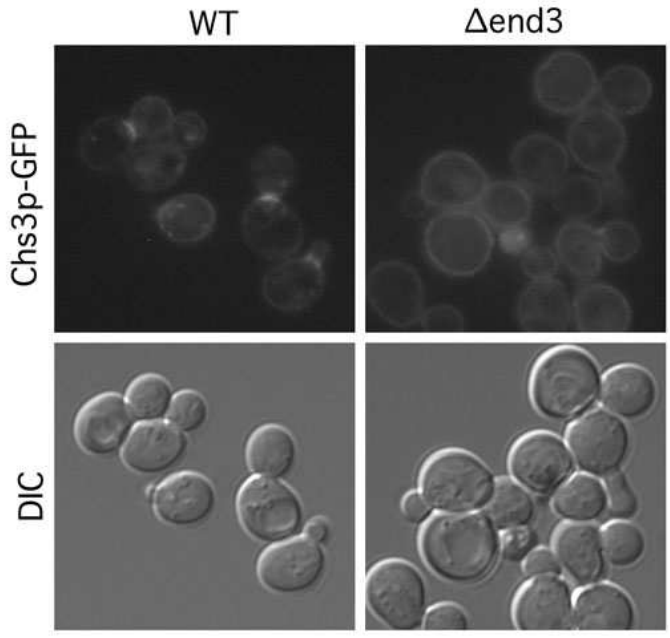

Fig. S2 Chs3p is not endocytosed in *Δend3* cells. Loss of *END3* causes Chs3p–GFP to be stuck at the plasma membrane. Note, that also the restricted localization to the bud neck is lost under these conditions.

Chapter 6

Cargo recognition by the ChAPs family

6. Making contact for specificity: The exomer complex has a three-dimensional cargo recognition domain

Uli Rockenbauch[*], Carlos Sacristan[†], Cesar Roncero[†] and Anne Spang[*‡]

[*]Biozentrum, Universität Basel, Klingelbergstrasse 70, 4056 Basel, Switzerland

[†]Instituto de Biología Funcional and Departamento de Microbiología y Genética, CSIC/Universidad de Salamanca, Salamanca, Spain.

[‡]Author for correspondence:
Anne Spang
Biozentrum, Universität Basel
Klingelbergstrasse 70
4056 Basel, Switzerland

Email: anne.spang@unibas.ch

Running Head: Cargo recognition by the ChAPs family

The following manuscript was submitted to *Molecular Biology of the Cell* and was under consideration at the time of submission of this thesis. The above authors have contributed to the manuscript as follows:

Uli Rockenbauch performed the experiments in Fig. 6.1 – 6.7, performed the pulldowns in Fig. 6.8 and wrote the manuscript together with Anne Spang.

Carlos Sacristan performed the initial experiments on the C-terminal truncations of Chs3p (Fig. 6.8, A and B)

Cesar Roncero provided critical comments on the manuscript.

Anne Spang supervised the experiments and wrote the manuscript together with U.R.

6.1. Abstract

The exomer complex is a putative vesicle coat required for the direct transport of a subset of cargoes from the trans-Golgi network (TGN) to the plasma membrane. Exomer comprises Chs5p as well as the ChAPs family of proteins (Chs6p, Bud7p, Bch1p and Bch2p), which are thought to act as cargo receptors. However, how the ChAPs associate with Chs5p and recognize cargo is not well understood. Here, we show that the ChAPs contain five conserved and functionally essential tetratricopeptide repeats (TPRs). These TPRs are interchangeable between the ChAP paralogues and form a structural backbone, which mediates Chs5p binding and provides stability to the exomer-cargo complex at the TGN. Using domain-switch chimeras of Chs6p and Bch2p, we determined the region that conveys cargo specificity to the ChAPs. Unlike the major coat complexes, which bind linear sorting motifs through small, folded domains, the ChAPs recognize cargoes using large polypeptide stretches distributed all over their sequence. This surprising finding suggests that ChAPs display an extensive, three-dimensional cargo recognition surface and thus provide a novel paradigm in protein sorting.

6.2. Introduction

The trans-Golgi network (TGN) is the central sorting station for exocytic and endocytic cargoes. In the yeast *Saccharomyces cerevisiae*, several sorting machineries and vesicular carriers operate along at least two routes to the cell surface, marked by high-density or low-density secretory vesicles (Harsay and Bretscher, 1995; Harsay and Schekman, 2002; Bard and Malhotra, 2006). Additionally, a subset of cargoes travels directly to the plasma membrane in low-density carriers requiring the exomer complex. This complex is a potential coat complex formed by the peripheral Golgi protein Chs5p and a protein family termed ChAPs, for "Chs5p and Arf1 binding proteins". In budding yeast, this family includes the paralogues Chs6p, Bud7p, Bch1p, and Bch2p (Ziman *et al.*, 1998; Sanchatjate and Schekman, 2006; Trautwein *et al.*, 2006; Wang *et al.*, 2006). Chs5p and the ChAPs are recruited from the cytosol to the TGN membrane by the small GTPase Arf1p. Together, they facilitate the incorporation of specific transmembrane cargoes into secretory vesicles (Trautwein *et al.*, 2006; Wang *et al.*, 2006).

Some specialized cargoes such as chitin synthase III (Chs3p) or Fus1p depend on exomer for their transport to the cell surface (Santos and Snyder, 1997; Ziman *et al.*, 1998; Barfield *et al.*, 2009). However, Chs3p and Fus1p do not share a common sorting motif, and the motif identified in Fus1p is also not transplantable (Barfield *et al.*, 2009). It is therefore likely that the exomer complex recognizes cargoes individually, perhaps in order to allow differential sorting. This provides an attractive model system for a protein trafficking pathway that is distinct from the major transport routes, allowing the cell to fine-tune the surface expression of cargoes depending on the cell cycle stage, or potentially also in response to the nutrient status and/or stress conditions.

The exomer components display a functional hierarchy: While individual ChAP deletions – or combinations thereof – lead to certain cellular defects, a deletion of *CHS5* collectively causes all ChAPs-associated defects (Trautwein *et al.*, 2006). Since these phenotypes are most likely due to the inability of specific cargoes to leave the TGN, this places Chs5p functionally upstream of the ChAPs. For example, *Δchs6* cells cannot export Chs3p and thus have chitin synthesis defects, while *Δbch1* cells are sensitive to ammonium (Trautwein *et al.*, 2006). Accordingly, cells lacking *CHS5* are both chitin-deficient and ammonium-sensitive. Interestingly, Chs3p export is also blocked when *BCH1* and *BUD7* are simultaneously deleted, suggesting that the ChAPs have partially overlapping functions. Alternatively, the ChAPs may also play a structural role in exomer complex assembly.

Chs5p requires activated Arf1p for TGN recruitment, while the ChAPs require both Chs5p and Arf1p, reflecting the functional hierarchy. The ChAPs do not co-precipitate in the absence of Chs5p, suggesting that they do not directly bind to each other (Sanchatjate and Schekman, 2006; Trautwein

et al., 2006). How Chs5p and the ChAPs associate into a complex has not been investigated in detail. Because of their association with distinct cargoes, it is believed that the ChAPs act as soluble receptors for transmembrane cargoes. However, their mode of cargo recognition has not been characterized.

In this study, we found that the ChAP family members contain five essential tetratricopeptide repeats (TPRs): While TPR5 appears to play a structural role in Chs6p function, TPRs 1-4 mediate Chs5p binding. The TPRs are all interchangeable between the ChAPs, thus forming a structural backbone. Importantly, we found that cargo specificity is conveyed by large sequence stretches that are likely to be distributed all over the protein surface. In contrast to the major eukaryotic coat complexes that bind their cargoes through small, folded domains, the ChAPs may thus harbor an extensive, three-dimensional interaction surface and utilize a novel mechanism to recognize specific target proteins.

6.3. Results

6.3.1. The ChAPs contain tetratricopeptide repeats

The ChAPs appear to interact directly with exomer-dependent cargoes. To gain a better understanding how cargo recognition and the interaction with other exomer components is achieved, we decided to examine the domain structure of the ChAPs. To this end, we performed a BLASTP search of the *S. cerevisiae* ChAP *CHS6* against other fungal genomes. The resulting alignment showed that particular stretches of the protein were highly conserved across species, while other sequences were more variable (Fig. S 6.1A). We expected the more conserved stretches to correspond to domains essential for function, while the sequences with a higher degree of variation might represent parts of the protein that are not involved in functions specific to the ChAPs family. Alternatively, those variable domains could be engaged in cargo recognition, since the cargoes studied thus far, Fus1p and Chs3p, do not share obvious motifs that are commonly recognized by all ChAPs (Barfield *et al.*, 2009).

To analyze the conserved regions in more detail, we used a number of different algorithms of the *Bioinformatics Toolkit* (http://toolkit.tuebingen.mpg.de) (Biegert *et al.*, 2006). Interestingly, the conserved regions contained tetratricopeptide repeats (TPRs) (Fig. 6.1A), four of which were clustered in the central region of Chs6p and a fifth one was located towards the C-terminus. The TPRs were conserved among the different *S. cerevisiae* ChAPs, indicating that they may represent a common feature of this protein family (Fig. 6.1A and Fig. S 6.1B). This hypothesis is supported by the

finding that automatic sequence annotation detected TPRs in ChAPs from *Kluyveromyces lactis*, *Ashbya gossypii*, and others (see e.g. http://www.ncbi.nlm.nih.gov/protein/CAG98421.1).

TPRs are highly versatile protein-protein interaction domains. Each repeat consists of a degenerate 34 amino acid motif, which exhibits a conserved helix-turn-helix fold and the ability to form clusters of multiple repeats (Blatch and Lassle, 1999; Zhang *et al.*, 2010). Interestingly, several cases of cargo recognition by TPRs have been described: Peroxin 5, which harbors a six-TPR tunnel recognizing the C-terminal "SKL" motif for peroxisomal import (Gatto *et al.*, 2000); Tom20, which facilitates mitochondrial import (Abe *et al.*, 2000), and kinesin light chain, which binds multiple cargoes via its TPR domain (Kamal *et al.*, 2000; Hammond *et al.*, 2008). Alternatively, TPRs can also have more structural roles, e.g. in the assembly of multiprotein complexes such as the COPI vesicle coat (Hsia and Hoelz, 2010) or the anaphase-promoting complex (APC) (Zhang *et al.*, 2010). Thus, finding TPRs in the ChAPs family members raised the possibility that these repeats would be of functional importance for the exomer complex.

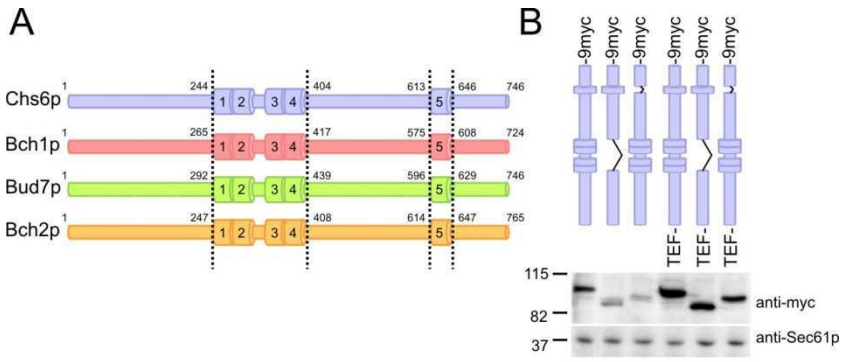

Fig. 6.1 Deletion of TPRs in ChAPs only mildly affects protein expression levels. (A) Domain structure of the ChAP family members. Numbers indicate the first and last amino acid of the TPR domains. The same coloring scheme is used in all subsequent figures. (B) Expression of 9myc-tagged TPR mutants of Chs6p, under the native and the TEF promoter. Immunoblot of yeast lysates; Sec61p serves as loading control. Note that all mutants were generated chromosomally.

6.3.2. The TPRs are essential for Chs6p function

Since TPRs are so versatile in function, they might serve several distinct purposes: As structural domains, as interaction modules for other exomer components, or as cargo recognition sites. To distinguish between these possibilities, we created two internal truncations in Chs6p: The first truncation, Chs6(ΔTPR1-4), lacked the entire central cluster of TPRs. In the second construct, Chs6(ΔTPR5), the last and most conserved repeat in the protein was deleted (Fig. 6.1A). The mutant proteins showed only a mild reduction in expression compared to wild-type, indicating that removing

one or more TPRs did not cause the protein to become significantly destabilized (Fig. 6.1B). The truncations did also not massively shorten the proteins: Removing TPR1-4 reduced the molecular weight by about 15 kDa, while eliminating TPR5 caused a 5 kDa reduction. Because the expression levels of the truncations were nevertheless consistently lower, we placed wild-type and mutant proteins under the control of the TEF promoter where indicated, ensuring that expression levels were comparable for all three constructs (Fig. 6.1B).

To assess the functionality of Chs6(ΔTPR1-4) and Chs6(ΔTPR5), we monitored the localization and activity of Chs3p, whose export depends on functional Chs6p. Both truncation mutants were unable to export Chs3p-2GFP from the TGN, as GFP staining was absent from the bud neck and Chs3p accumulated in intracellular structures, mimicking a *CHS6* deletion (Fig. 6.2A). Chs3p synthesizes a chitin ring around the yeast bud neck, which can be visualized by calcofluor staining (Lord *et al.*, 2002). The chitin ring was absent in *Δchs6*, Chs6(ΔTPR1-4) and Chs6(ΔTPR5). All three mutants were calcofluor-resistant, a hallmark of chitin synthesis-defective cells (Ziman *et al.*, 1998), demonstrating a lack of chitin synthase III activity at the plasma membrane (Fig. 6.2B).

The ChAPs are in complexes with Chs5p in varying stoichiometries. We were therefore wondering whether the truncations, when expressed together, could cross-complement and rescue the calcofluor-sensitivity. However, this was not the case, indicating that each Chs6p molecule must contain the full set of TPR motifs (Fig. 6.2B). In summary, these finding demonstrate that the TPRs of Chs6p are required for export of Chs3p from the TGN.

6.3.3. TPR function is conserved in the ChAPs

ChAPs share some degree of redundancy, indicated by the fact that some cellular phenotypes only arise upon deletion of multiple ChAPs (Trautwein *et al.*, 2006; Barfield *et al.*, 2009). For example, double deletion of *CHS6* and *BCH2* renders cells lithium-sensitive, a phenotype that could not be observed for either single deletion (Fig. 6.2C). This finding implicates Chs6p in the export of another – yet unidentified – cargo involved in lithium homeostasis.

We used this paradigm to test whether the TPRs in other ChAPs might be of equal importance for function. Indeed, Bch2(ΔTPR1-4 or ΔTPR5), combined with a *CHS6* deletion, also displayed the lithium-sensitivity phenotype (Fig. 6.2C). Moreover, we constructed analogous truncation mutants in Bch1p and tested these for ammonium-sensitivity, which is a characteristic phenotype of *Δbch1* cells (Trautwein *et al.*, 2006). In both cases, the TPR mutants behaved like the *BCH1* deletion (Fig. 6.2D), indicating that all ChAPs require their TPRs for functionality.

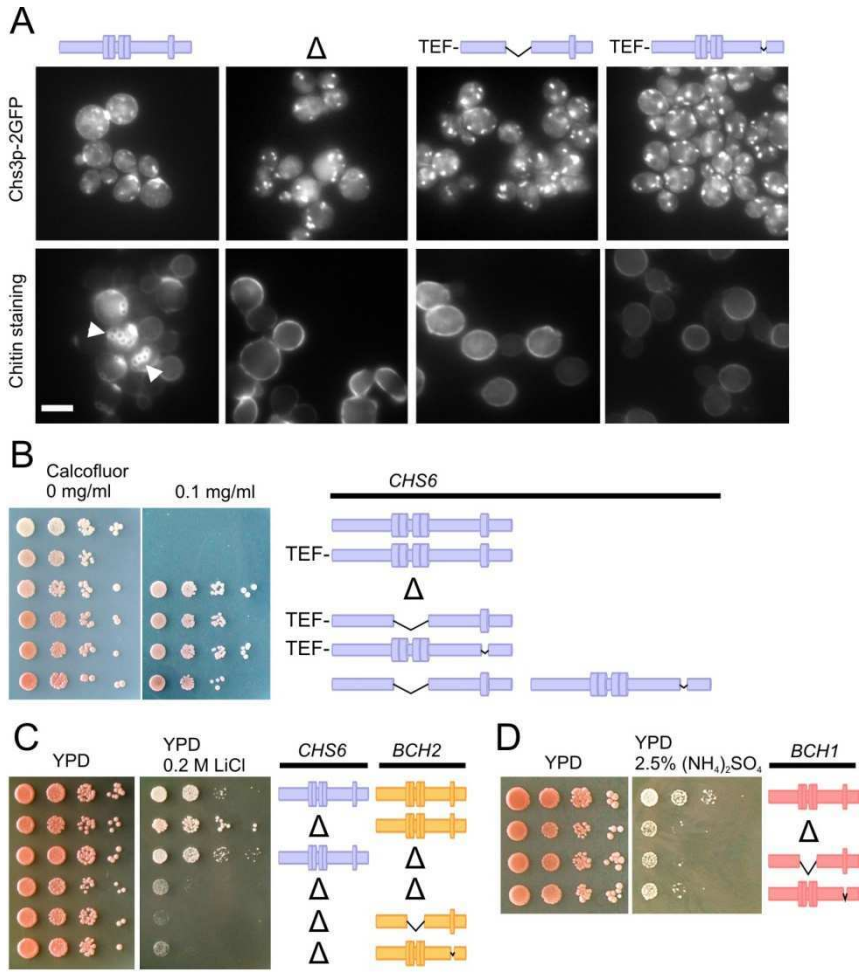

Fig. 6.2 The TPRs are essential for the function of the ChAPs. (A) Chs3p-2GFP localized exclusively to internal structures in *Δchs6*, Chs6(ΔTPR1-4) and Chs6(ΔTPR5) strains. Accordingly, while calcofluor-stained wild-type cells showed bud scar chitin staining (arrowheads), this was absent in the mutants. Scale bar: 5 µm. (B) Chs6(ΔTPR1-4) and Chs6(ΔTPR5) strains were resistant to calcofluor. This defect was as pronounced as for a *Δchs6* strain. The two mutant alleles showed not cross-complementation. Drop tests: Plates were incubated at 30°C for 2-3 days. Blue: Chs6p alleles. "Δ" refers to *Δchs6*. (C) Bch2p requires TPRs for functionality. A *CHS6* deletion in combination with a *Δbch2*, Bch2(ΔTPR1-4) or Bch2(ΔTPR5) allele led to lithium sensitivity. Drop tests were performed as above. Yellow: Bch2p alleles. "Δ" refers to *Δchs6* and *Δbch2*, respectively. (D) Bch1p requires TPRs for functionality. Bch1(ΔTPR1-4) and Bch1(ΔTPR5), like *Δbch1*, cells were sensitive to ammonium. Red: Bch1p alleles. "Δ" refers to *Δbch1*.

6.3.4. Chs6p requires its TPRs for efficient Golgi recruitment

The strong defect of the TPR mutants in cargo export could be explained by either impaired recruitment of the mutant proteins to the Golgi, or failure to form a productive exomer-cargo complex, or a combination of both. We therefore tested first whether the TPRs were required for Golgi association and determined the subcellular localization of the TPR mutants using differential centrifugation. Chs6(ΔTPR1-4)-9myc was more soluble, as the 100,000 g pellet, which contained the

Golgi membranes, was depleted of Chs6(ΔTPR1-4)-9myc (Fig. 6.3A), while the localization of Chs6(ΔTPR5)-9myc was not significantly distinct from the wild-type Chs6p-9myc distribution.

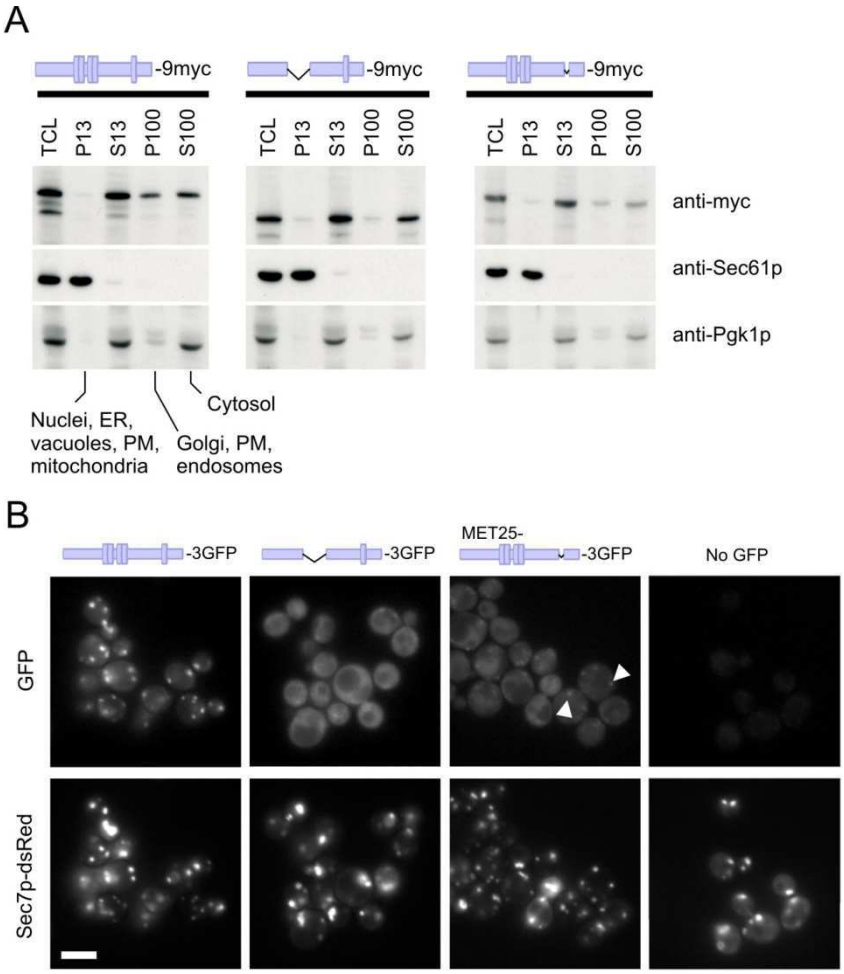

Fig. 6.3 Chs6(ΔTPR1-4) and Chs6(ΔTPR5) cannot be efficiently recruited to the Golgi. (A) Chs6(ΔTPR1-4)-9myc displays strongly reduced membrane association in cell lysates. Ten OD600 cells were lysed with glass beads, lysates were cleared of unbroken cells and subjected to differential centrifugation at 4°C. TCL, total cell lysate; S13, 13,000 g supernatant; P13, 13,000 g pellet; S100, 100,000 g supernatant; P100, 100,000 g pellet; PM, plasma membrane. All constructs were chromosomally expressed under the native *CHS6* promoter. (B) TPR mutants show inefficient Golgi localization *in vivo*. Chs6p-3GFP and Chs6(ΔTPR1-4)-3GFP were chromosomally expressed under the native *CHS6* promoter. Chs6(ΔTPR1-4)-3GFP was almost entirely cytoplasmic and showed no association with Golgi membranes. Chs6(ΔTPR5)-3GFP, expressed at a level similar to wild-type Chs6p using an inducible methionine promoter, was partially Golgi-localized (arrowheads). Scale bar: 5 µm.

To corroborate our findings, we also monitored the localization of the truncation mutants by live imaging. A 3xGFP-tagged version of wild-type Chs6p mostly localized to punctate structures, which overlapped with the TGN marker Sec7p-dsRed (Fig. 6.3B). Consistent with previous reports, some Chs6p-3GFP was also found in the cytoplasm (Ziman *et al.*, 1998; Trautwein *et al.*, 2006).

Interestingly, *in vivo*, both Chs6(ΔTPR1-4)-3GFP and Chs6(ΔTPR5)-3GFP were not efficiently recruited to the TGN: Chs6(ΔTPR1-4)-3GFP was found almost entirely in the cytoplasm, confirming the subcellular fractionation experiments (Fig. 6.3B). Consistent with the fractionation experiments, some Chs6(ΔTPR5) was present at the TGN, but the *in vivo* recruitment seemed to be less efficient for Chs6(ΔTPR5) than for wild-type Chs6p. Thus, all five TPRs contribute to efficient Golgi recruitment, whereby TPRs 1-4 seem to play a more predominant role.

6.3.5. The TPRs are dispensable for cargo binding

Next, we tested the second possibility, the failure of the TPR mutants to assemble a functional exomer-cargo complex. We first concentrated on the direct interaction of Chs6p and its cargo Chs3p. Since Chs3p is a polytopic membrane protein, we chose the split ubiquitin approach to detect the interaction *in vivo* (Johnsson and Varshavsky, 1994): Chs6p, Chs6(ΔTPR1-4) and Chs6(ΔTPR5) were expressed as fusion constructs with the N-terminal half of ubiquitin (Nub), and Chs3p or an unrelated protein (Ste14p) as fusions with the C-terminal half (Cub) and a reporter protein (Ura3p). The functionality of the Nub-Chs6p and Chs3p-Cub-Ura3 constructs was confirmed by complementation of the respective *Δchs6* and *Δchs3* mutations (data not shown). In this assay, a stable interaction between the two proteins of interest results in the formation of a full-length ubiquitin molecule, its cleavage by ubiquitin-specific proteases and subsequent degradation, including the reporter protein. Thus, the stronger the interaction, the less cells are able to grow on the selection medium. As a negative control, we used cells expressing Nub-Chs6p and Ste14p-Cub; these cells grew well on test plates, while cells expressing the well-characterized interactor pairs Nub-Sec22p/Arf1p-Cub and Nub-Chs6p/Chs5p-Cub grew slowly. The strain bearing Nub-Chs6p and Chs3p-Cub grew as slowly as the pair Chs6p/Chs5p (Fig. 6.4A), confirming previous interaction data (Sanchatjate and Schekman, 2006; Trautwein *et al.*, 2006; Wang *et al.*, 2006). Cells expressing Chs3p-Cub and Nub-Chs6(ΔTPR1-4) or Nub-Chs6(ΔTPR5) grew slightly but consistently faster than Chs3p-Cub/Nub-Chs6p, suggesting that both TPR mutants engaged in an exomer-cargo complex that was less stable compared to wild-type Chs6p. This result was in line with the live fluorescence data, which also suggested that Chs6(ΔTPR1-4) and Chs6(ΔTPR5) exhibited reduced Golgi association *in vivo* (Fig. 6.3B).

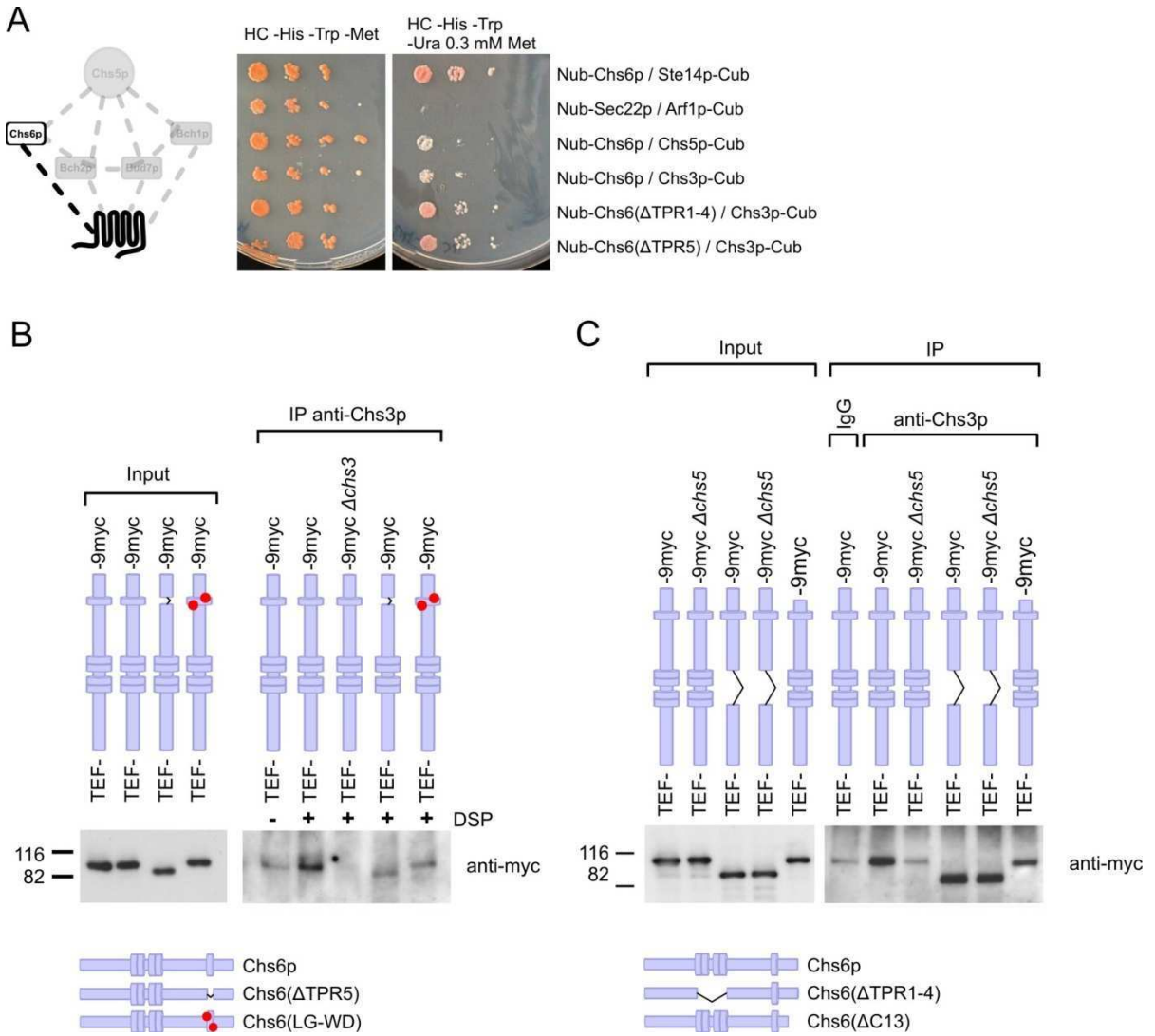

Fig. 6.4 TPRs are required for stable association with cargo *in vivo*, but dispensable for cargo binding *in vitro*. (A) Chs6(ΔTPR1-4) and Chs6(ΔTPR5) show reduced cargo interaction *in vivo*. Cells carrying plasmids encoding for fusion proteins of split ubiquitin (Nub and Cub) were assayed for growth on medium lacking uracil. Since the formation of a stable Nub-Cub complex leads to cleavage and degradation of the full-length ubiquitin-URA3 reporter molecule, reduced growth indicates an *in vivo* interaction of the two proteins of interest. The functionality of the assay was demonstrated using the pairs Chs6p/Ste14p (non-interacting) and Sec22p/Arf1p (interacting). Compared to wild-type Nub-Chs6p, both Nub-Chs6(ΔTPR1-4) and Nub-Chs6(ΔTPR5) showed a slightly but consistently reduced interaction with Chs3p-Cub. (B) Chs6(ΔTPR5) and Chs6(LG-WD) interact with cargo *in vitro*. Cargo interaction was assessed by precipitating Chs3p from DSP-crosslinked lysates and probing for the different Chs6p constructs. Chs6(ΔTPR5) and a double TPR5 point mutant Chs6(LG-WD) retained association with Chs3p. (C) Chs6(ΔTPR1-4) and Chs6(ΔC13) interact with cargo *in vitro*. A crosslinker IP was carried out as described in (B).

Nevertheless, the above experiment suggested that there was some degree of cargo association remaining in the TPR mutants. We therefore aimed to biochemically capture any interaction of Chs6p or the mutants with Chs3p. Since the binding reaction between a cargo and its cargo receptor is

usually transient (Appenzeller *et al.*, 1999; Muniz *et al.*, 2000; Zhang *et al.*, 2005), we employed a crosslinker-based immunoprecipitation approach, as published previously (Sanchatjate and Schekman, 2006; Trautwein *et al.*, 2006; Barfield *et al.*, 2009). Interestingly, both TPR mutants were still efficiently crosslinked to Chs3p (Fig. 6.4B and C), indicating that the actual cargo binding activity of Chs6p was not impaired in Chs6(ΔTPR1-4) or Chs6(ΔTPR5). We conclude that the TPR mutants could recognize cargo similarly to wild-type Chs6p. In addition, binding of Chs6(ΔTPR1-4) to Chs3p was even independent of Chs5p (Fig. 6.4C). However, the lack of Chs3p export suggests that no productive complex was formed, leading to rapid dissociation of the TPR mutants from the TGN.

The signal for Chs6(ΔTPR5) in the crosslinker IP appeared to be consistently weaker when the fifth TPR was missing. To corroborate this finding, we constructed a double point mutant, Chs6p-L619W/G620D (LG-WD), in which two critical residues of the TPR backbone were mutated (Magliery and Regan, 2004) but the protein was otherwise left intact. Again, we observed a reduction in the efficiency of the Chs3p-Chs6p interaction. Moreover, this mutant also caused Chs3p-2GFP to accumulate in the TGN (Fig. S 6.2). These results indicate that the TPR mutants can still be in close proximity to the cargo, but that in the case of Chs6(ΔTPR5) cargo recognition may be slightly impaired.

In a previous study, we had identified a truncation with similar features like the TPR mutants: removing the last 13 amino acids of a ChAP rendered the truncation construct cytoplasmic, and this effect was due to a failure to interact with Chs5p (Trautwein *et al.*, 2006). We asked whether the ability to recognize Chs3p as cargo is also still maintained in Chs6(ΔC13), again using crosslinker immunoprecipitation (Fig. 6.4C). Surprisingly, like the TPR mutants, Chs6(ΔC13) still bound Chs3p, suggesting that cargo recognition and TGN recruitment through Chs5p interaction are separable in ChAPs.

6.3.6. TPR1-4 are required for interaction with Chs5p and other ChAPs

Since Chs6(ΔC13) is not recruited efficiently to the Golgi due to the failure to interact with Chs5p (Trautwein *et al.*, 2006), we asked next whether Chs5p interaction was also impaired in the TPR mutants, and whether this was the cause for the cytoplasmic localization of the mutants. As expected, Chs6(ΔTPR1-4) could not be co-immunoprecipitated with Chs5p (Fig. 6.5A). Chs6(ΔTPR1-4) therefore shows similar characteristics to Chs6(ΔC13), which also cannot bind to Chs5p but efficiently recognizes cargoes. In contrast, Chs5p and Chs6(ΔTPR5) co-precipitated, suggesting that TPR5 is not involved in Chs5p binding.

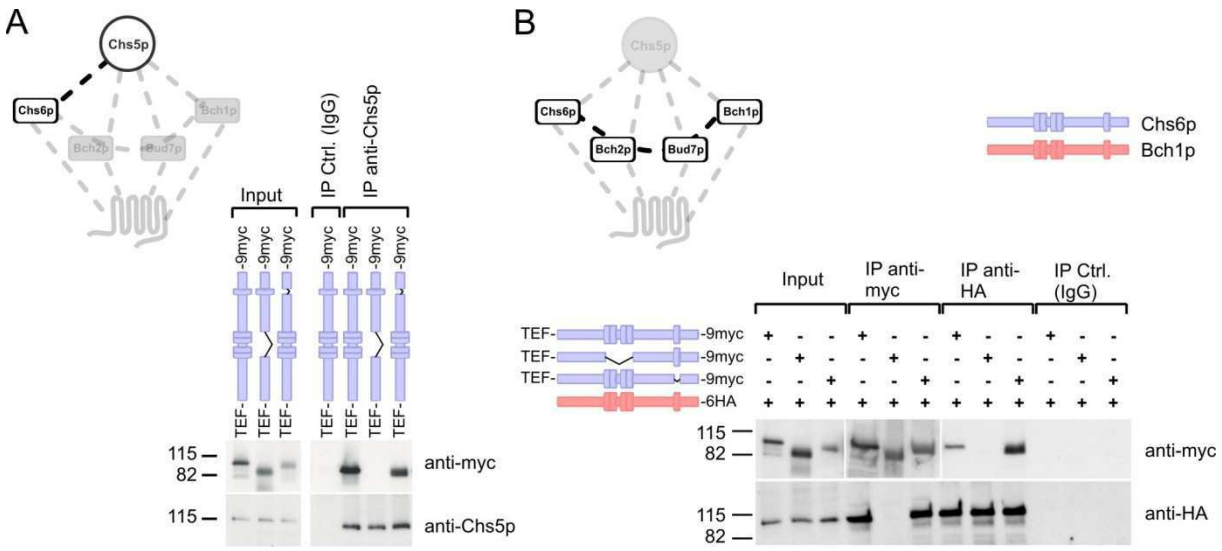

Fig. 6.5 Chs6(ΔTPR1-4) fails to interact with other exomer components. (A) Chs6(ΔTPR1-4) failed to bind to Chs5p, while Chs6(ΔTPR5) still interacted. Co-immunoprecipitation experiments were performed using an anti-Chs5p antibody and lysates generated from cells expressing chromosomally tagged Chs6(ΔTPR1-4)-9myc or Chs6(ΔTPR5)-9myc. (B) Chs6(ΔTPR1-4) also failed to co-precipitate with other ChAPs such as Bch1p. Blue: Chs6p alleles; red: Bch1p alleles. Two different exposures were cropped together because of the strong signal of the precipitated myc-tagged constructs.

Since Chs5p is required for co-precipitation of the ChAPs with each other (Sanchatjate and Schekman, 2006), we expected that Chs6(ΔTPR5) would still bind to other ChAPs, while Chs6(ΔTPR1-4) would not. Indeed, this was the case, as Chs6(ΔTPR1-4) specifically failed to interact with Bch1p (Fig. 6.5B) and Bud7p (Fig. S 6.3), while the binding of Chs6(ΔTPR5) was only marginally affected, if at all. So far our data suggest that the ChAPs require their first four TPRs for association with Chs5p and thus for assembly into a complex with other exomer components.

In contrast, Chs6(ΔTPR5) is inactive and Golgi recruitment is impaired. However, the *in vitro* interaction with Chs5p, the ChAPs and Chs3p are only mildly affected, indicating that TPR5 may be required for structural stability, i.e. a more flexible Chs6(ΔTPR5) could in principle interact with all of its binding partners, but these interactions may be much more short-lived.

6.3.7. The TPRs are transplantable between the ChAPs

Chs5p binding is a common feature of all ChAPs family members. One prediction from our results would therefore be that TPRs 1-4, which are conserved and required for Chs5p binding, should be interchangeable between the ChAPs without causing a phenotype. For this purpose, we constructed chimeric mutants of the ChAPs using a variation of the *delitto perfetto* protocol (Storici and Resnick, 2006). We chose *CHS6* and *BCH2* for these experiments because the functionality of Chs6p could be

monitored both by Chs3p localization and by chitin synthesis. Bch2p, on the other hand, is entirely dispensable for Chs3p traffic. As expected, transplantation of TPR1-4 from *BCH2* to *CHS6* had no effect on calcofluor-sensitivity or Chs3p localization (Fig. 6.6), demonstrating that this Chs6p chimera carrying the alien TPR1-4 was indeed functional. The repeats involved in Chs5p binding are therefore interchangeable between the ChAPs, confirming that TPR1-4 are part of a Chs5p interaction surface.

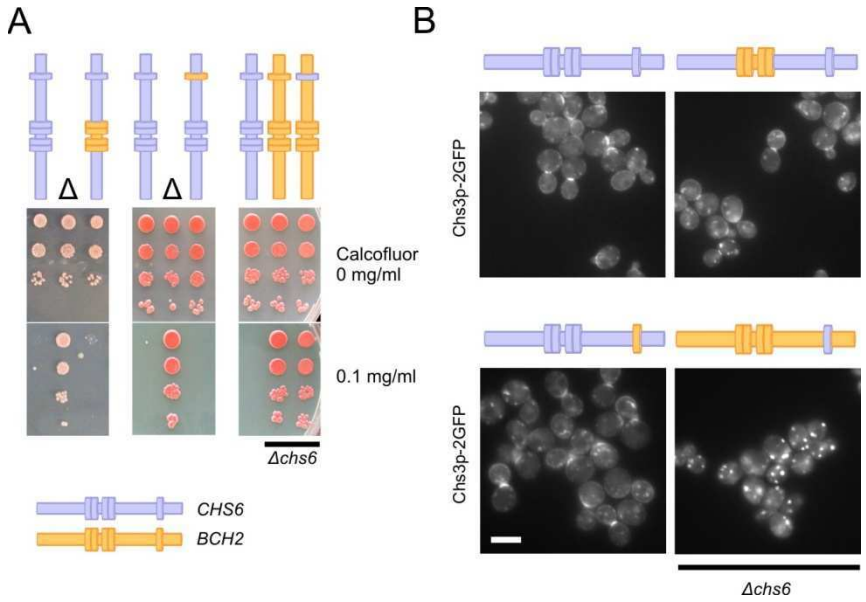

Fig. 6.6 The TPRs are interchangeable between ChAPs. (A) Chs6p bearing either TPR1-4 or TPR5 from Bch2p is fully functional. Chimeras in which TPRs from *CHS6* were grafted into *BCH2* (or vice versa) were created by *delitto perfetto*. Drop tests for calcofluor sensitivity were performed as in Fig. 6.2. Transplanting TPR5 from Chs6p to Bch2p did not restore calcofluor sensitivity in a *Δchs6* background. Blue: Chs6p domains; yellow: Bch2p domains. "Δ" refers to *Δchs6*. (B) Live fluorescence imaging of Chs3p-2GFP in the chimeras shown in (A) confirmed that the TPRs do not contribute to cargo specificity. Scale bar: 5 µm.

Similarly, TPR5 should also be exchangeable because our data indicate a structural role for this repeat. Indeed, when we repeated the chimera experiment, now transplanting TPR5, neither cargo specificity nor function of Chs6p seemed to be impaired (Fig. 6.6). Also, in a *Δchs6* background, a chimeric Bch2p carrying TPR5 from Chs6p was unable to export Chs3p. Taken together, these results support the notion that TPR1-4 form the interaction surface for Chs5p and that TPR5 plays a structural role. They furthermore indicate that cargo recognition must occur outside the TPRs.

6.3.8. Cargo specificity of the ChAPs is not conveyed by a simple linear sequence

The obvious next questions were: Where is the cargo recognition site located, and how is cargo specificity achieved? We used again our chimera approach to address these questions, and concentrated on the regions outside the TPRs (Fig. 6.7A). First, we exchanged the central domain (CD, located between TPR4 and TPR5) of Chs6p for the CD of Bch2p. This strain did not export Chs3p from the TGN and was calcofluor-resistant, suggesting that this chimeric Chs6p was unable to recognize Chs3p as a cargo (Fig. 6.7B). However, the inverse experiment – transplantation of the corresponding region from *CHS6* to *BCH2* – was not successful in changing the cargo specificity of Bch2p and rescuing *Δchs6* defects, indicating that the central domain of the ChAPs is necessary, but not sufficient, to convey cargo specificity (Fig. 6.7C). Strikingly, similar results were obtained when we individually exchanged longer sequences, like the C-terminal half (aa 409-765 of Bch2p) or even the N-terminus, TPR1-4 and central domain together (aa 1-613). These results were not due to a positioning effect in the genome, since insertion of the full-length *CHS6* ORF into the *BCH2* locus restored Chs3p export and calcofluor-sensitivity (Fig. 6.7C). Moreover, the chimeric constructs were expressed and stable (data not shown). In summary, these results suggested that the N-terminal, central and C-terminal domain were all necessary for cargo specificity, but none was sufficient by itself.

To test this hypothesis, we constructed a chimeric Bch2p protein, which retained only its original TPRs, but whose N-terminal, central and C-terminal domain had been replaced by the corresponding regions from Chs6p. In a *Δchs6* background, this triple chimera restored Chs3p export as well as most of the calcofluor-sensitivity (Fig. 6.7C). We therefore conclude that cargo recognition by the ChAPs family does not happen by means of a simple binary interaction motif, but that an extensive interaction surface is employed to achieve cargo specificity.

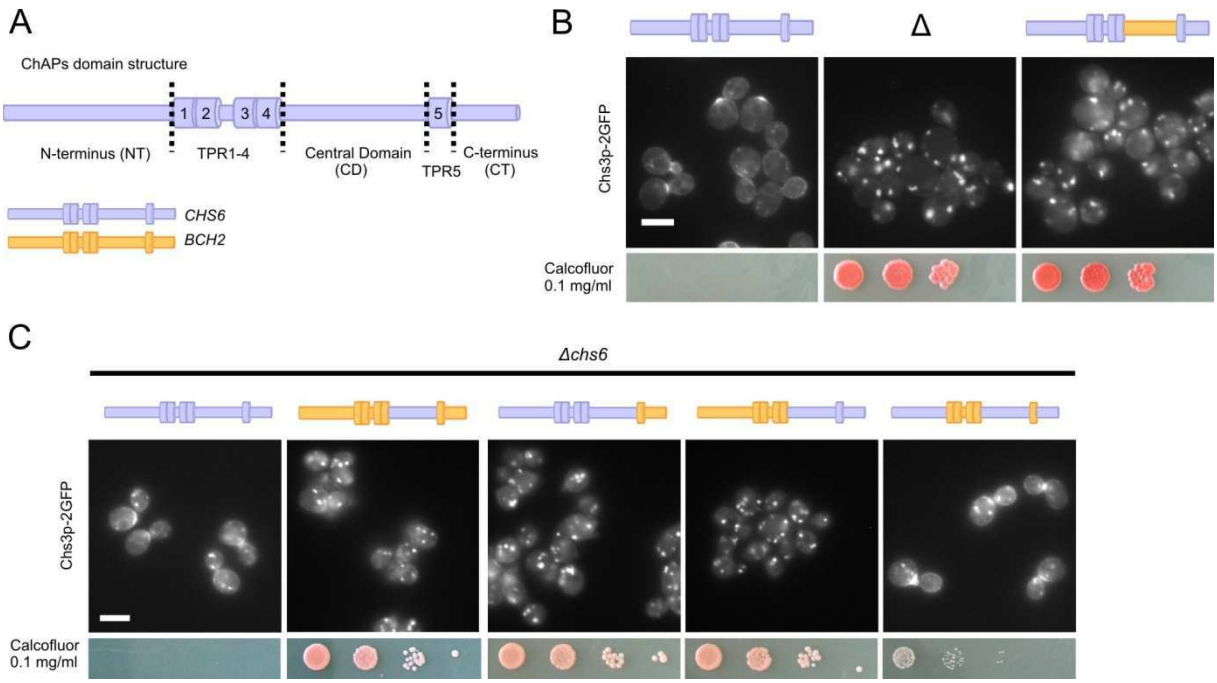

Fig. 6.7 The N-terminus, central domain and C-terminus of the ChAPs are individually necessary and only together sufficient to convey cargo specificity. (A) Schematic representation of the ChAPs' domain structure. (B) The central domain (CD) of the ChAPs is required for cargo specificity. Chimeric Chs6p bearing the CD of Bch2p was unable to export Chs3p-2GFP and rendered cells calcofluor-resistant, like a *Δchs6* strain. Chimeras were created by *delitto perfetto*. Blue: Chs6p domains; yellow: Bch2p domains. "Δ" refers to *Δchs6*. Drop assays were performed as in Fig. 6.2. Scale bar: 5 µm. (C) The N-terminus (NT), CD and C-terminus (CT) are necessary and together sufficient to determine cargo specificity. In a *Δchs6* background, calcofluor-sensitivity was restored by re-introduction of the *CHS6* full-length ORF into the *BCH2* locus, but not by transplantation of the following domains from Chs6p to Bch2p: CD, NT + TPR1-4 + CD, or CD + TPR5 + CT. Transplantation of NT, CD and CT together restored Chs3p export to the bud neck (by about 82% compared to wild-type cells). Scale bar: 5 µm.

6.3.9. Chs6p interacts with the C-terminus of Chs3p

Given the potentially large cargo interaction surface in Chs6p, one could assume that multiple parts of its cargo Chs3p would be involved in the interaction. On the other hand, we might be able to identify individual parts of Chs3p required for the interaction with Chs6p, similarly to the short, linear motif in Fus1p which binds to Bch1p/Bud7p (Barfield *et al.*, 2009). Since the topology of Chs3p is not quite resolved yet (Cos *et al.*, 1998; Meissner *et al.*, 2010), and since even the number of transmembrane (TM) domains is debated – varying between four and eight – we decided to focus on the C-terminal part of Chs3p. Cos et al. (1998) had generated two C-terminal truncations that rendered the cells calcofluor-resistant (Fig. 6.8A), suggesting a defect in either Chs3p function or localization. Interestingly, we found that GFP-tagged versions of these mutant proteins failed to reach the cell surface and were retained at the TGN, indicated by co-localization with Sec7p-dsRed

(Fig. 6.8B). These results suggest that the C-terminal 21 amino acids of Chs3p might be important for binding of the exomer complex and thus for incorporation into secretory vesicles.

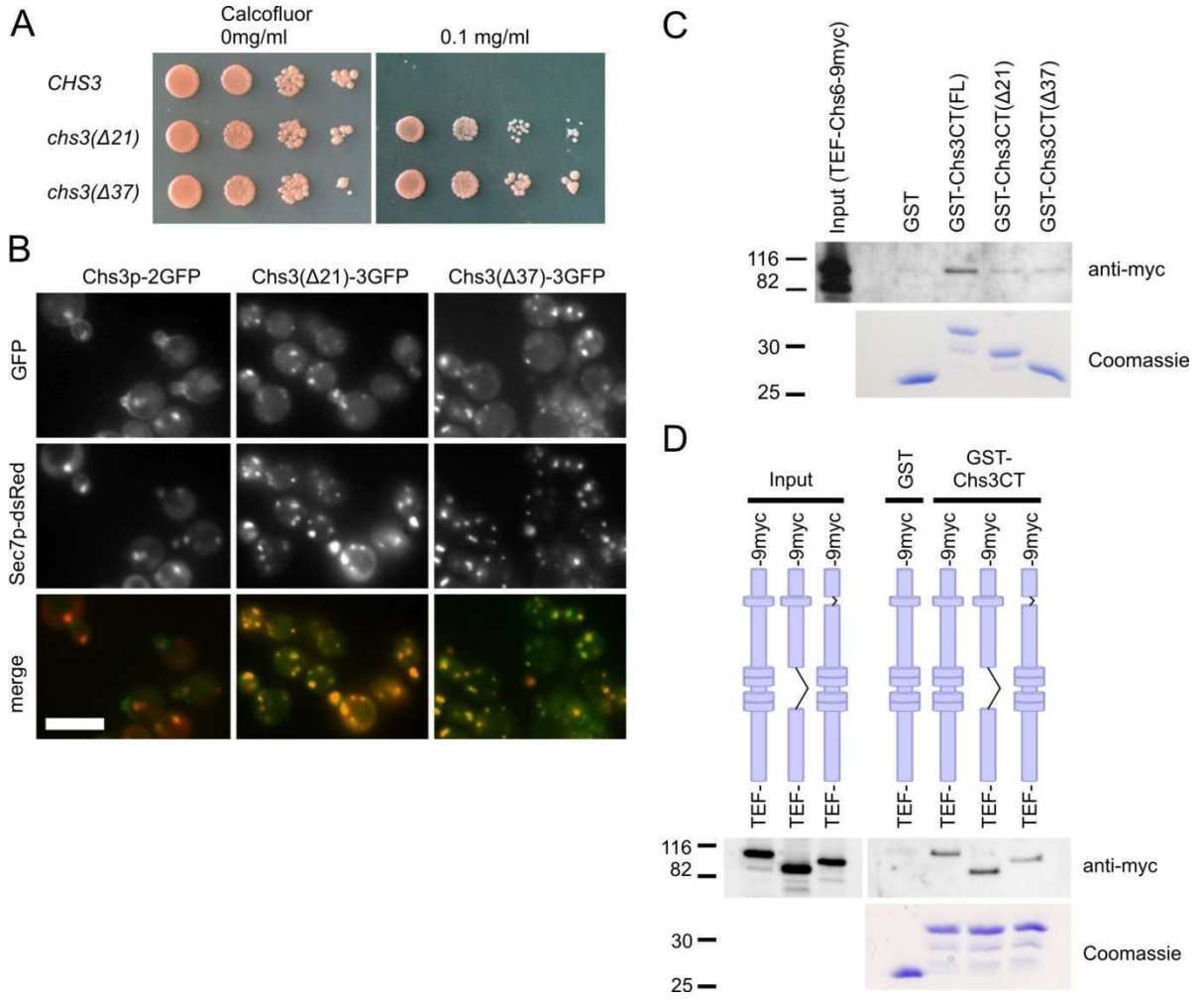

Fig. 6.8 The C-terminus of Chs3p contains an exomer-binding site required for Golgi export. (A) The last 21 amino acids of Chs3p are essential for chitin synthesis. Cells expressing Chs3p lacking the C-terminal 21 or 37 amino acids were calcofluor-resistant. (B) The C-terminus of Chs3p is required for Golgi export. Chromosomally generated Chs3(Δ21)-3GFP or Chs3(Δ37)-3GFP was trapped in internal membranes and co-localized with the TGN marker Sec7p-dsRed. Scale bar: 5 µm. (C) Chs6p binds to the C-terminus of Chs3p. Lysates from cells expressing Chs6p-9myc were incubated with immobilized GST, GST fused to the C-terminus of Chs3p (FL) or truncated C-terminal constructs (Δ21 and Δ37). Chs6p-9myc bound to the full C-terminus, but binding to the truncations was abolished. (D) Chs6p TPR mutants efficiently bind to the Chs3p C-terminus. GST pulldowns were performed as in (C) with lysates from cells expressing Chs6(ΔTPR1-4)-9myc or Chs6(ΔTPR5)-9myc.

We therefore performed GST pulldown experiments using the full C-terminal cytoplasmic tail of Chs3p, which has a total length of 55 amino acids following the last predicted TM domain. The corresponding truncation constructs lacked the final 21 and 37 amino acids, respectively. Immobilized GST fusion proteins were then incubated with whole cell lysate and analyzed for binding

of Chs6p. Chs6p-9myc bound to full-length GST-Chs3CT, but not to GST alone, GST-Chs3CT(Δ21) or GST-Chs3CT(Δ37) (Fig. 6.8C). This result suggests that the Chs3p C-terminus contains an exomer recognition site, which is necessary for Chs6p binding *in vitro* and for Chs3p export *in vivo*. This site is likely to be located within the last 21 amino acids, as the Δ21 mutation was sufficient to abolish Chs3p transport to the cell surface and abrogate Chs6 binding. As a control, we determined the binding of the TPR mutants to the Chs3p tail. As expected, both mutants interacted with the C-terminus of Chs3p to a similar level as wild-type Chs6p (Fig. 6.8D), validating our previous results.
Taken together, these results suggest that the C-terminal 21 amino acids of Chs3p are necessary and sufficient to interact with Chs6p. Given the large interaction surface in Chs6p, it is however likely that other sequences contribute to efficient Chs3p export from the TGN.

6.4. Discussion

The late secretory pathway controls the trafficking of proteins to the cell surface and the endosomal system, but how the multitude of cargoes is correctly sorted to control their spatial and temporal localization is not well understood. In recent years, the exomer complex, comprising Chs5p and the ChAPs family, has emerged as a crucial sorting determinant for a subset of cargoes (Santos and Snyder, 1997, 2003; Trautwein *et al.*, 2006). However, little is known about how exomer assembles at the TGN and recognizes specific cargo proteins. In this study, we investigated the role of conserved TPR motifs in ChAPs and found that they are essential for function. TPRs 1-4 of the ChAPs build up the interaction surface for Chs5p, because their deletion abolishes the binding of Chs5p. TPR5, however, does not seem to be engaged in direct binding of either Chs5p or cargo, but plays most likely a more structural role in perhaps providing more rigidity to the ChAPs. Either mutating critical TPR residues or deletion of the fifth TPR reduced the membrane association of Chs6p, consistent with such a structural role. Furthermore, our domain swapping experiments indicate that the TPRs may not be directly involved in cargo recognition or binding: TPR1-4 are interchangeable between the ChAPs without loss of function or specificity, and similarly, TPR5 also appears to be part of the structural ChAPs backbone since it is equally interchangeable.
The ChAPs alone, in the absence of Chs5p, are not sufficient to sort cargo into secretory vesicles, and neither are ChAPs mutants that fail to bind Chs5p (Santos and Snyder, 1997; Trautwein *et al.*, 2006). It has also been shown that the exomer complex depends on Chs5p to co-precipitate with cargo (Sanchatjate and Schekman, 2006), raising the possibility that the ChAPs cannot recognize cargo without Chs5p. We could now demonstrate that cargo recognition and Chs5p binding activities reside

in separate domains of Chs6p. Therefore, the role of Chs5p may be to stabilize the ChAPs-cargo complex on the TGN membrane. Cargo recognition, in contrast, required the N- and C-terminal and central domain of the ChAPs, probably forming a composite binding site.

In comparison, most coats feature several small, distinct cargo binding sites on their surface to allow for simultaneous recognition of small, linear sorting signals (Fig. 6.9A). For instance, COPI has two separate binding sites for KKXX and R-based motifs, respectively (Michelsen *et al.*, 2007). Likewise, the COPII subunit Sec24p harbors three independent cargo binding sites which consist of small, folded domains (Miller *et al.*, 2003; Mossessova *et al.*, 2003; Mancias and Goldberg, 2007). Similarly, AP-1 and AP-2 recognize cargoes through distinct binding sites in the μ subunit and in the γσ heterodimer (Owen and Evans, 1998; Janvier *et al.*, 2003; Jackson *et al.*, 2010).

Yet, at least some clathrin coats seem to be capable of recognizing more complex sorting signals in the form of three-dimensional surface motifs: an unconventional bipartite Golgi export motif, which is only formed in the folded protein was identified in the Kir2.1 channel (Ma *et al.*, 2011). The resulting surface patch is recognized by AP-1 and sufficient to drive export to the cell surface. Interestingly, the interaction between the clathrin adaptor epsinR and the Q-SNARE Vti1b also involves interactions of surface patches on both the cargo and the adaptor side (Miller *et al.*, 2007). While this may represent a special case of SNARE recruitment into clathrin-coated vesicles, the authors hypothesized that analogous mechanisms might in fact be the general paradigm for cargo sorting in more restricted, specialized routes. We therefore propose that the exomer-dependent Golgi export pathway could be such a route, since our data suggest that the ChAPs dedicate an unusually large fraction of their surface area to cargo recognition (Fig. 6.9B). Here, several large domains appear to form a composite, three-dimensional binding site for cargoes. This evolutionary step may have greatly increased the ChAPs' specificity towards individual cargoes, perhaps at the cost of being able to bind fewer cargo molecules at a time instead of harboring multiple binding sites within one subunit. The observed gene duplication and diversification of the original ChAP, Bch1p (Trautwein *et al.*, 2006), may compensate for this, as it allows a broader spectrum of traffic to pass through the exomer pathway. This would imply that exomer-dependent cargoes may not share a common sorting motif, which appears to be true for Chs3p and Fus1p.

An important question is: What kind of motifs or surfaces do the ChAPs recognize? The last 21 amino acids of Chs3p are necessary for Golgi export, and the C-terminal cytoplasmic domain is sufficient for Chs6p binding *in vitro*. Interestingly, the C-terminal residues of Chs3p are conserved among Chs3p homologues but absent in other chitin synthases like Chs1p or Chs2p (Cos *et al.*, 1998). This may provide an elegant explanation why, in *S. cerevisiae*, only Chs3p is exported via the exomer pathway (Ziman *et al.*, 1998 and data not shown). While the C-terminus appears to be necessary for

recognition, we hypothesize that is probably not sufficient, as in the case of Fus1p which harbors an IXTPK motif that is required for exomer-dependent export, but which only functions in a restricted context (Barfield *et al.*, 2009). The identification of more exomer-dependent cargoes may help to better understand how cargo recognition by the ChAPs is achieved.

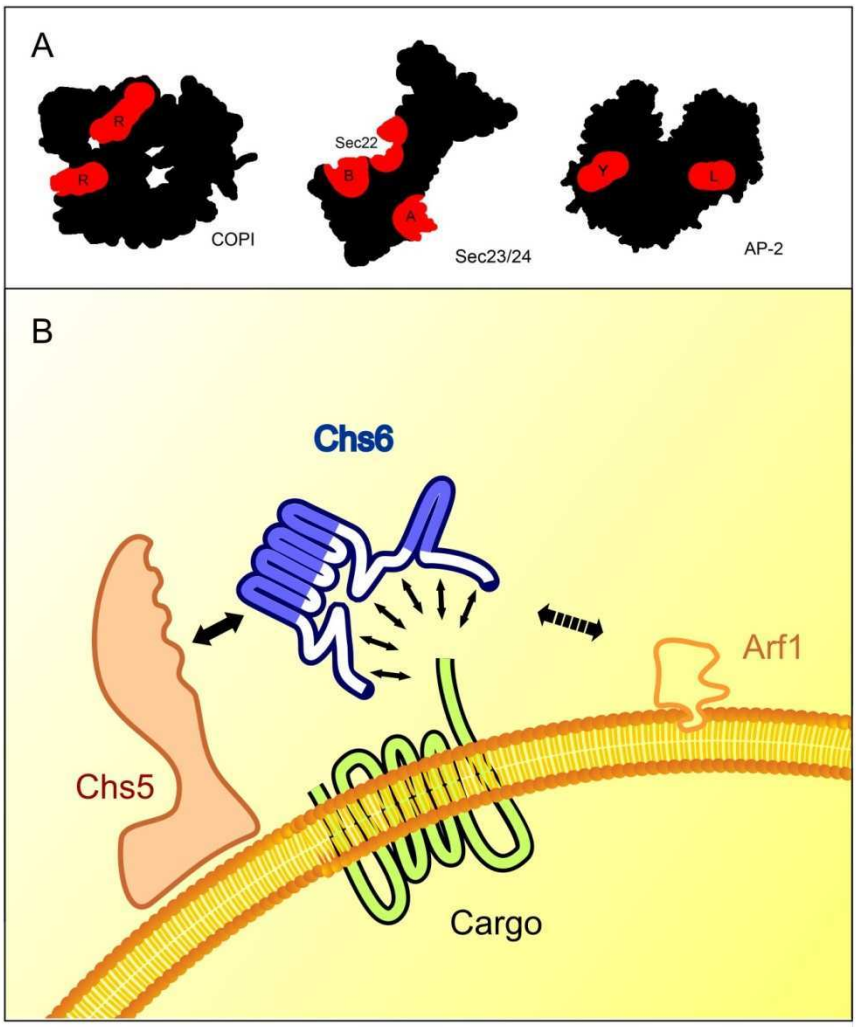

Fig. 6.9 Schematic depiction of cargo recognition modules. (A) The known cargo binding sites on COPI, COPII and AP-2 mostly map to small surface patches (shown in red). R: Binding site for arginine-based motifs for retrograde transport. A/B: Binding sites for Bet1 and Sed5. Sec22: Sec22 binding site. Y/L: Binding sites for tyrosine- and leucine-based endocytic signals. (B) Recruitment of the ChAPs to the TGN membrane requires Arf1p as well as Chs5p binding via TPR1-4. In contrast to other coats, cargo interaction is mediated by a large, composite binding surface.

6.5. Materials and Methods

Strains and growth conditions

Yeast strains used in this study are listed under 8.2. Standard yeast media were prepared as described (Sherman, 1991). Calcofluor plates were based on minimal medium containing additionally 0.1% yeast extract, 1% MES buffer pH 6.0 and 0.1 mg/ml Calcofluor White (Sigma).

Yeast genetic methods

Standard genetic techniques were used throughout (Sherman, 1991). Chromosomal tagging and deletions were performed as described (Güldener *et al.*, 1996; Knop *et al.*, 1999). For C-terminal tagging with 3xGFP, the plasmid pYM-3GFP was used (Zanolari *et al.*, 2011). All PCR-based chromosomal manipulations were confirmed by analytical colony PCR. The Sec7p-dsRed plasmid (pTPQ128) was described previously (Proszynski *et al.*, 2005). Marker-free chromosomal deletions were performed using the *delitto perfetto* method (Storici and Resnick, 2006) and confirmed by sequencing. Genetic chimeras were constructed using a modified version of the same technique: After insertion of the CORE cassette, the desired foreign genetic element was amplified from genomic DNA using chimeric primers, which were homologous to the 45 base pairs upstream and downstream of the *delitto perfetto* site. This PCR product was then directly used for transformation, thus recombining with the locus and replacing the CORE cassette.

Western Blot detection

Epitope tags and proteins were detected using the following antibodies: anti-myc (Sigma 9E10 1:1,000); anti-HA (Eurogentec HA11 1:1,000); anti-FLAG (Sigma M2 1:1,000); anti-Chs5p (affinity-purified, 1:500); anti-Chs3p (affinity-purified, 1:1,000); anti-Pgk1 (Invitrogen #A-6457 1:1,000) and anti-Sec61p serum (a gift from Prof. M. Spiess, Biozentrum Basel, 1:10,000). ECL (GE Healthcare) was used for detection.

For myc epitope detection in crosslinker immunoprecipitation experiments, anti-myc 9E10 (Sigma, 1:4,000) and TrueBlot-anti-mouse-HRP secondary antibody (eBioscience, 1:2,500) were employed, and ECL Advance (GE Healthcare) was used for detection according to the manufacturer's instructions.

Microscopy

Cells were grown to log phase in rich or selective medium supplemented with adenine, then harvested, washed and mounted. Images were acquired with an Axiocam mounted on a Zeiss Axioplan 2 fluorescence microscope, using filters for GFP, dsRed or DAPI.

Chitin staining was carried out as described (Lord *et al.*, 2002). Briefly, cells grown for at least 16 h to late log phase were stained after formaldehyde fixation in 1 mg/ml calcofluor, washed 3x in water and imaged directly.

Subcellular fractionation

Ten OD_{600} of mid-log cells were incubated in 1 ml DTT buffer (10 mM Tris pH 9.4, 10 mM DTT) for 5 min at 30°C, spun down and resuspended in 1 ml SP-buffer (75% YP medium, 0.7 M sorbitol, 0.5% glucose, 10 mM Tris pH 7.5). Thirty µl of zymolyase T20 (10 mg/ml) were added and the cells spheroplasted at 30°C for 40 min. Cells were gently spun down and lysed in 1 ml 50 mM Tris pH 7.5, 1 mM EDTA, 50 mM NaCl and protease inhibitors by pipetting up and down. The lysate was cleared at 500 g for 2 min and the supernatant (= "total cell lysate", TCL) subjected to centrifugation at 13,000 g (10 min). The supernatant (S13) was carefully taken off with a pipette and subjected to centrifugation at 100,000 g (1 h). Both pellets (P13 and P100) were washed once in lysis buffer and then resuspended in 1 ml lysis buffer. All steps were carried out at 4°C. Samples were taken from all final fractions and subjected to immunoblot analysis.

Co-immunoprecipitation

Yeast lysates from 10 OD_{600} of cells were prepared by spheroplasting as described above. Spheroplasts were sedimented (2 min, 1,000 g), lysed in B150Tw20 buffer (20 mM HEPES, pH 6.8, 150 mM KAc, 5 mM $Mg(Ac)_2$, 1% Tween-20) with protease inhibitors and cleared by centrifugation (10 min, 16,000 g). Immunoprecipitations were performed with 5 µg affinity purified rabbit IgG (Dianova), 5 µg affinity-purified anti-Chs5p antibody, 5 µg anti-HA (HA.11, Eurogentec), 5 µg anti-myc (9E10, Sigma) or 5 µg anti-AU5 (Abcam) and 100 µl 20% Protein A sepharose per 1 ml cleared lysate for 1 h at 4°C. The beads were washed, resuspended in sample buffer, and bound proteins analyzed by immunoblot.

Crosslinker immunoprecipitation

For each sample, yeast lysate from 6 OD_{600} of cells was prepared by glass bead lysis in 200 µl B88 buffer (20 mM HEPES, pH 6.8, 150 mM KAc, 5 mM $Mg(Ac)_2$, 250 mM sorbitol) with protease

inhibitors. The lysate was cleared by centrifugation at 13,000 g for 5 min at 4°C. DSP (Pierce) dissolved in DMSO was added to 140 µl lysate (2 mM final concentration). The crosslinking reaction took place for 30 min at RT and was stopped with 7 µl 1 M Tris (pH 7.5) for 15 min. Then, 8 µl 20% SDS were added, and the sample was incubated at 65°C for 15 min. Nine hundred µl IP buffer (50 mM Tris/HCl pH 7.5, 150 mM NaCl, 1% Triton X-100, 0.1% SDS) were added, and the sample was centrifuged for 10 min at 20,000 g. The supernatant was subjected to immunoprecipitation over night at 4°C using 5 µg affinity-purified anti-Chs3p antibody crosslinked to Protein A sepharose with DMP (Pierce). The washed precipitates were incubated at 95°C for 30 min in SDS sample buffer containing 100 mM DTT and analyzed by immunoblot.

BLAST analysis and TPR prediction

The Chs6p primary protein sequence was subjected to fungal BLAST search (available on *Saccharomyces Genome Database*, www.yeastgenome.org) using the default settings of the BLASTP algorithm on all available fungal nuclear genomes, excluding *Saccharomyces cerevisiae*. TPRs were predicted with the TPRPRED algorithm (Karpenahalli *et al.*, 2007), using the standard settings.

Split ubiquitin assay

CHS6, CHS6ΔTPR1-4 and CHS6ΔTPR5 were amplified from genomic DNA, and cloned into the pRS314-Nub vector (Johnsson and Varshavsky, 1994) using BamHI and NcoI restriction sites. *CHS3* and *STE14* were cloned into the pRS313-Cub vector using ClaI and SalI sites. Expression and functionality of the Nub-Chs6 and Chs3-Cub constructs were verified by rescue of chitin synthesis in *Δchs6* and *Δchs3* strains, respectively. Combinations of Nub and Cub plasmids were transformed into the YPH499 background yeast strain (Sikorski and Hieter, 1989) and assayed for growth as indicated.

GST Pulldowns

The C-terminal tail of Chs3p or C-terminally truncated versions ("Δ21" and "Δ37") were cloned into pGEX-6P-1 using EcoRI and XhoI restriction sites. The full-length tail comprised the last 55 amino acids (aa) following the last predicted transmembrane (TM) domain, while truncations of this tail lacked the C-terminal 21 and 37 aa, respectively. Expression in Rosetta *E. coli* cells was induced by addition of 1 mM IPTG and growth in LB medium at 37°C for 4 h. Cells were lysed in PBS/5% glycerol, and GST fusions were purified with GSH agarose (Sigma), eluted with 40 mM GSH and dialyzed against PBS/5% glycerol.

GST and GST-tagged Chs3p C-terminus were bound to GSH agarose. Yeast lysates were prepared by spheroplasting and subsequent lysis in B150Tw20 buffer. The lysates were incubated with the coupled resin for 1 h at 4°C. Beads were washed twice with B150Tw20 buffer, once with B150Tw20 buffer supplemented with 150 mM NaCl and then re-suspended in 40 µl SDS sample buffer, followed by incubation at 95°C for 10 min. Bound proteins were analyzed by immunoblot.

6.6. Acknowledgements

We are grateful to B. Zanolari and M. Trautwein for their initial observation of the lithium-sensitivity phenotype, and to M. Spiess for the anti-Sec61 serum. We would also like to thank all members of the Spang lab for technical advice and helpful discussion. This work was supported by a graduate student fellowship of the Werner Siemens Foundation to U.R., the University of Basel (A.S.) and the Swiss National Science Foundation (A.S.).

6.7. Supplementary figures

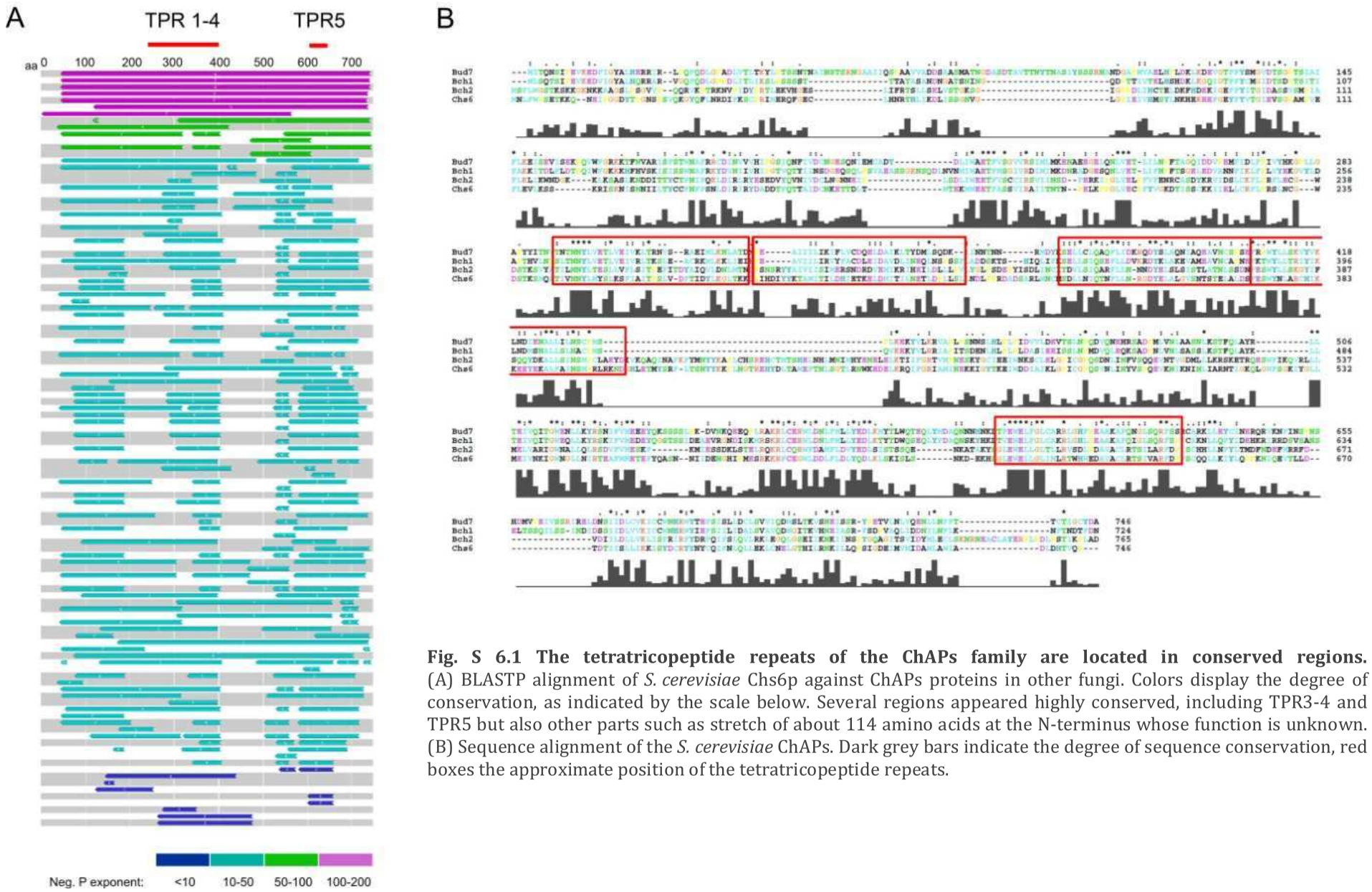

Fig. S 6.1 The tetratricopeptide repeats of the ChAPs family are located in conserved regions. (A) BLASTP alignment of *S. cerevisiae* Chs6p against ChAPs proteins in other fungi. Colors display the degree of conservation, as indicated by the scale below. Several regions appeared highly conserved, including TPR3-4 and TPR5 but also other parts such as stretch of about 114 amino acids at the N-terminus whose function is unknown. (B) Sequence alignment of the *S. cerevisiae* ChAPs. Dark grey bars indicate the degree of sequence conservation, red boxes the approximate position of the tetratricopeptide repeats.

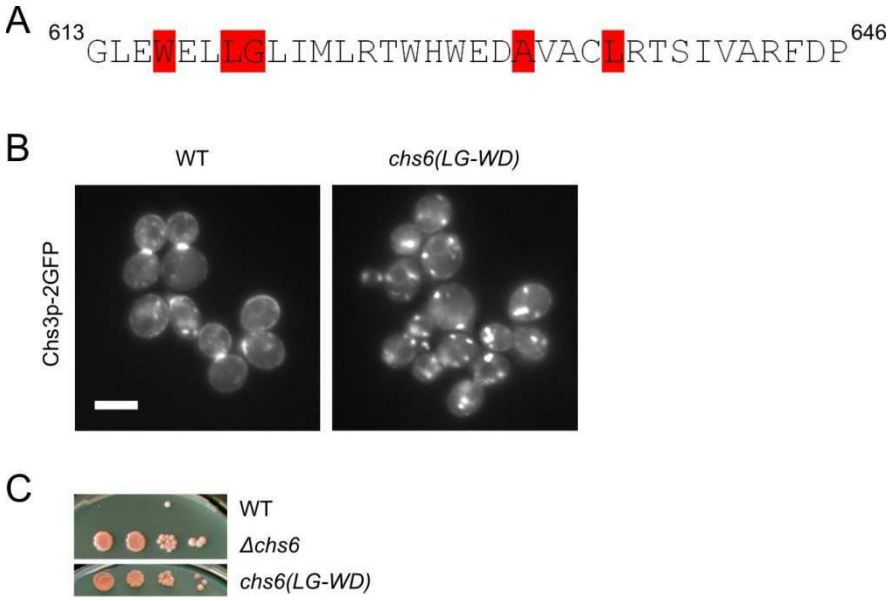

Fig. S 6.2 Chs6p requires an intact TPR fold for function. (A) Primary sequence of TPR5 in Chs6p. Residues which were considered part of the conserved TPR backbone are highlighted in red. Chs6p bearing a double point mutation in two neighboring TPR backbone residues (L619G/G620W) was non-functional, as judged by mis-localization of Chs3p (B) and calcofluor resistance (C). Scale bar: 5 µm.

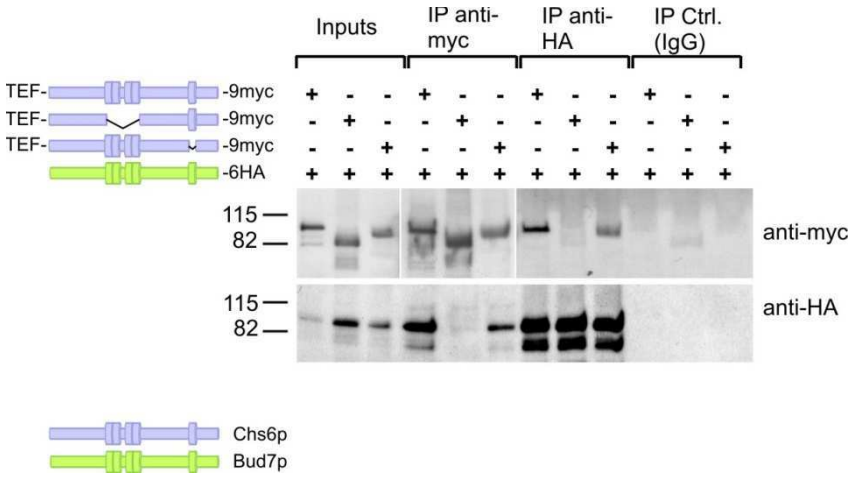

Fig. S 6.3 TPR1-4 is required for co-precipitation of Chs6p with Bud7p. Co-immunoprecipitation was performed as in Fig. 6.5. Interaction of Chs6(ΔTPR1-4) with Bud7p was entirely abolished, while Chs6(ΔTPR5) only showed a mild reduction in binding, suggesting that TPR1-4 is generally required for co-precipitation of the ChAPs family members. Two different exposures were cropped together because of the strong signal of the precipitated myc-tagged constructs.

Chapter 7

Approach to isolating and characterizing exomer-dependent secretory vesicles

7. Approach to isolating and characterizing exomer-dependent secretory vesicles

The data presented in Chapter 5 of this work suggested that more than the two described vesicular transport pathways to the cell surface may exist in yeast. In particular, the low-density secretory vesicle fraction may consist of several sub-species. A simple explanation would be that the exomer complex is involved in the formation of a specialized type of secretory vesicle, which has similar biophysical properties to the described low-density carriers and has therefore not been resolved by equilibrium density gradient centrifugation. However, this exomer-dependent vesicle would carry a set of cargoes (Chs3p, Fus1p, and other proteins) that is distinct from the general low-density vesicle type. To test this hypothesis and – if true – to characterize the cargo repertoire of exomer-dependent carriers, we sought to establish a procedure for differential isolation of secretory vesicles.

7.1. Approach towards the differential precipitation of secretory vesicles

To accumulate and enrich secretory vesicles, we devised a protocol based on previously described methods (Harsay and Schekman, 2002; Valdivia *et al.*, 2002; Klemm *et al.*, 2009). These studies employed the *sec6-4* temperature-sensitive allele, which blocks fusion of post-Golgi vesicles with the plasma membrane at 37°C (Novick *et al.*, 1980; Harsay and Bretscher, 1995), causing secretory vesicles to accumulate. However, as described previously (Valdivia and Schekman, 2003; Zanolari *et al.*, 2011), Chs3p delocalizes over the plasma membrane at 37°C, indicating that at higher temperatures Chs3p might potentially be delivered to the cell surface in a different type of vesicle compared to 30°C. We therefore tested two alternatives:

1. Constant accumulation by attenuation of vesicle fusion with the plasma membrane: To this end we used a *Δmsb3 Δmsb4* double mutant, which is viable but shows clouds of vesicles in the cytoplasm at steady state (Zanolari *et al.*, 2011).
2. A *GAL1* promoter shutoff of *SEC6* (Zanolari *et al.*, 2011). Accumulation of vesicles was achieved by shifting cells from galactose- to glucose-based medium.

Lysates from these strains were cleared by a 13,000 g spin and subjected to separation on a 200 µl sucrose step gradient as described previously (Valdivia *et al.*, 2002). In both the *Δmsb3/4* and

GAL1-SEC6 strains, Chs3p shifted to the lower fractions compared to wild-type (Fig. 7.1, compare also Chapter 5 Fig. 4). Thus, both accumulation strategies were suitable[1].

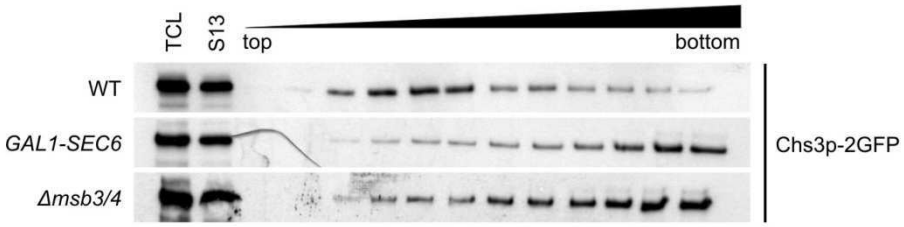

Fig. 7.1 Secretory vesicle accumulation is achieved by a *SEC6* promoter shutoff or by double deletion of *MSB3* and *MSB4*. *GAL1-SEC6* cells were pre-cultured in YP-galactose and grown in YP-glucose for 13 h to deplete Sec6p. Wild-type and *Δmsb3/4* cells were grown for 13 h in YP-glucose. Cells were lysed with glass beads, lysates cleared at 13,000 g and loaded on 200 µl sucrose step gradients. Gradients were centrifuged to equilibrium, fractions manually collected from the top and analyzed by immunoblot. TCL: total cell lysate; S13: 13,000 g supernatant.

For immunoprecipitation, Chs3p served as a suitable exomer-dependent cargo because, unlike Fus1p, it is expressed and exported during normal vegetative growth. Conversely, the plasma membrane ATPase Pma1p is exported independently of exomer and has been widely used as a model protein for surface delivery (Bagnat *et al.*, 2000; Gaigg *et al.*, 2006; Surma *et al.*, 2011). However, we considered it not to be the best cargo for this experiment because it is one of the most highly expressed proteins in yeast and may therefore be present in multiple secretory vesicle species (Harsay and Bretscher, 1995; Ghaemmaghami *et al.*, 2003). We therefore chose the Na^+/H^+ antiporter Nha1p, which was exported to the PM in *Δchs5* cells (Fig. 7.2A) and could be appended with several tags for IP and immunoblot detection. The strains used in the experiments shown here therefore co-expressed Nha1p-9myc and Chs3p (bearing various tags as indicated) under their native promoters.

Fractions 9-11 of the gradients showed a good enrichment of Chs3p and Nha1p (Fig. 7.2B) and were pooled for immunoprecipitation. Samples were pre-incubated with primary antibodies under native conditions and then added to magnetic secondary antibody beads for IP. Interestingly, Chs3p-2GFP and Nha1p-9myc co-precipitated above background levels, suggesting they were present in the same vesicle (Fig. 7.2C). However, we also detected Golgi and endosomal markers in the precipitate, such

[1] Over time we observed that the *Δmsb3/4* strain adapted, leading to inefficient vesicle accumulation. Therefore, while the experiments shown here employed both strategies, the *GAL1-SEC6* shutoff approach may present the best choice for future experiments.

as the endosomal SNARE Pep12p and the cis-Golgi-associated SNARE Sed5p (Fig. 7.2D). Since Chs3p recycles to the TGN via endosomes (Valdivia *et al.*, 2002), the presence of contaminating organelles in the IP input would likely co-precipitate many other exocytic and endocytic cargoes and thus mask the signal from the secretory vesicle fraction. Therefore, a higher purity of the vesicle preparation was required.

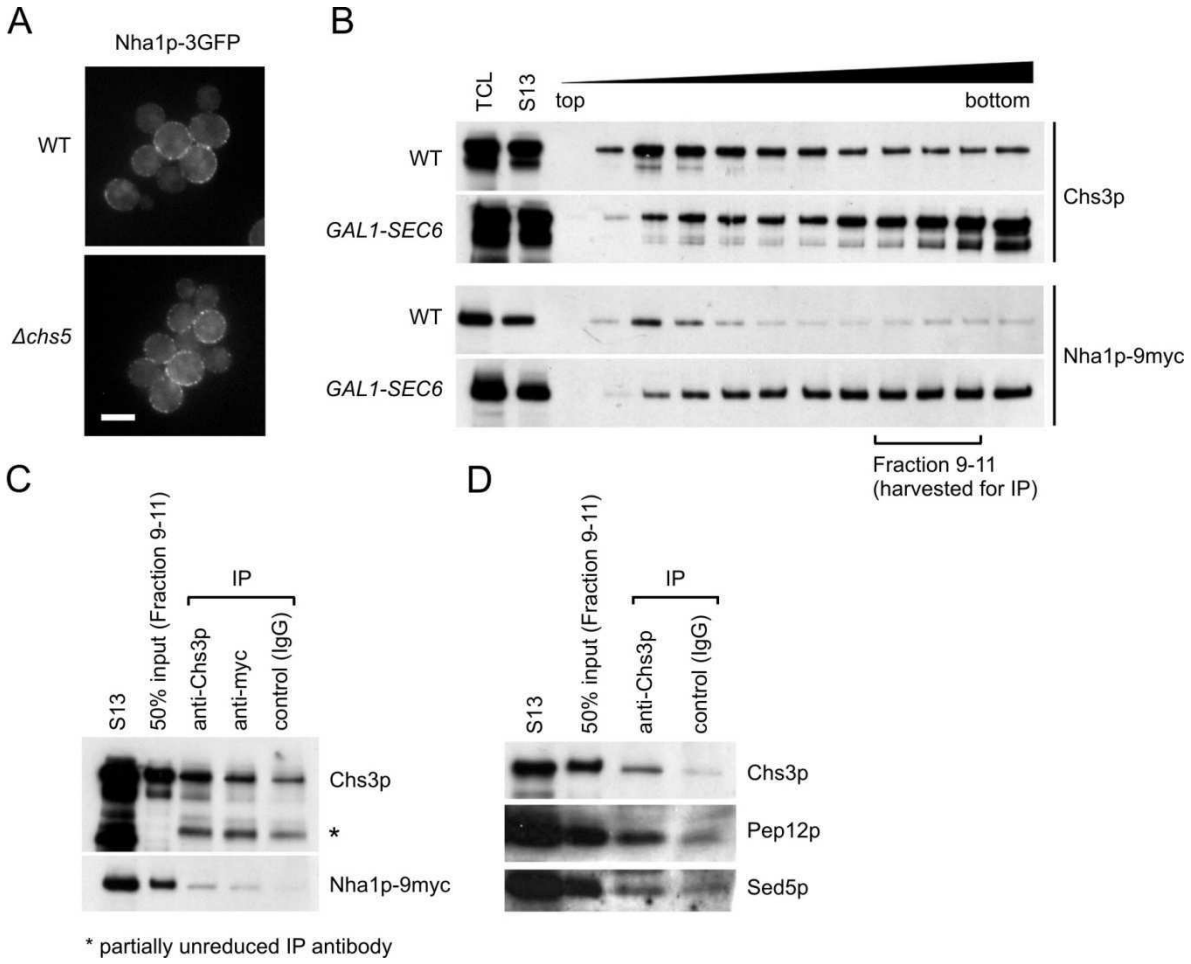

Fig. 7.2 Chs3p and Nha1p co-precipitate from an enriched secretory vesicle fraction, together with Golgi/endosomal contaminations. (A) Nha1p is an exomer-independent cargo. 3GFP-tagged Nha1p was exported to the cell surface in WT and *Δchs5* cells. Scale bar: 5 µm. (B) Both Chs3p and Nha1p accumulate in secretory vesicles upon Sec6p depletion. Cell lysates were prepared and separated as in Fig. 7.1. TCL: total cell lysate; S13: 13,000 g supernatant. (C) Chs3p and Nha1p co-precipitate from the secretory vesicle fraction. Gradient fractions 9-11 were harvested and subjected to IP under native conditions, using magnetic beads. Samples were incubated at 65°C in SDS sample buffer with DTT and analyzed by immunoblot. (D) Golgi and endosomal membranes contaminate the IP. The input and precipitate were analyzed for the endosomal SNARE Pep12p and the Golgi SNARE Sed5p. Both co-precipitated with Chs3p.

We aimed to reduce the endosomal contamination by three independent means: Firstly, we cleared the cell lysate by a 2 x 30 min pre-spin at 50,000 g, instead of 6 min at 13,000 g. This step depleted

the lysate of several Golgi/endosomal markers such as Sed5p, Pep12p and Kex2p, a prohormone-processing enzyme which cycles between the TGN and endosomes (Henkel *et al.*, 1999) (Fig. 7.3A). As expected, Chs3p was also partially depleted since a fraction of it pelleted together with the Golgi and endosomal membranes. However, the supernant still contains secretory vesicles under these conditions because these typically pellet above 100,000 g (Walworth and Novick, 1987; Zinser and Daum, 1995).

Secondly, because the 200 µl gradient provided only limited resolution, we increased the volume to 8.5 ml and added more gradient steps, which slightly improved the separation of internal organelles and secretory vesicles (Fig. 7.3B). Thirdly, to achieve a further depletion of endosomes, we chose the approach presented by Klemm *et al.* (2009): Fractions 9-11 of the sucrose gradient were pre-incubated with an antibody against Pep12p, and endosomal membranes were pelleted using cellulose fibers coupled to a secondary antibody. Since this resin showed a low signal-to-noise ratio, we also used it subsequent vesicle IPs. Although the efficiency was somewhat variable, this procedure depleted Pep12p from the gradient fractions (Fig. 7.3C). However, markers such as Kex2p and Tlg1p were still detectable after immunodepletion, indicating that Golgi and endosomal membranes were reduced, but not quantitatively removed.

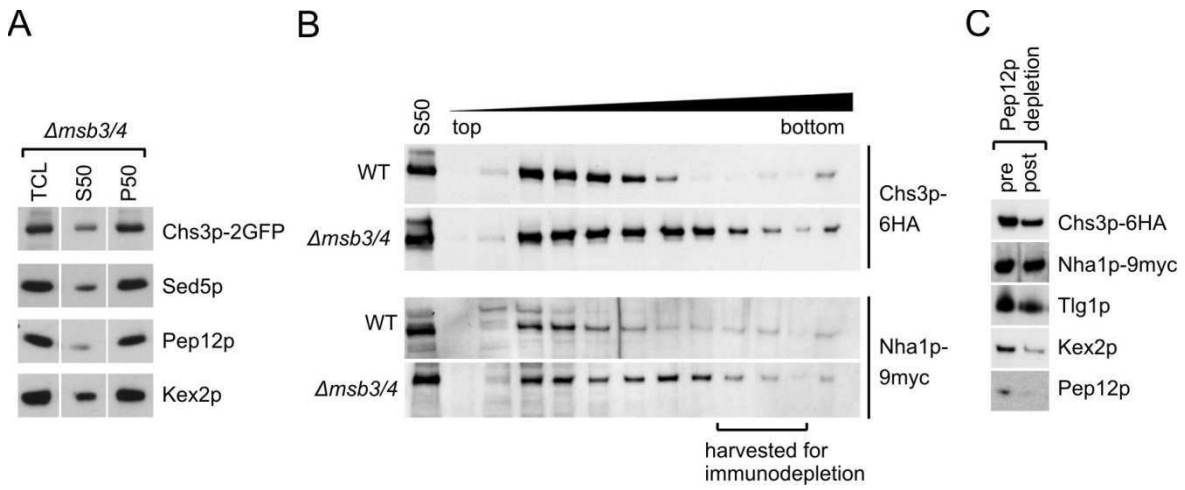

Fig. 7.3 An adapted protocol reduces contamination with Golgi and endosomal membranes. (A) Lysates from *Δmsb3/4* cells were prepared by spheroplasting and subjected to centrifugation for 2 x 30 min at 50,000 g. Immunoblot analysis showed that Golgi membranes (Sed5p, Kex2p) and endosomes (Pep12p) were depleted. TCL: total cell lysate; S50/P50: 50,000 g supernatant/pellet. (B) A larger gradient volume allows better separation of organelles. Cleared lysates were separated on a 8.5 ml sucrose step gradient. Separation of vesicles from other membranes was improved compared to a 200 µl gradient (compare Fig. 7.1). (C) Immunodepletion removes a large portion of Pep12p from the vesicle fraction, but only partially depletes other Golgi/endosomal markers. Gradient fractions 9-11 were harvested, incubated with an anti-Pep12p antibody, and membranes were pelleted using cellulose fibers coupled to secondary antibodies. Samples were analyzed by immunoblot.

While the adapted protocol allowed us to obtain a vesicle fraction of higher purity than before, the immunoblot signal for Nha1p was rather variable between individual experiments, perhaps owing to low abundance or aggregation, so that we were often unable to detect the protein. Enhancing the chemiluminescence signal by using more sensitive ECL reagents did not solve this problem since it caused the appearance of several high molecular weight bands in the IP (Fig. 7.4). These bands were present even when an untagged strain was used, demonstrating that they were unspecific and likely caused by small amounts of unreduced primary antibody, or by other proteins that bound unspecifically to the resin. Therefore, we had to replace Nha1p by an alternative, more abundant, exomer-independent cargo.

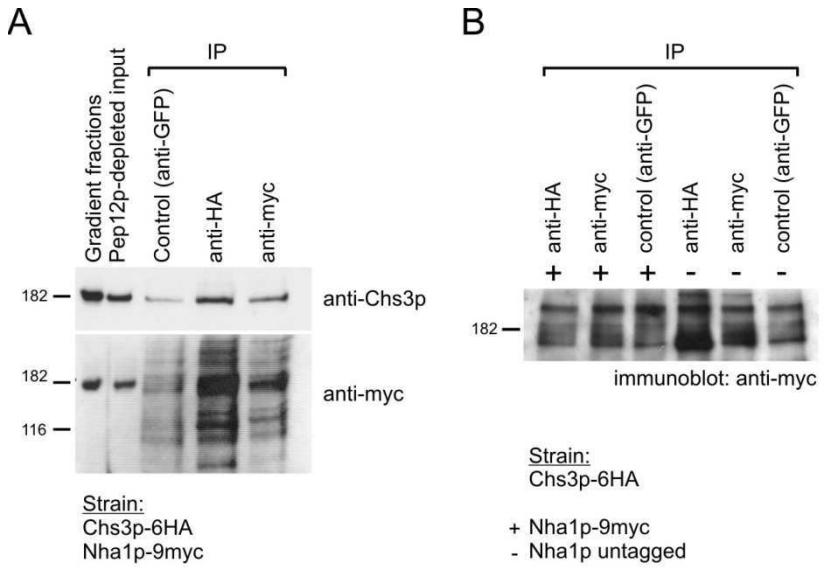

Fig. 7.4 Nha1p cannot be detected using enhanced ECL reagents. (A) Enhanced chemiluminescence detection causes multiple bands at a similar height where the Nha1p-9myc signal is expected. Secretory vesicles were prepared as in Fig. 7.3 and subjected to IP by pre-incubation with primary antibody and precipitation using cellulose fibers coupled to secondary antibody. Samples were incubated at 65°C in SDS sample buffer with DTT and analyzed by immunoblot, using enhanced ECL reagents. (B) The bands observed around 182 kDa were unspecific since they were also present for untagged strains.

We compared the immunoblot signal intensities of several other exomer-independent cargoes such as the zinc transporter Zrt1p (Zhao and Eide, 1996), the general amino acid permease Gap1p (Chen and Kaiser, 2002), the bud-localized membrane protein Skg6p (Gandhi *et al.*, 2006), and the osmosensor Sho1p (Posas and Saito, 1997). Skg6p, in particular, is currently being characterized in our lab as a model for exomer-independent transport. All four proteins showed expression levels above Nha1p (Fig. 7.5), although the Zrt1p and Gap1p signals appeared smeared and Skg6p-9myc

showed some degradation. The choice which of these cargoes is most suitable for a secretory vesicle IP will also be determined by other factors, such as the correct trafficking of the tagged proteins, accessibility of the tags to antibodies and the stability of the proteins during the vesicle preparation procedure.

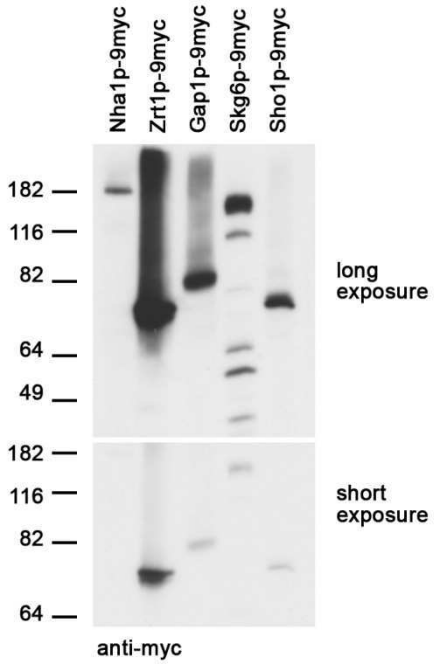

Fig. 7.5 Alternative cargoes for a secretory vesicle IP. Strains expressing 9myc-tagged forms of various plasma membrane proteins were created chromosomally under the native promoters. Lysates were prepared, cleared by a 2,000 g spin, and equal protein amounts were analyzed by immunoblot.

7.2. Steps towards identifying novel exomer-dependent cargoes

7.2.1. Exomer-dependent cargo entry into secretory vesicles

At present, the technical hurdles described above preclude the direct characterization of exomer-dependent vesicles and their protein content. Nevertheless, our centrifugation scheme allowed us to obtain an enriched secretory vesicle fraction. Therefore, we devised an approach to identify novel exomer-dependent cargoes using this preparation: Since Chs5p regulates the entry of a subset of proteins into post-Golgi vesicles, these proteins must be absent from vesicles in a strain deficient of Chs5p or ChAPs. This has been directly demonstrated for Chs3p (Valdivia *et al.*, 2002). We therefore separated lysates from wild-type, *Δmsb3/4* and *Δmsb3/4 Δchs5* strains on sucrose gradients, as described in the previous section (Fig. 7.6B). Surprisingly, however, the Chs3p signal in the vesicle fraction was not significantly reduced in *Δmsb3/4 Δchs5*. Because Chs3p is unable to leave the TGN in this strain, this suggested that the Golgi/endosomal membranes sedimented differently in a *Δmsb3/4 Δchs5* background and contaminated the secretory vesicle fraction. Since Valdivia *et al.* (2002) did not appear to face this problem, it may be specific to our strain background.

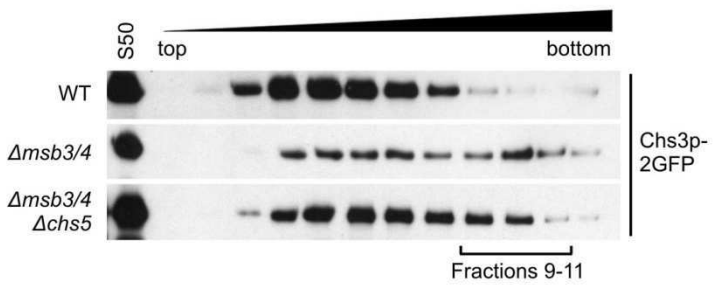

Fig. 7.6 Golgi/endosomal membranes contaminate the secretory vesicle fraction. *Δmsb3/4* cells accumulate Chs3p in secretory vesicles, but the signal in the corresponding fractions is not reduced in *Δmsb3/4 Δchs5*. Gradients were run as in Fig. 7.3. S50: 50,000 g supernatant.

7.2.2. Alternative approach: Exomer-dependent cargo localization to the plasma membrane

Since our secretory vesicle preparation was of insufficient purity, we wondered if there were other means to monitor global changes in protein trafficking upon *CHS5* deletion. We therefore reasoned that cargoes which are unable to leave the TGN will also be unable to reach the cell surface, as previously shown for Chs3p and Fus1p (Santos and Snyder, 1997; Ziman *et al.*, 1998; Barfield *et al.*, 2009). Comparing the plasma membrane proteome between wild-type and *Δchs5* cells might therefore present an alternative strategy to identifying exomer-dependent cargoes (Fig. 7.7A). An advantage of this approach would be that, unlike secretory vesicles, plasma membranes need no prior accumulation. Furthermore, yeast PM has a relatively high density compared to other organelles (Willsky, 1979; Franzusoff *et al.*, 1991), facilitating isolation. A drawback of this strategy is that the plasma membrane ATPase Pma1p is extremely abundant in PM preparations (Zinser and Daum, 1995; Navarre *et al.*, 2002; Ghaemmaghami *et al.*, 2003) and may thus mask rare protein species during mass spectrometry.

When we separated total yeast lysates by a combination of differential and equilibrium density gradient centrifugation, plasma membranes were found enriched at the bottom of the sucrose gradient while most other organelles such as Golgi, ER and endosomes peaked around the middle fractions (Fig. 7.7B) In lysates from wild-type cells, Chs3p was found in two peaks correlating with the Golgi and PM fractions, while the second peak was absent in *Δchs5*. The plasma membrane fractions from wild-type and *Δchs5* gradients were separately harvested and analyzed by SDS-PAGE. The band pattern of both preparations was similar (Fig. 7.7C), which was expected because the exomer pathway constitutes a specialized trafficking route in the cell and only few proteins show exomer-dependent trafficking (Zanolari *et al.*, 2011).

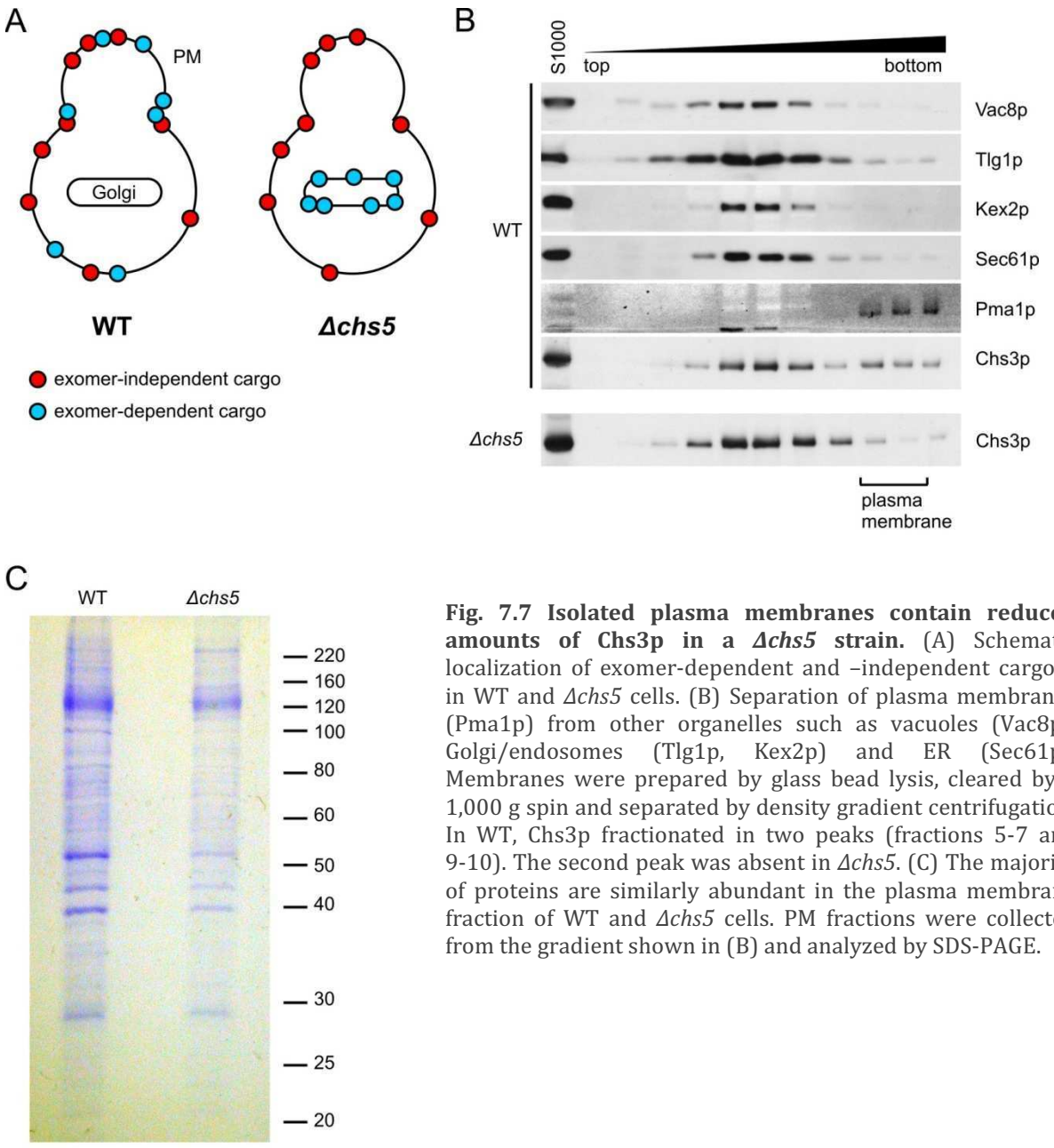

Fig. 7.7 Isolated plasma membranes contain reduced amounts of Chs3p in a *Δchs5* strain. (A) Schematic localization of exomer-dependent and –independent cargoes in WT and *Δchs5* cells. (B) Separation of plasma membranes (Pma1p) from other organelles such as vacuoles (Vac8p), Golgi/endosomes (Tlg1p, Kex2p) and ER (Sec61p). Membranes were prepared by glass bead lysis, cleared by a 1,000 g spin and separated by density gradient centrifugation. In WT, Chs3p fractionated in two peaks (fractions 5-7 and 9-10). The second peak was absent in *Δchs5*. (C) The majority of proteins are similarly abundant in the plasma membrane fraction of WT and *Δchs5* cells. PM fractions were collected from the gradient shown in (B) and analyzed by SDS-PAGE.

Samples were subsequently processed for liquid chromatography and tandem mass spectrometry (LC-MS/MS). The identified proteins from each fraction are listed in Suppl. Table 7.1. Among the most abundant proteins detected were not only Pma1p and other PM components like Fks1p, but also many contaminants from translating ribosomes (Eft1p, Tef1p, Ssb1p) and mitochondria (Ilv5p) (Table 7.1). Out of the 112 proteins identified in total, 39 were annotated as PM-localised proteins according to the *Saccharomyces Genome Database*. The coverage in this pilot experiment was therefore rather low, and the purity of the preparation could be improved. Furthermore, due to this low coverage, only 68 proteins (60%) were found in both the wild-type and *Δchs5* sample. Clearly, additional optimization steps will be required for a large-scale study.

Gene	*Peptides identified*		PM-localized protein	Function
	WT	*Δchs5*		
PMA1	27	27	●	Plasma membrane ATPase
EFT1	19	17		Translation elongation factor 2
FKS1	13	22	●	Catalytic subunit of 1,3-beta-D-glucan synthase
LSP1	12	12		Eisosome component
PIL1	11	11		Eisosome component
TEF1	11	8		Translational elongation factor EF-1 alpha
ILV5	11	7		Mitochondrial acetohydroxyacid reductoisomerase
SSB1	10	9		ATPase, ribosome-associated molecular chaperone
PDR12	10	0	●	ABC transporter, conveys resistance to organic acids

Table 7.1 Highly abundant proteins detected in plasma membrane preparations from WT and *Δchs5* cells. Table shows the results of one experiment. Only proteins with ten or more identified peptides are shown. The full list is found in Suppl. Table 7.1.

For those proteins found in at least one sample, the number of identified peptides allowed a preliminary comparison of protein amounts at the PM. Several proteins displayed changes in abundance upon *CHS5* deletion (Table 7.1). Importantly, three out of the four most up-regulated proteins (Fks1p, Gas3p and Chs1p) were factors involved in cell wall synthesis, suggesting that in *Δchs5* cells the expression of cell wall remodeling enzymes at the PM was increased in response to chitin synthesis defects (Table 7.2). This finding indicated that we were able to detect some physiologically relevant changes, although in this case they probably reflected transcriptional up-regulation rather than increased surface delivery (Valdivieso *et al.*, 2000). Unfortunately, neither Chs3p nor Fus1p was identified in the experiment, so that we do not know what magnitude of change can be expected for an exomer-dependent cargo.

The most strongly down-regulated protein was Pdr12p, an ABC transporter involved in resistance to weak organic acids (Piper *et al.*, 1998). However, Pdr12p-GFP efficiently reached the cell surface in wild-type and *Δchs5* cells, indicating that Pdr12p is not an exomer-dependent cargo (Fig. 7.8). Instead, we noticed consistently lower levels of fluorescence in the mutant cells, suggesting that the differences observed by mass spectrometry were due to a transcriptional response and not a trafficking defect. We had previously observed a similar effect for the Ena1p and Ena2p sodium transporters (Wieland *et al.*, 1995), which displayed PM localization independently of exomer but whose expression levels were reduced in *Δchs5* strains (unpublished observations).

Gene	Peptides identified			PM-localised protein	Function
	WT	*Δchs5*	Diff.		
FKS1	13	22	9	●	Catalytic subunit of 1,3-beta-D-glucan synthase
TIF1	0	6	6		Translation initiation factor eIF4A
GAS3	3	8	5	●	Beta-1,3-glucanosyltransferase
CHS1	0	4	4	●	Chitin synthase 1
NDE1	0	4	4		Mitochondrial external NADH dehydrogenase
ILV5	11	7	-4		Mitochondrial acetohydroxyacid reductoisomerase
KAR2	6	2	-4		ATPase involved in protein import into the ER
HXT1	4	0	-4	●	Low-affinity glucose transporter
ILV3	4	0	-4		Dihydroxyacid dehydratase
PAN1	5	0	-5		Part of actin-regulatory complex Pan1p-Sla1p-End3p
TCB3	6	0	-6	●	Tricalbin 3, role in vesicle-mediated transport
BAT1	6	0	-6		Mitochondrial amino acid aminotransferase
PDR12	10	0	-10	●	ABC transporter, conveys resistance to organic acids

Table 7.2 Proteins with altered abundance in plasma membrane preparations of *Δchs5* compared to WT cells. Table shows results from the same experiment as in Table 7.1, ordered by the difference ("Diff.") in the number of peptides. Only proteins with an absolute difference of 4 or higher are shown.

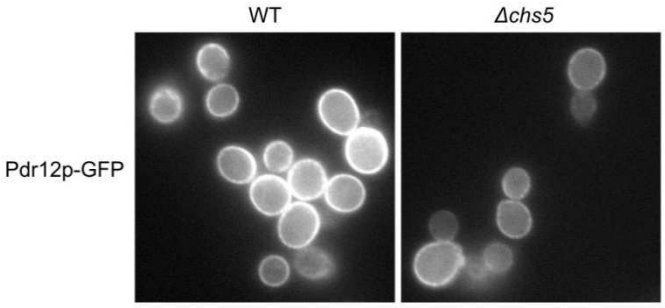

Fig. 7.8 Pdr12p is an exomer-independent cargo. The localization of Pdr12p-GFP was similar in WT and *Δchs5* cells. However, total fluorescence levels were lower in the mutant strain.

7.3. Section summary and outlook

The first goal of this section was to test whether vesicles containing exomer-dependent cargo could be separated from those carrying exomer-independent cargo. We were able to produce an enriched secretory vesicle fraction and precipitate Chs3p- and Nha1p-containing membranes from this preparation. The result of this experiment suggested that Chs3p and Nha1p were present in the same vesicle; however, the presence of contaminating organelles such as Golgi and endosomes (through which both Chs3p and Nha1p may traverse) rendered the experiment inconclusive.

While attempting to reduce endosomal contaminations, we faced a trade-off of yield vs. purity: Through a combination of higher pre-spins, larger sucrose gradients and specific immunodepletion of endosomal membranes we were able to obtain a rather pure vesicle preparation, but we also lost a large amount of material during this procedure. More abundant cargoes than Nha1p will thus be required for reliable detection. However, another important question remains: What degree of secretory vesicle purity must be obtained so that co-precipitation of exomer-dependent and -independent cargoes can be believed to reflect sorting into a common vesicle, and not a contamination? A useful control would be the differential IP of high-density and low-density vesicles, which are known to contain different cargoes. However, the enzymes known to be secreted via the high-density secretory vesicle (HDSV) pathway lack cytoplasmic domains and therefore inaccessible to antibodies (Harsay and Bretscher, 1995; Lustgarten and Gerst, 1999; Gurunathan *et al.*, 2002). In summary, despite our intensive efforts to differentially precipitate exomer-dependent and -independent cargoes, we are still unable to conclude whether or not they travel in the same transport vesicle.

A recent report described the immunoisolation and characterization of yeast post-Golgi vesicles marked by Pma1p, Mid2p or a mutant form of Gap1p (Surma *et al.*, 2011). These three proteins have mostly overlapping, but also some distinct, requirements for delivery to the PM (Bagnat *et al.*, 2001; Chen and Kaiser, 2002). All three vesicle preparations showed a similar cargo content and lipid composition, suggesting that the low-density vesicle fraction might in fact be homogeneous and lack sub-populations. Instead, packaging of different cargoes into one common vesicle may require individual sorting machineries. Unfortunately, the study was not extended to Chs3p or Fus1p, so that it is still unknown whether or not these cargoes enter the same type of secretory vesicle as Pma1p, Gap1p or Mid2p.

It is also currently unclear why a subset of cargoes requires exomer for Golgi exit, while the majority of secreted proteins does not. In order to better understand this difference in behavior, we aimed to identify more exomer-dependent cargoes. The secretory vesicle preparation we obtained proved unsuitable for analysis due to endosomal contaminations. Instead, we were able to obtain a PM fraction that was depleted of Golgi, endosomal, vacuolar and ER membranes, and which contained reduced amounts of Chs3p in *Δchs5* compared to wild-type. To extend this analysis to other proteins on a much larger scale, the SILAC technique (Stable Isotope Labeling of Amino acids in Cell culture) would be the method of choice (Ong *et al.*, 2002). However, we faced several problems: Firstly, the proteome coverage in a pilot experiment was rather low, so that quite some optimization would be required. This should be feasible, e.g. by pre-separation of the samples by SDS-PAGE and performing

LC-MS/MS on individual gel strips (Soulard *et al.*, 2010). New and more sensitive technology would certainly facilitate this process.

Secondly, we identified numerous mitochondrial and ribosome-associated proteins in our preparations, indicating that additional washing steps might be required. This could considerably lengthen the protocol and the time to establish it (Navarre *et al.*, 2002). Thirdly, neither Chs3p nor Fus1p were among the proteins detected in the wild-type PM sample. This is not unexpected, as Chs3p is only found at the bud neck in small- and large-budded cells, but not in the unbudded or medium-budded stage (Chuang and Schekman, 1996; Ziman *et al.*, 1996). In an asynchronous culture, cargoes with a Chs3p-like localization and abundance may therefore be very difficult to detect. A synchronized yeast population, obtained e.g. by elutriation, would allow us to focus specifically on small-budded cells. On the other hand, this would greatly increase the volume of SILAC medium required and, accordingly, the cost of the experiment.

Taken together, we can conclude that performing a SILAC experiment on plasma membrane preparations would probably be technically possible. However, there are alternative and more straightforward strategies to identify novel exomer-dependent cargoes, e.g. searching for physical exomer interactors by crosslinking and tandem-affinity purification (Tagwerker *et al.*, 2006).

7.4. Supplementary Material

Gene	*Peptides identified*		PM-localized protein
	WT	*Δchs5*	
PMA1	27	27	●
EFT1	19	17	
FKS1	13	22	●
LSP1	12	12	
PIL1	11	11	
TEF1	11	8	
ILV5	11	7	
SSB1	10	9	
PDR12	10	0	●
FAA1	9	7	
GAS1	8	8	●
ATP2	8	7	
PGK1	8	7	
ENO1	8	7	
TY1B	8	6	
ZEO1	8	6	●
PDR5	7	7	●
PYK1	7	5	
POR1	6	7	
PDC1	6	6	
KAR2	6	2	
TCB3	6	0	●
BAT1	6	0	
RHO1	5	7	
MIR1	5	7	
SNQ2	5	6	●
SSC1	5	6	
YCP4	5	4	
SSO2	5	3	●
FAT2	5	3	
YCK1	5	2	●
OLA1	5	2	
PAN1	5	0	
SSA1	4	7	
HXT3	4	6	●
AAC2	4	6	
HSC82	4	5	
ATP1	4	5	
RSN1	4	4	●
ECM33	4	4	●

GAS5	4	4	●
EXG2	4	4	●
HSP60	4	4	
YCK2	4	3	●
ERG6	4	3	
PST2	4	3	
SCS2	4	3	
RTN1	4	3	
PDB1	4	2	
PDI1	4	2	
SAC1	4	2	
HXT1	4	0	●
ILV3	4	0	
GAS3	3	8	●
YEF3	3	6	
ITR1	3	4	●
RPL12A	3	3	
BMH1	3	3	
SUR7	3	3	●
SAM3	3	0	●
ILV2	3	0	
FMP52	3	0	
CIT1	3	0	
SSO1	2	4	●
FET3	2	3	●
ENO2	2	3	
YJL171C	2	3	●
TDH1	2	3	
PDR10	2	3	●
GPM1	2	3	
HXT2	2	3	●
RAS2	2	2	●
YHM2	2	2	
SSH1	2	2	
RPS3	2	2	
AHP1	2	2	
RPS18A	2	2	
RPS16A	2	2	
YGR266W	2	0	●
IDP1	2	0	
MDH1	2	0	
PDA2	2	0	
RCR1	2	0	
PDA1	2	0	
YJU3	2	0	
TDH2	2	0	
GND1	2	0	

RHO5	2	0	
ELO3	2	0	
TPO1	2	0	●
TCB2	2	0	●
STE2	2	0	●
NCE102	2	0	●
YLR413W	2	0	●
TCB1	2	0	●
SEC4	2	0	
TIF1	0	6	
CHS1	0	4	●
NDE1	0	4	
PHO88	0	3	●
RPS13	0	3	
YMR295C	0	3	
FAS3	0	2	
ARF1	0	2	
ATP4	0	2	
GSC2	0	2	●
KRE6	0	2	●
PDR15	0	2	●
RPL4A	0	2	
RPS1B	0	2	
RPS6A	0	2	
TOM40	0	2	

Suppl. Table 7.1 Full list of proteins identified in plasma membrane preparations from WT and *Δchs5* cells. Table shows the results of one experiment.

Materials and Methods

8. Materials and Methods

8.1. Materials

8.1.1. Instruments

Instrument	Manufacturer
Axiocam MRm camera	Zeiss
Axioplan 2 epi-fluorescence microscope	Zeiss
Cooling centrifuge 5417 R	Eppendorf
Cooling centrifuge 5810 R	Eppendorf
Cooling centrifuge Discovery 90SE	Sorvall
Ultracentrifuge Optima	Beckman
Rotor GS3	Kendro
Rotor SS34	Kendro
Rotor TH-641	Sorvall
Rotor TLA-55	Beckman
Rotor TLS 55	Beckman
Rotor TLA 100	Beckman
Spectrophotometer UltroSpec 3100 pro	Amersham Biosciences
Chemiluminescence imager LAS-4000	Fujifilm
Lyophilisator Speedvac Plus Sc110A	Savant

Only non-standard instruments are listed.

8.1.2. Kits

Name	Order #	Supplier
Biorad protein assay kit	500-0001	Biorad
Expand High Fidelity PCR system	1732641	Roche
Expand Long Template PCR System	11681842001	Roche
NucleoSpin Plasmid Mini Kit	740588.5	Macherey & Nagel
NucleoSpin Gel & PCR Cleanup Kit	740609.5	Macherey & Nagel
ECL Advanced Kit	RPN 2135	Amersham Bioscience
ECL Kit	RPN 2106	Amersham Bioscience
Rapid DNA ligation kit	1635379	Roche

8.1.3. Chemicals and Consumables

Standard chemicals were obtained from Sigma, Roth or Merck.

Material	Ordner #	Supplier
Difco™ Agar granulated	214510	BD
Bacto™ Peptone	211830	BD
Bacto™ Tryptone	211701	BD
Bacto™ Yeast extract	212730	BD
Difco™ Yeast nitrogen base (YNB) w/o amino acids	291920	BD
Benchmark Protein Ladder	10747-012	Invitrogen
Benchmark Protein Ladder Prestained	10748-010	Invitrogen
Brillant Blue G250	35050	Serva
Brillant Blue R250	35051	Serva
Calcofluor white dye	F-3543	Sigma
Cellulose, microgranular	C6413	Sigma
Complete mini EDTA-free protease inhibitors	1836170	Roche
Concanavalin A	C2631	Sigma
Dextrose	A1349	Applichem
Dimethylpimelimidate (DMP)	21667	Thermo Scientific
Dithiobis(succinimidylpropionate) (DSP)	22586	Thermo Scientific
Dynabeads M-280 sheep-anti-rabbit	112-03D	Invitrogen
Galactose	G0750	Sigma
Glass beads 0.25 – 0.5 mm	A553.1	Roth
Glutathione (GSH)	737038	Roche
GSH agarose	G4510	Sigma
Iodoacetamide (IAA)	I-1149	Sigma
Leupeptin	L-8511	Sigma
Pepstatin A	P-5318	Sigma
Protein A-sepharose CL-4B	17-0780-01	Amersham Bioscience
Raffinose	5241	Roth
Trypsin	V5111	Promega

Only non-standard chemicals and consumables are listed.

8.1.4. Media

Standard yeast media were prepared (Sherman, 1991) and autoclaved at 121°C for 20 min. Distilled or double-distilled water was used exclusively. "YNB" stands for "yeast nitrogen base".

LB medium:	10 g tryptone (BD) 5 g yeast extract (BD) 10 g NaCl (Roth) ad 1 l dH_2O and autoclaved 1 ml 1000x ampicillin was added after autoclaving.
LB agar:	5 g tryptone (BD) 2.5 g yeast extract (BD) 5 g NaCl (Roth) 10 g agar (BD) ad 500 ml dH_2O and autoclaved 0.5 ml 1000x ampicillin was added after autoclaving.
SOC-medium:	5 g yeast extract (BD) 20 g peptone (BD) 20 g dextrose 10 mM NaCl 2.5 mM KCl 10 mM $MgSO_4$ ad 1 l dH_2O and autoclaved
HC medium:	800 ml dH_2O 100 ml 10x HC-XX (without the component to select for) 100 ml 10x YNB w/o amino acids Complemented with 2% (w/v) dextrose after autoclaving.
Calcofluor white plates:	50 ml 10x YNB w/o amino acids 20 ml 50% dextrose 50 ml 10x HC complete 50 ml 10% MES buffer pH 6.0 5 ml 10% yeast extract 350 ml autoclaved agar (60°C), final conc. 2% 1 ml calcofluor white solution (50 mg/ml) was added while stirring. Plates were poured immediately.

HC agar:	hot sterile agar (10 g dissolved in 350 ml H_2O) 50 ml 20% dextrose 50 ml 10x YNB w/o amino acids 50 ml 10x HC-XX (without the component to select for)
YP medium:	1% yeast extract (BD) 2% peptone (BD) Complemented with 2% (w/v) dextrose after autoclaving. For induction of genes under control of the *GAL1* promoter, the mixture was complemented with 1% raffinose and 2% galactose instead of dextrose.
YP agar:	10 g peptone (BD) 5 g yeast extract (BD) 10 g agar (BD) ad 450 ml dH_2O and autoclaved Complemented with 50 ml 20% (w/v) dextrose before plates were poured. For induction of genes under control of the *GAL1* promoter, the mixture was complemented with 1% raffinose and 2% galactose instead of glucose.
5-FOA-plates:	0.34 g w/o amino acids 0.05 g 5-fluoroorotic acid (Biovectra 1555) 1 g dextrose 5 ml 10x HC-XX (without the component to select for) ad 20 ml dH_2O and filter sterilized into 25 ml warm (55°C) sterile agar (1 g in 25 ml H_2O)

8.1.5. Common solutions and buffers

Double-distilled H_2O was used exclusively for preparation of all solutions and buffers.

1000x ampicillin	100 mg/ml in dH_2O, filter-sterilized
100x G418	20 mg/ml geneticin in dH_2O, filter-sterilized

2000x ClonNAT	200 mg/ml nourseotricin in ddH_2O, filter-sterilized
150x IPTG:	150 mM, filter sterilized
50x lysozyme:	50 mg/ml
1000x pepstatin A	1 mg/ml in DMSO
1000x leupeptin	1 mg/ml in DMSO
1000x antipain	1 mg/ml in ddH_2O
100x PMSF:	0.1 M in isopropanol
10x HC mixture	0.2 mg/ml adenine hemi-sulfate 0.35 mg/ml uracil 0.8 mg/ml L-tryptophan 0.2 mg/ml L-histidine-HCl 0.8 mg/ml L-leucine 1.2 mg/ml L-lysine-HCl 0.2 mg/ml L-methionine 0.6 mg/ml L-tyrosine 0.8 mg/ml L-isoleucine 0.5 mg/ml L-phenylalanine 1.0 mg/ml L-glutamic acid 2.0 mg/ml L-threonine 1.0 mg/ml L-aspartic acid 1.5 mg/ml L-valine 4.0 mg/ml L-serine 0.2 mg/ml L-arginine-HCl autoclaved for selection media, the components to select for were omitted
Calcofluor white stock:	50 mg/ml NaOH added dropwise to dissolve
6x loading buffer for agarose gel-electrophoresis:	0.25% Bromophenol Blue 0.25% Xylene Cyanol 30% glycerol
B88 buffer:	20 mM HEPES/KOH pH 6.8 250 mM sorbitol 150 mM KAc 5 mM $Mg(Ac)_2$

	filter sterilized
5x Laemmli buffer:	62.5 mM Tris/HCl pH 6.8 5% β-mercaptoethanol 10% glycerol 2% SDS 0.0025% Bromophenol Blue
50x TAE buffer:	2 M Tris/HAc pH 7.7 5 mM EDTA
20x TBS:	60 g Tris/HCl pH 7.4 160 g NaCl 4 g KCl ad 1 l with H_2O
20x PBS	46.6 g $Na_2HPO_4 \cdot 12\ H_2O$ 4.2 g KH_2PO_4 175.2 g NaCl 44.8 g KCl ad 1 l with H_2O
TBS-T:	TBS with 0.1% Tween-20
Coomassie staining solution:	7.5% acetic acid 50% methanol 0.25% Serva Brilliant Blue R250
Destaining solution:	7.5% acetic acid 50% methanol
Carrier DNA for transformations:	200 mg Salmon Sperm DNA (Sigma D1626) TE buffer ad 100 ml
B150Tw20:	20 mM HEPES/KOH pH 6.8 150 mM KAc 5 mM $Mg(Ac)_2$ 1% Tween-20
Transfer buffer:	25 mM Tris 192 mM glycine 0.25% SDS 20% methanol
Ponceau S solution	1 g Ponceau S (Roth) 485 ml ddH_2O 15 ml 100% trichloroacetic acid (TCA)

10x YNB:	33.5 g Yeast Nitrogen Base w/o amino acids (BD) ad 500 ml dH_2O wrapped in aluminum foil and autoclaved the same day.

8.1.6. Plasmids

Plasmid	Description	Reference / Source
pUG series	amplification of PCR cassettes for deletions of genes by chromosomal integration	(Güldener *et al.*, 2002)
pYM series	amplification of PCR cassettes for C-terminal tagging by chromosomal integration	(Janke *et al.*, 2004)
pYM-3GFP	3xGFP and TRP1-cassette; integrates as 1xGFP, 2xGFP or 3xGFP	(Zanolari *et al.*, 2011)
pYM-N series	amplification of PCR cassettes for N-terminal tagging or promoter exchange by chromosomal integration	(Janke *et al.*, 2004)
pSH series	expression of Cre recombinase for chromosomal excision of auxotrophy markers	(Güldener *et al.*, 2002)
pRS series	allele replacement and ectopic protein expression in yeast	(Sikorski and Hieter, 1989)
pRS314-Nui	expression of fusion proteins for split ubiquitin assay	(Johnsson and Varshavsky, 1994)
pRS313-Cub	expression of fusion proteins for split ubiquitin assay	(Johnsson and Varshavsky, 1994)
pCORE	amplification of CORE cassette (KanMX4-klURA3) for *delitto perfetto*	(Storici and Resnick, 2006)
pTPQ128	Sec7p-dsRed	(Proszynski *et al.*, 2005)
pGS99	pRS315-*exo84-117*	Wei Guo
Pma1p-GFP	TEF-Pma1p-GFP	Aaron Neiman
GFP-Cwp2	GFP-Cwp2	Howard Riezman
pGEX-6P-1	cloning and bacterial expression of N-terminally tagged GST fusion proteins	GE Healthcare

8.2. Strains

Name	Genotype	Reference
YPH499	*MAT a ade2 his3 leu2 lys2 trp1 ura3*	Sikorski and Hieter, 1989
YAS328	*MAT a ade2 his3 leu2 lys2 trp1 ura3 CHS6::CHS6-9myc (Kl TRP1)*	Trautwein *et al.*, 2006
YAS2413	*MAT α ade2 his3 leu2 lys2 trp1 ura3 CHS3::CHS3-2GFP (Kl TRP1) CHS6::CHS6(Δ730-1212)-9myc (HIS3MX6)*	This study
YAS2414	*MAT α ade2 his3 leu2 lys2 trp1 ura3 CHS3::CHS3-2GFP (Kl TRP1) CHS6::CHS6(Δ1837-1938)-9myc (HIS3MX6)*	This study
YAS2506	*MAT a ade2 his3 leu2 lys2 trp1 ura3 CHS6::TEF(natNT2)-CHS6-9myc (Kl TRP1)*	This study
YAS2475	*MAT α ade2 his3 leu2 lys2 trp1 ura3 CHS3::CHS3-2GFP (Kl TRP1) CHS6::TEF(natNT2)-CHS6(Δ730-1212)-9myc (HIS3MX6)*	This study
YAS2476	*MAT α ade2 his3 leu2 lys2 trp1 ura3 CHS3::CHS3-2GFP (Kl TRP1) CHS6::TEF(natNT2)-CHS6(Δ1837-1938)-9myc (HIS3MX6)*	This study
YAS563-2a	*MAT a ade2 his3 leu2 lys2 trp1 ura3 CHS6::URA3*	Trautwein *et al.*, 2006
YAS2855	*MAT a/α ade2/ade2 his3/his3 leu2/leu2 lys2/lys2 trp1/trp1 ura3/ura3 CHS3::CHS3-2GFP (Kl TRP1) CHS6::CHS6(Δ730-1212)-9myc (HIS3MX6) CHS6::CHS6(Δ1837-1938)*	This study
YAS563-4A	*MAT a ade2 his3 leu2 lys2 trp1 ura3 BCH2::KAN (Tn903)*	Trautwein *et al.*, 2006
YAS525	*MAT a ade2 his3 leu2 lys2 trp1 ura3 CHS6::URA3 BCH2::KAN (Tn903)*	Trautwein *et al.*, 2006
YAS2938	*MAT a ade2 his3 leu2 lys2 trp1 ura3 CHS6::LEU2 BCH2::BCH2(Δ739-1224)*	This study
YAS2939	*MAT a ade2 his3 leu2 lys2 trp1 ura3 CHS6::LEU2 BCH2::BCH2(Δ1840-1941)*	This study
YAS563-5a	*MAT a ade2 his3 leu2 lys2 trp1 ura3 BCH1::HIS5 (S. pombe)*	Trautwein *et al.*, 2006
YAS2852	*MAT a ade2 his3 leu2 lys2 trp1 ura3 BCH1::BCH1(Δ793-1251)*	This study
YAS2853	*MAT a ade2 his3 leu2 lys2 trp1 ura3 BCH1::BCH1(Δ1723-1824)*	This study
YAS2923	*MAT a ade2 his3 leu2 lys2 trp1 ura3 CHS6::CHS6-3GFP (Kl TRP1) pTPQ128*	This study
YAS2924	*MAT α ade2 his3 leu2 lys2 trp1 ura3 CHS3::CHS3 (URA3)* CHS6::CHS6(Δ730-1212)-3GFP (Kl TRP1) pTPQ128*	This study
YAS2925	*MAT α ade2 his3 leu2 lys2 trp1 ura3 CHS3::CHS3 (URA3)* CHS6::MET25(natNT2)-CHS6(Δ1837-1938)-3GFP (Kl TRP1) pTPQ128*	This study
YAS2700	*MAT a ade2 his3 leu2 lys2 trp1 ura3 pTPQ128*	This study
YAS2561	*MAT a ade2 his3 leu2 lys2 trp1 ura3 CHS6::TEF(natNT2)-CHS6-9myc (URA3) BCH1::BCH1-6HA (KanMX4)*	This study
YAS2570	*MAT α ade2 his3 leu2 lys2 trp1 ura3 CHS3::CHS3-2GFP (Kl TRP1) CHS6::CHS6(Δ730-1212)-9myc (HIS3MX6) BCH1::BCH1-6HA (KanMX4)*	This study
YAS2508	*MAT α ade2 his3 leu2 lys2 trp1 ura3 CHS3::CHS3-2GFP (Kl TRP1) CHS6::CHS6(Δ1837-1938)-9myc (HIS3MX6) BCH1::BCH1-6HA (KanMX4)*	This study
YAS2854	*MAT α ade2 his3 leu2 lys2 trp1 ura3 CHS3::CHS3-2GFP (Kl TRP1) CHS6::TEF(natNT2)-CHS6(L619W/G620D)-9myc (HIS3MX6)*	This study
YAS2851	*MAT α ade2 his3 leu2 lys2 trp1 ura3 CHS3::CHS3-2GFP (Kl TRP1) CHS6::CHS6-BCH2(739-1224)*	This study
YAS2850	*MAT α ade2 his3 leu2 lys2 trp1 ura3 CHS3::CHS3-2GFP (Kl TRP1) CHS6::CHS6-BCH2(1840-1941)*	This study

YAS3083	*MAT α ade2 his3 leu2 lys2 trp1 ura3 CHS3::CHS3-2GFP (Kl TRP1) CHS6::LEU2 BCH2::BCH2-CHS6(1837-1938)*	This study
YAS2927	*MAT α ade2 his3 leu2 lys2 trp1 ura3 CHS3::CHS3-2GFP (Kl TRP1) CHS6::CHS6-BCH2(1225-1839)-9myc (HIS3MX6)*	This study
YAS3084	*MAT α ade2 his3 leu2 lys2 trp1 ura3 CHS3::CHS3-2GFP (Kl TRP1) BCH2::BCH2-CHS6(1213-1836)-9myc (HIS3MX6) CHS6::LEU2*	This study
YAS3021	*MAT α ade2 his3 leu2 lys2 trp1 ura3 CHS3::CHS3-2GFP (Kl TRP1) BCH2::CHS6 CHS6::LEU2*	This study
YAS3019	*MAT α ade2 his3 leu2 lys2 trp1 ura3 CHS3::CHS3-2GFP (Kl TRP1) BCH2::BCH2-CHS6(1-1836)-9myc (HIS3MX6) CHS6::LEU2*	This study
YAS3085	*MAT α ade2 his3 leu2 lys2 trp1 ura3 CHS3::CHS3-2GFP (Kl TRP1) BCH2::BCH2-CHS6(1213-2241)-9myc (HIS3MX6) CHS6::LEU2*	This study
YAS3087	*MAT α ade2 his3 leu2 lys2 trp1 ura3 CHS3::CHS3-2GFP (Kl TRP1) BCH2::BCH2-CHS6(1-729,1213-1836, 1939-2241) CHS6::LEU2*	This study
YAS3091	*MAT α ade2 his3 leu2 lys2 trp1 ura3 CHS3::CHS3(Δ3433-3498)-3GFP (Kl TRP1) pTPQ128*	This study
YAS3093	*MAT α ade2 his3 leu2 lys2 trp1 ura3 CHS3::CHS3(Δ3385-3498)-3GFP (Kl TRP1) pTPQ128*	This study
YAS1516	*MAT α ade2 his3 leu2 lys2 trp1 ura3 CHS3::LEU2*	This study
YAS3077	*MAT α ade2 his3 leu2 lys2 trp1 ura3 CHS6::TEF(natNT2)-CHS6-9myc (Kl TRP1) CHS3::LEU2*	This study
YAS2632	*MAT α ade2 his3 leu2 lys2 trp1 ura3 CHS6::TEF(natNT2)-CHS6-9myc (Kl TRP1) CHS5::LEU2*	This study
YAS2712	*MAT α ade2 his3 leu2 lys2 trp1 ura3 CHS3::CHS3-2GFP (Kl TRP1) CHS6::CHS6(Δ730-1212)-9myc (HIS3MX6) CHS5::LEU2*	This study
YAS2562	*MAT α ade2 his3 leu2 lys2 trp1 ura3 CHS6::TEF(natNT2)-CHS6-9myc (URA3) BUD7::BUD7-6HA (KanMX4)*	This study
YAS2571	*MAT α ade2 his3 leu2 lys2 trp1 ura3 CHS3::CHS3-2GFP (Kl TRP1) CHS6::CHS6(Δ730-1212)-9myc (HIS3MX6) BUD7::BUD7-6HA (KanMX4)*	This study
YAS2510	*MAT α ade2 his3 leu2 lys2 trp1 ura3 CHS3::CHS3-2GFP (Kl TRP1) CHS6::CHS6(Δ1837-1938)-9myc (HIS3MX6) BUD7::BUD7-6HA (KanMX4)*	This study
YAS1291	*MAT α ade2 his3 leu2 lys2 trp1 ura3 CHS3-2GFP::TRP1 HXT2-eqFP611::KanMX4*	This study
YAS1322	*MAT α ade2 his3 leu2 lys2 trp1 ura3 CHS3-2GFP::TRP1 HXT2-eqFP611::KanMX4 chs5::LEU2*	This study
YAS1311	*MAT α ade2 his3 leu2 lys2 trp1 ura3 CHS3-2GFP::TRP1 HXT2-eqFP611::KanMX4 ypt7::URA3*	This study
YAS1328	*MAT α ade2 his3 leu2 lys2 trp1 ura3 CHS3-2GFP::TRP1 HXT2-eqFP611::KanMX4 msb3::URA3*	This study
YAS1342	*MAT α ade2 his3 leu2 lys2 trp1 ura3 CHS3-2GFP::TRP1 HXT2-eqFP611::KanMX4 msb4::LEU2*	This study
YAS1344	*MAT α ade2 his3 leu2 lys2 trp1 ura3 CHS3-2GFP::TRP1 HXT2-eqFP611::KanMX4 msb3::URA3 msb4::LEU2*	This study
YAS1310	*MAT α ade2 his3 leu2 lys2 trp1 ura3 CHS3-2GFP::TRP1 HXT2-eqFP611::KanMX4 ypt6::URA3*	This study
YAS1312	*MAT α ade2 his3 leu2 lys2 trp1 ura3 CHS3-2GFP::TRP1 HXT2-eqFP611::KanMX4 ypt10::URA3*	This study
YAS1313	*MAT α ade2 his3 leu2 lys2 trp1 ura3 CHS3-2GFP::TRP1 HXT2-eqFP611::KanMX4 ypt11::URA3*	This study
YAS1325	*MAT α ade2 his3 leu2 lys2 trp1 ura3 CHS3-2GFP::TRP1 HXT2-eqFP611::KanMX4 ypt51::LEU2*	This study
YAS1345	*MAT α ade2 his3 leu2 lys2 trp1 ura3 CHS3-2GFP::TRP1 HXT2-eqFP611::KanMX4 ypt51::LEU2 ypt52::HIS5 ypt53::URA3*	This study
YAS1321	*MAT α ade2 his3 leu2 lys2 trp1 ura3 CHS3-2GFP::TRP1 HXT2-eqFP611::KanMX4 ypt31::LEU2*	This study
YAS1314	*MAT α ade2 his3 leu2 lys2 trp1 ura3 CHS3-2GFP::TRP1 HXT2-eqFP611::KanMX4 ypt32::URA3*	This study
YAS1839	*MAT α ade2 his3 leu2 lys2 trp1 ura3 CHS3-2GFP::TRP1 HXT2-eqFP611::KanMX4 ypt31::LEU2 ypt32A141D::HIS*	This study
YAS2346	*MAT α ade2 his3 leu2 lys2 trp1 ura3 CHS3-2GFP::TRP1 HXT2-eqFP611::KanMX4 sur2::LEU2*	This study
YAS2347	*MAT α ade2 his3 leu2 lys2 trp1 ura3 CHS3-2GFP::TRP1 HXT2-eqFP611::KanMX4 elo3::LEU2*	This study
YAS1630	*MAT α ade2 his3 leu2 lys2 trp1 ura3 CHS3-2GFP::TRP1 clonNAT-GAL1p-SEC6*	This study

YAS1484	*MAT a ade2 his3 leu2 lys2 trp1 ura3 SEC8-GFP::KanMX4*	This study
YAS1489	*MAT α ade2 his3 leu2 lys2 trp1 ura3 CHS3-2GFP::TRP1 HXT2-eqFP611::KanMX4 sec6-4*	This study
YAS1450	*MAT a ade2 his3 leu2 ura3 CHS3-2GFP::TRP1 HXT2-eqFP611::KanMX4 sec3-2*	This study
YAS1452	*MAT a ade2 his3 lys2 ura3 CHS3-2GFP::TRP1 HXT2-eqFP611::KanMX4 ypt1-3*	This study
YAS1415	*MAT a ade2 leu2 lys2 ura3 CHS3-2GFP::TRP1 HXT2-eqFP611::KanMX4 sec2-41*	This study
YAS1597	*MAT α ade2 his3 leu2 lys2 trp1 ura3 CHS3-2GFP::TRP1 HXT2-eqFP611::KanMX4 sec4-8*	This study
YAS1352	*MAT α ade2 his3 leu2 lys2 trp1 ura3 CHS3-2GFP::TRP1 HXT2-eqFP611::KanMX4 sro7::URA3*	This study
YAS1420	*MAT α ade2 his3 leu2 lys2 trp1 ura3 CHS3-2GFP::TRP1 HXT2-eqFP611::KanMX4 sro77::LEU2*	This study
YAS1421	*MAT α ade2 his3 leu2 lys2 trp1 ura3 CHS3-2GFP::TRP1 HXT2-eqFP611::KanMX4 sro7::URA3 sro77::LEU2*	This study
YAS946	*MAT α ade2 his3 leu2 lys2 trp1 ura3 CHS3-2GFP::TRP1*	Trautwein *et al.*, 2006
YAS2674	*MAT a ade2 his3 leu2 lys2 trp1 ura3 ITR1-GFP::TRP1*	This study
YAS2675	*MAT a ade2 his3 leu2 lys2 trp1 ura3 ITR1-GFP::TRP1 sro7::LEU2 sro77::HIS3*	This study
YAS2676	*MAT a ade2 his3 leu2 lys2 trp1 ura3 ITR1-GFP::TRP1 ypt32::LEU2*	This study
YAS2677	*MAT a ade2 his3 leu2 lys2 trp1 ura3 ITR1-GFP::TRP1 sro77::HIS3*	This study
YAS2678	*MAT a ade2 his3 leu2 lys2 trp1 ura3 ITR1-GFP::TRP1 ypt31::LEU2*	This study
YAS2679	*MAT a ade2 his3 leu2 lys2 trp1 ura3 ITR1-GFP::TRP1 sro7::LEU2*	This study
YAS2680	*MAT a ade2 his3 leu2 lys2 trp1 ura3 ITR1-GFP::TRP1 ypt51:LEU2 ypt52::HIS3 ypt53::KanMX4*	This study
YAS2681	*MAT a ade2 his3 leu2 lys2 trp1 ura3 ITR1-GFP::TRP1 chs5::LEU2*	This study
YAS2682	*MAT a ade2 his3 leu2 lys2 trp1 ura3 ITR1-GFP::TRP1 ypt7::LEU2*	This study
YAS2687	*MAT a ade2 his3 leu2 lys2 trp1 ura3 ypt31::LEU2 ypt32A141D::HIS3*	This study
YAS2686	*MAT a ade2 his3 leu2 lys2 trp1 ura3 ypt51::LEU2 ypt52::HIS3 ypt53::KanMX4*	This study
YAS2688	*MAT a ade2 his3 leu2 lys2 trp1 ura3 ypt7::LEU2*	This study
YAS2715	*MAT a ade2 his3 leu2 lys2 trp1 ura3 ITR1-GFP::TRP1 exo84::HIS3 pG599*	This study
YAS2714	*MAT a ade2 his3 leu2 lys2 trp1 ura3 Chs3-2GFP::TRP1 sec5-24*	This study
YAS2717	*MAT a ade2 his3 leu2 lys2 trp1 ura3 sec10-2*	This study
YAS2716	*MAT a ade2 his3 leu2 lys2 trp1 ura3 sec5-24*	This study
YAS2718	*MAT a ade2 his3 leu2 lys2 trp1 ura3 exo84::HIS3 pG599*	This study
YAS2613	*MAT a ade2 his3 leu2 lys2 trp1 ura3 sro7::LEU2*	This study
YAS2614	*MAT a ade2 his3 leu2 lys2 trp1 ura3 sro77::HIS3*	This study
YAS431	*MAT a ade2 his3 leu2 lys2 trp1 ura3 chs5::LEU2*	Trautwein *et al.*, 2006
YAS2719	*MAT a ade2 his3 leu2 lys2 trp1 ura3 ypt31::HIS3*	This study
YAS2720	*MAT a ade2 his3 leu2 lys2 trp1 ura3 ypt32::LEU2*	This study
YAS2721	*MAT a ade2 his3 leu2 lys2 trp1 ura3 sro7::LEU2 sro77::HIS3*	This study
YAS2722	*MAT a ade2 his3 leu2 lys2 trp1 ura3 sec5-24 ITR1-GFP::TRP1*	This study

YAS2723	*MAT a ade2 his3 leu2 lys2 trp1 ura3 ypt31::LEU2 ypt32A141D::HIS3 ITR1-GFP::TRP1*	This study
YAS2724	*MAT a ade2 his3 leu2 lys2 trp1 ura3 sec8-9 CHS3-2GFP::TRP1*	This study
YAS957	*MAT a ade2 his3 leu2 lys2 trp1 ura3 end3::LEU2 CHS3-2GFP::TRP1*	This study
YAS2752	*MAT a ade2 his3 leu2 lys2 trp1 ura3 sec10-2 CHS3-2GFP::TRP1*	This study
YAS2753	*MAT a ade2 his3 leu2 lys2 trp1 ura3 sec10-2 ITR1-GFP::TRP1*	This study
YAS2754	*MAT a ade2 his3 leu2 lys2 trp1 ura3 exo84::HIS3 CHS3-GFP::TRP1 pG599*	This study
YAS1385	*MAT a ade2 his3 leu2 lys2 trp1 ura3 NHA1::NHA1-3GFP (KanMX6)*	This study
YAS1394	*MAT a ade2 his3 leu2 lys2 trp1 ura3 NHA1::NHA1-3GFP (KanMX6) CHS5::LEU2*	This study
YAS2564	*MAT a ade2 his3 leu2 lys2 trp1 ura3 clonNAT-GAL1p-SEC6 NHA1::NHA1-9myc (HIS3)*	This study
YAS2416	*MAT a ade2 his3 leu2 lys2 trp1 ura3 CHS3::CHS3-6HA (TRP1) NHA1::NHA1-9myc (HIS3) MSB3::URA3 MSB4::LEU2*	This study
YAS2287	*MAT a ade2 his3 leu2 lys2 trp1 ura3 CHS3::CHS3-6HA (TRP1) MSB3::URA3 MSB4::LEU2*	This study
YAS2609	*MAT a ade2 his3 leu2 lys2 trp1 ura3 NHA1::NHA1-9myc (HIS3)*	This study
YAS1999	*MAT α ade2 his3 leu2 lys2 trp1 ura3 CHS3-2GFP::TRP1 ZRT1::ZRT1-9myc (HIS3)*	This study
YAS2000	*MAT α ade2 his3 leu2 lys2 trp1 ura3 CHS3-2GFP::TRP1 GAP1::GAP1-9myc (HIS3)*	This study
YAS2109	*MAT α ade2 his3 leu2 lys2 trp1 ura3 CHS3-2GFP::TRP1 SKG6::SKG6-9myc (HIS3)*	This study
YAS2116	*MAT α ade2 his3 leu2 lys2 trp1 ura3 CHS3-2GFP::TRP1 SHO1::SHO1-9myc (HIS3)*	This study
YAS2230	*MAT α ade2 his3 leu2 lys2 trp1 ura3 CHS3::CHS3-2GFP MSB3::KAN(Tn903) MSB4::URA3 CHS5::LEU2*	This study
YAS2511	*MAT a ade2 his3 leu2 lys2 trp1 ura3 PDR12::PDR12-GFP(HIS3)*	This study
YAS2568	*MAT a ade2 his3 leu2 lys2 trp1 ura3 PDR12::PDR12-GFP(HIS3) CHS5::LEU2*	This study

* A 3xGFP-tag was inserted into the *CHS3* locus and later replaced with a *URA3* cassette, thus removing the tag and restoring WT Chs3p expression.

8.3. Oligonucleotides

Number	Designation	Sequence	Purpose
UR061	pUG72-URA3_rev	ggacagaaaattcgccgata	Cassette-specific primer for colony PCR
UR062	pUG27-HIS5_rev	tgttctccctttttggtttgc	Cassette-specific primer for colony PCR
UR063	pUG73-LEU2_rev	ctaacgtgcttgcctcttcc	Cassette-specific primer for colony PCR
UR064	pYM_Kan/HIS_rev	tgggcctccatgtcgctgg	Cassette-specific primer for colony PCR
UR072	hxt2_c_for	aaatctggtagctggatctcaaaagaaaaaaagagtttccgaggaacgtacgctgcaggtcgac	C-terminal tagging of *HXT2*
UR073	hxt2_c_rev	cattagccttaaaaaaatcagtgctagtttaagtataatctcttaatcgatgaattcgagctcg	C-terminal tagging of *HXT2*
UR074	hxt2_con_for	gtcttcatgggctgtttggt	control PCR for C-terminal tagging
UR079	Sec6_n_for	tgggccgagagcagagatattatcaagtatctagttactaagatg cagctgaagcttcgtacgc	promoter exchange of *CHS6*
UR080	Sec6_n_rev	atctccctttattaaatcacaaacttgctgcaagggatctgaaga catcgatgaattctctgtcg	promoter exchange of *CHS6*
UR081	Sec6_n_con_for	gaatgggcctggaagtgata	control PCR for promoter exchange
UR099	nha1_S3	gctgctgttaagtcggcgctatcaaaaacgcttggtctcaataagcgtacgctgcaggtcgac	C-terminal tagging of *NHA1*
UR100	nha1_S2	cgtttatatatatactaaaataatatatctttgtgtattaataaagcataggccactagtggatctg	C-terminal tagging of *NHA1*
UR101	nha1_con_for	aacgatggtccaggtacagc	control PCR for C-terminal tagging
UR105	gap1_S3	atggccacaaagccaagatggtatagaatctggaatttctggtgtcgtacgctgcaggtcgac	C-terminal tagging of *GAP1*
UR106	gap1_S2	tgattatctaaaaaataaagtctttttttgtcgttgttcgattcagcataggccactagtggatctg	C-terminal tagging of *GAP1*
UR107	gap1_con_for	agcttttcatcccagcagaa	control primer for C-terminal tagging
UR108	zrt1_S3	actcttttcggtgctggtatcatggctttgatcggtaagtgggctcgtacgctgcaggtcgac	C-terminal tagging of *ZRT1*
UR109	zrt1_S2	atatgaaatagaatctatatggaacatgcagaatttcgctttggtgcataggccactagtggatctg	C-terminal tagging of *ZRT1*
UR110	zrt1_con_for	tgcgcttgttatctctggtg	control primer for C-terminal tagging
UR111	S3-Chs6	gccatgcttgcgtggatagccgacctagatcacacagtacaacctcgtacgctgcaggtcgac	C-terminal tagging of *CHS6*
UR112	S2-Chs6	tccaaccgtagtggttatataataatactaagagcaccgttttgtatcgatgaattcgagctcg	C-terminal tagging of *CHS6*
UR113	S3-Bud7	ttgctcaatttcttcactacttgcaccattggatgctacgatgcacgtacgctgcaggtcgac	C-terminal tagging of *BUD7*
UR114	S2-Bud7	attttttttggattatatatacgtattaatgtctttttatcgtatatcgatgaattcgagctcg	C-terminal tagging of *BUD7*
UR115	S3-Ymr237w	attctaaattttctgaagaatttcacgaatgacactttcgataatcgtacgctgcaggtcgac	C-terminal tagging of *BCH1*
UR116	S2-ymr237w	ttaattgatttctttcacctttttattgattgtattcatctttttatcgatgaattcgagctcg	C-terminal tagging of *BCH1*
UR117	tag-Ykr027-for S3	cgccctcttccagatcttccttccactatcaaacctctggcagaccgtacgctgcaggtcgac	C-terminal tagging of *BCH2*
UR118	tag-Ykr027-rev S2	cacacacagtatatatatatagattcattaaatcaatttgatcagatcgatgaattcgagctcg	C-terminal tagging of *BCH2*
UR119	tag-cont-Chs6-for	cagcggattagagtgggaac	control primer for C-terminal tagging

UR120	tag-cont-Bud7-for	gcgaggaaactgctggaata	control primer for C-terminal tagging
UR121	tag-cont-ymr237w-for	gggaattattcggcctttgt	control primer for C-terminal tagging
UR122	Contr-Bch2-for2	cccgatgcagtagcgtgtctacg	control primer for C-terminal tagging
UR123	KO-Chs5-for	gcgtagatgctaaatgttatcgcggtttagcttgcatgttacgttccagctgaagcttcgtacgtgc	deletion of *CHS5*
UR124	KO-Chs5-rev	gcttggcggctactgagtacccctctcaagaaaatgaagtgatcgcataggccaactagtggatc	deletion of *CHS5*
UR125	KO-cont-Ch5-for	cggtcggcccttcaagttctcc	control primer for deletion
UR133	TRP_rev	gctattcatccagcaggcctc	cassette-specific primer for colony PCR
UR155	MAT_for	agtcacatcaagatcgtttatgg	mating type PCR
UR156	MATa_rev	actccacttcaagtaagagtttg	mating type PCR
UR157	MATalpha_rev	gcacggaatatgggactacttcg	mating type PCR
UR158	Sho1_S2	ttttttcctttgactcgagaatccatgctataagattgttaatca gcataggccactagtggatctg	C-terminal tagging of *SHO1*
UR159	Sho1_S3	agcaattatgttcaactaatcgatggtccagaagaaatgcatcgt cgtacgctgcaggtcgac	C-terminal tagging of *SHO1*
UR160	Sho1_con_for	attgaaggcagatggtggaa	control primer for C-terminal tagging
UR161	msb3_S1	ttgtaggagtcaaagagttgcgcacccagaaccattgtaattagccagctgaagcttcgtacgc	deletion of *MSB3*
UR162	msb3_S2	ttatcacatatttgtttatgcaaaaacaaaaacaggaagcaaaaggcataggccactagtggatctg	deletion of *MSB3*
UR163	msb3_del_con_for	tttctgttcgggcagtatca	control primer for deletion
UR164	msb4_S1	tcgcacacttttacaatcacagaaggcaaaacccggcatgacaggcagctgaagcttcgtacgc	deletion of *MSB4*
UR165	msb4_S2	acttgttattttacacagttgcgctttttatcacggttgcgcttagcataggccactagtggatctg	deletion of *MSB4*
UR166	msb4_del_con_for	ttgtacatttggcaccgaag	control primer for deletion
UR193	Chs3_S3	ggaagatattctcaatcggaaggaggaaagtgactccttcgttgcacgtacgctgcaggtcgac	C-terminal tagging of *CHS3*
UR194	Chs3_S2	atatatcaacttgtaagtatcacagtaaaaatattttcatactgtatcgatgaattcgagctcg	C-terminal tagging of *CHS3*
UR195	Chs3_c_con_for	ggcagattacggggctaatgg	control primer for C-terminal tagging
UR204	Itr1_S3	catgaattgaaatatgaaccaactcaagagattatagaggatatacgtacgctgcaggtcgac	C-terminal tagging of *ITR1*
UR205	Itr1_S2	tttgaatattcaattgcgtctccttccttttacctcgtgaaaggagcataggccactagtggatctg	C-terminal tagging of *ITR1*
UR206	Itr1_c_con_for	ccagaattatcgggattgga	control primer for C-terminal tagging
UR211	Chs6_CORE_729_for	cggtcactgaattgcgggtgggattctaccaagagtatgcaagccgagctcgttttcgacactgg	integration of CORE cassette into *CHS6*
UR212	Chs6_CORE_729_rev	aataaaacttttaaactatacattaaatagttattgacaatggttccttaccattaagttgatc	integration of CORE cassette into *CHS6*
UR213	Chs6_729_con_for	tcctcttgcaaaaagatcatagaa	control PCR for CORE integration
UR214	Chs6_729_con_rev	catggattggatctttcttgg	control PCR for CORE integration
UR215	Chs6_dp_730-1212	actgaattgcgggtgggattctaccaagagtatgcaagccggacacctggaaacaatgtacagtaggtttcttacctcca	*delitto perfetto* of bp 730-1212 of *CHS6*
UR216	Chs6_CORE1836_for	aaattgagcaagattagcctaagcaataaagatgaaaaacacagcgagctcgttttcgacactgg	integration of CORE cassette into *CHS6*
UR217	Chs6_CORE1836_rev	ccaggtacgcagcatgatcaaacccaaaagttcccactctaatcctccttaccattaagttgatc	integration of CORE cassette into *CHS6*
UR218	Chs6_1836_con_for	ggttttgtgaagggtggcta	control PCR for CORE integration
UR219	Chs6_1836_con_rev	cgttgcatagcttttctagcag	control PCR for CORE integration

UR220	Chs6_dp_1837-1938	gagcaagattagcctaagcaataaagatgaaaaacacagcgtaagttgccagcagctgctaaaaatatacctgcaacctc	*delitto perfetto* of bp 1837-1938 of *CHS6*
UR237	CORE_front_rev	ccagatgcgaagttaagtgc	cassette-specific primer for colony PCR
UR238	CORE_rear_for	aaaccattacaaccattgcg	cassette-specific primer for colony PCR
UR241	Chs6_729_con2_rev	gtagtgttcgcgggtaccat	*delitto perfetto* of bp 730-1212 of *CHS6*
UR270	Bch1_CORE_792_for	gaaaaaggtgtttatttagatgcacctactcacgttttaaatcccgagctcgttttcgacactgg	integration of CORE cassette into *BCH1*
UR271	Bch1_CORE_792_rev	aactatttccactaaagtttccactaaataattattggttaacgatccttaccattaagttgatc	integration of CORE cassette into *BCH1*
UR272	Bch1_792_con_for	agataatcgtgcggatggag	control PCR for CORE integration
UR273	Bch1_792_con_rev	gaggcatccaatggtaatgg	control PCR for CORE integration
UR274	Bch1_dp_793-1251	aggtgtttatttagatgcacctactcacgttttaaatcccaaatacgttcttagaagaattgcgcctattacttcagatg	*delitto perfetto* of bp 793-1251 of *BCH1*
UR275	Bch2_S1	gtataagtagtaaagtacagttaacagatcaattggcctcgaggaatccagctgaagcttcgtacgtgc	deletion of *BCH2*
UR276	Bch2_S2	ggatattacccgcgctaaagtattagcattatcgccgtaaatttgcataggccaactagtggatc	deletion of *BCH2*
UR277	Bch2_del_con_for	ggtttccgaggcattgttacaccg	control primer for deletion
UR282	Pdr12_S3	attttccaaacagttccaggtgacgaaaataaaatcacgaagaaacgtacgctgcaggtcgac	C-terminal tagging of *PDR12*
UR283	Pdr12_S2	aattgtgtgttaaaccacgaaatacaaatatatttgcttgcttgtgcataggccactagtggatctg	C-terminal tagging of *PDR12*
UR284	Pdr12_c_con_for	tgccgctatgttgatttgtt	control primer for C-terminal tagging
UR287	Chs6_S1	tttcttaagctgttggtgcaaaaaaggattacatctattgcccttcagctgaagcttcgtacgc	promoter exchange of *CHS6*
UR288	Chs6_S4	aggtatttcattttgctttttggtttccgatggccaaaacaaattcatcgatgaattctctgtcg	promoter exchange of *CHS6*
UR300	Chs3_S3_STOP_for	gaagatattctcaatcggaaggaggaaagtgactccttcgttgcatagcagctgaagcttcgtacgc	removal of C-terminal tag from *CHS3*
UR301	Chs3_S2_pUG_rev	atatatcaacttgtaagtatcacagtaaaaatattttcatactgtgcataggccactagtggatctg	removal of C-terminal tag from *CHS3*
UR305	Chs3_Cla1_for	cctccatcgatatgaccggcttgaatggagatga	cloning of *CHS3-Cub*
UR306	Chs3_Sal1_rev	cctccgtcgaccctgcaacgaaggagtcactttcctccttccg	cloning of *CHS3-Cub*
UR307	Chs5_Cla1_for	cctccatcgatatgtcttcagttgatgtactgtta	cloning of *CHS5-Cub*
UR308	Chs5_Sal1_rev	cctccgtcgacccttttcttttttccctttcttcttattcttctt	cloning of *CHS5-Cub*
UR309	Chs6_BamH1_for	cgcggatccctgggtctgggaatttgttttggccatcggaaacc	cloning of Nub-*CHS6*
UR310	Chs6_Nco1_rev	cctccccatggccctgttcaacagtttagctaatgg	cloning of Nub-*CHS6*
UR311	Ypt31_S1	tttaggccagcaaagggattctgacggcgtctggggatttcaacacagctgaagcttcgtacgc	deletion of *YPT31*
UR312	Ypt31_S2	gaagagtcattcacatgcaagtgcgcaactgctgcaaaatatctcgcataggccactagtggatctg	deletion of *YPT31*
UR313	Ypt31_del_con_for	tttgtttaggccagcaaagg	control primer for deletion
UR314	Ypt32_S1	aaagcgtggtgataaagagcgaaccaagcatattgttttccaagacagctgaagcttcgtacgc	deletion of *YPT32*
UR315	Ypt32_S2	cagaatatgcatgaaaccatgcgaccttagtagggcacaaaatttgcataggccactagtggatctg	deletion of *YPT32*
UR316	Ypt32_del_con_for	agagaggaaaagcgtggtga	control primer for deletion
UR317	Ypt51_S1	acttatctaagctataaaaaaatatccctttttatcacacaaaaaacagctgaagcttcgtacgc	deletion of *YPT51*
UR318	Ypt51_S2	caatttgcccagacttttttttttatatatatttatttttcccctctgcataggccactagtggatctg	deletion of *YPT51*
UR319	Ypt51_del_con_for	gaggtgaaaatacgagcagctt	control primer for deletion

UR320	Ypt52_S1	aagaaggtttaacttatttggagtaaacgtatatattattaacagcagctgaagcttcgtacgc	deletion of *YPT52*
UR321	Ypt52_S2	aagcaacttctgttgtttttcctctaaaacacaaatcataggatacataggccactagtggatctg	deletion of *YPT52*
UR322	Ypt52_del_con_for	gcgagggtaggaagaaggtt	control primer for deletion
UR323	Ypt53_S1	attcaaattatttattacatttttcagcatcgaagttaagtagacagctgaagcttcgtacgc	deletion of *YPT53*
UR324	Ypt53_S2	ctaagacgctgaatatgccgcgtttgctgttgttttgcttgcagtcataggccactagtggatctg	deletion of *YPT53*
UR325	Ypt53_del_con_for	ggccttctgaatgcacgtat	control primer for deletion
UR326	Ypt7_S1	tcttatccatatagaaacccttctgtatcaattcaaattaagtgcagctgaagcttcgtacgc	deletion of *YPT7*
UR327	Ypt7_S2	gctataaaggattacataatagaagatacaattaagtagtacagcgcataggccactagtggatctg	deletion of *YPT7*
UR328	Ypt7_del_con_for	ggaataagctcatccagtcca	control primer for deletion
UR329	Exo84_S1	tagaccaggtaagagactgaaagttgaaatatttgtactgtgaaacagctgaagcttcgtacgc	deletion of *EXO84*
UR330	Exo84_S2	acacatcatatatattgaagtgaggtttattttctgtgatcttgtgcataggccactagtggatctg	deletion of *EXO84*
UR340	Sro7_S1	atactatttctgactaattctctatacacataagagcaaaacaaa cagctgaagcttcgtacgc	deletion of *SRO7*
UR341	Sro7_S2	atagaaggaagttgctcattaccctgtatgaattagtgtatgtat gcataggccactagtggatctg	deletion of *SRO7*
UR342	Sro7_del_con_for	cggcgcttttgttaaaagtaa	control primer for deletion
UR343	Sro77_S1	aaaagttacaaaattgtcaattgaacagatacaaaaattttataa cagctgaagcttcgtacgc	deletion of *SRO77*
UR344	Sro77_S2	cgagcaagggcaacctgatcgaattttataaaaactatttatgga gcataggccactagtggatctg	deletion of *SRO77*
UR345	Sro77_del_con_for	atgcgaagccgtatgttca	control primer for deletion
UR352	Sec5_BamH1_for	gatcggatcctcgtttcactcgtacatctgct	cloning of *SEC5* +-500bp into pRS305
UR353	Sec5_Not1_rev	gatcgcggccgctcagcatttagcaccaccaa	cloning of *SEC5* +-500bp into pRS305
UR356	Sec10_BamH1_for	gatcggatcctcgcactaaagacttcacca	cloning of *SEC10* +-500bp into pRS305
UR357	Sec10_Not1_rev	gatcgcggccgcgaaatcaagaaattatatttaggacca	cloning of *SEC10* +-500bp into pRS305
UR360	Bch1_CORE1722_for	gagcaattgtattttgatgctcaaaacagtaaatatcacaaattagagctcgttttcgacactgg	integration of CORE cassette into *BCH1*
UR361	Bch1_CORE1722_rev	cttatgctcgtcaatgtaaaactgtaatagattctttgcgcatactccttaccattaagttgatc	integration of CORE cassette into *BCH1*
UR362	Bch1_1722_con_for	agacgagtaccaaggctcca	control PCR for CORE integration
UR363	Bch1_1722_con_rev	taccaacgatgattccagca	control PCR for CORE integration
UR364	Bch1_dp_1723-1824	attgtattttgatgctcaaaacagtaaatatcacaaattagtatgcgcaaagaatctattacagttttacattgacgagc	deletion of bp 1723-1824 of *BCH1*
UR365	Bch2_CORE1839_for	cacttcatctcaagaaaataaggctacggcgaaatacagcgagctcgttttcgacactgg	integration of CORE cassette into *BCH2*
UR366	Bch2_CORE1839_rev	ccatggttaaataaaagttcaacagatggtgacaactaattccttaccattaagttgatc	integration of CORE cassette into *BCH2*
UR367	Bch2_1839_con_for	tctgacgttttcgttatggaga	control PCR for CORE integration
UR368	Bch2_1839_con_rev	cttgaagggaaaatatctgaaatc	control PCR for CORE integration
UR369	Bch2_dp_1840-1941	cacttcatctcaagaaaataaggctacggcgaaatacagcattagttgtcaccatctgttgaacttttatttaaccatgg	deletion of bp 1840-1941 of *BCH2*
UR377	Exo84_del_con2for	acctcgtgtcccatctcttg	control primer for deletion of *EXO84*
UR378	Chs6TPR5_Bch2_for	attagcacttcatctcaagaaaataaggctacggcgaaatacagcggattagagtgggaactttt	transplantation of TPR5 into BCH2
UR379	Chs6TPR5_Bch2_rev	aaaatccatggttaaataaaagttcaacagatggtgacaactaatggggtcgaatcgagctacta	transplantation of TPR5 into BCH2

UR380	Bch2_seq_TPR5	tccacagaattacgccagaa	sequencing of TPR5 in *BCH2*
UR381	Bch1_seq_TPR1-4	tacctcgggtgagttggaag	sequencing of TPR1-4 in *BCH1*
UR382	Bch1_seq_TPR5	agaggctatgcgaaagatgg	sequencing of TPR5 in *BCH1*
UR387	CHS6-pUGDelfor	atgaatttgttttggccatcggaaaccaaaaagcaaaatgaaatacagctgaagcttcgtacgc	deletion of *CHS6*
UR388	CHS6-pUGDelrev	tcaaggttgtactgtgtgatctaggtcggctatccacgcaagcatgcataggccactagtggatct g	deletion of *CHS6*
UR389	Bch2TPR5_Chs6_for	aaattgagcaagattagcctaagcaataaagatgaaaaacacagcgggttggaatgggaactact	transplantation of TPR5 into CHS6
UR390	Bch2TPR5_Chs6_rev	ttttggaggttgcaggtatatttttagcagctgctggcaacttacagggtcaaaccttgccaaaa	transplantation of TPR5 into CHS6
UR391	Bch1_dp2_793-1251	catctgaagtaataggcgcaattcttctaagaacgtatttgggatttaaaacgtgagtaggtgcatctaaataaacacct	*delitto perfetto* of bp 793-1251 of *BCH1*
UR392	Chs6TPR5_dp_mut1	gagcaagattagcctaagcaataaagatgaaaaacacagcggattagagtgggaactttgggatttgatcatgctgcgta	mutagenesis of TPR5 of *CHS6*
UR397	Bch2mid_Chs6_for	gctctcttcgcaataaattcaatgcctcgtttgcgcaaaaatgatatcgttaaacaagcccagat	transplanting central domain into *CHS6*
UR398	Bch2mid_Chs6_rev	ccaggtacgcagcatgatcaaacccaaaagttcccactctaatccgctgtatttcgccgtagcct	transplanting central domain into *CHS6*
UR399	Bch2_1-4_Chs6_for	cggtcactgaattgcgggtgggattctaccaagagtatgcaagccacgatactgaataactacct	transplanting TPR1-4 into *CHS6*
UR400	Bch2_1-4_Chs6_rev	ataattggaggtaagaaacctactgtacattgtttccaggtgtccatcatattccgctaaacagg	transplanting TPR1-4 into *CHS6*
UR401	Bch1_dp_1-4_new	ctatgaaaaaggtgtttatttagatgcacctactcacgttttaaatcccaaatacgttcttagaagaat	*delitto perfetto* of TPR1-4 of *BCH1*
UR402	Chs6_seq_mid	ctagcgagatgccacatcaa	sequencing of central domain of *CHS6*
UR413	Chs6mid_Bch2_for	gcactgctctcaatcaattcgatgccctgtttagcggaatatgatggacacctggaaacaatgta	transplanting central domain into *BCH2*
UR414	Chs6mid_Bch2_rev	actcactcgaagcagagttaagccaagtagttcccattccaacccgctgtgtttttcatctttat	transplanting central domain into *BCH2*
UR418	Chs6_CORE1a_1377f	ttgaggaattggaaagaggatgagttaaaacggcaaatttttggagagctcgttttcgacactgg	integration of CORE cassette into *CHS6*
UR419	Chs6_CORE1a_1377r	ttcctttgtataaccgatttttttttcgtttatcattgcgattcttccttaccattaagttgatc	integration of CORE cassette into *CHS6*
UR420	Chs6_dp_1213-1377	cttcgcaataaattcaatgcctcgtttgcgcaaaaatgatagaatcgcaatgataaacg	deletion of *CHS6* bp 1213-1377
UR421	Chs6_dp_1687-1836	agaagctttcatgatggaaactgaattctatcaagcttctggattagagtgggaacttttg	deletion of *CHS6* bp 1213-1377
UR422	Bch2_CORE_738_for	agatttttagaatgtggttgggattctacaaagagcgtctatgcagagctcgttttcgacactgg	integration of CORE cassette into *BCH2*
UR423	Bch2_CORE_738_rev	cagaaatactaataatgattcagttaggtagttattcagtatcgttccttaccattaagttgatc	integration of CORE cassette into *BCH2*
UR424	Bch2_CORE1_con_f	tgtttatcaagttaatatcgttgactg	control PCR for cassette integration
UR425	Bch2_CORE1_con_r	tcttcaactccaactcattttca	control PCR for cassette integration
UR426	Bch2_dp_739-1224	gatttttagaatgtggttgggattctacaaagagcgtctatgcaatcgttaaacaagcccaga	*delitto perfetto* of bp 739-1224 of *BCH2*
UR427	Bch2_TPR1-4_seq	gggaagaaactttcgttagctg	sequencing of TPR1-4 of *BCH2*
UR428	Bch2_CORE1a_for	gcactgctctcaatcaattcgatgccctgtttagcggaatatgatgagctcgttttcgacactgg	integration of CORE cassette into *BCH2*
UR429	Bch2_CORE1a_rev	gttcatataaaacttaaaagcgttaatctgggcttgtttaacgattccttaccattaagttgatc	integration of CORE cassette into *BCH2*
UR430	Bch2_CORE1a_con	tttctttatccatttccacattg	control PCR for CORE integration
UR433	Chs6start_Bch2_for	ataagtagtaaagtacagttaacagatcaattggcctcgaggaatatgaatttgttttggccatc	transplantation of *CHS6* into *BCH2*
UR434	Chs6end_Bch2_rev	cacacacagtatatatatatagattcattaaatcaatttgatcagtcaaggttgtactgtgtgat	transplantation of *CHS6* into *BCH2*
UR435	Bch2_end_amp	tatcgccgtaaatttgtcca	amplification of *BCH2* locus
UR436	Chs6_Y2H_for3	gatctcgaggtctcgaattcatgaatttgttttggccatc	cloning of *CHS6* into vector pJG4-5

UR437	Chs6Start_Bch2_rev	cagaaatactaataatgattcagttaggtagttattcagtatcgtggcttgcatactcttggtag	transplanting N-terminus into *BCH2*
UR438	Bch2_S1	ataagtagtaaagtacagttaacagatcaattggcctcgaggaatcagctgaagcttcgtacgc	promoter exchange of *BCH2*
UR439	Bch2_S4	tttattcttgcctttcttggactttgtagacccccataaaaaaactcatcgatgaattctctgtcg	promoter exchange of *BCH2*
UR443	Chs3_S1	ttcttcaaaggtcctgtttagactatccgcaggaaagaaattagacagctgaagcttcgtacgc	deletion of *CHS3*, use with UR301
UR444	Bch2_CORE3_for	gcagtagcgtgtctacgaactagtattttggcaaggtttgaccctgagctcgttttcgacactgg	integration of CORE cassette after TPR5
UR445	Chs6end_Bch2_for	gcagtagcgtgtctacgaactagtattttggcaaggtttgaccctgtaagttgccagcagctgc	transplanting C-terminus into *BCH2*
UR461	Chs3_Cterm_for	gatcgaattcgacttctcatggggtgatacgagaactattg	cloning of *CHS6*-CT into pGEX-6P-1
UR462	Chs3_Cterm_rev	gatcctcgagctatgcaacgaaggagtcactttcctcctt	cloning of *CHS6*-CT into pGEX-6P-1
UR463	Chs3_Delta21_rev	gatcctcgagctatgtcctcattttaatctttgagtgatcaaa	cloning of *CHS6*-CTΔ21 into pGEX-6P-1
UR464	Chs3_Delta37_rev	gatcctcgagctattgtgccttttttattacctcccgcaatagt	cloning of *CHS6*-CTΔ37 into pGEX-6P-1
UR465	Chs3_Delta21_S3	gagaatgaaggtgaatttgatcactcaaagattaaaatgaggacacgtacgctgcaggtcgac	C-terminal tagging of *CHS3*-Δ21
UR466	Chs3_Delta37_S3	tggggtgatacgagaactattgcgggaggtaataaaaaggcacaacgtacgctgcaggtcgac	C-terminal tagging of *CHS3*-Δ37
UR471	Chs3_Cterm_for2	gatcgaattcctggaagttctgttccaggggcccctgggatccgacttctcatggggtgatacgagaactattg	cloning of *CHS6*-CT into pGEX-6P-1
BZ001	ypt6del	ctgttgattctgaacagtaaaagataaacaaagaagagattaacacagctgaagcttcgtacgc	deletion *YPT6*
BZ002	yptdelR	cacaaagagttctccttatgccctatagaactgaaatattaggtggcataggccactagtggatctg	deletion *YPT6*
BZ003	ypt6-920	gggcacttaaggttgtgtgaa	control primer for deletion
MT288	Ypt10-pUGf	ttactccaggaaatacaagtagcacaaaatacggaggaatacgatcagctgaagcttcgtacgc	deletion *YPT10*
MT289	Ypt10-pUGr	ggtgatatctaagtaattatgatttaaaatcaaatactttatgtagcataggccactagtggatctg	deletion *YPT10*
MT290	Ypt10-deltestf	tcgcttccagtaaatgcaga	control primer for deletion
MT316	Ypt11-pUGf	aatgttcatcatggtggcacggttttgaatcctgggttgggcatacagctgaagcttcgtacgc	deletion *YPT11*
MT317	Ypt11-pUGr	tggacaatggctgcctgcgaatcttgttgtataatttgtcgaagagcataggccactagtggatctg	deletion *YPT11*
MT318	Ypt11-deltestf	cagtgcaccgatacggacta	control primer for deletion
BZ160	sur2del	taacattctagtccgaagagggtgtatacgaaaagaaaatatacgcagctgaagcttcgtacgc	deletion *SUR2*
BZ161	sur2delR	gacattgcctttacccagcaattgaacgggaggtatgcaaaaggggcataggccactagtggatctg	deletion *SUR2*
BZ162	sur2-822	catcctgctgcgctgttgttg	control primer for deletion
BZ163	elo3del	tatttattcggcttt tttccgtttgtttacgaaacataaacagtccagctgaagcttcgtacgc	deletion *ELO3*
BZ164	elo3delR	aatttttttctttttcattcgctgtcaaaaattctcgcttcctatgcataggccactagtggatctg	deletion *ELO3*
BZ165	elo3-850	ttaccccagttaggtactgtg	control primer for deletion
MT269	Sec6-4-klonf	tccccccgggggccgagagcagagatatt	cloning of *sec6-4* into pRS406
MT270	Sec6-4-klonr	ggaccgcggacacgaatgaagggaaaactatac	cloning of *sec6-4* into pRS406
MT271	Sec6-401	ccctggaaactggttgtc	sequencing of *SEC6*
MT272	Sec6-801	agaatatccgacaaacaa	sequencing of *SEC6*
MT273	Sec6-1201	tttaccaaaagcgaagtc	sequencing of *SEC6*
MT274	Sec6-1601	aagatgagtgtccaggag	sequencing of *SEC6*

MT275	Sec6-2001	tttatcgttcgagcattc	sequencing of *SEC6*
MT276	Sec6-415rev	gacaaccagtttccaggg	sequencing of *SEC6*
MT277	Sec6-2f	tgtcttcagatcccttgcag	sequencing of *SEC6*
MT456	Sec4-8f	tccccccggggcgtatcgttcaccagaaag	cloning of *sec4-8* into pRS406
MT457	Sec4-8r	ggaccgcggttctcaaagaagcaaaaatcttc	cloning of *sec4-8* into pRS406
BZ029	ypt1-1001/Bam	cgcggatccatgaatagcgagtacgattacctg	cloning of *YPT1*
BZ030	ypt1-1650R/Xho	ccgccgctcgagatgggtctgcaaggtagagg	cloning of *YPT1*
BZ035	sec2-976/Bam	cgcggatccagctgtgtttgataaaggtttca	cloning of *SEC2*
BZ036	sec2-3335R/Xho	ccgccgctcgagcatcttaaggaactcaaatgtcca	cloning of *SEC2*
BZ037	sec3-939/Bam	cgcggatccagactgagtcggtgccagat	cloning of *SEC3*
BZ038	sec3-5033R/Xho	ccgccgctcgaggaagcgacaatgcagaggtt	cloning of *SEC3*

8.4. Biochemical Methods

As the methods applied in the lab were standardized as much as possible, part of the Methods section has been taken from the dissertations of two former lab members, Mark Trautwein (Trautwein, 2004) and Cornelia Kilchert (Kilchert, 2011). Changes have only been made where necessary.

8.4.1. Production of yeast cell lysates by spheroplasting

Ten OD_{600} of logarithmically growing yeast cells were incubated in 1 ml DTT-buffer (10 mM Tris/HCl pH 9.4, 10 mM DTT) for 5 min at 30°C. The buffer was replaced by 1 ml SP-buffer (0.76% YPD, 0.7 M sorbitol, 10 mM Tris/HCl pH 7.5), supplemented with 30 µl zymolyase T-20 (10 mg/ml). Cells were spheroplasted for 40 min at 30°C. The spheroplasts were sedimented (2 min, 1,000 g) and lysed in B150Tw20 buffer supplemented with the standard concentrations of proteinase inhibitors (PMSF, leupeptin, pepstatin, and antipain). The lysates were cleared by a centrifugation step depending on the experiment.

8.4.2. Immunoblot

Proteins were transferred onto nitrocellulose using the wet-blot method (Towbin *et al.*, 1979) in transfer buffer (3 h at RT), 30 V, 250 mA. After the transfer, the nitrocellulose was stained in Ponceau S solution for 1 min (optional) and rinsed with water to remove background staining. Unspecific binding sites were blocked by incubation for 1 h in 5% milk (non-fat milk powder in TBS; 0.02% NaN_3). Unless otherwise stated, the membrane was decorated with primary antibodies diluted in 5% milk for 1 h at RT or overnight at 4°C. Epitope tags and proteins were detected using the following primary antibodies: anti-myc (Sigma 9E10 1:1,000); anti-HA (Eurogentec HA.11 1:1,000); anti-FLAG (Sigma M2 1:1,000); anti-Chs5p (affinity-purified, 1:500); anti-Chs3p: (affinity-purified, 1:1,000); anti-Pgk1 (Invitrogen #A-6457 1:1,000) and anti-Sec61p serum (a gift from Prof. M. Spiess, Biozentrum Basel, 1:10,000).

The membrane was briefly rinsed with water and washed in TBS-T (3 x 10 min). The secondary antibody coupled to horseradish peroxidase (HRP) was diluted in TBS-T and incubated for 1 h at RT. Goat-anti-mouse-HRP (Pierce) and goat-anti-rabbit-HRP (Pierce) were diluted 1:20,000 and 1:15,000, respectively. After repeated washes in TBS-T, the signals were detected using either the ECL or ECL Advance system (Amersham Bioscience) according to the manufacturer's recommendations with ECL

hyperfilms (GE Healthcare) or a LAS-4000 chemiluminescence imager. Exposure times were chosen such that none of the relevant signals were outside the linear range.

8.4.3. Co-immunoprecipitation

Co-immunoprecipitation experiments were performed essentially as described previously (Harlow and Lane, 1988). Yeast lysates from 10 OD_{600} cells were prepared by spheroplasting and cleared (10 min, 16,000 x g, 4°C). Immunoprecipitations were performed using 5 µg affinity-purified rabbit IgG, 5 µg affinity-purified anti-Chs5p antibody, 5 µg anti-HA (HA.11, Eurogentec), 5 µg anti-myc (9E10, Sigma) or 5 µg anti-AU5 (Abcam) and 100 µl 20% Protein A sepharose per 1 ml cleared lysate for 1 h at 4°C. The beads were washed with B150Tw20 buffer, resuspended in 40 µl sample buffer and incubated at 65°C for 10 min. Aliquots were analyzed by SDS-PAGE and subsequent immunoblotting.

IP buffer
50 mM Tris (pH 7.5)
150 mM NaCl
1% Triton-X 100
0.1% SDS

8.4.4. Crosslinker immunoprecipitation

For each sample, 6 OD_{600} yeast cells were harvested, washed and resuspended in 220 µl B88 buffer supplemented with protease inhibitors. One hundred µl of glass beads were added and cells lysed by vortexing for 10 min at 4°C. The lysate was cleared by centrifugation at 13,000 g for 5 min at 4°C, protein concentrations of the supernatants were determined by the Bradford method (Bradford, 1976) and adjusted with B88 buffer. Twenty µl of DSP (Pierce) dissolved in DMSO was added to 140 µl lysate to a final concentration of 2 mM. The crosslinking reaction took place for 30 min at RT and was stopped with 7 µl 1M Tris (pH 7.5) for 15 min. Then, 8 µl of 20% SDS were added, and the sample heated to 65°C for 15 min. Nine hundred µl IP buffer were added and the sample was centrifuged for 10 min at 20,000 g to remove aggregates. The supernatant was subjected to immunoprecipitation overnight at 4°C using 5 µg affinity-purified anti-Chs3p antibody crosslinked to Protein A sepharose. The resin was pelleted for 1 min at 1,500 g (4°C), washed once with IP buffer and twice with IP buffer supplemented with 250 mM NaCl. The resin was transferred to new tubes, 40 µl of Laemmli buffer containing 100 mM DTT were added and the samples incubated at 65°C for 30 min. For SDS-PAGE and immunoblot, the following primary and secondary antibodies were used:

anti-Chs3p (rabbit, affinity-purified, 1:1,000), TrueBlot anti-rabbit (eBioscience, 1:2,000), development with ECL; anti-myc (mouse monoclonal, 9E10, 1:2,500), TrueBlot anti-mouse (eBioscience, 1:4,000), development with ECL Advance. For membrane blocking and dilution of primary antibodies, 2% ECL Advance Blocking Reagent dissolved in TBS was used.

IP buffer
50 mM Tris/HCl (pH 7.5)
150 mM NaCl
1% Triton X-100
0.1% SDS

8.4.5. Covalent antibody coupling to protein A sepharose

Per IP, 100 µl 20% protein A sepharose were washed in PBS and rotated with 5 µg antibody for 1.5 h at 4°C. The resin was pelleted for 1 min at 1,500 g (4°C), washed twice with PBS and once with 0.2 M triethanolamine (TEA), pH 8.2. For crosslinking, the sepharose/antibody complexes were resuspended in 50 µl TEA / 6.5 mg/ml dimethylpimelimidate (DMP) and rotated at RT for 1 h. The reaction was stopped by adding 50 µl 1 M Tris (pH 8.0) and rotating at RT for 1 h. The resin was washed twice and either used directly for immunoprecipitation or stored in PBS at 4°C for up to two weeks.

8.4.6. Purification of GST-tagged constructs from *E. coli*

The C-terminal tail of Chs3p or C-terminally truncated versions ("Δ21" and "Δ37") were cloned into the pGEX-6P-1 vector using EcoRI and XhoI restriction sites. The full-length tail comprised the last 55 aa following the last predicted transmembrane (TM) domain, while truncations of this tail lacked the C-terminal 21 and 37 aa, respectively. Expression in Rosetta *E. coli* cells was induced at OD_{600} 1.0 by addition of 1 mM IPTG and growth in LB medium at 37°C for 4 h.

The pellet of a 200 ml culture was incubated for 30 min on ice in 2.7 ml PBS/5% glycerol supplemented with 1 mM DTT, proteinase inhibitor cocktail (Roche), DNase I (0.02 mg/ml) and lysozyme (1 mg/ml). Cells were broken by sonication and centrifuged for 20 min at 38,000 g (4°C). The supernatant was incubated with 500 µl GSH-agarose at 4°C for 1 h. The resin was washed four times in PBS / glycerol and bound proteins eluted with 12 x 1 ml PBS / 5% glycerol / 40 mM GSH (pH 7.5). Proteins were dialyzed against PBS / glycerol and stored at -80°C. Aliquots were thawed on ice and aggregates removed by centrifugation (10 min, 16,000 g, 4°C) before every experiment.

8.4.7. GST Pulldowns

GST and GST-tagged Chs3p C-terminus (GST-Chs3CT) were bound to 25 µl GSH agarose per pulldown. Since the binding of GST-Chs3CT to the resin appeared to be significantly weaker than GST alone, 10 µg GST and 60 µg GST-Chs3CT (or the respective truncations) were used as input to achieve comparable Coomassie signals in the final pulldown. Protein binding was performed for 1 h at 4°C in 1 ml PBS / 5% glycerol, the resin was washed three times with B150Tw20 buffer and stored in 200 µl buffer until the lysates were prepared. Beads were always spun at 1,000 g for 1 min at 4°C.

Yeast lysates from 10 OD_{600} cells were prepared as follows: Cells were washed in H_2O, resuspended in B88 buffer supplemented with protease inhibitors, and 120 µl of glass beads were added. Cells were broken by vortexing for 10 min at 4°C and the supernatant cleared by centrifugation (5 min, 13,000 g, 4°C). Protein levels were determined by the Bradford method and adjusted with B88 buffer. One ml B150Tw20 buffer was added to 200 µl lysate, the mixture incubated on ice for 3 min and added to the GST-coupled beads. Binding took place for 1 h at 4°C on a rotator. The beads were washed once with B150Tw20 buffer and twice with B150Tw20 buffer supplemented with 150 mM NaCl. The resin was transferred to a new tube and incubated with 40 µl 5x Laemmli buffer at 65°C for 10 min. Bound proteins were analyzed by immunoblot.

8.4.8. Accumulation of secretory vesicles

Secretory vesicles were accumulated *in vivo* by one of the following methods:

1. By double deletion of *MSB3* and *MSB4*. Usually a 1 l culture was grown overnight at 30°C to an OD_{600} of 0.3 – 0.7.
2. By means of a *GAL1* promoter shutoff of the *SEC6* gene. *GAL1-SEC6* cells were pre-cultured for 48 h in YP medium supplemented with 1% raffinose and 2% galactose. Usually a 1 l culture was inoculated from this to grow overnight at 30°C. The medium was supplemented with 2% glucose, causing depletion of Sec6p within 13 h. The culture was harvested at an OD_{600} of 0.3 – 0.7.
3. Using the *sec6-4* allele (Potenza *et al.*, 1992). Cultures between 0.5 and 1 l were grown in rich medium at 23°C to an OD_{600} of 0.5. Cells were harvested, resuspended in pre-warmed medium and incubated for 1 h at 23°C or 37°C, respectively, before harvesting.

8.4.9. Purification and immunoisolation of secretory vesicles

Cells were harvested and subsequently incubated in the following buffers:

- 10 ml cold N_3/F solution, incubation on ice for 10 min
- 1 ml cold Tris/N_3/F solution per 50 OD_{600}, supplemented with 10 mM DTT, incubation at RT for 2 min
- 1 ml spheroplast solution per 50 OD_{600}, supplemented with 1 mM DTT and 18 µl lyticase (60,000 U/ml) per ml, incubation at 30°C for 10 min

Cells were gently pelleted for 1 min at 500 g, and the supernatant carefully removed. Spheroplasts were very gently resuspended in 10 ml cold ConA solution and incubated on ice for 10 min. After pelleting the cells for 1 min at 500 g, the supernatant was aspirated with a glass pipette, cells were resuspended in 5.5 ml cold lysis buffer supplemented with protease inhibitors and homogenized on ice with a glass pipette by pipetting up and down 15 – 20 times. The lysate was then centrifuged for 30 min at 50,000 g (4°C), the supernatant transferred to a new tube, and the spin repeated. The final supernatant was loaded on three identical sucrose step gradients. Steps listed below are w/w sucrose concentrations in gradient buffer.

Top to bottom:

Lysate	1.5 ml
30%	1.5 ml
35%	2.0 ml
40%	1.0 ml
42,5%	1.5 ml
45%	1.0 ml
55%	1.0 ml
60%	0.5 ml

The gradient was centrifuged for 4.5 h at 39,300 rpm in a TH-641 or TST41.14 rotor. Alternatively, longer times and lower speeds were used if the run was to be performed overnight (see section 8.6.5). Per gradient, twelve fractions of 850 µl were collected from top to bottom with a pipette. Secretory vesicles and endosomes were typically found enriched in fractions 9, 10 and 11. These were pooled and diluted 1:2 in gradient buffer. For depletion of endosomal contaminations (Klemm *et al.*, 2009), 5 µg anti-pep12 antibody (Invitrogen) were added and incubated with the vesicle/endosome mixture on a rotator for 2 h at 4°C. Cellulose fibers coupled to 50 µg sheep-anti-mouse antibody (see section 8.4.12) were washed in PBS and added to the sample. After rotation O/N at 4°C, cellulose-antibody-endosome complexes were pelleted for 4 min at 1,500 g (4°C). The supernatant was transferred to a new tube and the spin repeated. The final supernatant was split into three tubes and incubated with 7.5 µg of one of the following antibodies: mouse anti-HA (HA.11,

Eurogentec), mouse anti-myc (9E10, Sigma), or mouse anti-AU5 (Abcam) as a control. Samples were rotated for 2 h at 4°C, and washed cellulose fibers coupled to 50 µg sheep-anti-mouse antibody (see above) were added. After rotation O/N, fibers were pelleted for 4 min at 1,500 g (4°C), washed three times with PBS, resuspended in 80 µl 5x Laemmli buffer supplemented with 20 mM DTT, and incubated at 65°C for 10 min. Samples were analyzed by immunoblot or silver staining.

N_3/F solution	Tris/N_3/F solution	Spheroplast solution
20 mM NaN_3	100 mM Tris/HCl pH 9.4	10 mM Tris/HCl pH 7.5
20 mM NaF	20 mM NaN_3	20 mM NaN_3
	20 mM NaF	20 mM NaF
		1 M Sorbitol
		0.6x YP medium

ConA solution	Gradient buffer	Lysis buffer
50 mM Tris/HCl pH 7.5	20 mM Triethanolamine (TEA)	gradient buffer containing
10 mM $MgSO_4$	1 mM EDTA	5% (w/w) sucrose
20 mM NaN_3	adjusted to pH 7.2 with KOH	
20 mM NaF	Different amounts of sucrose	
1 M Sorbitol	(w/w) were added.	
1 mg/ml ConA		

8.4.10. Enrichment of plasma membrane from yeast lysates

Cells were grown in 500 ml HC/glucose medium O/N at 30°C to an OD_{600} of 0.5. Two hundred OD_{600} were harvested, resuspended in 3 ml lysis buffer supplemented with protease inhibitors and transferred to a 25 ml Corex glass tube. One ml of glass beads were added and vortexed 5 x 30 sec, with 30 sec pause on ice. The lysate was retrieved with a Pasteur pipette, filled up to 3.5 ml with lysis buffer and spun for 5 min at 1,000 g (4°C). One ml of supernatant was loaded on each of two identical sucrose gradients. Steps listed below are w/w sucrose concentrations in gradient buffer.

Top to bottom:

Lysate	1 ml
30%	1.5 ml
40%	2.5 ml
45%	2.5 ml
50%	2.5 ml
60%	1 ml

The gradients were centrifuged for 18 h at 35,000 rpm in a TH-641 rotor at 4°C. Per gradient, 13 fractions of 850 µl were collected from top to bottom with a pipette. Samples from one gradient were used for immunoblot analysis. Plasma membranes were typically enriched in Fraction 12, which

was diluted 1:2 with gradient buffer. Membranes were pelleted by centrifugation for 1 h at 100,000 g in a TLS 55 swing-out rotor (Beckman) at 4°C, the supernatant removed, the pellet resuspended in 2 ml gradient buffer and the spin repeated to remove all traces of sucrose. For analysis by SDS-PAGE, the pellet was resuspended in 50 µl 5x Laemmli buffer and incubated at 65°C for 15 min. Alternatively, for analysis by LC-MS/MS, the membrane pellets were processed as described under 8.4.11.

Lysis and gradient buffers: see section 8.4.9.

8.4.11. Identification of proteins from yeast membrane preparations using LC-MS/MS

Isolated membranes were incubated on ice for 1 h in 50 µl 100 mM Tris (pH 8.0) / 0.1% SDS and thoroughly resuspended. Disulfide bridges were reduced by adding 4.5 µl of 100 mM DTT, followed by incubation at 37°C for 1 h. Side chains were alkylated by adding 5 µl of 500 mM iodoacetamide (IAA) and incubation for 15 min at RT in the dark. Proteins were digested by adding 1 µl trypsin (0.25 mg/ml), incubation in a shaker at 37°C for 2 h, addition of a further 1 µl trypsin and incubation O/N at 37°C. The resulting peptides were freeze-dried. Further processing of this sample and mass spectrometric analysis using LC-MS/MS was carried out by Suzette Moes in the lab of Paul Jenö, Biozentrum Basel.

8.4.12. Production of cellulose-coupled immunoglobulins

The cellulose based sheep anti-mouse-coupled immunoadsorbent was prepared as previously described (Hales and Woodhead, 1980; Wandinger-Ness et al., 1990). The procedure consisted of three steps: Production of aminocellulose, production of highly reactive diazocellulose, and antibody coupling.

Production of aminocellulose: A measure of 0.5 g water-free NaAc was dissolved in 2 ml H_2O and 1.4 g N-(3-nitrobenzyloxymethyl)-pyridinium chloride was dissolved in 18 ml absolute ethanol. Both solutions were mixed, 5 g of cellulose powder were added and stirred to a slurry, which was poured into a large glass Petri dish (15 cm diameter). The mixture was dried for 30 min at 70˚C and then for an additional 40 min at 125˚C. The cellulose was washed three times with 100 ml benzene in a sintered glass funnel (10 cm) and sucked dry. The powder was washed with 1 l H_2O and suspend in 150 ml H_2O containing 30 g sodium dithionite. The mixture was heated to 55-60˚C in a water bath for 30 min and occasionally stirred with a glass rod. This step was followed by three washes with H_2O, two washes with 30% acetic acid (v/v) and one wash again with H_2O using a Büchner funnel and

Whatman filter paper. The resulting product was dried and stored in a desiccator at RT until further processing.

Production of diazocellulose: Copper(II)chloride (750 mg) was dissolved in 1 ml H_2O, and 10 ml fresh 1 M NaOH were added while stirring. Afterwards the tube was placed on ice. The turquoise/dark blue precipitate was filtered through three layers of Whatman paper in a Büchner funnel and washed with ~500 ml H_2O until the pH of the wash fraction was below 9. The precipitate was partially dried on the funnel, transferred to a 50 ml tube and dissolved in 20 ml 32% ammonia to give a saturated solution. The tube was rotated for 15 min at RT and centrifuged at 2,000 rpm for 2 min. Two hundred and fifty mg aminocellulose were then dissolved in 20 ml of the ammonium-cupric-hydroxide solution, the lid sealed with parafilm and rotation continued for 15 min. The tube was centrifuged as above and the supernatant (containing the dissolved cellulose) decanted into 750 ml distilled H_2O in a 1 l glass beaker. The pellet was discarded. One hundred ml of 10% (v/v) H_2SO_4 was added until the solution turned almost colorless and the pH dropped below 4. The solution was left to stand for 30-60 min, allowing the cellulose to sediment. The supernatant was carefully decanted or sucked off and the remaining ~100 ml were transferred to two 50 ml Falcon tubes. The cellulose was pelleted as above and washed four times with distilled H_2O. It was then suspended in 25 ml 2 M HCl at 4˚C, and 200 µl fresh 10% (w/v) sodium nitrite were added. The mixture was rotated for 20 min at 4˚C. Washing was performed at 4˚C: three times with 50 ml distilled H_2O and twice with 0.2 M borate / 0.2 M KCl buffer ($Na_2B_4O_7$) pH 8.2. The final product was resuspended in 25 ml borate/KCl buffer and used immediately for antibody coupling.

Coupling of antibody to diazocellulose: Antibody coupling was performed by mixing equal masses of antibody (in 25 ml borate/KCl buffer) and diazocellulose (usually 10 mg + 10 mg). The tube was wrapped with aluminum foil and incubated overnight at 4˚C on a rotator. The immunoadsorbent was pelleted by centrifuging for 5 min at 2,500 rpm and washed three times with borate/KCl buffer. This procedure usually resulted in 15-20% coupling efficiency when commercially available antibody was used. After determination of the protein concentration the immunoadsorbent was stored at 4˚C either in borate buffer or in PBS / BSA (5 mg/ml) / NaN_3 (0.02%). The resin was stable for several weeks, but gradual hydrolysis of the diazo-bonds was observed over time.

8.4.13. Subcellular fractionation

Ten OD_{600} of mid-log cells were spheroplasted and lysed in 1 ml 50 mM Tris (pH 7.5), 1 mM EDTA, 50 mM NaCl and protease inhibitors by pipetting up and down. The lysate was cleared at 500 g for 2 min and the supernatant (= "total cell lysate", TCL) subjected to centrifugation at 13,000 g (10 min). The supernatant was carefully taken off with a pipette and subjected to centrifugation at 100,000 g

(1 h). Both pellets (P13 and P100) were washed once in lysis buffer and then resuspended in 1 ml lysis buffer. All steps were carried out at 4°C. Samples were taken from all final fractions and subjected to immunoblot analysis.

8.5. Molecular biology techniques

Standard techniques for nucleic acid manipulations were used throughout in this study (Sambrook *et al.*, 1989).

8.5.1. Chromosomal manipulation of yeast DNA

To delete or manipulate genes in yeast cells, established methods were followed (Güldener *et al.*, 1996; Knop *et al.*, 1999; De Antoni and Gallwitz, 2000; Güldener *et al.*, 2002). Briefly, PCR was performed on template plasmids with primers having 45 bp 5'-overhangs homologous to the desired target site in the yeast genome. The PCR-product was transformed directly into yeast cells without further purification. Cells were selected for with the corresponding auxotrophy/resistance markers, correct integrations were confirmed by analytical colony PCR. Wherever possible, the expression was checked by immunoblotting of total yeast lysates. Occasionally, the chromosomal manipulation had to be sequenced. In this case, the PCR product using the proof-reading Expand PCR system (Roche) on genomic yeast DNA was sequenced to confirm the desired manipulation.

8.5.2. Yeast transformation

Yeast cells were transformed by a high-efficiency lithium acetate transformation method (Gietz *et al.*, 1995). Cells were grown overnight in liquid culture to logarithmic phase. Best results were obtained with an OD_{600} of about 0.1. Five OD_{600} of cells were harvested and incubated for 5 min at 30°C in 100 mM LiAc. Subsequently, they were resuspended in 360 µl transformation mix and mixed thoroughly for 1 min. A heat-shock was employed for 40 min at 42°C, after which the cells were pelleted for 1 min at 3,000 g. The cell pellet was resuspended in sterile water and spread on appropriate selection plates. In case a G418 or ClonNAT resistance cassette was transformed, cells were first incubated in YPD for 3 h at 30°C before plating on YPD-G418 plates. Colonies usually appeared after 2 – 3 days and were tested by analytical PCR.

Transformation mix
240 µl 50% (w/v) PEG
36 µl 1 M LiAc
50 µl 2 mg/ml single-stranded salmon sperm DNA
(obtained by heating for 5 min at 95°C and fast cooling on ice)
5 µl of PCR product or 0.5-2 µl plasmid DNA
H_20 ad 360 µl

8.5.3. Analytical PCR of yeast colonies

Analytical PCR of yeast colonies was performed to confirm chromosomal manipulations of yeast cells or to determine the mating type. The primers were chosen in a way that the resulting PCR product indicated a successful manipulation either through its presence or size. Single colonies were picked with a pipette tip and incubated in 3 µl 20 mM NaOH at 100°C for 10 min, then the PCR reaction mix was added. A typical reaction contained 18.9 µl H_2O, 2.5 µl 10x reaction buffer, 2.5 µl 2 mM dNTPs, 2x 0.5 µl 10 µM oligonucleotide primer, 0.15 µl *Taq* DNA-polymerase (Roche). Usually, the annealing temperature was 54°C, the elongation time was 1 min per kb of expected product, and 40 cycles were used for amplification. Routinely, 10 µl of the reaction were analyzed by agarose gel electrophoresis.

8.5.4. Staining of cell wall chitin

Staining of cell wall chitin was carried out as described previously (Lord et al., 2002). A stationary yeast liquid culture was diluted and grown for at least 16 h to logarithmic phase. Cells were fixed directly in growth medium by adding 2 ml 37% formaldehyde to 18 ml culture and incubation for 1 h at RT under gentle agitation. Cells were washed twice in H_2O, resuspended in 250 µl 1 mg/ml calcofluor white solution and incubated for 5 min at RT. The cells were washed twice with H_2O and resuspended in 1 ml H_2O. Cells were observed using a DAPI filter on a Zeiss Axioplan 2 epifluorescence microscope.

8.5.5. Drop assays

Strains were grown overnight, diluted and grown to logarithmic phase. After adjusting to equal cell concentrations (OD_{600} between 0.2 and 0.25), four serial dilutions (1:10) were dropped onto different plates using a “frogger” stamp (custom-built). The plates were incubated for 2 – 5 days at 30°C unless indicated otherwise, and photographed for documentation.

8.5.6. Split ubiquitin yeast two-hybrid assays

CHS6, CHS6ΔTPR1-4 and CHS6ΔTPR5 were amplified from genomic DNA and cloned into the pRS314-Nui vector (Johnsson and Varshavsky, 1994) using BamHI and NcoI restriction sites. *CHS3* and *STE14* were cloned into the pRS313-Cub vector using ClaI and SalI sites. Expression and functionality of the Nui-Chs6 and Chs3-Cub constructs was verified by rescue of chitin synthesis in *Δchs6* and *Δchs3* strains, respectively. The plasmids encoding for Nui-Arf1 and Sec22-Cub were described previously (Nickel, 2004).

Combinations of Nui and Cub plasmids were transformed into the YPH499 background yeast strain (Sikorski and Hieter, 1989) and assayed for growth as indicated in the figures.

8.5.7. Chromosomal manipulations using *delitto perfetto*

Marker-free chromosomal deletions were performed using the *delitto perfetto* method (Storici and Resnick, 2006). This technique is based on the genomic integration of a counterselectable reporter (CORE) cassette and subsequent replacement by a fragment carrying the desired mutation, deletion or insertion. Primers were designed so that the cassette inserted next to the chromosomal base pair (or region) to be manipulated. In the first step, transformants were selected on HC-URA or YPD-G418 plates. By transforming a second PCR cassette into the resulting strain, the CORE cassette was then replaced, yielding a mutated site. Transformants of the second step were selected by plating the cells on YPD and replica plating on 5-FOA plates after 24 h. Due to the large number of false positives, all 5-FOA-resistant colonies were tested for simultaneous loss of $G418^R$ before analytical colony PCR was performed.

The original publication suggested the use of double-stranded 80-mer oligonucleotides for the second recombination event. However, we found that PCR products of ~500 bp, amplified from yeast genomic DNA, were cheaper and yielded a much higher recombination efficiency. The following design rules for the primers of these PCR cassettes were drawn up:

a) Deletions:
   forward primer – 45 bp upstream and 20 bp downstream of the deletion site
   Reverse primer – 500 bp downstream of the deletion site (reverse-complement)

b) Point mutations:
   forward primer – 45 bp upstream and 20 bp downstream of the mutation site, including the point mutation(s)
   Reverse primer – 500 bp downstream of the deletion site (reverse-complement)

c) Replacement of sequences by longer foreign genetic elements, such as sequences from other ORFs:

forward primer – 45 bp upstream of the sequence to be replaced, first 20 bp of the foreign sequence

Reverse primer – 45 bp downstream of the sequence to be replaced, last 20 bp of the foreign sequence (reverse complement)

8.5.8. Preparation of genomic yeast DNA

Crude yeast DNA was obtained as previously described (Hoffman and Winston, 1987). Briefly, 5 ml of yeast culture were grown to saturation. The cells were harvested and resuspended in 200 µl buffer A. Approximately 200 µl glass beads and 200 µl phenol:chloroform:isoamylalcohol 25:24:1 were added. After vigorous vortexing for 5 min, 200 µl H_2O were added. Phase separation was accomplished by centrifugation (5 min, 20,000 g, 4°C). The aqueous phase was transferred to a fresh reaction tube and 1 ml 100% EtOH (RT) was added. The DNA was pelleted by centrifugation for 2 min (20,000 g). The resulting DNA pellet was dried at 65°C for about 5 min and resuspended in 40 µl H_2O.

Buffer A
10 mM Tris/HCl pH 8.0
100 mM NaCl
1 mM EDTA
2% Triton X-100
1% SDS

8.5.9. Live fluorescence microscopy

Cells were grown overnight to logarithmic phase in rich medium or the appropriate selection medium. Cultures contained 50 mg/l adenine to suppress cellular autofluorescence. An aliquot of cells was harvested by spinning at RT for 1 min at 3,000 g. Cells were briefly washed in H_2O or HC complete medium and visualized directly under a Zeiss Axioplan 2 epifluorescence microscope using filters for GFP, dsRed or DAPI. Pictures were taken using an Axiocam MRm CCD camera and Axiovision software. Image processing was performed using Adobe Photoshop. All pictures from the same experiment were treated equally. Per strain, a minimum of one hundred cells from at least three independent experiments was counted when quantification was required.

8.6. Formulas and web resources

8.6.1. BLAST analysis

BLAST and BLASTP analysis was performed using the *Saccharomyces Genome Database* (www.yeastgenome.org/cgi-bin/blast-sgd.pl). The same website provides a fungal BLAST search tool specifically to search for homologues in other fungal species. In this work, the algorithm's standard settings were used.

8.6.2. Retrieval of annotated data on genes and proteins

Information on protein function, abundance, localization and topology was usually obtained from the *Saccharomyces Genome Database* (www.yeastgenome.org) or from *Biobase Biological Databases* (https://portal.biobase-international.com/cgi-bin/build_ghpywl/idb/1.0/searchengine/start.cgi). The localization of C-terminally GFP-tagged proteins, as determined by high-throughput, was obtained from the *Yeast Resource Center* (www.yeastrc.org/pdr/pages/front.jsp).

8.6.3. TPR prediction

Tetratricopeptide repeats were predicted using the TPRPRED algorithm (Karpenahalli *et al.*, 2007, available on http://toolkit.tuebingen.mpg.de/tprpred), using the standard settings.

8.6.4. Determination of yeast generation times

The following formula was used to determine the generation time of a yeast strain under defined conditions:

$$t_g = T \times \frac{\log 2}{\log(\frac{OD_2}{OD_1})}$$

t_g: generation time

T: time of logarithmic growth

OD_1: OD_{600} value at the beginning of the growth phase

OD_2: OD_{600} value at the end of the growth phase

(Note that the formula can only be used for logarithmically growing cells.)

When cultures were inoculated from a stationary pre-culture, cells typically required one additional generation time to adjust to logarithmic growth again.

8.6.5. Conversion of centrifugation run times

To facilitate experimental planning, run times of centrifugation steps were sometimes shortened or prolonged by adjusting the centrifugation speed accordingly. Assuming that the same rotor is used, the following formula can be employed to convert centrifugation conditions:

$$\omega_1{}^2 \times T_1 = \omega_2{}^2 \times T_2$$

ω: rotation speed in rotations per minute (rpm)

T: time

This formula assumes that ω is constant, i.e. that the time required for acceleration and deceleration is significantly smaller than the total run time. Since the centrifuges used in this study typically required ~15 min for acceleration and deceleration, this assumption can be considered valid for overnight runs.

Appendix

9. Appendix

9.1. Abbreviations

5-FOA	5-fluoroorotic acid
aa	amino acid
Ac	acetate
AMW	average molecular weight
AP	adaptor protein
ARF1	ADP ribosylation factor 1
ATP	adenosine-5'-triphosphate
BLAST	basic local alignment and sequencing tool
bp	base pair
BSA	bovine serum albumin
ChAPS	Chs5p-Arf1p-binding proteins
CFW	calcofluor white
ConA	concanavalin A
COPI	coat protein complex I
COPII	coat protein complex II
ddH_2O	water bidest.
dH_2O	water dest.
DMP	dimenthylpimelimidate
DMSO	dimethylsulfoxide
DNA	desoxyribonucleic acid
DNase	DNA-hydrolyzing enzyme
dNTPs	desoxynucleotide triphosphates
dsRed	drFP583 red fluorescent protein (from *Discosoma species*)
DTT	dithiothreitol
E. coli	*Escherichia coli*
ECL	enhanced chemoluminescence
EDTA	ethylenediaminetetraacetic acid
EGFP	enhanced GFP
eqFP611	*Entacmaea quadricolor* fluorescent protein, emission maximum at 611 nm
ER	endoplasmic reticulum
EtOH	ethanol
g	gravitational acceleration constant (also: gram)
$G418^R$	resistance to G418 (geneticin)
GAP	GTPase-activating protein
GDP	guanosin-5'-diphosphate
GEF	guanine nucleotide exchange factor
GFP	green fluorescent protein
GPI	glycosylphosphatidylinositol
GST	glutathion-S-transferase

GTP	guanosine-5'-triphosphate
GTPase	GTP hydrolyzing enzyme
h	hours
HDSV	high-density secretory vesicle
HEPES	N-(2-hydroxyethyl)piperazine-N'-(2-ethanesulfonic acid)
HRP	horseradish peroxidase
IF	immunofluorescence
IP	immunoprecipitation
K. lactis	*Kluyveromyces lactis*
kb	kilobase
LB	lysogeny broth
LC-MS/MS	liquid chromatography coupled to tandem mass spectrometry
LDSV	low-density secretory vesicle
min	minutes
mRNA	messenger RNA
MVB	multivesicular body
MW	molecular weight
n.d.	not determined
O/N	over night
OD_{600}	optical density at 600 nm
PAGE	polyacrylamide gel electrophoresis
PBS	phosphate-buffered saline
PCR	polymerase chain reaction
PEG	polyethylene glycol
PM	plasma membrane
PMSF	phenylmethylsulfonylfluoride
RNA	ribonucleic acid
rpm	revolutions per minute
RT	room temperature
S. cerevisiae	*Saccharomyces cerevisiae*
SDS	sodium dodecyl sulfate
sec	seconds
SILAC	Stable Isotope Labeling of Amino acids in Cell culture
TBS	Tris-buffered saline
TEA	triethanolamine
TGN	trans-Golgi network
TPR	tetratricopeptide repeat (also: total protonic reversal)
Tris	tris(hydroxymethylaminomethane)
ts	temperature-sensitive
w/o	without
w/v	weight per volume
w/w	weight per weight
WT	wild-type
yeGFP	yeast codon-optimized GFP
YNB	yeast nitrogen base

9.2. Acknowledgements

I would like to express my sincere gratitude to the following people:

Anne Spang, for her supervision and her continued efforts that a valuable story would eventually emerge out of every project – be it ever so difficult and frustrating. In the four years that I worked in her lab, I have not heard her say "I don't have time for this" a single time. Especially for someone who has a so many other commitments, she is still remarkably close to the bench (not just spatially), a fact from which I benefitted a lot throughout my PhD. I also much appreciated that she always kept the lab both well-funded and well-organized – this made a tremendous difference. Finally, despite my plans to leave academic research, I am convinced that much of what I learned from her will be invaluable to me and my work in the future.

My Thesis Committee members, **Margaret "Scottie" Robinson and Francis Barr**, for their efforts to guide me through the different projects over the years, even if we never actually got down to doing the real SILAC experiment. I greatly appreciated their suggestions and all their input on my experimental problems, of which there were many, no doubt. Furthermore, I would like to thank **Markus Affolter** for chairing my PhD defense.

Mark Trautwein, for an inspiring start at the Biozentrum and a rich scientific heritage.

Julia Stevens, Dominik Sutter, Sabine Probst, Lucas Thiel and Alejandra Fernández Belmonte, for running the lab behind the scenes and making sure that I could always focus on my work, rather than pouring gels. Also, **Isabel, Sangmo and Adela** for being a great kitchen team, always keeping our flasks clean and the pipette boxes filled. I cannot emphasize enough how much of a difference this made.

Julia Stevens, again, for never getting tired of showing me the obvious location of a chemical I was looking for. I am sure this was the main reason why she eventually came up with her "What is where?" list.

Julie Weidner, for her miraculous 50% PEG solution that made even untransformable strains grow.

Cornelia Kilchert, for introducing me to the secrets of elutriation, and for being a very fine bench neighbor.

Alejandro Fernández Estrada, for spicy things you can find in a fly.

All past and present members of the Spang Lab, for the great and co-operative atmosphere, their advice, encouragement and friendship. And for their willingness to bear with me even on days when I slammed the office door on them...

Paul Jenö and Suzette Moes, for a very enjoyable lab rotation in early 2008, and for the plasma membrane mass spectrometry analysis.

Stefan Hümmer, for his *Vesicle Dance* and for giving me a role in it (behind the camera, luckily).

Brigitte Olufsen, for going out of her way many times and taking administrative matters into her hands.

Robin Klemm, for the immunocellulose protocol and helpful hints on the vesicle IP.

The **Werner Siemens Foundation** for funding.

Alice Krudewig, Julia Sommer and Aaron Robitaille, for a truly memorable *I love science but I don't know what to do with it* Dinner.

My parents, for their continued support, even from far away.

Silke, for her encouragement, her understanding, and her love.

References

10. References

Abe, Y., Shodai, T., Muto, T., Mihara, K., Torii, H., Nishikawa, S., Endo, T., and Kohda, D. (2000). Structural basis of presequence recognition by the mitochondrial protein import receptor Tom20. Cell *100*, 551-560.

Adamo, J.E., Moskow, J.J., Gladfelter, A.S., Viterbo, D., Lew, D.J., and Brennwald, P.J. (2001). Yeast Cdc42 functions at a late step in exocytosis, specifically during polarized growth of the emerging bud. J Cell Biol *155*, 581-592.

Amor, J.C., Harrison, D.H., Kahn, R.A., and Ringe, D. (1994). Structure of the human ADP-ribosylation factor 1 complexed with GDP. Nature *372*, 704-708.

Antonny, B., Madden, D., Hamamoto, S., Orci, L., and Schekman, R. (2001). Dynamics of the COPII coat with GTP and stable analogues. Nat Cell Biol *3*, 531-537.

Appenzeller, C., Andersson, H., Kappeler, F., and Hauri, H.P. (1999). The lectin ERGIC-53 is a cargo transport receptor for glycoproteins. Nat Cell Biol *1*, 330-334.

Arighi, C.N., Hartnell, L.M., Aguilar, R.C., Haft, C.R., and Bonifacino, J.S. (2004). Role of the mammalian retromer in sorting of the cation-independent mannose 6-phosphate receptor. J Cell Biol *165*, 123-133.

Bagnat, M., Chang, A., and Simons, K. (2001). Plasma membrane proton ATPase Pma1p requires raft association for surface delivery in yeast. Mol Biol Cell *12*, 4129-4138.

Bagnat, M., Keranen, S., Shevchenko, A., Shevchenko, A., and Simons, K. (2000). Lipid rafts function in biosynthetic delivery of proteins to the cell surface in yeast. Proc Natl Acad Sci U S A *97*, 3254-3259.

Balch, W.E., Glick, B.S., and Rothman, J.E. (1984). Sequential intermediates in the pathway of intercompartmental transport in a cell-free system. Cell *39*, 525-536.

Bard, F., and Malhotra, V. (2006). The formation of TGN-to-plasma-membrane transport carriers. Annu Rev Cell Dev Biol *22*, 439-455.

Barfield, R.M., Fromme, J.C., and Schekman, R. (2009). The exomer coat complex transports Fus1p to the plasma membrane via a novel plasma membrane sorting signal in yeast. Mol Biol Cell *20*, 4985-4996.

Barlowe, C., d'Enfert, C., and Schekman, R. (1993). Purification and characterization of SAR1p, a small GTP-binding protein required for transport vesicle formation from the endoplasmic reticulum. J Biol Chem *268*, 873-879.

Barlowe, C., Orci, L., Yeung, T., Hosobuchi, M., Hamamoto, S., Salama, N., Rexach, M.F., Ravazzola, M., Amherdt, M., and Schekman, R. (1994). COPII: a membrane coat formed by Sec proteins that drive vesicle budding from the endoplasmic reticulum. Cell *77*, 895-907.

Barlowe, C., and Schekman, R. (1993). SEC12 encodes a guanine-nucleotide-exchange factor essential for transport vesicle budding from the ER. Nature *365*, 347-349.

Barral, Y., Mermall, V., Mooseker, M.S., and Snyder, M. (2000). Compartmentalization of the cell cortex by septins is required for maintenance of cell polarity in yeast. Mol Cell *5*, 841-851.

Beck, R., Rawet, M., Wieland, F.T., and Cassel, D. (2009). The COPI system: molecular mechanisms and function. FEBS Lett *583*, 2701-2709.

Beites, C.L., Campbell, K.A., and Trimble, W.S. (2005). The septin Sept5/CDCrel-1 competes with alpha-SNAP for binding to the SNARE complex. Biochem J *385*, 347-353.

Biegert, A., Mayer, C., Remmert, M., Soding, J., and Lupas, A.N. (2006). The MPI Bioinformatics Toolkit for protein sequence analysis. Nucleic Acids Res *34*, W335-339.

Bigay, J., Casella, J.F., Drin, G., Mesmin, B., and Antonny, B. (2005). ArfGAP1 responds to membrane curvature through the folding of a lipid packing sensor motif. Embo J *24*, 2244-2253.

Bigay, J., Gounon, P., Robineau, S., and Antonny, B. (2003). Lipid packing sensed by ArfGAP1 couples COPI coat disassembly to membrane bilayer curvature. Nature *426*, 563-566.

Blatch, G.L., and Lassle, M. (1999). The tetratricopeptide repeat: a structural motif mediating protein-protein interactions. Bioessays *21*, 932-939.

Boehm, M., Aguilar, R.C., and Bonifacino, J.S. (2001). Functional and physical interactions of the adaptor protein complex AP-4 with ADP-ribosylation factors (ARFs). Embo J *20*, 6265-6276.

Bonifacino, J.S., and Glick, B.S. (2004). The mechanisms of vesicle budding and fusion. Cell *116*, 153-166.

Bonifacino, J.S., and Rojas, R. (2006). Retrograde transport from endosomes to the trans-Golgi network. Nat Rev Mol Cell Biol *7*, 568-579.

Bradford, M.M. (1976). A rapid and sensitive method for the quantitation of microgram quantities of protein utilizing the principle of protein-dye binding. Anal Biochem *72*, 248-254.

Brennwald, P., and Rossi, G. (2007). Spatial regulation of exocytosis and cell polarity: yeast as a model for animal cells. FEBS Lett *581*, 2119-2124.

Brown, H.A., Gutowski, S., Moomaw, C.R., Slaughter, C., and Sternweis, P.C. (1993). ADP-ribosylation factor, a small GTP-dependent regulatory protein, stimulates phospholipase D activity. Cell *75*, 1137-1144.

Bulawa, C.E. (1992). CSD2, CSD3, and CSD4, genes required for chitin synthesis in Saccharomyces cerevisiae: the CSD2 gene product is related to chitin synthases and to developmentally regulated proteins in Rhizobium species and Xenopus laevis. Mol Cell Biol *12*, 1764-1776.

Bulawa, C.E. (1993). Genetics and molecular biology of chitin synthesis in fungi. Annu Rev Microbiol *47*, 505-534.

Bulawa, C.E., Slater, M., Cabib, E., Au-Young, J., Sburlati, A., Adair, W.L., Jr., and Robbins, P.W. (1986). The S. cerevisiae structural gene for chitin synthase is not required for chitin synthesis in vivo. Cell *46*, 213-225.

Cabib, E., Sburlati, A., Bowers, B., and Silverman, S.J. (1989). Chitin synthase 1, an auxiliary enzyme for chitin synthesis in Saccharomyces cerevisiae. J Cell Biol *108*, 1665-1672.

Cai, H., Reinisch, K., and Ferro-Novick, S. (2007). Coats, tethers, Rabs, and SNAREs work together to mediate the intracellular destination of a transport vesicle. Dev Cell *12*, 671-682.

Cai, H., Yu, S., Menon, S., Cai, Y., Lazarova, D., Fu, C., Reinisch, K., Hay, J.C., and Ferro-Novick, S. (2007). TRAPPI tethers COPII vesicles by binding the coat subunit Sec23. Nature *445*, 941-944.

Canuel, M., Lefrancois, S., Zeng, J., and Morales, C.R. (2008). AP-1 and retromer play opposite roles in the trafficking of sortilin between the Golgi apparatus and the lysosomes. Biochem Biophys Res Commun *366*, 724-730.

Carlton, J., Bujny, M., Peter, B.J., Oorschot, V.M., Rutherford, A., Mellor, H., Klumperman, J., McMahon, H.T., and Cullen, P.J. (2004). Sorting nexin-1 mediates tubular endosome-to-TGN transport through coincidence sensing of high- curvature membranes and 3-phosphoinositides. Curr Biol *14*, 1791-1800.

Chavrier, P., and Goud, B. (1999). The role of ARF and Rab GTPases in membrane transport. Curr Opin Cell Biol *11*, 466-475.

Chen, E.J., and Kaiser, C.A. (2002). Amino acids regulate the intracellular trafficking of the general amino acid permease of Saccharomycescerevisiae. Proc Natl Acad Sci U S A *99*, 14837-14842.

Chuang, J.S., and Schekman, R.W. (1996). Differential trafficking and timed localization of two chitin synthase proteins, Chs2p and Chs3p. J Cell Biol *135*, 597-610.

Collins, B.M., Praefcke, G.J., Robinson, M.S., and Owen, D.J. (2003). Structural basis for binding of accessory proteins by the appendage domain of GGAs. Nat Struct Biol *10*, 607-613.

Cos, T., Ford, R.A., Trilla, J.A., Duran, A., Cabib, E., and Roncero, C. (1998). Molecular analysis of Chs3p participation in chitin synthase III activity. Eur J Biochem *256*, 419-426.

Dancourt, J., and Barlowe, C. (2010). Protein sorting receptors in the early secretory pathway. Annu Rev Biochem *79*, 777-802.

De Antoni, A., and Gallwitz, D. (2000). A novel multi-purpose cassette for repeated integrative epitope tagging of genes in Saccharomyces cerevisiae. Gene *246*, 179-185.

De Matteis, M.A., and Luini, A. (2008). Exiting the Golgi complex. Nat Rev Mol Cell Biol *9*, 273-284.

Dell'Angelica, E.C., Mullins, C., and Bonifacino, J.S. (1999). AP-4, a novel protein complex related to clathrin adaptors. J Biol Chem *274*, 7278-7285.

Dell'Angelica, E.C., Ohno, H., Ooi, C.E., Rabinovich, E., Roche, K.W., and Bonifacino, J.S. (1997). AP-3: an adaptor-like protein complex with ubiquitous expression. Embo J *16*, 917-928.

Deloche, O., and Schekman, R.W. (2002). Vps10p cycles between the TGN and the late endosome via the plasma membrane in clathrin mutants. Mol Biol Cell *13*, 4296-4307.

Deloche, O., Yeung, B.G., Payne, G.S., and Schekman, R. (2001). Vps10p transport from the trans-Golgi network to the endosome is mediated by clathrin-coated vesicles. Mol Biol Cell *12*, 475-485.

DeMarini, D.J., Adams, A.E., Fares, H., De Virgilio, C., Valle, G., Chuang, J.S., and Pringle, J.R. (1997). A septin-based hierarchy of proteins required for localized deposition of chitin in the Saccharomyces cerevisiae cell wall. J Cell Biol *139*, 75-93.

Dobbelaere, J., and Barral, Y. (2004). Spatial coordination of cytokinetic events by compartmentalization of the cell cortex. Science *305*, 393-396.

Eugster, A., Frigerio, G., Dale, M., and Duden, R. (2004). The alpha- and beta'-COP WD40 domains mediate cargo-selective interactions with distinct di-lysine motifs. Mol Biol Cell *15*, 1011-1023.

Fath, S., Mancias, J.D., Bi, X., and Goldberg, J. (2007). Structure and organization of coat proteins in the COPII cage. Cell *129*, 1325-1336.

Fölsch, H. (2008). Regulation of membrane trafficking in polarized epithelial cells. Curr Opin Cell Biol *20*, 208-213.

Foote, C., and Nothwehr, S.F. (2006). The clathrin adaptor complex 1 directly binds to a sorting signal in Ste13p to reduce the rate of its trafficking to the late endosome of yeast. J Cell Biol *173*, 615-626.

Forster, R., Weiss, M., Zimmermann, T., Reynaud, E.G., Verissimo, F., Stephens, D.J., and Pepperkok, R. (2006). Secretory cargo regulates the turnover of COPII subunits at single ER exit sites. Curr Biol *16*, 173-179.

Fotin, A., Cheng, Y., Sliz, P., Grigorieff, N., Harrison, S.C., Kirchhausen, T., and Walz, T. (2004). Molecular model for a complete clathrin lattice from electron cryomicroscopy. Nature *432*, 573-579.

Franzusoff, A., Rothblatt, J., and Schekman, R. (1991). Analysis of polypeptide transit through yeast secretory pathway. Methods Enzymol *194*, 662-674.

Fucini, R.V., Navarrete, A., Vadakkan, C., Lacomis, L., Erdjument-Bromage, H., Tempst, P., and Stamnes, M. (2000). Activated ADP-ribosylation factor assembles distinct pools of actin on golgi membranes. J Biol Chem *275*, 18824-18829.

Gaidarov, I., and Keen, J.H. (1999). Phosphoinositide-AP-2 interactions required for targeting to plasma membrane clathrin-coated pits. J Cell Biol *146*, 755-764.

Gaigg, B., Toulmay, A., and Schneiter, R. (2006). Very long-chain fatty acid-containing lipids rather than sphingolipids per se are required for raft association and stable surface transport of newly synthesized plasma membrane ATPase in yeast. J Biol Chem *281*, 34135-34145.

Gall, W.E., Geething, N.C., Hua, Z., Ingram, M.F., Liu, K., Chen, S.I., and Graham, T.R. (2002). Drs2p-dependent formation of exocytic clathrin-coated vesicles in vivo. Curr Biol *12*, 1623-1627.

Gandhi, M., Goode, B.L., and Chan, C.S. (2006). Four novel suppressors of gic1 gic2 and their roles in cytokinesis and polarized cell growth in Saccharomyces cerevisiae. Genetics *174*, 665-678.

Garrus, J.E., von Schwedler, U.K., Pornillos, O.W., Morham, S.G., Zavitz, K.H., Wang, H.E., Wettstein, D.A., Stray, K.M., Cote, M., Rich, R.L., Myszka, D.G., and Sundquist, W.I. (2001). Tsg101 and the vacuolar protein sorting pathway are essential for HIV-1 budding. Cell *107*, 55-65.

Gatto, G.J., Jr., Geisbrecht, B.V., Gould, S.J., and Berg, J.M. (2000). Peroxisomal targeting signal-1 recognition by the TPR domains of human PEX5. Nat Struct Biol *7*, 1091-1095.

Ghaemmaghami, S., Huh, W.K., Bower, K., Howson, R.W., Belle, A., Dephoure, N., O'Shea, E.K., and Weissman, J.S. (2003). Global analysis of protein expression in yeast. Nature *425*, 737-741.

Gietz, R.D., Schiestl, R.H., Willems, A.R., and Woods, R.A. (1995). Studies on the transformation of intact yeast cells by the LiAc/SS-DNA/PEG procedure. Yeast *11*, 355-360.

Gladfelter, A.S., Pringle, J.R., and Lew, D.J. (2001). The septin cortex at the yeast mother-bud neck. Curr Opin Microbiol *4*, 681-689.

Güldener, U., Heck, S., Fielder, T., Beinhauer, J., and Hegemann, J.H. (1996). A new efficient gene disruption cassette for repeated use in budding yeast. Nucleic Acids Res *24*, 2519-2524.

Güldener, U., Heinisch, J., Koehler, G.J., Voss, D., and Hegemann, J.H. (2002). A second set of loxP marker cassettes for Cre-mediated multiple gene knockouts in budding yeast. Nucleic Acids Res *30*, e23.

Gurunathan, S., David, D., and Gerst, J.E. (2002). Dynamin and clathrin are required for the biogenesis of a distinct class of secretory vesicles in yeast. Embo J *21*, 602-614.

Hales, C.N., and Woodhead, J.S. (1980). Labeled antibodies and their use in the immunoradiometric assay. Methods Enzymol *70*, 334-355.

Hammond, J.W., Griffin, K., Jih, G.T., Stuckey, J., and Verhey, K.J. (2008). Co-operative versus independent transport of different cargoes by Kinesin-1. Traffic *9*, 725-741.

Hanson, P.I., Shim, S., and Merrill, S.A. (2009). Cell biology of the ESCRT machinery. Curr Opin Cell Biol *21*, 568-574.

Harlow, E., and Lane, D. (1988). Antibodies: A Laboratory Manual. Cold Spring Harbor Laboratory.

Harsay, E., and Bretscher, A. (1995). Parallel secretory pathways to the cell surface in yeast. J Cell Biol *131*, 297-310.

Harsay, E., and Schekman, R. (2002). A subset of yeast vacuolar protein sorting mutants is blocked in one branch of the exocytic pathway. J Cell Biol *156*, 271-285.

He, B., and Guo, W. (2009). The exocyst complex in polarized exocytosis. Curr Opin Cell Biol *21*, 537-542.

He, B., Xi, F., Zhang, J., TerBush, D., Zhang, X., and Guo, W. (2007). Exo70p mediates the secretion of specific exocytic vesicles at early stages of the cell cycle for polarized cell growth. J Cell Biol *176*, 771-777.

Henkel, M.K., Pott, G., Henkel, A.W., Juliano, L., Kam, C.M., Powers, J.C., and Franzusoff, A. (1999). Endocytic delivery of intramolecularly quenched substrates and inhibitors to the intracellular yeast Kex2 protease1. Biochem J *341 (Pt 2)*, 445-452.

Hirschberg, K., Miller, C.M., Ellenberg, J., Presley, J.F., Siggia, E.D., Phair, R.D., and Lippincott-Schwartz, J. (1998). Kinetic analysis of secretory protein traffic and characterization of golgi to plasma membrane transport intermediates in living cells. J Cell Biol *143*, 1485-1503.

Hirst, J., Barlow, L.D., Francisco, G.C., Sahlender, D.A., Seaman, M.N., Dacks, J.B., and Robinson, M.S. (2011). The fifth adaptor protein complex. PLoS Biol *9*, e1001170.

Hirst, J., Bright, N.A., Rous, B., and Robinson, M.S. (1999). Characterization of a fourth adaptor-related protein complex. Mol Biol Cell *10*, 2787-2802.

Hirst, J., Sahlender, D.A., Choma, M., Sinka, R., Harbour, M.E., Parkinson, M., and Robinson, M.S. (2009). Spatial and functional relationship of GGAs and AP-1 in Drosophila and HeLa cells. Traffic *10*, 1696-1710.

Hoffman, C.S., and Winston, F. (1987). A ten-minute DNA preparation from yeast efficiently releases autonomous plasmids for transformation of Escherichia coli. Gene *57*, 267-272.

Hsia, K.C., and Hoelz, A. (2010). Crystal structure of alpha-COP in complex with epsilon-COP provides insight into the architecture of the COPI vesicular coat. Proc Natl Acad Sci U S A *107*, 11271-11276.

Hsu, S.C., Hazuka, C.D., Roth, R., Foletti, D.L., Heuser, J., and Scheller, R.H. (1998). Subunit composition, protein interactions, and structures of the mammalian brain sec6/8 complex and septin filaments. Neuron *20*, 1111-1122.

Huotari, J., and Helenius, A. (2011). Endosome maturation. Embo J *30*, 3481-3500.

Ito, H., Atsuzawa, K., Morishita, R., Usuda, N., Sudo, K., Iwamoto, I., Mizutani, K., Katoh-Semba, R., Nozawa, Y., Asano, T., and Nagata, K. (2009). Sept8 controls the binding of vesicle-associated membrane protein 2 to synaptophysin. J Neurochem *108*, 867-880.

Jackson, L.P., Kelly, B.T., McCoy, A.J., Gaffry, T., James, L.C., Collins, B.M., Honing, S., Evans, P.R., and Owen, D.J. (2010). A large-scale conformational change couples membrane recruitment to cargo binding in the AP2 clathrin adaptor complex. Cell *141*, 1220-1229.

Janke, C., Magiera, M.M., Rathfelder, N., Taxis, C., Reber, S., Maekawa, H., Moreno-Borchart, A., Doenges, G., Schwob, E., Schiebel, E., and Knop, M. (2004). A versatile toolbox for PCR-based tagging of yeast genes: new fluorescent proteins, more markers and promoter substitution cassettes. Yeast *21*, 947-962.

Janvier, K., Kato, Y., Boehm, M., Rose, J.R., Martina, J.A., Kim, B.Y., Venkatesan, S., and Bonifacino, J.S. (2003). Recognition of dileucine-based sorting signals from HIV-1 Nef and LIMP-II by the AP-1 gamma-sigma1 and AP-3 delta-sigma3 hemicomplexes. J Cell Biol *163*, 1281-1290.

Johnsson, N., and Varshavsky, A. (1994). Split ubiquitin as a sensor of protein interactions in vivo. Proc Natl Acad Sci U S A *91*, 10340-10344.

Jones, D.H., Morris, J.B., Morgan, C.P., Kondo, H., Irvine, R.F., and Cockcroft, S. (2000). Type I phosphatidylinositol 4-phosphate 5-kinase directly interacts with ADP-ribosylation factor 1 and is responsible for phosphatidylinositol 4,5-bisphosphate synthesis in the golgi compartment. J Biol Chem *275*, 13962-13966.

Kahn, R.A., Cherfils, J., Elias, M., Lovering, R.C., Munro, S., and Schurmann, A. (2006). Nomenclature for the human Arf family of GTP-binding proteins: ARF, ARL, and SAR proteins. J Cell Biol *172*, 645-650.

Kamal, A., Stokin, G.B., Yang, Z., Xia, C.H., and Goldstein, L.S. (2000). Axonal transport of amyloid precursor protein is mediated by direct binding to the kinesin light chain subunit of kinesin-I. Neuron *28*, 449-459.

Karpenahalli, M.R., Lupas, A.N., and Soding, J. (2007). TPRpred: a tool for prediction of TPR-, PPR- and SEL1-like repeats from protein sequences. BMC Bioinformatics *8*, 2.

Kilchert, C. (2011). mRNA localization and turnover in mutants of the small GTPase Arf1p in S. cerevisiae, Universität Basel, Basel.

Kilchert, C., and Spang, A. (2011). Cotranslational transport of ABP140 mRNA to the distal pole of S. cerevisiae. Embo J *30*, 3567-3580.

Kilchert, C., Weidner, J., Prescianotto-Baschong, C., and Spang, A. (2010). Defects in the secretory pathway and high Ca2+ induce multiple P-bodies. Mol Biol Cell *21*, 2624-2638.

Kirchhausen, T. (2000). Three ways to make a vesicle. Nat Rev Mol Cell Biol *1*, 187-198.

Klemm, R.W., Ejsing, C.S., Surma, M.A., Kaiser, H.J., Gerl, M.J., Sampaio, J.L., de Robillard, Q., Ferguson, C., Proszynski, T.J., Shevchenko, A., and Simons, K. (2009). Segregation of sphingolipids and sterols during formation of secretory vesicles at the trans-Golgi network. J Cell Biol *185*, 601-612.

Knop, M., Siegers, K., Pereira, G., Zachariae, W., Winsor, B., Nasmyth, K., and Schiebel, E. (1999). Epitope tagging of yeast genes using a PCR-based strategy: more tags and improved practical routines. Yeast *15*, 963-972.

Kumari, S., Mg, S., and Mayor, S. (2010). Endocytosis unplugged: multiple ways to enter the cell. Cell Res *20*, 256-275.

Kweon, H.S., Beznoussenko, G.V., Micaroni, M., Polishchuk, R.S., Trucco, A., Martella, O., Di Giandomenico, D., Marra, P., Fusella, A., Di Pentima, A., Berger, E.G., Geerts, W.J., Koster, A.J., Burger, K.N., Luini, A., and Mironov, A.A. (2004). Golgi enzymes are enriched in perforated zones of golgi cisternae but are depleted in COPI vesicles. Mol Biol Cell *15*, 4710-4724.

Lee, C., and Goldberg, J. (2010). Structure of coatomer cage proteins and the relationship among COPI, COPII, and clathrin vesicle coats. Cell *142*, 123-132.

Lippincott-Schwartz, J., Yuan, L., Tipper, C., Amherdt, M., Orci, L., and Klausner, R.D. (1991). Brefeldin A's effects on endosomes, lysosomes, and the TGN suggest a general mechanism for regulating organelle structure and membrane traffic. Cell *67*, 601-616.

Lord, C., Bhandari, D., Menon, S., Ghassemian, M., Nycz, D., Hay, J., Ghosh, P., and Ferro-Novick, S. (2011). Sequential interactions with Sec23 control the direction of vesicle traffic. Nature *473*, 181-186.

Lord, M., Chen, T., Fujita, A., and Chant, J. (2002). Analysis of budding patterns. Methods Enzymol *350*, 131-141.

Losev, E., Reinke, C.A., Jellen, J., Strongin, D.E., Bevis, B.J., and Glick, B.S. (2006). Golgi maturation visualized in living yeast. Nature *441*, 1002-1006.

Love, H.D., Lin, C.C., Short, C.S., and Ostermann, J. (1998). Isolation of functional Golgi-derived vesicles with a possible role in retrograde transport. J Cell Biol *140*, 541-551.

Lustgarten, V., and Gerst, J.E. (1999). Yeast VSM1 encodes a v-SNARE binding protein that may act as a negative regulator of constitutive exocytosis. Mol Cell Biol *19*, 4480-4494.

Ma, D., Taneja, T.K., Hagen, B.M., Kim, B.Y., Ortega, B., Lederer, W.J., and Welling, P.A. (2011). Golgi export of the Kir2.1 channel is driven by a trafficking signal located within its tertiary structure. Cell *145*, 1102-1115.

Madden, K., and Snyder, M. (1998). Cell polarity and morphogenesis in budding yeast. Annu Rev Microbiol *52*, 687-744.

Magliery, T.J., and Regan, L. (2004). Beyond consensus: statistical free energies reveal hidden interactions in the design of a TPR motif. J Mol Biol *343*, 731-745.

Malsam, J., Kreye, S., and Sollner, T.H. (2008). Membrane fusion: SNAREs and regulation. Cell Mol Life Sci *65*, 2814-2832.

Mancias, J.D., and Goldberg, J. (2007). The transport signal on Sec22 for packaging into COPII-coated vesicles is a conformational epitope. Mol Cell *26*, 403-414.

Marsh, B.J., Volkmann, N., McIntosh, J.R., and Howell, K.E. (2004). Direct continuities between cisternae at different levels of the Golgi complex in glucose-stimulated mouse islet beta cells. Proc Natl Acad Sci U S A *101*, 5565-5570.

Martin-Garcia, R., de Leon, N., Sharifmoghadam, M.R., Curto, M.A., Hoya, M., Bustos-Sanmamed, P., and Valdivieso, M.H. (2010). The FN3 and BRCT motifs in the exomer component Chs5p define a conserved module that is necessary and sufficient for its function. Cell Mol Life Sci *68*, 2907-2917.

Martinez-Menarguez, J.A., Prekeris, R., Oorschot, V.M., Scheller, R., Slot, J.W., Geuze, H.J., and Klumperman, J. (2001). Peri-Golgi vesicles contain retrograde but not anterograde proteins consistent with the cisternal progression model of intra-Golgi transport. J Cell Biol *155*, 1213-1224.

Matsuoka, K., Orci, L., Amherdt, M., Bednarek, S.Y., Hamamoto, S., Schekman, R., and Yeung, T. (1998). COPII-coated vesicle formation reconstituted with purified coat proteins and chemically defined liposomes. Cell *93*, 263-275.

Matsuura-Tokita, K., Takeuchi, M., Ichihara, A., Mikuriya, K., and Nakano, A. (2006). Live imaging of yeast Golgi cisternal maturation. Nature *441*, 1007-1010.

Mayor, S., and Pagano, R.E. (2007). Pathways of clathrin-independent endocytosis. Nat Rev Mol Cell Biol *8*, 603-612.

McGough, I.J., and Cullen, P.J. (2011). Recent advances in retromer biology. Traffic *12*, 963-971.

McNew, J.A., Parlati, F., Fukuda, R., Johnston, R.J., Paz, K., Paumet, F., Sollner, T.H., and Rothman, J.E. (2000). Compartmental specificity of cellular membrane fusion encoded in SNARE proteins. Nature *407*, 153-159.

Meissner, D., Odman-Naresh, J., Vogelpohl, I., and Merzendorfer, H. (2010). A novel role of the yeast CaaX protease Ste24 in chitin synthesis. Mol Biol Cell *21*, 2425-2433.

Meyer, C., Zizioli, D., Lausmann, S., Eskelinen, E.L., Hamann, J., Saftig, P., von Figura, K., and Schu, P. (2000). mu1A-adaptin-deficient mice: lethality, loss of AP-1 binding and rerouting of mannose 6-phosphate receptors. Embo J *19*, 2193-2203.

Meyer, D.M., Crottet, P., Maco, B., Degtyar, E., Cassel, D., and Spiess, M. (2005). Oligomerization and dissociation of AP-1 adaptors are regulated by cargo signals and by ArfGAP1-induced GTP hydrolysis. Mol Biol Cell *16*, 4745-4754.

Michelsen, K., Schmid, V., Metz, J., Heusser, K., Liebel, U., Schwede, T., Spang, A., and Schwappach, B. (2007). Novel cargo-binding site in the beta and delta subunits of coatomer. J Cell Biol *179*, 209-217.

Miller, E.A., Beilharz, T.H., Malkus, P.N., Lee, M.C., Hamamoto, S., Orci, L., and Schekman, R. (2003). Multiple cargo binding sites on the COPII subunit Sec24p ensure capture of diverse membrane proteins into transport vesicles. Cell *114*, 497-509.

Miller, S.E., Collins, B.M., McCoy, A.J., Robinson, M.S., and Owen, D.J. (2007). A SNARE-adaptor interaction is a new mode of cargo recognition in clathrin-coated vesicles. Nature *450*, 570-574.

Mossessova, E., Bickford, L.C., and Goldberg, J. (2003). SNARE selectivity of the COPII coat. Cell *114*, 483-495.

Mulholland, J., Wesp, A., Riezman, H., and Botstein, D. (1997). Yeast actin cytoskeleton mutants accumulate a new class of Golgi-derived secretary vesicle. Mol Biol Cell *8*, 1481-1499.

Muniz, M., Nuoffer, C., Hauri, H.P., and Riezman, H. (2000). The Emp24 complex recruits a specific cargo molecule into endoplasmic reticulum-derived vesicles. J Cell Biol *148*, 925-930.

Nakano, A., and Luini, A. (2010). Passage through the Golgi. Curr Opin Cell Biol *22*, 471-478.

Nakatsu, F., and Ohno, H. (2003). Adaptor protein complexes as the key regulators of protein sorting in the post-Golgi network. Cell Struct Funct *28*, 419-429.

Navarre, C., Degand, H., Bennett, K.L., Crawford, J.S., Mortz, E., and Boutry, M. (2002). Subproteomics: identification of plasma membrane proteins from the yeast Saccharomyces cerevisiae. Proteomics *2*, 1706-1714.

Nickel, P. (2004). Identifizierung neuer membranständiger Regulatoren der kleinen GTPase Arf1p in Saccharomyces cerevisiae, Universität Tübingen, Tübingen.

Nishimura, N., and Balch, W.E. (1997). A di-acidic signal required for selective export from the endoplasmic reticulum. Science *277*, 556-558.

Novick, P., Field, C., and Schekman, R. (1980). Identification of 23 complementation groups required for post-translational events in the yeast secretory pathway. Cell *21*, 205-215.

Nufer, O., Guldbrandsen, S., Degen, M., Kappeler, F., Paccaud, J.P., Tani, K., and Hauri, H.P. (2002). Role of cytoplasmic C-terminal amino acids of membrane proteins in ER export. J Cell Sci *115*, 619-628.

Oh, Y., and Bi, E. (2011). Septin structure and function in yeast and beyond. Trends Cell Biol *21*, 141-148.

Ong, S.E., Blagoev, B., Kratchmarova, I., Kristensen, D.B., Steen, H., Pandey, A., and Mann, M. (2002). Stable isotope labeling by amino acids in cell culture, SILAC, as a simple and accurate approach to expression proteomics. Mol Cell Proteomics *1*, 376-386.

Orci, L., Stamnes, M., Ravazzola, M., Amherdt, M., Perrelet, A., Sollner, T.H., and Rothman, J.E. (1997). Bidirectional transport by distinct populations of COPI-coated vesicles. Cell *90*, 335-349.

Owen, D.J., and Evans, P.R. (1998). A structural explanation for the recognition of tyrosine-based endocytotic signals. Science *282*, 1327-1332.

Park, H.O., and Bi, E. (2007). Central roles of small GTPases in the development of cell polarity in yeast and beyond. Microbiol Mol Biol Rev *71*, 48-96.

Parlati, F., Varlamov, O., Paz, K., McNew, J.A., Hurtado, D., Sollner, T.H., and Rothman, J.E. (2002). Distinct SNARE complexes mediating membrane fusion in Golgi transport based on combinatorial specificity. Proc Natl Acad Sci U S A *99*, 5424-5429.

Pasqualato, S., Renault, L., and Cherfils, J. (2002). Arf, Arl, Arp and Sar proteins: a family of GTP-binding proteins with a structural device for 'front-back' communication. EMBO Rep *3*, 1035-1041.

Pelham, H.R. (2001). Traffic through the Golgi apparatus. J Cell Biol *155*, 1099-1101.

Piper, P., Mahe, Y., Thompson, S., Pandjaitan, R., Holyoak, C., Egner, R., Muhlbauer, M., Coote, P., and Kuchler, K. (1998). The pdr12 ABC transporter is required for the development of weak organic acid resistance in yeast. Embo J *17*, 4257-4265.

Posas, F., and Saito, H. (1997). Osmotic activation of the HOG MAPK pathway via Ste11p MAPKKK: scaffold role of Pbs2p MAPKK. Science *276*, 1702-1705.

Potenza, M., Bowser, R., Muller, H., and Novick, P. (1992). SEC6 encodes an 85 kDa soluble protein required for exocytosis in yeast. Yeast *8*, 549-558.

Proszynski, T.J., Klemm, R.W., Gravert, M., Hsu, P.P., Gloor, Y., Wagner, J., Kozak, K., Grabner, H., Walzer, K., Bagnat, M., Simons, K., and Walch-Solimena, C. (2005). A genome-wide visual screen reveals a role for sphingolipids and ergosterol in cell surface delivery in yeast. Proc Natl Acad Sci U S A *102*, 17981-17986.

Proszynski, T.J., Simons, K., and Bagnat, M. (2004). O-glycosylation as a sorting determinant for cell surface delivery in yeast. Mol Biol Cell *15*, 1533-1543.

Pylypenko, O., Lundmark, R., Rasmuson, E., Carlsson, S.R., and Rak, A. (2007). The PX-BAR membrane-remodeling unit of sorting nexin 9. Embo J *26*, 4788-4800.

Rapoport, T.A. (2007). Protein translocation across the eukaryotic endoplasmic reticulum and bacterial plasma membranes. Nature *450*, 663-669.

Rein, U., Andag, U., Duden, R., Schmitt, H.D., and Spang, A. (2002). ARF-GAP-mediated interaction between the ER-Golgi v-SNAREs and the COPI coat. J Cell Biol *157*, 395-404.

Reyes, A., Sanz, M., Duran, A., and Roncero, C. (2007). Chitin synthase III requires Chs4p-dependent translocation of Chs3p into the plasma membrane. J Cell Sci *120*, 1998-2009.

Rink, J., Ghigo, E., Kalaidzidis, Y., and Zerial, M. (2005). Rab conversion as a mechanism of progression from early to late endosomes. Cell *122*, 735-749.

Robinson, M., Poon, P.P., Schindler, C., Murray, L.E., Kama, R., Gabriely, G., Singer, R.A., Spang, A., Johnston, G.C., and Gerst, J.E. (2006). The Gcs1 Arf-GAP mediates Snc1,2 v-SNARE retrieval to the Golgi in yeast. Mol Biol Cell *17*, 1845-1858.

Robinson, M.S. (2004). Adaptable adaptors for coated vesicles. Trends Cell Biol *14*, 167-174.

Rodriguez-Pena, J.M., Rodriguez, C., Alvarez, A., Nombela, C., and Arroyo, J. (2002). Mechanisms for targeting of the Saccharomyces cerevisiae GPI-anchored cell wall protein Crh2p to polarised growth sites. J Cell Sci *115*, 2549-2558.

Rohde, G., Wenzel, D., and Haucke, V. (2002). A phosphatidylinositol (4,5)-bisphosphate binding site within mu2-adaptin regulates clathrin-mediated endocytosis. J Cell Biol *158*, 209-214.

Sambrook, J., Fritsch, E.F., and Maniatis, T. (1989). Molecular cloning: A Laboratory Manual. Second Edition. Cold Spring Habor Laboratory Press.

Sanchatjate, S., and Schekman, R. (2006). Chs5/6 complex: a multiprotein complex that interacts with and conveys chitin synthase III from the trans-Golgi network to the cell surface. Mol Biol Cell *17*, 4157-4166.

Santiago-Tirado, F.H., Legesse-Miller, A., Schott, D., and Bretscher, A. (2011). PI4P and Rab inputs collaborate in myosin-V-dependent transport of secretory compartments in yeast. Dev Cell *20*, 47-59.

Santos, B., Duran, A., and Valdivieso, M.H. (1997). CHS5, a gene involved in chitin synthesis and mating in Saccharomyces cerevisiae. Mol Cell Biol *17*, 2485-2496.

Santos, B., and Snyder, M. (1997). Targeting of chitin synthase 3 to polarized growth sites in yeast requires Chs5p and Myo2p. J Cell Biol *136*, 95-110.

Santos, B., and Snyder, M. (2003). Specific protein targeting during cell differentiation: polarized localization of Fus1p during mating depends on Chs5p in Saccharomyces cerevisiae. Eukaryot Cell *2*, 821-825.

Scheiffele, P., Peranen, J., and Simons, K. (1995). N-glycans as apical sorting signals in epithelial cells. Nature *378*, 96-98.

Schindler, C., and Spang, A. (2007). Interaction of SNAREs with ArfGAPs precedes recruitment of Sec18p/NSF. Mol Biol Cell *18*, 2852-2863.

Schott, D.H., Collins, R.N., and Bretscher, A. (2002). Secretory vesicle transport velocity in living cells depends on the myosin-V lever arm length. J Cell Biol *156*, 35-39.

Sherman, F. (1991). Getting started with yeast. Methods Enzymol *194*, 3-21.

Sikorski, R.S., and Hieter, P. (1989). A system of shuttle vectors and yeast host strains designed for efficient manipulation of DNA in Saccharomyces cerevisiae. Genetics *122*, 19-27.

Silverman, S.J., Sburlati, A., Slater, M.L., and Cabib, E. (1988). Chitin synthase 2 is essential for septum formation and cell division in Saccharomyces cerevisiae. Proc Natl Acad Sci U S A *85*, 4735-4739.

Simmen, T., Honing, S., Icking, A., Tikkanen, R., and Hunziker, W. (2002). AP-4 binds basolateral signals and participates in basolateral sorting in epithelial MDCK cells. Nat Cell Biol *4*, 154-159.

Soulard, A., Cremonesi, A., Moes, S., Schutz, F., Jeno, P., and Hall, M.N. (2010). The rapamycin-sensitive phosphoproteome reveals that TOR controls protein kinase A toward some but not all substrates. Mol Biol Cell *21*, 3475-3486.

Spang, A., Herrmann, J.M., Hamamoto, S., and Schekman, R. (2001). The ADP ribosylation factor-nucleotide exchange factors Gea1p and Gea2p have overlapping, but not redundant functions in retrograde transport from the Golgi to the endoplasmic reticulum. Mol Biol Cell *12*, 1035-1045.

Spang, A., Matsuoka, K., Hamamoto, S., Schekman, R., and Orci, L. (1998). Coatomer, Arf1p, and nucleotide are required to bud coat protein complex I-coated vesicles from large synthetic liposomes. Proc Natl Acad Sci U S A *95*, 11199-11204.

Spang, A., Shiba, Y., and Randazzo, P.A. (2010). Arf GAPs: gatekeepers of vesicle generation. FEBS Lett *584*, 2646-2651.

Spiliotis, E.T., Hunt, S.J., Hu, Q., Kinoshita, M., and Nelson, W.J. (2008). Epithelial polarity requires septin coupling of vesicle transport to polyglutamylated microtubules. J Cell Biol *180*, 295-303.

Springer, S., and Schekman, R. (1998). Nucleation of COPII vesicular coat complex by endoplasmic reticulum to Golgi vesicle SNAREs. Science *281*, 698-700.

Springer, S., Spang, A., and Schekman, R. (1999). A primer on vesicle budding. Cell *97*, 145-148.

Stagg, S.M., Gurkan, C., Fowler, D.M., LaPointe, P., Foss, T.R., Potter, C.S., Carragher, B., and Balch, W.E. (2006). Structure of the Sec13/31 COPII coat cage. Nature *439*, 234-238.

Stearns, T., Kahn, R.A., Botstein, D., and Hoyt, M.A. (1990). ADP ribosylation factor is an essential protein in Saccharomyces cerevisiae and is encoded by two genes. Mol Cell Biol *10*, 6690-6699.

Storici, F., and Resnick, M.A. (2006). The delitto perfetto approach to in vivo site-directed mutagenesis and chromosome rearrangements with synthetic oligonucleotides in yeast. Methods Enzymol *409*, 329-345.

Surma, M.A., Klose, C., Klemm, R.W., Ejsing, C.S., and Simons, K. (2011). Generic sorting of raft lipids into secretory vesicles in yeast. Traffic *12*, 1139-1147.

Sutton, R.B., Fasshauer, D., Jahn, R., and Brunger, A.T. (1998). Crystal structure of a SNARE complex involved in synaptic exocytosis at 2.4 A resolution. Nature *395*, 347-353.

Tagwerker, C., Flick, K., Cui, M., Guerrero, C., Dou, Y., Auer, B., Baldi, P., Huang, L., and Kaiser, P. (2006). A tandem affinity tag for two-step purification under fully denaturing conditions: application in ubiquitin profiling and protein complex identification combined with in vivocross-linking. Mol Cell Proteomics *5*, 737-748.

Takizawa, P.A., DeRisi, J.L., Wilhelm, J.E., and Vale, R.D. (2000). Plasma membrane compartmentalization in yeast by messenger RNA transport and a septin diffusion barrier. Science *290*, 341-344.

Towbin, H., Staehelin, T., and Gordon, J. (1979). Electrophoretic transfer of proteins from polyacrylamide gels to nitrocellulose sheets: procedure and some applications. Proc Natl Acad Sci U S A *76*, 4350-4354.

Traub, L.M. (2005). Common principles in clathrin-mediated sorting at the Golgi and the plasma membrane. Biochim Biophys Acta *1744*, 415-437.

Trautwein, M. (2004). Die kleine GTPase Arf1p aus Saccharomyces cerevisiae geht neue Wege: Neue Funktionen im mRNA Transport und bei der Bildung von spezialisierten Golgi-Vesikeln, Eberhard-Karls-Universität, Tübingen.

Trautwein, M., Dengjel, J., Schirle, M., and Spang, A. (2004). Arf1p provides an unexpected link between COPI vesicles and mRNA in Saccharomyces cerevisiae. Mol Biol Cell *15*, 5021-5037.

Trautwein, M., Schindler, C., Gauss, R., Dengjel, J., Hartmann, E., and Spang, A. (2006). Arf1p, Chs5p and the ChAPs are required for export of specialized cargo from the Golgi. Embo J *25*, 943-954.

Trilla, J.A., Cos, T., Duran, A., and Roncero, C. (1997). Characterization of CHS4 (CAL2), a gene of Saccharomyces cerevisiae involved in chitin biosynthesis and allelic to SKT5 and CSD4. Yeast *13*, 795-807.

Trucco, A., Polishchuk, R.S., Martella, O., Di Pentima, A., Fusella, A., Di Giandomenico, D., San Pietro, E., Beznoussenko, G.V., Polishchuk, E.V., Baldassarre, M., Buccione, R., Geerts, W.J., Koster, A.J., Burger, K.N., Mironov, A.A., and Luini, A. (2004). Secretory traffic triggers the formation of tubular continuities across Golgi sub-compartments. Nat Cell Biol *6*, 1071-1081.

Valdivia, R.H., Baggott, D., Chuang, J.S., and Schekman, R.W. (2002). The yeast clathrin adaptor protein complex 1 is required for the efficient retention of a subset of late Golgi membrane proteins. Dev Cell *2*, 283-294.

Valdivia, R.H., and Schekman, R. (2003). The yeasts Rho1p and Pkc1p regulate the transport of chitin synthase III (Chs3p) from internal stores to the plasma membrane. Proc Natl Acad Sci U S A *100*, 10287-10292.

Valdivieso, M.H., Ferrario, L., Vai, M., Duran, A., and Popolo, L. (2000). Chitin synthesis in a gas1 mutant of Saccharomyces cerevisiae. J Bacteriol *182*, 4752-4757.

Vogel, K., and Roche, P.A. (1999). SNAP-23 and SNAP-25 are palmitoylated in vivo. Biochem Biophys Res Commun *258*, 407-410.

Walworth, N.C., and Novick, P.J. (1987). Purification and characterization of constitutive secretory vesicles from yeast. J Cell Biol *105*, 163-174.

Wandinger-Ness, A., Bennett, M.K., Antony, C., and Simons, K. (1990). Distinct transport vesicles mediate the delivery of plasma membrane proteins to the apical and basolateral domains of MDCK cells. J Cell Biol *111*, 987-1000.

Wang, C.W., Hamamoto, S., Orci, L., and Schekman, R. (2006). Exomer: A coat complex for transport of select membrane proteins from the trans-Golgi network to the plasma membrane in yeast. J Cell Biol *174*, 973-983.

Weber, T., Zemelman, B.V., McNew, J.A., Westermann, B., Gmachl, M., Parlati, F., Sollner, T.H., and Rothman, J.E. (1998). SNAREpins: minimal machinery for membrane fusion. Cell *92*, 759-772.

Wendeler, M.W., Nufer, O., and Hauri, H.P. (2007). Improved maturation of CFTR by an ER export signal. Faseb J *21*, 2352-2358.

Wendeler, M.W., Paccaud, J.P., and Hauri, H.P. (2007). Role of Sec24 isoforms in selective export of membrane proteins from the endoplasmic reticulum. EMBO Rep *8*, 258-264.

Wieland, J., Nitsche, A.M., Strayle, J., Steiner, H., and Rudolph, H.K. (1995). The PMR2 gene cluster encodes functionally distinct isoforms of a putative Na+ pump in the yeast plasma membrane. Embo J *14*, 3870-3882.

Willsky, G.R. (1979). Characterization of the plasma membrane Mg2+-ATPase from the yeast, Saccharomyces cerevisiae. J Biol Chem *254*, 3326-3332.

Wood, S.A., Park, J.E., and Brown, W.J. (1991). Brefeldin A causes a microtubule-mediated fusion of the trans-Golgi network and early endosomes. Cell *67*, 591-600.

Yoshihisa, T., Barlowe, C., and Schekman, R. (1993). Requirement for a GTPase-activating protein in vesicle budding from the endoplasmic reticulum. Science *259*, 1466-1468.

Zahner, J.E., Harkins, H.A., and Pringle, J.R. (1996). Genetic analysis of the bipolar pattern of bud site selection in the yeast Saccharomyces cerevisiae. Mol Cell Biol *16*, 1857-1870.

Zanetti, G., Pahuja, K.B., Studer, S., Shim, S., and Schekman, R. (2011). COPII and the regulation of protein sorting in mammals. Nat Cell Biol *14*, 20-28.

Zanolari, B., Rockenbauch, U., Trautwein, M., Clay, L., Barral, Y., and Spang, A. (2011). Transport to the plasma membrane is regulated differently early and late in the cell cycle in Saccharomyces cerevisiae. J Cell Sci *124*, 1055-1066.

Zerial, M., and McBride, H. (2001). Rab proteins as membrane organizers. Nat Rev Mol Cell Biol *2*, 107-117.

Zhang, B., Kaufman, R.J., and Ginsburg, D. (2005). LMAN1 and MCFD2 form a cargo receptor complex and interact with coagulation factor VIII in the early secretory pathway. J Biol Chem *280*, 25881-25886.

Zhang, Z., Kulkarni, K., Hanrahan, S.J., Thompson, A.J., and Barford, D. (2010). The APC/C subunit Cdc16/Cut9 is a contiguous tetratricopeptide repeat superhelix with a homo-dimer interface similar to Cdc27. Embo J *29*, 3733-3744.

Zhao, H., and Eide, D. (1996). The yeast ZRT1 gene encodes the zinc transporter protein of a high-affinity uptake system induced by zinc limitation. Proc Natl Acad Sci U S A *93*, 2454-2458.

Ziman, M., Chuang, J.S., and Schekman, R.W. (1996). Chs1p and Chs3p, two proteins involved in chitin synthesis, populate a compartment of the Saccharomyces cerevisiae endocytic pathway. Mol Biol Cell *7*, 1909-1919.

Ziman, M., Chuang, J.S., Tsung, M., Hamamoto, S., and Schekman, R. (1998). Chs6p-dependent anterograde transport of Chs3p from the chitosome to the plasma membrane in Saccharomyces cerevisiae. Mol Biol Cell *9*, 1565-1576.

Zink, S., Wenzel, D., Wurm, C.A., and Schmitt, H.D. (2009). A link between ER tethering and COP-I vesicle uncoating. Dev Cell *17*, 403-416.

Zinser, E., and Daum, G. (1995). Isolation and biochemical characterization of organelles from the yeast, Saccharomyces cerevisiae. Yeast *11*, 493-536.